NUREG/CR-4599
BMI-2173
Vol. 1, No. 2

Short Cracks in Piping and Piping Welds

Semiannual Report
October 1990–March 1991

Prepared by
G. M. Wilkowski, F. Brust, R. Francini,
N. Ghadiali, T. Kilinski, P. Krishnaswamy, M. Landow,
C. W. Marschall, S. Rahman, F. Scott

Battelle

Prepared for
U.S. Nuclear Regulatory Commission

AVAILABILITY NOTICE

Availability of Reference Materials Cited in NRC Publications

Most documents cited in NRC publications will be available from one of the following sources:

1. The NRC Public Document Room, 2120 L Street, NW., Lower Level, Washington, DC 20555

2. The Superintendent of Documents, U.S. Government Printing Office, P.O. Box 37082, Washington, DC 20013-7082

3. The National Technical Information Service, Springfield, VA 22161

Although the listing that follows represents the majority of documents cited in NRC publications, it is not intended to be exhaustive.

Referenced documents available for inspection and copying for a fee from the NRC Public Document Room include NRC correspondence and internal NRC memoranda; NRC bulletins, circulars, information notices, inspection and investigation notices; licensee event reports; vendor reports and correspondence; Commission papers; and applicant and licensee documents and correspondence.

The following documents in the NUREG series are available for purchase from the GPO Sales Program: formal NRC staff and contractor reports, NRC-sponsored conference proceedings, international agreement reports, grant publications, and NRC booklets and brochures. Also available are regulatory guides, NRC regulations in the *Code of Federal Regulations*, and *Nuclear Regulatory Commission Issuances*.

Documents available from the National Technical Information Service include NUREG-series reports and technical reports prepared by other Federal agencies and reports prepared by the Atomic Energy Commission, forerunner agency to the Nuclear Regulatory Commission.

Documents available from public and special technical libraries include all open literature items, such as books, journal articles, and transactions. *Federal Register* notices, Federal and State legislation, and congressional reports can usually be obtained from these libraries.

Documents such as theses, dissertations, foreign reports and translations, and non-NRC conference proceedings are available for purchase from the organization sponsoring the publication cited.

Single copies of NRC draft reports are available free, to the extent of supply, upon written request to the Office of Administration, Distribution and Mail Services Section, U.S. Nuclear Regulatory Commission, Washington, DC 20555.

Copies of industry codes and standards used in a substantive manner in the NRC regulatory process are maintained at the NRC Library, 7920 Norfolk Avenue, Bethesda, Maryland, for use by the public. Codes and standards are usually copyrighted and may be purchased from the originating organization or, if they are American National Standards, from the American National Standards Institute, 1430 Broadway, New York, NY 10018.

NUREG/CR-4599
BMI-2173
Vol. 1, No. 2

Short Cracks in Piping and Piping Welds

Semiannual Report
October 1990–March 1991

Manuscript Completed: August 1991
Date Published: April 1992

Prepared by
G. M. Wilkowski, F. Brust, R. Francini,
N. Ghadiali, T. Kilinski, P. Krishnaswamy, M. Landow,
C. W. Marschall, S. Rahman, P. Scott

Battelle
505 King Avenue
Columbus, OH 43201

Prepared for
Division of Engineering
Office of Nuclear Regulatory Research
U.S. Nuclear Regulatory Commission
Washington, DC 20555
NRC FIN B5702

ABSTRACT

This is the second semiannual report of the U.S. Nuclear Regulatory Commission's Short Cracks in Piping and Piping Welds research program. The program began in March 1990 and will extend for 4 years. The intent of this program is to verify and improve fracture analyses for circumferentially cracked large-diameter nuclear piping with crack sizes typically used in leak-before-break analyses or in-service flaw evaluations. Only quasi-static loading rates are evaluated since the NRC's International Piping Integrity Research Group (IPIRG) program is evaluating the effects of seismic loading rates on cracked piping systems.

Progress for through-wall-cracked pipe involved (1) conducting a 28-inch diameter stainless steel SAW and 4-inch diameter French TP316 experiments, (2) conducting a matrix of FEM analyses to determine GE/EPRI functions for short TWC pipe, (3) comparison of uncracked pipe maximum moments to various analyses and FEM solutions, and (4) development of a J-estimation scheme that includes the strength of both the weld and base metals.

Progress for surface-cracked pipe involved (1) conducting two experiments on 6-inch diameter (Sch. 40 and XXS) pipe with $d/t = 0.5$ and $\theta/\pi = 0.25$ cracks, (2) comparisons of the pipe experiments to Net-Section-Collapse predictions, and (3) modification of the SC.TNP and SC.TKP J-estimation schemes to include external surface cracks.

High-temperature hardness testing appears to be a useful screening criteria parameter for assessing the susceptibility of ferritic pipe to dynamic strain aging. For anisotropic fracture evaluations, it was found that only one of five ferritic pipes had the low toughness direction in a helical direction, the rest had low toughness in the axial direction.

For crack-opening area analyses, predictive capabilities were expanded so that load versus crack opening can be calculated from the LBB.NRC, GE/EPRI, LBB.GE, LBB.ENG, and Tada/Paris analyses. These include loading due to tension, bending, and combined tension and bending. The LBB.ENG analysis was also modified to account for the weld and base metals strengths. Elastic FEA showed that for pressure loading, a crack close to a terminal end (i.e., a nozzle) will have lower crack opening due to restraint of the induced bending. This could affect LBB analyses.

CONTENTS

Page

ABSTRACT iii

LIST OF FIGURES ix

LIST OF TABLES xiv

PREVIOUS REPORTS IN SERIES xvii

EXECUTIVE SUMMARY xix

ACKNOWLEDGEMENTS xxi

NOMENCLATURE xxiii

1. INTRODUCTION 1-1

2. TASK 1 SHORT TWC PIPE EVALUATIONS 2-1

2.1 Task Objective 2-1
2.2 Task Rationale 2-1
2.3 Task Approach 2-1

2.3.1 Subtask 1.1 Material Characterization for Short TWC Pipe Experiments 2-1
2.3.2 Subtask 1.3 Large Diameter Pipe Fracture Experiments 2-14
2.3.3 Subtask 1.4 Analyses for Short Through-Wall Cracks in Pipes 2-24

2.4 Plans for Next Fiscal Year 2-61

2.4.1 Subtask 1.1 Material Characterization for Short TWC Pipe Experiments 2-61
2.4.2 Subtask 1.2 Upgrading of the Large-Pipe Testing System 2-61
2.4.3 Subtask 1.3 Large Diameter Pipe Fracture Experiments 2-62
2.4.4 Subtask 1.4 Analyses for Short Through-Wall Cracks in Pipes 2-62
2.4.5 Subtask 1.5 Prepare Topical Report on Short TWC Experiments and Analyses 2-63

2.5 References 2-63

3. TASK 2 SHORT SC PIPE EVALUATIONS 3-1

3.1 Task Objective 3-1
3.2 Task Rationale 3-1

CONTENTS

Page

3.3 Task Approach 3-1

3.3.1 Subtask 2.1 Material Characterization for Surface-Cracked Pipe Experiments 3-1
3.3.2 Subtask 2.2 Smaller Diameter Pipe Fracture Experiments in Pure Bending for Limit-Load Ovalization Correction 3-1
3.3.3 Subtask 2.4 Analysis of Short Surface Cracks in Pipes 3-8

3.4 Plans for Next Fiscal Year 3-15

3.4.1 Subtask 2.1 Material Characterization for Surface-Cracked Pipe Experiments 3-15
3.4.2 Subtask 2.2 Smaller Diameter Pipe Fracture Experiments in Pure Bending for Limit-Load Ovalization Correction 3-16
3.4.3 Subtask 2.3 Large Diameter Surface-Cracked Pipe Fracture Experiment in Combined Bending and Tension (Pressure) 3-16
3.4.4 Subtask 2.4 Analysis of Short Surface Cracks in Pipes 3-16

3.5 References 3-16

4. TASK 3 BIMETALLIC WELD CRACK EVALUATIONS 4-1

5. TASK 4 DYNAMIC STRAIN AGING 5-1

5.1 Task Objective 5-1
5.2 Task Rationale 5-1
5.3 Task Approach 5-1

5.3.1 Background 5-1
5.3.2 Subtask 4.1 Establish a Screening Criterion to Predict Unstable Crack Jumps in Ferritic Steels 5-3

5.4 Plans for Next Fiscal Year 5-21

5.4.1 Subtask 4.1 Establish a Screening Criterion to Predict Unstable Crack Jumps in Ferritic Steels 5-21
5.4.2 Subtask 4.2 Evaluate Procedures for Assessing Fracture Resistance During Crack Jumps in Laboratory Specimens 5-21
5.4.3 Subtask 4.3 Assess Current Procedures for Predicting Crack Jump Magnitude in Pipes 5-21
5.4.4 Subtask 4.4 Prepare Interim and Topical Reports on Dynamic Strain Aging Induced Crack Instabilities in Ferritic Nuclear Piping Steels at LWR Temperatures 5-22
5.4.5 Optional Subtask 4.5 Refine Procedures for Assessing Fracture Resistance During Crack Jumps in Laboratory Specimens 5-22
5.4.6 Optional Subtask 4.6 Refine Procedures for Predicting Crack Jump Magnitude in Pipes 5-22

CONTENTS

Page

5.5 References 5-22

6. TASK 5 FRACTURE EVALUATIONS OF PIPE ANISOTROPY 6-1

6.1 Task Objective 6-1
6.2 Task Rationale 6-1
6.3 Task Approach 6-1

6.3.1 Background 6-1
6.3.2 Subtask 5.1 Assess Effect of Toughness Anisotropy on Pipe Fracture Under Combined Loads 6-2
6.3.3 Subtask 5.2 Determine Magnitude of Toughness Anisotropy and Establish a Screening Criterion to Predict Out-of-Plane Crack Growth 6-6

6.4 Plans for Next Fiscal Year 6-24

6.4.1 Subtask 5.1 Assess Effect of Toughness Anisotropy on Pipe Fracture Under Combined Loads 6-24
6.4.2 Subtask 5.2 Determine Magnitude of Toughness Anisotropy and Establish a Screening Criterion to Predict Out-of-Plane Crack Growth 6-25
6.4.3 Subtask 5.3 Prepare Interim and Topical Reports on Anisotropy and Mixed-Mode Studies 2-25
6.4.4 Optional Subtask 5.4 Establish Ductile Crack Growth Resistance Under Mixed-Mode Loading 6-25
6.4.5 Optional Subtask 5.5 Refine J-Estimation Scheme Analyses for Pipes 6-25

6.5 References 6-25

7. TASK 6 CRACK OPENING AREA EVALUATIONS 7-1

7.1 Task Objective 7-1
7.2 Task Rationale 7-1
7.3 Task Approach 7-1

7.3.1 Subtask 6.1 Create Combined Loading Improvements 7-1
7.3.2 Subtask 6.3 Improve Weld Crack Evaluations 7-9
7.3.3 Subtask 6.6 Leak Rate Quantification 7-14

7.4 Plans for Next Fiscal Year 7-17

7.4.1 Subtask 6.1 Create Combined Loading Improvements 7-17
7.4.2 Subtask 6.2 Implement Short TWC Crack-Opening Improvements 7-19
7.4.3 Subtask 6.3 Improve Weld Crack Evaluations 7-19

CONTENTS

Page

7.4.4 Subtask 6.4 Modify SQUIRT Code 7-19
7.4.5 Subtask 6.5 Prepare Topical Report on Crack Opening Area Improvements 7-19
7.4.6 Subtask 6.6 Leak Rate Quantification 7-20

7.5 References 7-20

8. TASK 7 NRCPIPE IMPROVEMENTS 8-1

8.1 Task Objective 8-1
8.2 Task Rationale 8-1
8.3 Task Approach 8-1
8.4 Plans for Next Fiscal Year 8-1

8.4.1 Subtask 7.1 Improve Efficiency of Current Version 8-2
8.4.2 Subtask 7.2 Incorporate TWC Improvements in NRCPIPE 8-2
8.4.3 Subtask 7.3 Make Surface Crack Version of NRCPIPE 8-2

APPENDIX A WELD PROCEDURE A-1
APPENDIX B PLASTIC SOLUTION OF EQUIVALENT PIPE B-1
APPENDIX C PARTIAL DERIVATIVES $\partial I_B/\partial\theta$ AND $\partial L^d{}_B/\partial\theta$ C-1

LIST OF FIGURES

Figure		Page
2.1	Engineering stress-strain curves for submerged-arc weld (DP2-A45W2) tested at 288 C (550 F)	2-7
2.2	J-resistance curves for non-side-grooved C(T) specimens machined from submerged-arc weld (DP2-A45W2) and a typical TP304 stainless steel base metal	2-8
2.3	J-resistance curves for C(T) specimens having 20% side grooves machined from submerged-arc weld (DP2-A45W2)	2-9
2.4	Engineering stress-strain curves for tensile specimens machined from French TP316LN stainless steel pipe (Pipe IP-A2)	2-13
2.5	J-resistance curves for compact specimens machined from French TP316LN stainless steel pipe (Pipe IP-A2) in the L-C orientation	2-13
2.6	Schematic of experimental setup for EDF-24	2-16
2.7	Moment versus rotation at 85 mm from crack plane for EDF Experiment No. 24	2-17
2.8	Schematic of Experiment 1.1.1.26	2-18
2.9	Total load versus load-time displacement from Experiment 1.1.1.26	2-19
2.10	Schematic and dimensions of Experiment 1.1.1.23	2-21
2.11	Total load versus load-line displacement data from Experiment 1.1.1.23 (Stainless steel SAW with short crack)	2-22
2.12	Photographs of crack growth from stainless steel SAW Experiment 1.1.1.23	2-23
2.13	Circumferentially cracked pipe loaded in four-point bending	2-28
2.14	Comparison of predicted to experimental maximum moments for JAERI uncracked stainless steel unpressurized pipe bending experiments	2-32
2.15	Comparison of experimental to finite element analyses of uncracked stainless steel pipe test results (JAERI Experiment S-17)	2-33
2.16	Comparison of Sanders' F-functions for $F_m/t = 5$ and polynominal fit assuming F = 1 as crack angle approaches zero	2-34

LIST OF FIGURES

Figure		Page
2.17	Typical finite element (a) mesh used for analysis (1/4 model), and (b) circumferential cracked pipe geometry	2-38
2.18	Plasticity function h_1 (ABAQUS - Solid Element Results) for pipe under bending. $R/t = 10$, $n = 3$, and $\theta/\pi = 0.0625$	2-44
2.19	Comparison of maximum loads from Experiments 1.1.1.21 and 4111-2 on a 28-inch-diameter Schedule A516, Grade 70 pipe to predictions by various analyses	2-46
2.20	Comparison of maximum load predictions by various analyses to two 28-inch-diameter, Schedule 80, TP316 stainless steel, through-wall-cracked pipe experiments	2-46
2.21	Circumferential crack in a pipe butt weld	2-49
2.22	Idealized pipe weld with a crack	2-50
2.23	Schematics of pipe weldments with a circumferential flaw	2-50
2.24	Reduced section analogy	2-51
2.25	Comparisons of computed J versus M ($R/t \sim 6$)	2-56
2.26	Comparisons of computed J versus M ($R/t \sim 15$)	2-56
2.27	Plots of I_B^d versus M	2-57
2.28	Comparisons of computed J versus M ($n_1 = 3$, $n_2 = 8$)	2-59
2.29	Comparisons of computed J versus M ($n_1 = 3$, $n_2 = 12$)	2-59
2.30	Comparisons of computed J versus M ($n_1 = 7$, $n_2 = 8$)	2-60
2.31	Comparison of computed J versus M ($n_1 = 7$, $n_2 = 12$)	2-60
2.32	Circumferential through-wall crack in a weld showing plastic zone sizes	2-61
3.1	Plot of the ratio of the maximum experimental stress to the predicted net-section-collapse stress as a function of the pipe R/t ratio for a series of surface-cracked pipe experiments for which the DPZP is greater than 0.2	3-2
3.2	Pretest calculations for 6-inch-diameter Schedule 40 stainless steel pipe test (Experiment 1.2.1.22)	3-5

LIST OF FIGURES

Figure Page

3.3 Total load versus load-line displacement of Experiment 1.2.1.22 6-inch-diameter Schedule 40 TP304 pipe with short surface crack ($d/t = 0.5$, $\theta/\pi = 0.25$) 3-6

3.4 Post-test photograph of 6-inch Schedule 40 stainless steel internal surface crack showing buckling (Experiment 1.2.1.22) 3-6

3.5 Total load versus load-line displacement of Experiment 1.2.1.21 6-inch-diameter Schedule XXS TP304 pipe with short surface crack ($d/t = 0.5$, $\theta/\pi = 0.25$) 3-7

3.6 Flaw geometry and loading configuration for surface-cracked pipe 3-11

3.7 Comparison between J-estimation scheme (INTCRK7) and FE results for internal-surface-cracked pipe Experiment 4131-4, neglecting effects of internal pressure 3-12

3.8 Comparison of J-estimation scheme (INTCRK7) and FE results for Experiment 4131-8, including effects of internal pressure 3-12

3.9 Comparison of experiment maximum moment/net-section-collapse moment versus R_m/t for short and long surface-cracked pipe experiments 3-14

5.1 Location of thermocouples and Brinell hardness impressions on carbon steel plates 5-6

5.2 Yield strength, ultimate tensile strength, and Brinell hardness as functions of test temperature for five carbon steels 5-9

5.3 Elongation and reduction of area as functions of test temperature for five carbon steels 5-10

5.4 Engineering stress-strain curves at various temperatures for five carbon steels tested in tension 5-11

5.5 Load versus displacement curves for C(T) specimens of three different carbon steels tested at various temperatures 5-14

5.6 J-resistance curves for C(T) specimens of three different carbon steels tested at various temperatures 5-15

5.7 J_i and dJ/da versus test temperature for C(T) specimens from Pipe DP2-F11 5-16

LIST OF FIGURES

Figure Page

5.8 J_i and dJ/da versus test temperature for C(T) specimens from Pipe DP2-F26 5-17

5.9 J_i and dJ/da versus test temperature for C(T) specimens from Pipe DP2-F30 5-18

6.1 Orientation of skewed specimens machined from Pipe DP2-F11: (a) tensile specimens and (b) C(T) specimens 6-5

6.2 Tensile properties as functions of specimen orientation for Pipe DP2-F11 (A333 Grade 6) 6-7

6.3 Engineering stress-strain curves for several different tensile specimen orientations in Pipe DP2-F11 6-8

6.4 Load versus displacement curves for several different C(T) specimen orientations in Pipe DP2-F11 6-9

6.5 J-resistance curves for several different C(T) specimen orientations in Pipe DP2-F11 6-9

6.6 J_i and dJ/da as functions of C(T) specimen orientation in Pipe DP2-F11 6-10

6.7 Load versus displacement curves for two different C(T) specimen orientations in Pipe DP2-F30 6-11

6.8 J-resistance curves for two different C(T) specimen orientations in Pipe DP2-F30 6-11

6.9 J_i, J at $\Delta a = 2$ mm, and dJ/da as functions of C(T) specimen orientation in Pipe DP2-F30 6-12

6.10 Photomicrographs of sulfide inclusions in carbon steel pipes: (a) Pipe DP2-F9, (b) Pipe DP2-F11, (c) Pipe DP2-F26, (d) Pipe DP2-F29, and (e) Pipe DP2-F30 6-17

6.11 Photographs and X-ray dot maps of selected inclusions in Pipe DP2-F9 (A333 Grade 6 carbon steel) to verify presence of manganese sulfides 6-18

6.12 Examples of skewed crack extension in tests on three different carbon steel pipes 6-19

6.13 Comparison of single shear and double shear fractures in carbon steel C(T) specimens 6-20

LIST OF FIGURES

Figure | Page

6.14 Energy absorbed by Charpy V-notch impact specimens as a function of specimen orientation 6-23

7.1 Crack-opening displacement in Experiment 4111-1 up to load at crack initiation 7-4

7.2 Crack-opening displacement in Experiment 4111-2 up to load at crack initiation 7-4

7.3 Crack-opening displacement in Experiment 4111-3 up to load at crack initiation 7-5

7.4 Comparison of various analyses to center-crack-opening displacement for pressurized pipe Experiment 4121-1 on 6-inch-diameter TP304 stainless steel pipe 7-7

7.5 Comparison of predictions of various analyses to experimental center-crack-opening displacement for pressure and bend Experiment 4131-1 on 6-inch-diameter TP304 stainless steel pipe 7-8

7.6 Comparison of predictions of various analyses to experimental center-crack-opening displacement for pressure and bend Experiment 4131-9 on 10-inch nominal diameter A333 Grade 6 pipe 7-8

7.7 Schematics of pipe weldments with a circumferential flaw 7-11

7.8 Reduced section analogy 7-11

7.9 Comparisons of M versus COD (R/t ~ 6) 7-13

7.10 Comparisons of M versus COD (R/t ~ 15) 7-13

7.11 Comparisons of applied load versus computed crack-opening displacement 7-14

7.12 Finite element analysis in linear elastic restraint of COD study 7-18

7.13 Effect of fully restrained bending conditions from crack location on COD normalized by unrestrained COD 7-19

LIST OF TABLES

Table Page

1.1 Summary of proposed pipe experiments 1-2

2.1 Chemical composition of the submerged-arc weld (DP2-A45W2) in TP304 austenitic stainless steel plate 2-4

2.2 Tensile properties at 288 C (550 F) of submerged-arc weld metal (DP2-A45W2) in a TP304 stainless steel plate 2-5

2.3 Charpy V-notch impact tests on submerged-arc weld (DP2-A45W2) in TP304 stainless steel plate (Full-size specimens) 2-5

2.4 J_i and dJ/da values obtained from compact specimens machined from a submerged-arc weld (DP2-A45W2) in TP304 stainless steel plate 2-6

2.5 Chemical composition of French TP316LN stainless steel pipe (Pipe IP-A2) 2-11

2.6 Tensile properties of French TP316LN steel pipe (Pipe IP-A2) in the longitudinal direction at room temperature 2-12

2.7 Summary of J_i and dJ/da values for French TP316LN stainless steel pipe (Pipe IP-A2) obtained from compact specimens tested at room temperature 2-12

2.8 Critical parameters from EDF and 1.1.1.26 experiments 2-17

2.9 Material properties of 28-inch-diameter stainless steel weld at 288 C 2-22

2.10 Critical parameters from Experiments 4111-5 and 1.1.1.23 2-23

2.11 Summary of uncracked JAERI experiments analyzed 2-32

2.12 Matrix of finite element calculations 2-37

2.13 F, V_1, V_2, V_3 functions (tension - elastic) 2-41

2.14 h functions (tension-fully plastic) (n = 3) 2-41

2.15 F, V_1, V_3 functions (bending-elastic) 2-42

2.16 h functions (bending - fully plastic) (n = 3) 2-42

2.17 h functions (bending - fully plastic) (n = 5) 2-43

LIST OF TABLES

Table — Page

2.18 h functions (bending - fully plastic) (n = 7) 2-43

2.19 Parameters of material constitutive law 2-55

3.1 Smaller diameter pipe with short cracks under bending for Subtask 2.2 3-3

3.2 Short versus long surface crack maximum moment/net-section-collapse predicted moments 3-15

5.1 Description of Activity 4.1.1 pipes used in study of dynamic strain aging 5-4

5.2 Chemical composition of Activity 4.1.1 pipes used in study of dynamic strain aging 5-5

5.3 Tensile strength ratios and hardness ratios for carbon steel pipes at selected temperatures 5-20

6.1 Description of Activity 5.2.1 pipes used in study of anisotropy 6-14

6.2 Chemical composition of Activity 5.2.1 pipes used in study of anisotropy 6-14

6.3 Appearance of stringer-type inclusions in pipes used in study of anisotropy 6-16

6.4 Ratio of transverse to longitudinal toughness in Charpy V-notch impact specimens machined from carbon steel pipes 6-23

7.1 Crack-opening displacement analysis of past Degraded Piping Program data 7-6

7.2 Ramberg-Osgood coefficients of experiment analyzed 7-12

PREVIOUS REPORTS IN SERIES

Previous Reports from this Program

"Short Cracks in Piping and Piping Welds," First Semiannual Report, NUREG/CR-4599, Vol. 1, No. 1, March 1991.

Previous Related Documents from NRC's Degraded Piping Program

"Degraded Piping Program - Phase II," Semiannual Report, NUREG/CR-4082, Vol. 1, October 1984.

"Degraded Piping Program - Phase II," Semiannual Report, NUREG/CR-4082, Vol. 2, June 1985.

"Degraded Piping Program - Phase II," Semiannual Report, NUREG/CR-4082, Vol. 3, March 1986.

"Degraded Piping Program - Phase II," Semiannual Report, NUREG/CR-4082, Vol. 4, July 1986.

"Degraded Piping Program - Phase II," Semiannual Report, NUREG/CR-4082, Vol. 5, December 1986.

"Degraded Piping Program - Phase II," Semiannual Report, NUREG/CR-4082, Vol. 6, April 1988.

"Degraded Piping Program - Phase II," Semiannual Report, NUREG/CR-4082, Vol. 7, March 1989.

"Degraded Piping Program - Phase II," Semiannual Report, NUREG/CR-4082, Vol. 8, March 1989.

"NRC Leak-Before-Break (LBB.NRC) Analysis Method for Circumferentially Through-Wall Cracked Pipes Under Axial Plus Bending Loads," Topical Report, NUREG/CR-4572, March 1986.

"Elastic-Plastic Finite Element Analysis of Crack Growth in Large Compact Tension and Circumferentially Through-Wall-Cracked Pipe Specimen--Results of the First Battelle/NRC Analysis Round Robin," Topical Report, NUREG/CR-4573 September 1986.

"An Experimental and Analytical Assessment of Circumferential Through-Wall Cracked Pipes Under Pure Bending," Topical Report, NUREG/CR-4574, June 1986.

"Predictions of J-R Curves With Large Crack Growth From Small Specimen Data," Topical Report, NUREG/CR-4575, August 1986.

"An Assessment of Circumferentially Complex-Cracked Pipe Subjected to Bending," Topical Report, NUREG/CR-4687, September 1986.

Previous Reports in Series

"Analysis of Cracks in Stainless Steel TIG Welds," Topical Report, NUREG/CR4806, November 1986.

"Approximate Methods for Fracture Analyses of Through-Wall Cracked Pipes," Topical Report, NUREG/CR-4853, January 1987.

"Assessment of Design Basis for Load-Carrying Capacity of Weld-Overlay Repair," Topical Report," NUREG/CR-4877, February 1987.

"Analysis of Experiments on Stainless Steel Flux Welds," Topical Report, NUREG/CR-4878, February 1987.

"Experimental and Analytical Assessment of Circumferentially Surface-Cracked Pipes Under Bending," Topical Report, NUREG/CR-4872, April 1987.

Previous Related Documents from NRC's International Piping Integrity Research Group (IPIRG) Program

"Evaluation and Refinement of Leak-Rate Estimation Models," NUREG/CR-5128, April 1991.

EXECUTIVE SUMMARY

This is the second semiannual report of the U.S. NRC's Short Cracks in Piping and Piping Welds Research Program. The program began in March of 1990, and will extend for four years. The intent of this program is to verify and improve fracture analyses for circumferentially cracked large diameter nuclear piping using integrated results from analytical, material characterization, and full-scale pipe fracture efforts. Only quasi-static loading rates are evaluated, since the NRC's International Piping Integrity Research Group (IPIRG) Program evaluated the effects of seismic loading rates on cracked piping systems.

The term "short cracks" encompasses crack sizes typically considered in leak-before-break (LBB) or pragmatic in-service flaw evaluations. A typical LBB size crack for a large diameter pipe is 6 percent of the circumference. This is much less than the circumferential crack lengths of 20 to 40 percent investigated in many past pipe fracture programs. Hence, the term "short cracks" in this program does not refer to microscopic cracks often of technical interest to the aerospace industry.

Additional efforts involve investigating phenomena discovered during the course of conducting the Degraded Piping Program. These include the evaluation of the occurrence of unstable crack jumps in ferritic steels at light water reactor temperatures and the occurrence of anisotropic fracture properties causing helical crack growth. Both of these phenomena may reduce the actual safety margins in LBB analyses when compared to real behavior. Other investigations deal with the fracture behavior of bi-metallic welds and improvements in crack opening area analyses used in LBB analyses. Some key points from this reporting period are presented below.

Short Through-Wall-Cracked Pipe

Progress was made in several subtasks, but final conclusions cannot be made yet for most of these efforts. An experiment on a 28-inch-diameter pipe with a short through-wall crack (TWC) of 6 percent of the circumference in a stainless steel submerged-arc weld (SAW) experiment was conducted and analyzed. Results differed from the ferritic pipe tests on similar size pipe reported in the last semiannual report in that the experimental failure loads for this stainless steel SAW experiment were below the predicted loads from the various analyses except for the predictions based on the IWB-3640 source equations. Conversely, the ferritic pipe tests had maximum loads above most predictions, except for predictions based on the net-section-collapse and some J-estimation schemes for the short crack experiment ($2c/\pi D = 0.06$) results.

A 4-inch-diameter pipe test on a French TP316 stainless steel showed that the maximum loads from the EDF and Battelle pipe test systems agreed within 4 percent of each other.

The h, V, and F-functions for the GE/EPRI method were calculated for short TWC pipe under tension and bending loads. Initial results showed good agreement with elastic solutions, but fully plastic solutions for the displacement function and the function to calculate J (h_1) were higher than in the original GE/EPRI solutions. The higher h_1 values would result in load predictions closer to experimental results. Further calculations are under way. A J-estimation scheme

(LBB.ENG2) was also developed to account for stress-strain properties of the weld and base metal for the case of a TWC in a weld.

Short Surface-Cracked Pipe

Two experiments were conducted on 6-inch-diameter TP304 stainless steel pipe, one on Schedule 40 pipe and the other on Schedule XXS pipe. The crack geometries were 25 percent of the pipe circumference in length and 50 percent of the wall thickness in depth. The Schedule 40 pipe first buckled and then fractured after significant load drop and further applied displacements during the buckling. Both experiments had maximum loads significantly below the net-section-collapse predicted loads. These results agreed with past EPRI data generated at Battelle that used similar crack lengths. However, further data are needed to quantify a trend with pipe R/t ratio. Interestingly, uncracked stainless steel pipe data were used to assess buckling loads by finite element analyses (FEA). The FEA underpredicted the experimental loads by 20 percent. This result agrees with trends from finite element analyses of many stainless steel TWC pipe bending experiments, suggesting a basic problem in FEA of stainless steel pipe.

The SC.TNP and SC.TKP analyses were modified to include external as well as internal finite length circumferential surface cracks.

Unstable Crack Jumps and Dynamic Strain Aging

A screening criterion that assesses dynamic strain-aging sensitivity of ferritic steels by high-temperature hardness testing appears to be successful. This could be used for material selection for new reactors or in-plant assessment of piping.

Anisotropic Fracture Properties

Only one of five carbon steel pipes evaluated had inclusions occurring in a helical direction; the rest of the pipe samples had inclusions oriented in the axial crack growth direction. The direction of the inclusions corresponded to the direction of lowest toughness for all five pipes.

Crack-Opening Area Analyses

Crack-opening displacement capabilities were added to the LBB.ENG and LBB.GE J-estimation schemes in addition to the existing capability for the GE/EPRI, Tada-Paris, and LBB.NRC analyses. Comparisons were made to experimental results under pure bending, pure pressure loading, and combined pressure and bending. The LBB.ENG2 analysis was also modified to predict opening of a crack in a weld where the weld and base metal strengths were included. For tension loading of a crack in a piping system, FEA showed that if the crack were close to a terminal end, the crack opening from the induced bending would be restrained. This was found to be a function of the length of the through-wall crack and the distance from the terminal end (e.g., a nozzle). For a TWC length less than 1/8 of the circumference, the restraint of the induced bending has negligible effect on the crack opening. For cracks longer than 25 percent of the circumference, the effect of the restrained bending can be significant if the crack is close to a terminal end (i.e., the crack is within 10 pipe diameters of a nozzle).

ACKNOWLEDGMENTS

This work is supported by the U.S. Nuclear Regulatory Commission through the Materials Engineering Branch of the Office of Nuclear Regulatory Research under Contract No. NRC-04-90-069. Mr. M. Mayfield was the NRC program manager during this period, and the current NRC program manager is Mr. A. Hiser.

We would also like to thank others at Battelle who have helped in these efforts. Technicians who have contributed to the initial efforts are: Mr. R. Gertler, Mr. P. Held, Mr. J. Kramer, Mr. P. Mincer, Mr. D. Rider, Mr. J. Ryan, Mr. D. Shoemaker, and Mr. J. Woods. We thank Mrs. B. Blanton for typing this report and Mr. D. Hayes for drafting assistance.

NOMENCLATURE

1. SYMBOLS

A	Crack area
a	Crack length
$\hat{a}$	Axial length in LBB.ENG analysis
a_o	Initial crack length
a_e	Effective crack length
C	Constant in fatigue crack growth equation
c	Half the circumferential crack length
D	Nominal pipe diameter
D_m	Mean pipe diameter
D_o	Outside diameter
d	Surface crack depth
E	Young's modulus
E'	$E/(1-\nu^2)$
$F_b(\theta)$	Dimensionless function for calculation of linear elastic stress intensity factor for pipe in bending with circumferential half crack length of θ.
G_n	Function used in SC.TKP J-estimation scheme for J_p
H_n	Function used in SC.TNP J-estimation scheme for J_p
h_1,h_2,h_3,h_4	Functions tabulated in GE/EPRI method
I	Moment of inertia

Nomenclature

J	J-integral fracture parameter
J_D-R	Deformation J-R curve
J_e	Elastic component of J-integral
J_i	J-integral at crack initiation but not necessarily a valid J_{Ic} by ASTM E813-81
J_I, J_{II}, J_{III}	J applied for Modes I, II, and III.
J_{Ic}	Plane strain J at crack initiation by ASTM E813
J_p	Plastic component of J-integral
J-R	J-integral resistance (curve)
J_T	Total J
K	Elastic stress intensity factor
L	Pipe length
$L\omega$	Axial length of weld
M	Moment
m	Exponent for fatigue crack growth
M_{mes}	Buckling moment calculated by Mesloh analysis
M_i	Moment at a nominal stress of σ_i
M_{nsc}	Moment calculated by Net-Section-Collapse analysis
M_o	Moment at a nominal stress of σ_o
N	1/n, also used for number of cycles
n	Ramberg-Osgood strain-hardening exponent

P	Applied load
Q	Generalized load
q	Generalized displacement
R	Pipe radius
R_m	Mean pipe radius
R_o	Outside pipe radius
r_y	Plastic-zone radius
S_m	ASME design stress
T	Axial tension load
t	Thickness of pipe
t_e	Effective thickness in LBB.ENG analysis
U	Electric potential
U_o	Initial electric potential
V_1, V_2, V_3	Displacement functions in GE/EPRI analysis
w	Width of C(T) specimen
Z	A stress multiplier in ASME IWB-3640 and -3650 analyses
α	Ramberg-Osgood parameter
Δ	Displacement for axial tension
Δa	Increment of crack growth
Δ_{cpt}	Tension component of crack opening
δ	Displacement at center of crack

Nomenclature

δ_e	Elastic displacement at center of crack
δ_p	Plastic displacement at center of crack
δ_T	Total displacement
δ_t	Crack tip displacement
η	Eta factor, a geometric factor (η) times the energy = J
ε	Strain
ε_o	Ramberg-Osgood reference strain
θ	Half crack angle of through-wall crack in a pipe
θ_o	Initial crack angle
υ	Poisson's ratio
ϕ	Half rotation angle of pipe
ϕ^e	Half of elastic component of pipe rotation due to the crack
ϕ^p	Half of plastic component of pipe rotation due to the crack
Π	Strain energy - work of external forces
σ	Stress
σ_f	Flow stress
σ_i	Stress at crack initiation
σ_{nsc}	Net-Section Collapse analysis predicted stress
σ_o	Ramberg-Osgood reference stress
σ_u	Ultimate strength
σ_y	Yield strength

$\sigma_{0.005}$	Stress at a strain of 0.005

2. ACRONYMS AND INITIALISMS

ACO	Area of crack opening
ASME	American Society of Mechanical Engineers
ASTM	American Society of Testing and Materials
BHN	Brinell hardness number
BHN_{RT}	Brinell hardness number at room temperature
BHN_{288}	Brinell hardness number at 288 C
BWR	Boiling water reactor
CEA	Commissariat a l'Energie Atomique
C-L	Circumferential-longitudinal orientation (axial through-wall crack growth direction)
COA	Crack opening angle
COD	Crack opening displacement
CMOD	Crack mouth opening displacement
CTOA	Crack tip opening angle
C(T)	Compact (tension) specimen
CVN	Charpy V-notch
DSA	Dynamic strain aging
DP^3II	Degraded Piping Program - Phase II
EDF	Electricité de France

Nomenclature

EPFM	Elastic-plastic fracture mechanics
EPRI	Electric Power Research Institute
FE	Finite element
FEM	Finite element method
FY	Fiscal Year
GE	General Electric Company
HAZ	Heat-affected zone
IPIRG	International Piping Integrity Research Group
JAERI	Japanese Atomic Energy Research Institute
LBB	Leak-before-break
L-C	Longitudinal-circumferential orientation (direction of through-wall crack growth around pipe circumference)
LEFM	Linear-elastic fracture mechanics
LWR	Light water reactor
LLD	Load-line displacement
NDT	Non-destructive testing
NRC	Nuclear Regulatory Commission
NRC-RES	Nuclear Regulatory Commission - Office of Nuclear Regulatory Research
NRC-NRR	Nuclear Regulatory Commission - Office of Nuclear Reactor Regulation
NSC	Net-section-collapse

OD	Outside diameter
PC	Personal computer
PVP	Pressure vessel and piping
RT	Room temperature
SAW	Submerged arc weld
SC	Surface crack
Sch.	Schedule (pipe thickness)
SMAW	Shielded metal arc weld
SSE	Safe shut-down earthquake
TWC	Through-wall crack
UTS	Ultimate tensile strength
XXS	Schedule extra extra strong pipe

1. INTRODUCTION

The "Short Cracks in Piping and Piping Welds" program was initiated to address Nuclear Regulatory Commission (NRC) licensing needs and to resolve some critical findings from the NRC's Degraded Piping Program. The term "short cracks" refers to the type of cracks assessed in leak-before-break (LBB) or pragmatic in-service flaw evaluations. A typical LBB-size crack for a large diameter pipe is 6 percent of the circumference, which is much less than the circumferential lengths of 20 to 40 percent investigated in other past pipe fracture programs. Hence, the term "short cracks" in this project does not refer to microscopic cracks in the sense of the technical interests of the aerospace industry.

This 4-year program started on March 23, 1990. This report covers progress to date, along with details and plans for the entire program.

The nine tasks addressed in this program are:

(1) Short through-wall cracked (TWC) pipe evaluations

(2) Short surface-cracked (SC) pipe evaluations

(3) Bi-metallic weld crack evaluations

(4) Dynamic strain aging and crack instabilities evaluations

(5) Fracture evaluations of anisotropic pipe

(6) Crack-opening-area evaluations

(7) NRCPIPE Code improvements

(8) Additional tasks, if needed

(9) Interprogram cooperation and program management.

Of these, significant work has started in Tasks 1, 2, 4, 5, and 6. No work has been identified under Task 8 at this time.

Most of the tasks in this program involve integrated analytical, material characterization, and full-scale pipe fracture experimental efforts. The specific efforts in this program are limited to circumferential cracks in straight pipe, and loads that are applied at quasi-static rates. A summary of all the pipe experiments is given in Table 1.1. Seismic loading rate behavior is being investigated in the NRC's International Piping Integrity Research Group program (IPIRG).

The progress reported in this report includes work from October 1, 1990 to March 31, 1991.

Table 1.1 Summary of proposed pipe experiments

Expt. No.[a]	Diameter	Schedule	Material	Temperature	Test[b] Date	Task No.
Unpressurized through-wall-cracked pipe experiments						
1.1.1.21	28 inch	60	A516 Gr70	288C (550F)	10/25/90	1
1.1.1.22	36 inch	160	A516 Gr70	288C (550F)	(5/93)	1
1.1.1.23	28 inch	80	TP316 SAW	288C (550F)	5/23/91	1
1.1.1.24	24 inch	100	A333 Gr6 SAW	288C (550F)	(7/92)	1
1.1.1.26	4 inch	80	TP316LN	20C (72F)	2/27/91	1
Unpressurized uncracked pipe experiment						
1.1.1.25	28 inch	60	A516 Gr70	288C (550F)	(2/92)	1
Bi-metallic weld fusion line experiments - TWC						
1.1.3.8	36 inch	160	A516/SS-SAW	288C (550F)	(1/94)	3
Unpressurized surface-cracked pipe experiments						
1.2.1.20	16 inch	40S	TP316	100C (212F)	(1/92)	2
1.2.1.21	6 inch	XXS	TP304	288C (550F)	4/16/91	2
1.2.1.22	6 inch	40	TP304	288C (550F)	3/15/91	2
Pressurized surface-cracked pipe experiments						
1.2.3.15	28 inch	60	A516	288C (550F)	11/03/91	2
1.2.3.16	28 inch	80	TP316 SAW	288C (550F)	9/05/91	2
1.2.3.17	36 inch	160	A516 SAW	288C (550F)	(9/93)	2
Bi-metallic weld fusion line experiments - SC						
1.2.3.21	36 inch	160	A516/SS-SAW	288C (550F)	(7/94)	3

(a) Experiment numbers are consecutive with Degraded Piping Program Data Record Book entries.
(b) Anticipated test dates in parenthesis.

2. TASK 1 SHORT TWC PIPE EVALUATIONS

2.1 Task Objective

The objective of this task is to modify and verify analyses for short through-wall-cracked (TWC) pipe using existing and new data on large diameter pipe.

2.2 Task Rationale

The results of this task will help to refine the fracture analyses in LBB procedures used to evaluate through-wall cracks in large diameter pipes.

2.3 Task Approach

The five subtasks in this task are:

Subtask 1.1	Material characterization of pipes to be tested
Subtask 1.2	Facility modifications for large diameter pipe experiments
Subtask 1.3	Conduct large diameter pipe experiments
Subtask 1.4	Analysis modification and verifications
Subtask 1.5	Topical report.

During this reporting period progress was made in Subtasks 1.1, 1.3, and 1.4; hence, only these subtasks will be discussed.

2.3.1 Subtask 1.1 Material Characterization for Short TWC Pipe Experiments

2.3.1.1 Objective

The objective of this activity is to generate the necessary data to document the material strength and toughness for analysis in Subtask 1.4.

2.3.1.2 Rationale

The material property data needed for the analysis procedures in Subtask 1.4 will be determined from each pipe and weld to be tested. These data are also of value for the NRC PIFRAC database (Ref. 2.1).

2.3.1.3 Approach

Material property data, i.e., Charpy, chemical analysis, tensile, and J-R curves, need to be generated for the 28-inch-diameter stainless steel weld and the 24-inch-diameter carbon steel

SAW used in Subtask 1.3. The 24-inch-diameter pipe weld will be the same as the 36-inch-diameter pipe weld used in Task 2. Hence, only the larger diameter carbon steel pipe weld needs to be characterized. This characterization will be done in Task 2.1. The French TP316LN stainless steel pipe used in the new 4-inch diameter TWC pipe experiment has been fully characterized and those results are given in this report. We have the material property data on the other materials from the Degraded Piping Program (Ref. 2.2).

The full-size Charpy data will be determined as a function of temperature for the carbon steel weld and at 22 and 288 C (72 and 550 F) for the austenitic stainless steel weld. The tensile and J-R curve tests will be conducted at room temperature and at 288 C (550 C). Duplicate specimens will be tested for each specimen type. The tensile specimens will be longitudinally oriented, and will be tested for both the base and weld materials. The Charpy and C(T) specimens for the J-R curve tests will have an L-C orientation. The thickness of the C(T) specimens will be at least 80 percent of the pipe thickness and will be the largest planform size that the curvature of the pipe allows. If weld specimens are taken from plate welds, then the standard size specimen for the plate thickness will be used.

The data will be recorded digitally, and reduced to a format identical to that used in past Degraded Piping Program data record book entries. These data would also be available for input into the NRC PIFRAC database.

2.3.1.4 Progress

During the past reporting period, a submerged-arc weldment was prepared in 25.4-mm- (1-inch) thick TP304 stainless steel plate and material characterization tests were completed. The weldment was prepared at the United McGill Corporation in Columbus, Ohio, following procedures that were nominally identical to those employed in girth welding the 28-inch-diameter stainless steel pipe that is to be subjected to a short TWC pipe experiment.

In addition to the work on the plate weld, characterization tests were completed on the 4-inch-diameter French pipe, identified as Pipe IP-A2. That pipe was originally thought to be TP316L, but chemical analysis showed it to meet the ASTM specifications for TP316LN.

Characterization of Submerged-Arc Weld in TP304 Stainless Steel

Chemical analysis, tensile, Charpy V-notch, and J-R curve tests were conducted on a submerged-arc weld in 25.4-mm- (1-inch) thick TP304 stainless steel plate. The plate in which the weld was prepared was identified as DP2-A45 and the weld metal as DP2-A45W2. The tensile tests, Charpy tests, and J-R curve tests were conducted in duplicate at room temperature and at 288 C (550 F).

The tensile specimens, which were threaded-end, round bar specimens having a gage diameter of 3.2 mm (0.125 inch) and a gage length of 12.7 mm (0.5 inch), were oriented such that the specimen axis was normal to the weld centerline. Prior to the machining of the reduced gage-section, the specimen blanks were etched to reveal the weld to ensure that the entire reduced section was weld metal. Testing was done in a servohydraulic testing machine at a strain rate of approximately 3 x 10^{-4} s^{-1} to obtain the complete stress-strain curves, in addition to values of yield strength, tensile strength, elongation, and reduction of area.

The Charpy V-notch specimens and the compact specimens were machined such that the crack extended along the centerline of the weld in the direction of the plate width. The compact specimens were fatigue precracked; half of them contained no side grooves and the other half contained side grooves of 10 percent per side. Those without side grooves were to simulate TWC pipe tests in Task 1, while those with side grooves were to simulate surface-cracked pipe tests in Task 2. Charpy tests were conducted in a Tinius Olson pendulum machine having a capacity of 356 Joules (264 ft-lb). Compact specimens were tested in a screw-driven Instron machine under crosshead control; the crosshead speed was selected to produce crack initiation in approximately 5 to 10 minutes. Data obtained included load, load-line displacement, and direct-current electric potential. The electric potential data were used to estimate the onset of crack extension and the amount of crack growth as the test progressed.

The chemical analysis of the weld metal is given in Table 2.1. Included for comparison is the chemical analysis of the base metal (Plate DP2-45). Notice that the weld metal contains more nickel and chromium than does the base metal because the TP308 stainless steel weld wire that was used contains more of those two elements than does TP304 stainless steel plate.

Tensile properties of the weld metal are given in Table 2.2 and engineering stress-strain curves are shown in Figure 2.1. Included for comparison in Table 2.2 and Figure 2.1 are results for the base metal plate material tested in the principal rolling direction.

Energy absorption values in full-size Charpy tests of the weld metal at two different temperatures are shown in Table 2.3. Very little difference in energy absorption was discernible at the two different temperatures.

Results of compact specimen tests are given in Table 2.4, including both the 0 percent and the 20 percent side-grooved specimens. Included for comparison in Table 2.4 are values obtained from the base metal plate material (DP2-A45). Notice in Table 2.4 that the J values at crack initiation for the weld metal are less than 5 percent of the values for the base metal.

Figures 2.2 and 2.3 show J-resistance curves for the 0 percent side grooved specimens and the 20 percent side-grooved specimens, respectively. For comparison, each figure includes a J-R curve for base metal specimens from the plate that contained the weld, tested at 288 C (550 F). Also included in the figures are vertical lines indicating the point at which the crack extension reaches 30 percent of the original uncracked ligament. From previous experimental work on both compact specimens and pipe, that amount of crack extension appears to represent an engineering limit for using J to analyze the data (Ref. 2.3). The J-resistance curves shown in Figures 2.2 and 2.3 indicate that the toughness of the weld metal is significantly lower at 288 C (550 F) than at room temperature. For reference, a typical TP304 base metal J-R curve is shown. That result differs from the result obtained using Charpy V-notch impact specimens (see Table 2.3), where energy absorption values were found to be approximately the same at the two different temperatures. Figures 2.2 and 2.3 show also that the toughness of the base metal at 288 C (550 F) is much greater than that of the weld metal at the same temperature.

Table 2.1 Chemical composition of the submerged-arc weld (DP2-A45W2) in TP304 austenitic stainless steel plate

Included for comparison is the chemical composition of the base metal plate (DP2-A45)

	Percent by Weight of Indicated Element	
Element	**Weld Metal (DP2-A45W2)**	**Base Metal (DP2-A45)**
C	0.03	0.048
Mn	2.26	1.87
P	0.032	0.027
S	0.010	0.005
Si	0.89	0.63
Cu	0.26	0.42
Sn	0.010	0.016
Ni	9.6	8.0
Cr	19.7	18.4
Mo	0.10	0.22
Al	0.015	0.002
V	0.070	0.09
Nb	0.012	0.026
Zr	0.015	0.002
Ti	0.006	0.003
B	0.0008	0.0008
Ca	0.0008	N.D.
Co	0.13	0.12
W	0.0	0.01
Se	0.00	N.D.

Table 2.2 Tensile properties at 288 C (550 F) of submerged-arc weld metal (DP2-A45W2) in a TP304 stainless steel plate

(Properties of the base metal are included for comparison)

Specimen Number	Material	0.2% Offset Yield Strength, MPa	0.2% Offset Yield Strength, ksi	Ultimate Tensile Strength, MPa	Ultimate Tensile Strength, ksi	Elongation, pct in 12.7 mm (0.5 in)	Reduction of Area, pct
A45-1	TP304 Base Metal	169	24.5	475	68.9	47.0	79.0
A45-2	TP304 Base Metal	145	21.1	466	67.6	47.5	78.9
A45W2-3	SAW in TP304 Plate	374	54.3	510	74.0	15.5	63.0
A45W2-4	SAW in TP304 Plate	357	51.8	495	71.8	13.7	54.0

Table 2.3 Charpy V-notch impact tests on submerged-arc weld (DP2-A45W2) in TP304 stainless steel plate (Full-size specimens)

Test Temperature, C (F)	Energy Absorbed, J (ft-lb)
22 (72)	56 (41)
22 (72)	62 (46)
288 (550)	64 (47)
288 (550)	67 (49.5)

Table 2.4 J_i and dJ/da values obtained from compact specimens machined from a submerged-arc weld (DP2-A45W2) in TP304 stainless steel plate

[Included for comparison are results for the TP304 base metal plate (DP2-A45) tested at 288 C (550 F)]

Specimen Number	Material	Test Temp., C (F)	Side Grooves, pct	J_i kJ/m^2	J_i in-lb/in^2	dJ/da MJ/m^3	dJ/da in-lb/in^3
A45W2-1	Weld metal	20 (68)	20	114	(649)	334	(48,400)
A45W2-2	Weld metal	288 (550)	20	58	(332)	169	(24,500)
A45W2-3	Weld metal	288 (550)	20	61	(350)	152	(22,000)
A45W2-4	Weld metal	20 (68)	0	106	(605)	289	(41,900)
A45W2-5	Weld metal	288 (550)	0	38	(215)	111	(16,100)
A45W2-6	Weld metal	288 (550)	0	57	(326)	183	(26,600)
A45-37	Base metal	288 (550)	0	2,190	(12,500)	395	(57,300)
A45-38	Base metal	288 (550)	20	1,370	(7,830)	556	(80,700)

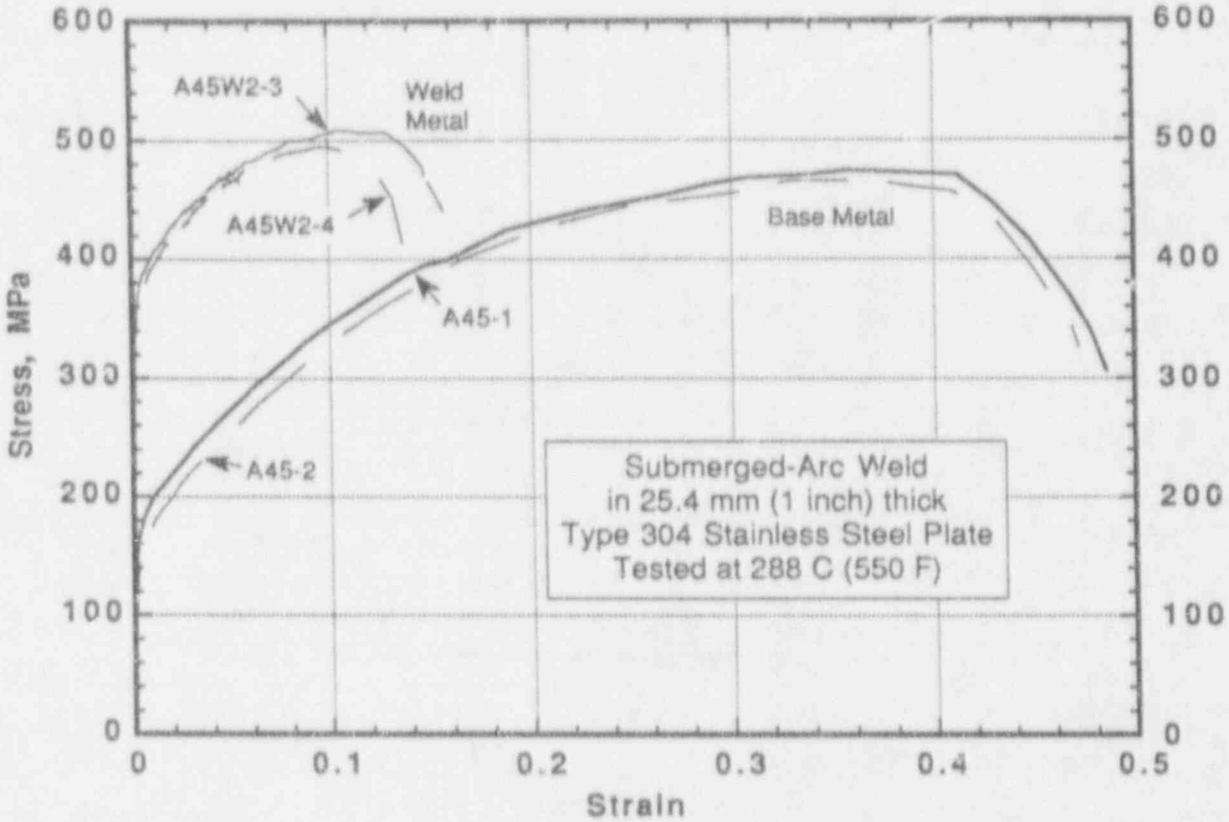

Figure 2.1 Engineering stress-strain curves for submerged-arc weld (DP2-A45W2) tested at 288C (550F)

SC-M-6/91-F1

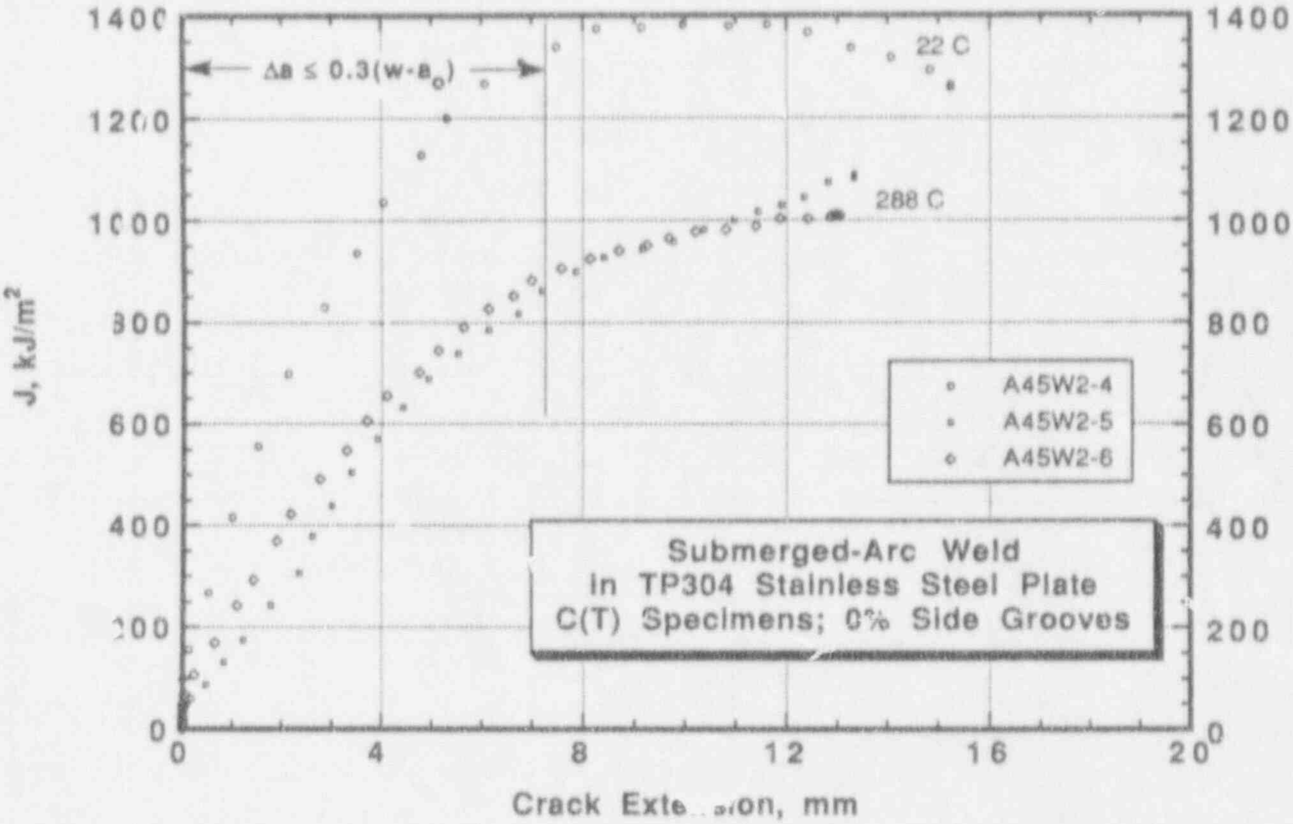

Figure 2.2 J-resistance curves for non-side-grooved C(T) specimens machined from submerged-arc weld (DP2-A45W2) and a typical TP304 stainless steel base metal

SC-M-6/91-F2

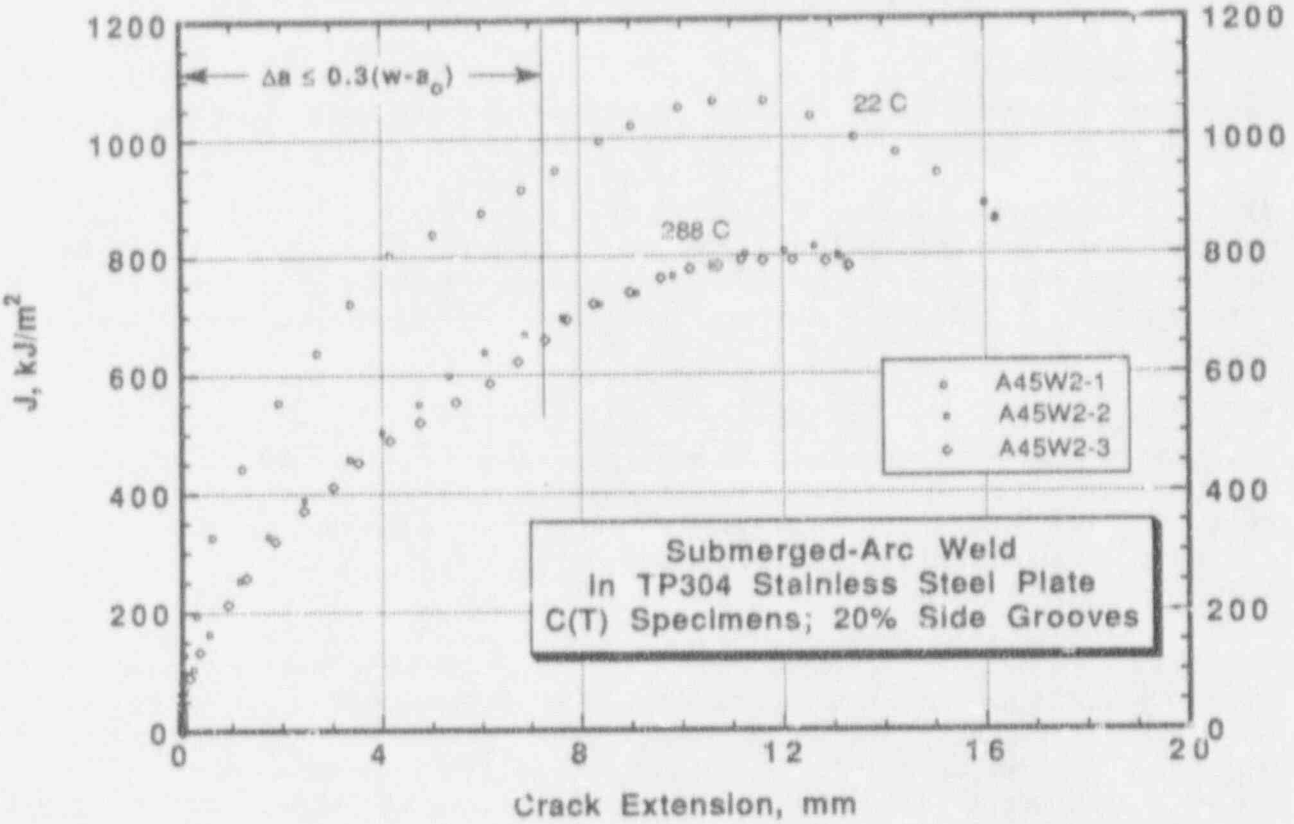

Figure 2.3 J-resistance curves for C(T) specimens having 20% side grooves machined from submerged-arc weld (DP2-A45W2)

SC-M-6/91-F3

Characterization of French TP316LN Pipe

This pipe was furnished to Battelle by Commissariat a l'Energie Atomique (CEA) where a section of the same pipe had been subjected to a room temperature pipe fracture experiment. The pipe originally was in the possession of Électricité de France (EDF) and carried the designation Z3 CND 18-12 (316L) stainless steel. It came from EDF Tube Experiment No. 24. Its diameter is approximately 114 mm (4.5 inches) and its wall thickness is approximately 12.7 mm (0.5 inch). The Battelle identification number is IP-A2.

The pipe was subjected to tensile tests, J-R curve tests, and a dynamic test to determine modulus of elasticity, all at room temperature. In addition, samples of the pipe were subjected to chemical analysis tests and to metallographic examination.

The room temperature tensile tests were conducted in duplicate on round-bar, threaded-end specimens machined from the midwall region of the pipe; the tensile axis was parallel with the pipe axis. Each specimen had a 6.35-mm- (0.25-inch) diameter by 31.8-mm- (1.25-inch) long reduced section. Tests were conducted in a servohydraulic testing machine at an average strain rate of 10^{-3} to 10^{-4} s^{-1}.

To verify the reportedly low values of elastic modulus for this pipe, a dynamic modulus determination was conducted at room temperature in a Magnaflux Type FM-500 Elastomat. The specimen was a cylinder having a diameter and length of 12.7 and 107 mm (0.5 and 4.2 inches), respectively. Its axis was parallel with the pipe axis. The Elastomat was used to determine the frequency of longitudinal vibrations in the bar, from which the modulus of elasticity could be calculated.

To determine the pipe's fracture resistance, three 0.5T-planform-size compact type specimens, 10.2 mm (0.4 inch) thick, were machined such that crack growth would be in the circumferential direction (L-C orientation). The specimens were not side-grooved. They were tested at room temperature in a screw-driven Instron machine at a crosshead speed of 1.25 mm/min. (0.05 in. min.). Quantities recorded during each test included load, load-line displacement, and direct-current electrical potential. The latter was obtained to indicate the point of crack initiation and the amount of crack extension. The procedures used to calculate J values were those specified in ASTM E1152-87, Standard Test Method for Determining J-R Curves.

The chemical analysis of Pipe IP-A2 is shown in Table 2.5. Included in the analysis is nitrogen because metallographic evidence suggested the presence of nitrogen in the steel. The nitrogen content of 0.164 percent by weight, shown in Table 2.5, indicates that nitrogen was added deliberately and that the steel meets the composition specifications for TP316LN in ASTM A376, Seamless Austenitic Steel Pipe for High Temperature Central-Station Service.

Tensile properties of Pipe IP-A2 at room temperature are shown in Table 2.6. Engineering stress-strain curves are presented in Figure 2.4. The dynamic modulus of elasticity test produced a value of 157.5 GPa (22.84 x 10^6 psi). That value is significantly lower than the handbook value of 193 GPa (28 x 10^6 psi). The most likely explanation for the low modulus value is preferred

Table 2.5 Chemical composition of French TP316LN stainless steel pipe (Pipe IP-A2)

	Percent by Weight	
Element	Pipe IP-A2	ASTM A376 Requirement for TP316LN
C	0.02	0.035 max
Mn	1.68	2.00 max
P	0.024	0.040 max
S	0.009	0.030 max
Si	0.48	0.75 max
Cu	0.13	(a)
Sn	0.008	(a)
Ni	12.9	11.0-14.0
Cr	17.0	16.0-18.0
Mo	2.5	2.00-3.00
Al	0.015	(a)
V	0.059	(a)
Nb	0.008	(a)
Zr	0.000	(a)
Ti	0.014	(a)
B	0.0012	(a)
Ca	0.0009	(a)
Co	0.076	(a)
W	0.0	(a)
Se	0.00	(a)
N	0.164[b]	0.10-0.16

(a) Not specified.
(b) Determined by Kjeldahl analysis.

orientation, or texture, of the individual crystalline grains making up the pipe. Rather than being randomly oriented, each grain is hypothesized to be crystallographically oriented similar to neighboring grains. This condition can give rise to significant directionality in elastic modulus values. X-ray diffraction studies would be required to confirm that a preferred orientation condition is present. A consequence of preferred orientation in this particular pipe is that the unusually low modulus value in the axial direction is almost certainly accompanied by an unusually high modulus value in another direction, probably the circumferential direction. If that is the case, hoop strains arising from internal pressure would be lower than values calculated on the basis of typical elastic modulus values.

J-resistance curves from room temperature tests on compact specimens are shown in Figure 2.5. Included in the figure is a line which indicates the point at which the crack extension reaches 30 percent of the original uncracked ligament. Values of J_i and dJ/da from the compact specimen tests are summarized in Table 2.7. The values of dJ/da were for crack extension values in the range of approximately 0.15 to 1.5 mm (0.006 to 0.060 inch).

Table 2.6 Tensile properties of French TP316LN steel pipe (Pipe IP-A2) in the longitudinal direction at room temperature[(a)]

Spec. Ident. No.	Strain Rate, s^{-1}	0.2 Pct Offset Yield Str.		Ult. Tensile Str.		Elongation, pct. in 25.4 mm (1 inch)	Area Reduction pct.
		MPa	ksi	MPa	ksi		
IP-A2-1	$1.6x10^{-3}$	250	36.2	536	77.7	55	~84[(b)]
IP-A2-2	$3.1x10^{-4}$	258	37.4	527	76.5	58	~83[(b)]
	Avg.	254	36.8	531.5	77.1	56.5	~83.5

(a) The modulus of elasticity in the direction of the pipe axis was found to be 157.5 GPa (22.84 x 10^6 psi) on the basis of a resonant frequency experiment.

(b) The final cross section was elliptical; the ratio of the ellipse minor axis to the ellipse major axis was approximately 0.58. The average of the two values was used in the calculation of the reduction of area.

Table 2.7 Summary of J_i and dJ/da values for French TP316LN stainless steel pipe (Pipe IP-A2) obtained from compact specimens tested at room temperature

L-C orientation; no side grooves

Spec. Ident. No.	J at Initiation		dJ/da	
	kJ/m^2	$in\text{-}lb/in^2$	MJ/m^3	$in\text{-}lb/in^3$
IP-A2-1	1050	6000	90.3	131,000
IP-A2-2	910	5195	70.3	102,000
IP-A2-3	680	3865	75.8	110,000
Avg.	880	5020	78.8	114,300

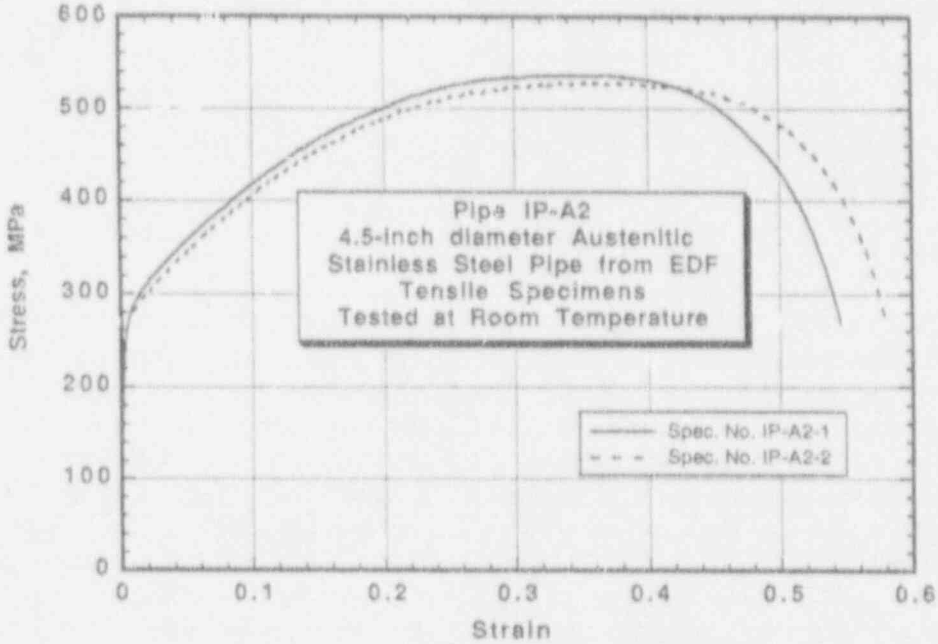

Figure 2.4 Engineering stress-strain curves for tensile specimens machined from French TP316LN stainless steel pipe (Pipe IP-A2)

DRB/1.1.1.26/FA-2

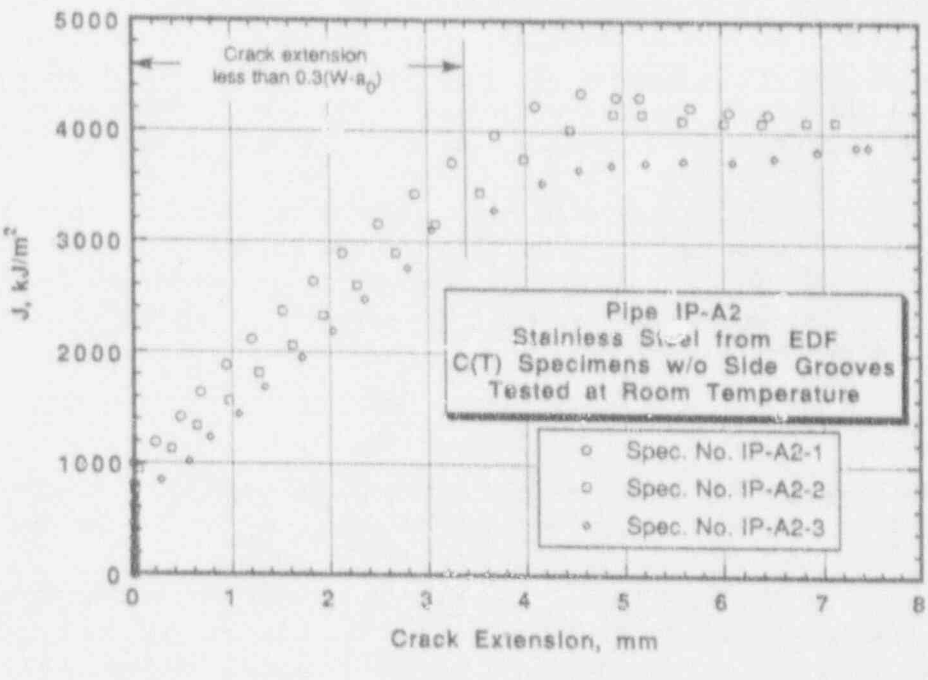

Figure 2.5 J-resistance curves for compact specimens machined from French TP316LN stainless steel pipe (Pipe IP-A2) in the L-C orientation

DRB/1.1.1.26/FA-6

2.3.2 Subtask 1.3 Large Diameter Pipe Fracture Experiments

2.3.2.1 Objective

The objective of this activity is to develop data for the verification of fracture analyses used in LBB evaluations of large diameter pipe.

2.3.2.2 Rationale

Past work in the Degraded Piping Program (Ref. 2.2) on long circumferential through-wall cracks showed different results for thinner versus thicker large diameter pipe. A thin steam-line pipe had failure stresses well below those predicted by net-section-collapse (NSC) but agreed well with the prediction of J-estimation scheme. On the other hand, a thicker cold-leg pipe reached the NSC stress, which is much higher than that predicted by the J-estimation scheme predictions. In the thicker cold-leg pipe, however, the circumferential crack grew in the axial direction even though it was unpressurized. This was an unexpected failure mode, and is believed to be due to the toughness anisotropy of that pipe. Additional large diameter pipe experiments with shorter through-wall crack lengths and sufficiently low enough toughness are needed to assess the elastic-plastic fracture analyses.

2.3.2.3 Approach

Four through-wall-cracked pipe experiments and one uncracked-pipe experiment on large diameter pipe will be conducted as part of the initial program. These are on 24-, 28-, and 36-inch-diameter pipe with different R/t ratios. Battelle's large pipe bending frame will be used in these experiments. The pipe bend test system will be upgraded for the 36-inch-diameter, cold-leg experiments in this subtask and the bi-metal weld subtask. The upgrading of the large-pipe test frame (strong-back) system was described in the last Semiannual Report (November 1990).

An additional 4-inch-diameter pipe experiment was added to the initial test matrix. This was done with the objective of comparing a French (EDF) pipe test system and the Battelle pipe test facilities. The piece of French pipe received was from the moment arm of their Experiment No. 24. We reproduced their test with the same size crack and machined the pipe to close to the same thickness and diameter as they did in their experiment.

General Test Procedures

As with the prior Degraded Piping Program pipe fracture experiments, the large diameter pipe experiments are being conducted with a sharp machine notch, except for the test involving the carbon steel weld and the new French pipe experiment. The carbon steel weld is sufficiently low in toughness that it is susceptible to notch acuity effects. High toughness steels are not sensitive to notch acuity effects, as seen in the data on fatigue and sharp machine notches in the Degraded Piping Program (Ref. 2.2). The through-wall crack in the 4-inch-diameter pipe section was fatigue precracked to duplicate the French test procedures.

The data to be recorded in these experiments include:

- applied load,
- load-line displacement,
- rotation due to the crack,
- crack-opening displacement at the crack center line, initial crack tips, and one location betweer n initial crack tip and the center of the crack
- ovalization of the pipe in the horizontal and vertical directions at the crack plane,
- d-c electric potential at the crack centerline and each crack tip, and
- temperature at various locations along the pipe.

2.3.2.4 Progress

The first pipe fracture test on the 28-inch-diameter A516 Grade 70 steam line pipe has been completed and was reported on in the first program report for this project (Ref. 2.4).

Experiment 1.1.1.26 - 4-inch Diameter French TP316 Pipe

The specific objective of this experiment was to conduct a comparison of a French pipe test system with one of the Battelle pipe test systems. The French experiment was conducted at the Électricité de France (EDF) facilities. In the IPIRG program it was found that there was excellent agreement with finite element predictions of this experiment (Ref. 2.5). However, for another stainless steel TWC experiment conducted during the IPIRG program, the finite element results underpredicted the experimental loads by 30 percent. For both of these experiments, several finite element analyses were conducted by different organizations. The finite element results are in very good agreement with each other, but not necessarily with the experimental results (Ref. 2.6). Furthermore, for other past finite element analyses, it has been observed that for a few stainless steel TWC experiments there was good agreement between other experimental and finite element results. However, in most of the cases there was not good agreement (Ref. 2.6). Hence this experiment was a verification test between the Battelle and EDF systems to see if experimental differences could be the cause of the disagreement with the finite element results.

EDF Test Results

EDF conducted a series of stainless steel TWC pipe experiments on 4-inch nominal diameter stainless steel pipe. Two of these of specific interest were EDF Experiment Numbers 5 and 24. EDF Experiment Number 5 was analyzed by FEM (Ref. 2.6). This pipe had a through-wall circumferential crack with a length of 1/3 of the pipe circumference. However, no extra material from that pipe remained for a comparison test.

EDF Experiment Number 24 was another EDF experiment. In this case there was remaining material for a comparison experiment. The remaining material was from the moment arms of the specimen (see Figure 2.6). The pipe used in EDF Experiment 24 was from a different heat than the pipe used in EDF Experiment 5.

EDF Experiment 24 had a TWC with a length of 25 percent of the circumference. As noted in Figure 2.6, the center span had a reduced thickness, where the pipe was machined on the outside diameter. The pipe dimensions are given in Table 2.8. The crack was fatigue precracked. Moment-rotation data are shown in Figure 2.7.

Experiment 1.1.1.26 Results

This experiment was intended to duplicate EDF Experiment 24. The specimen was machined to the dimensions shown in Table 2.8 and as indicated in Figure 2.8. Since the inside surface was very rough, a small amount of inside machining was done. This allowed for the thickness of the pipe to be the same as the EDF specimen, but the diameter differed slightly. It is believed that EDF only machined the outside of the pipe.

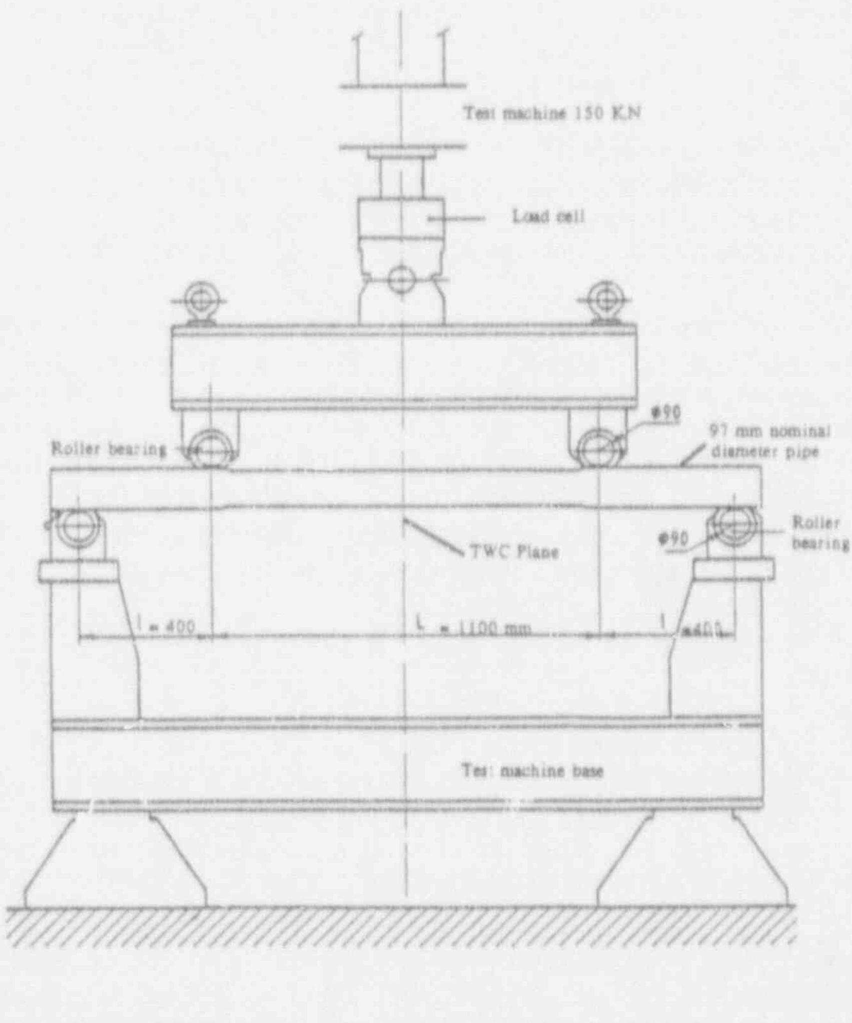

Figure 2.6 Schematic of experimental setup for EDF-24

SC-SA-7/9.-F2.6

Table 2.8 Critical parameters from EDF and 1.1.1.26 experiments

Expt. No.	Outer Diameter, mm	Thickness, mm	$2c/\pi D$	Max. Moment, kN-m	Max. NSC[a]
EDF #24	105.00	8.260	0.25	15.52	0.895
1.1.1.26	106.17	8.255	0.24	17.05	0.931
			Difference		3.6%

(a) NSC = net-section-collapse predicted load using σ_f = 393 MPa for both experiments.
[$\sigma_f = (\sigma_y + \sigma_u)/2$ using Battelle tensile test data.]

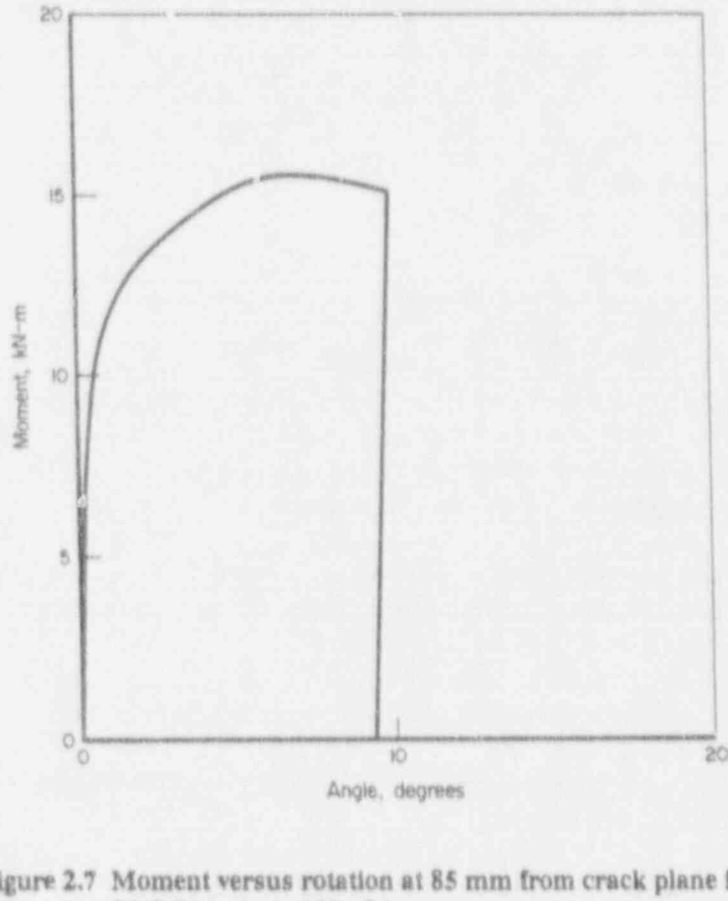

Figure 2.7 Moment versus rotation at 85 mm from crack plane for EDF Experiment No. 24

SC-SA-7/91-F2.7

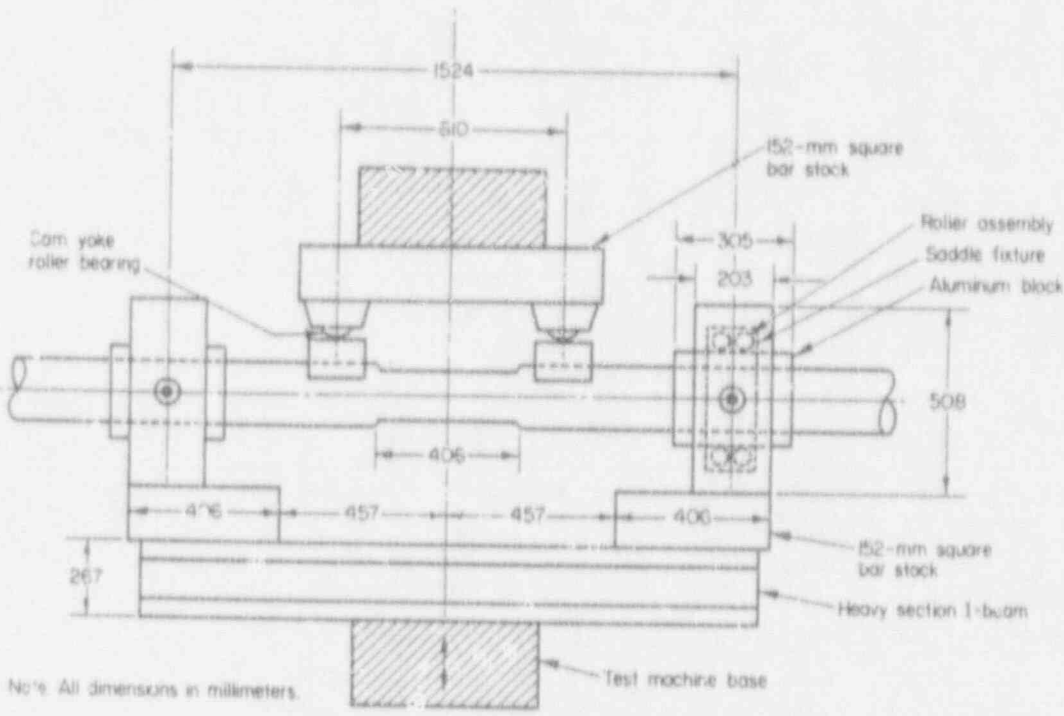

Figure 2.8 Schematic of Experiment 1.1.1.26

DRB/1.1.1.26/F1

As with the EDF pipe, this specimen was fatigue precracked. The specimen was instrumented to measure load, load-line displacement, rotation, crack opening at the tips and the center of the crack, and d-c electric potential measurements to determine crack initiation and crack growth. Both experiments were conducted at room temperature.

After chemical analyses, it was found that the material was a TP316LN stainless steel. The material properties from the pipe sent to Battelle are given in Tables 2.5 to 2.7. This pipe was given a Battelle pipe number of IP-A2.

The experimental load versus load-line displacement record from Experiment 1.1.1.26 is shown in Figure 2.9. The two major unloadings were done to mark the crack, while the other smaller unloadings were done to measure the ovalization of the pipe during the test. No unstable crack jumps occurred during the experiment.

The maximum moment was calculated using a kinematic correction for the rollers used at the outside load points. The maximum moment is given in Table 2.8. Because of slight differences between the EDF specimen and this experiment, due to actual pipe dimensions from the

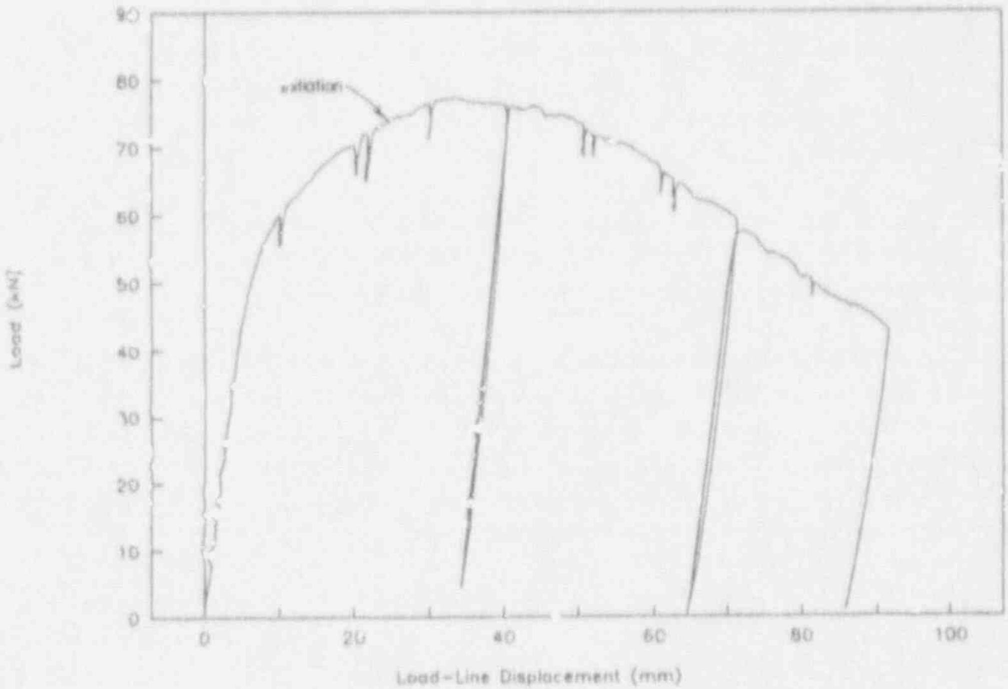

Figure 2.9 Total load versus load-time displacement from Experiment 1.1.1.26

DRB/1.1.1.26/F7

machining and flaw length, the maximum moments were normalized by the predicted NSC moments. A comparison of the maximum moments normalized by the NSC moments shows that there was 3.6 percent difference in the two experiments. This is within the typical ±5 percent difference observed in multiple experiments at Battelle on the same test frame or experiments conducted on different test systems at Battelle.

Consequently, the Battelle and EDF systems compare well. This means that the discrepancies between the FEA and many stainless steel TWC pipe experiments are not due to pipe test experimental differences. Hence, the differences must be in the computer modelling, i.e., mesh refinement, constitutive law representation of the materials being analyzed, etc.

Experiment 1.1.1.23 - 28-inch-Diameter TP304 SAW

The objective of this experiment was to develop data to be used in assessing the load-carrying capacity of an LBB size through-wall crack. This size of pipe was used in a similar test in the Degraded Piping Program, Experiment 4111-5. The pipe was a BWR recirculation line pipe. Experiment 4111-5 involved a 28-inch-diameter TP316 stainless steel pipe with a SMAW that was a section of pipe removed from the recirculation system at the Nine Mile Point Plant. The pipe section was decontaminated before testing. That experiment had a 37-percent long circumferential through-wall crack in the center of the weld. The weld crown was left on. Details of that experiment are in Reference 2.7.

No additional pipe from that plant exists, so a new weld had to be manufactured. The pipe used was 28-inch-diameter pipe that was purchased from excess inventory of replacement pipe from the Nine Mile Point Plant.

Experiment 1.1.1.23 - Results

A schematic of this test specimen in the test machine is shown in Figure 2.10. The specimen was not fatigue precracked since past data on the effect of a sharp machine notch (radius 0.127 mm) and a fatigue precrack in C(T) specimens showed no differences.

The welding procedures for this experiment are given in Appendix A. This was a SAW weld, whereas the past Experiment 4111-5 had a field SMAW. Both welds, however, have generally the same toughness (Ref. 2.7). The material properties of the pipe and weld from Experiment 1.1.1.23 are given in Table 2.9. The pipe (A51) used in Experiment 1.1.1.23 has not had its tensile properties determined yet, but typical values from Nine Mile Point Plant piping removed from service (Pipe A50) are given as approximate values.

In this experiment it was decided to grind the weld crown off. This was done since about 10 percent of the welds in service have the outside weld crowns removed for ease of NDT inspection. The removal of the weld crown may also have some effect on the loads at crack initiation. It was also of interest to see if the crack would stay in the weld.

In the process of sharpening the crack tips with a jeweler's saw, it was observed that at Crack Tip A many of the very thin jeweler's saw blades were worn away during the cutting operation. This was an indicator that the weld may have been harder at Tip A than Tip B.

Figure 2.11 shows the load versus load-line displacement from the experiment. The loads at crack initiation and maximum load are given in Table 2.10.

Post-test photographs of the two crack tips show that the crack grew down the center of the weld from Crack Tip B, but immediately turned into the base metal at Crack Tip A (see Figure 2.12). It can also be seen that the amount of crack growth from Tip A was substantially greater than from Tip B, due, at least partially, to the fact that the crack growth from Tip A is essentially in the tougher base metal. Further metallographic work is to be done to assess why the crack turned out of the weld and determine whether Tip A was harder, as suspected by the technician who sharpened the notch tips.

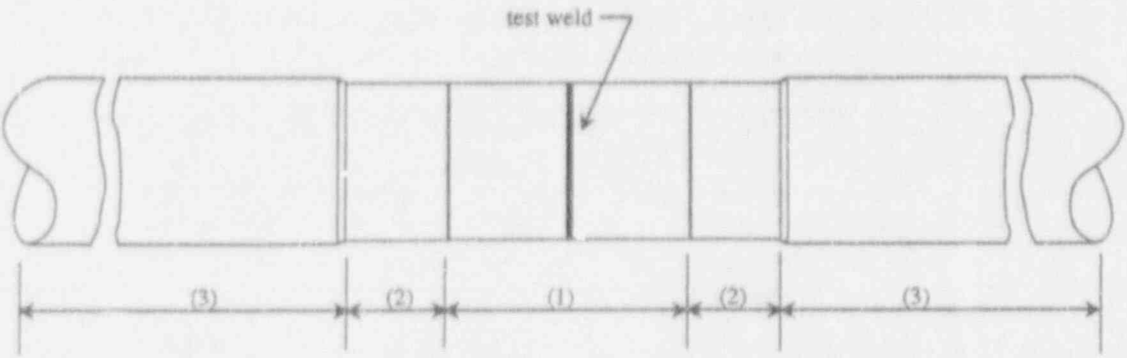

	ID	OD (mm)	t (mm)	Length (m)
(1)	DP2-A51	711.2	30.2	1.32
(2)	DP2-F90	711.2	31.8	0.51
(3)	IP-F5	762.0	38.1	6.35

(a) Details of test specimen

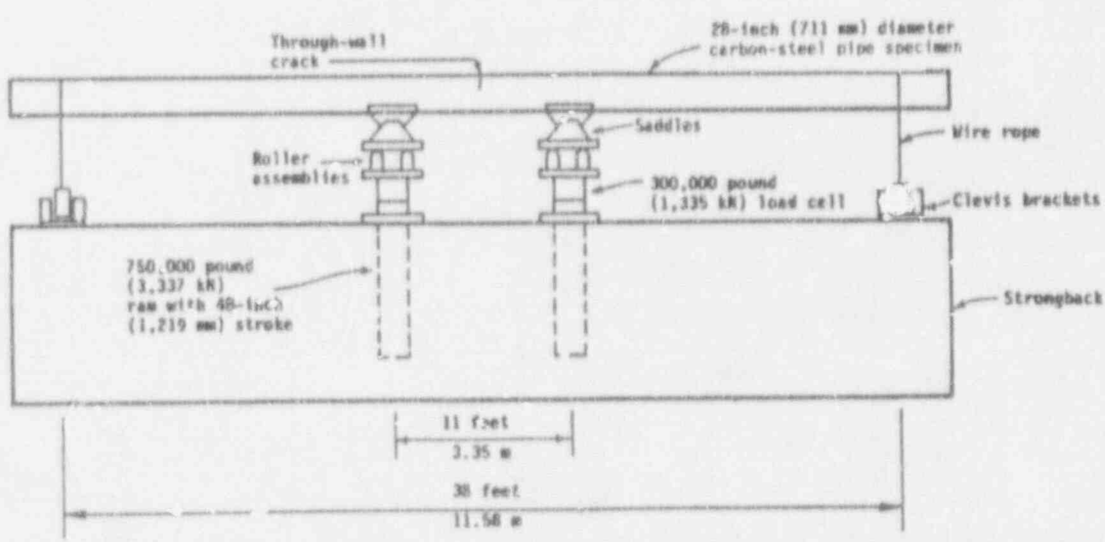

(b) Schematic of test apparatus

Figure 2.10 Schematic and Dimensions of Experiment 1.1.1.23

DRB/1.1.1.23/F1&2

Table 2.9 Material properties of 28-inch-diameter stainless steel weld at 288 C

	Weld Metal (A45W2)	Base Metal[a] (A50)
Yield Strength,[b] MPa (ksi)	366 (53.1)	228.9 (33.2)
Ultimate Strength,[b] MPa (ksi)	503 (72.9)	501.3 (72.7)
Reduction of Area,[b,c] percent	58.5	67.3
J_p,[d] MJ/m^2 ($in\text{-}lb/in^2$)	47.5 (270)	N.D.
dJ/da,[d,e] MJ/m^3 ($in\text{-}lb/in^3$)	147 (21,350)	N.D.

(a) To be determined for Pipe A51. Approximate values from another pipe (A50) given for reference. N.D. = not determined.
(b) Average of two specimens for weld data. One specimen for Pipe A50.
(c) 6.35-mm-diameter round-bar specimen.
(d) No side grooves, average of two specimens.
(e) Calculated within the ASTM exclusion lines.

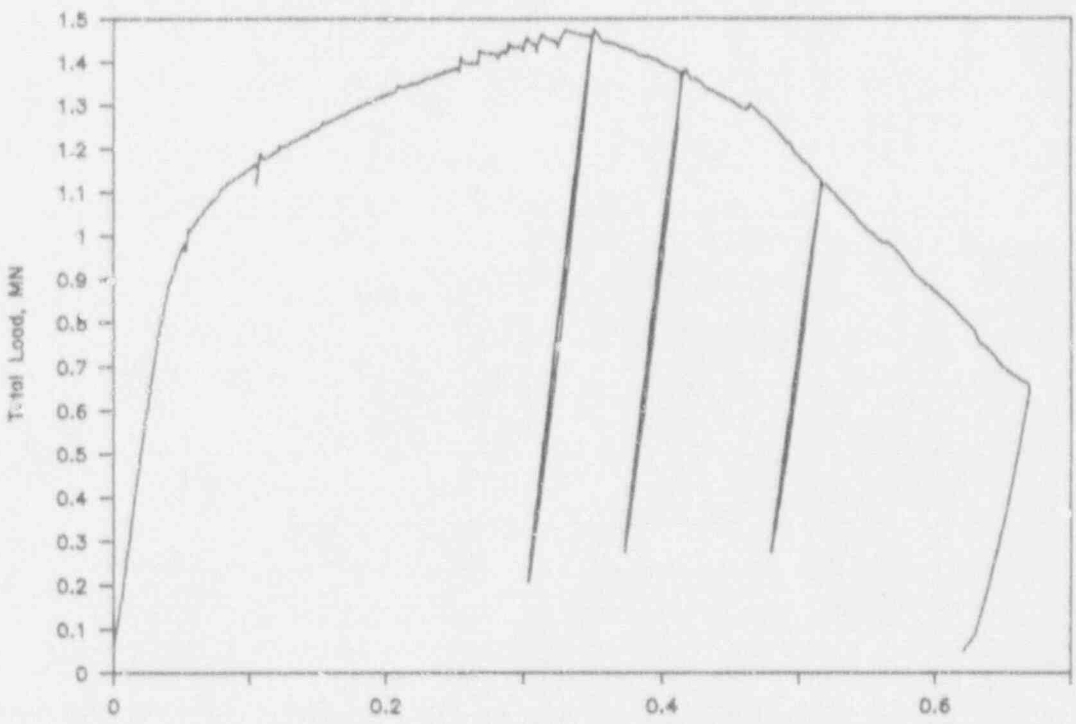

Figure 2.11 Total load versus load-line displacement data from Experiment 1.1.1.23 (Stainless steel SAW with short crack)

DRB/1.1.1.23/F7

Table 2.10 Critical parameters from Experiments 4111-5 and 1.1.1.23

Exp. No.	Outer Diameter, mm	Thickness, mm	2c/πD	Maximum Moment, MN-m
4111-5	719.6	30.2	0.370	1.258
1.1.1.23	711.2	30.2	0.063	2.987

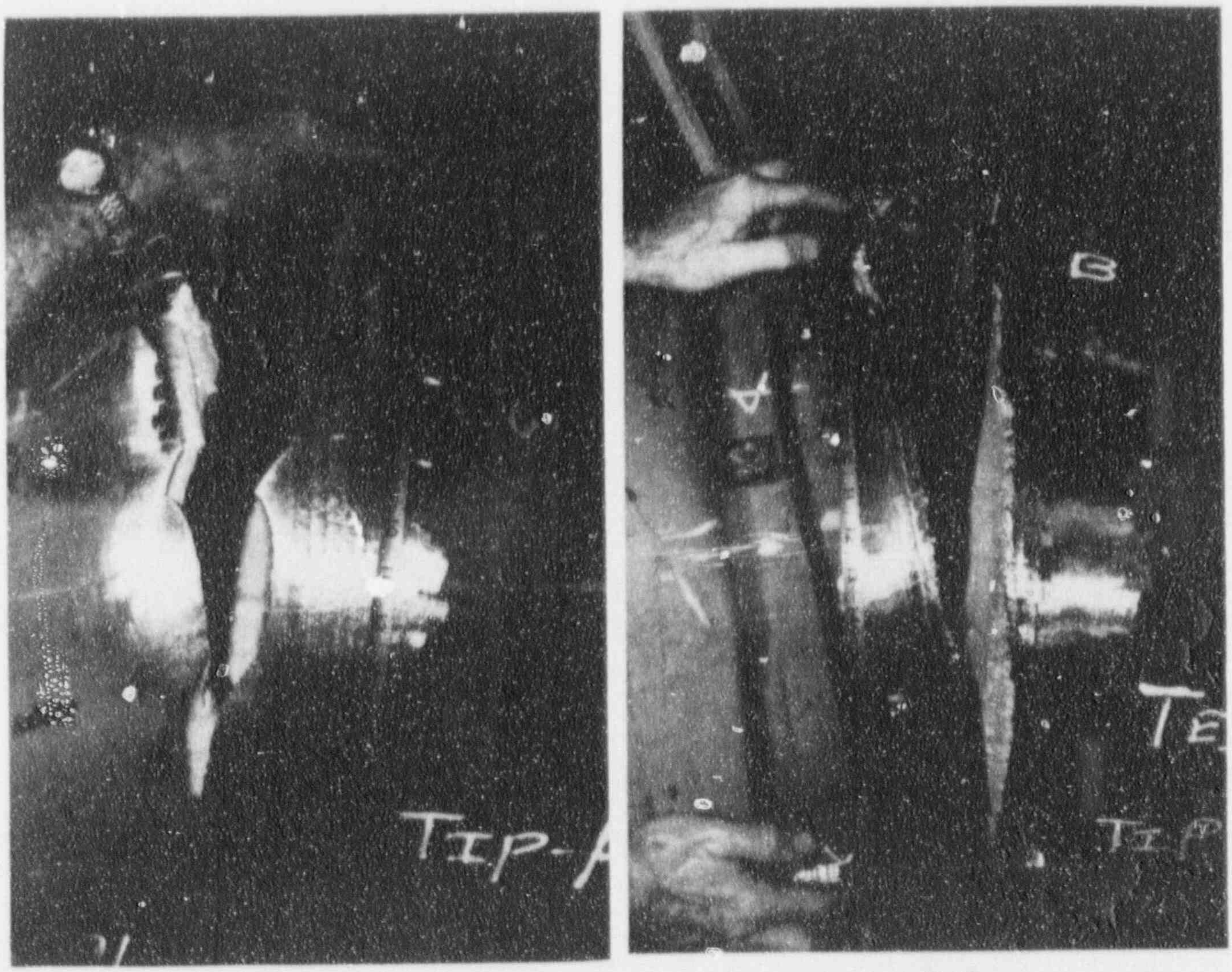

Tip A Tip B

Figure 2.12 Photographs of crack growth from stainless steel SAW Experiment 1.1.1.23

DRB/1.1.1.23/F14

2.3.3 Subtask 1.4 Analyses for Short Through-Wall Cracks in Pipes

2.3.3.1 Objective

The objective of this subtask is to develop, improve, and verify the engineering analyses for short circumferential through-wall cracked pipe.

2.3.3.2 Rationale

The short through-wall-cracked pipe analysis improvements are aimed at LBB fracture evaluations for larger diameter pipe.

2.3.3.3 Approach

The three activities in this subtask are:

Activity 1.4.1	Improve short through-wall cracked analysis and compare predictions to existing data
Activity 1.4.2	Analyze large diameter pipe TWC test results
Activity 1.4.3	Analyze through-wall cracks in welds.

Theoretical Background for Elastic-Plastic Fracture Models

All the elastic-plastic fracture mechanics (EPFM) simplified methods for crack stability assessment are based on the deformation plasticity theory, which assumes that all loadings are proportional and monotonically increasing (basic hypothesis, H_1). This makes the plastic computations simpler, allowing for separate treatments of elasticity and plasticity. The fracture criterion used in simplified J-estimation methods requires that the crack will not initiate as long as the computed J is less than a critical value J_{Ic}. Furthermore, the crack will not propagate in an unstable manner unless the driving force J is growing faster than the critical material parameter J_R, which increases with crack growth. These two conditions are summarized in the following equation.

$$J(Q,a) \leq J_R(\Delta a) \tag{2-1}$$

where $J_R(0) = J_{Ic}$, Q is a load parameter, and a is crack length. In these methods only Mode I crack growth is considered.

J Definitions

All J-estimation schemes refer to the same definition of J, which is expressed as the rate of decrease of potential energy with respect to crack area.

$$J = -\frac{d\Pi}{dA} \tag{2-2}$$

where

$$\Pi = \int_v w(\epsilon)\, dv - \int_s Q \cdot q\, ds, \tag{2-3}$$

i.e., Π = strain e... v - work of external forces.

A is the crack area, q are the generalized displacements due to the generalized load $Q^{(a)}$, and

$$w(\epsilon) = \int_o^{\epsilon} \sigma_{ij}\, d\epsilon_{ij}. \tag{2-4}$$

Rice (Ref. 2.8) proved that J could be evaluated by a path-independent integral encompassing the crack tip, thus showing the relationship between crack tip stress strain fields and the loading parameter Q. These conclusions were further extended in References 2.9 through 2.11.

As long as history effects may be neglected, this link between local parameters associated to the crack tip damaged zone and global parameters defining the loading permits one to describe the fracture process through a global approach.

This definition holds only for nonlinear elasticity in forms for which the potential energy is defined, and for non-growing cracks. A second basic hypothesis (H_2) is then formulated, which extends the previous definition of J assuming the product (J·A) is given by the difference between the two potential energies of the cracked body before and after the small crack extension ΔA. Thus, under fixed displacement loading:

$$J = -\left[\frac{\partial}{\partial A}\int_o^q Q\, dq\right]_q \tag{2-5}$$

or

$$J = \int_o^q \frac{\partial Q}{\partial A}\bigg|_q dq \tag{2-6}$$

(a) For through-wall cracked pipes of concern here, Q is the moment (M) and q is the rotation (ϕ) for bending; Q is the total axial tension load (T) and q is the axial displacement (Δ) for tension loading.

Under fixed load, we have

$$J = \int_0^Q \frac{\partial q}{\partial A}\bigg|_Q dQ \tag{2-7}$$

The difference between the forms in Equations 2-2 and 2-6 for a given configuration is of the second order of magnitude. The GE/EPRI estimation scheme uses the forms in Equations 2-2 and 2-3, where $\partial\Pi/\partial A$ is computed by virtual crack extension technique. All the other J-estimation schemes use the formula in Equation 2-6 (Refs. 2.12 and 2.13).

Elastic-Plastic Problem Partition

Even in the case of monotonically increasing radial loads, the elastic-plastic behavior is not so easy to analyze because of the presence of elastic regions in the loaded body. This makes stress and strain nonproportional to any load parameter.

For a given cracked body subjected to a monotonically increasing radial load Q, one may consider two extremes in materials behavior. In linear elasticity, the uniaxial tensile stress-strain relation is $\sigma = E \cdot \epsilon$ and J is proportional to Q^2. In full plasticity, or completely incompressible nonlinear elasticity, Shih and Hutchinson (Refs. 2.14 and 2.15) established that J is proportional to Q^{n+1}.

This scaling law based on Ilyushin theorem (Ref. 2.16) is only realized in nonlinear elasticity assuming a fixed value of Poisson's ratio or considering only the plastic deformation.

In the elastic-plastic case, <u>if the displacements are small</u> (basic hypothesis H_3), the strains may always be separated into elastic and plastic components:

$$\varepsilon_{ij} = \varepsilon_{ij}^e + \varepsilon_{ij}^p \ . \tag{2-8}$$

The displacement field, for a <u>body free of any initial strain</u> (basic hypothesis H_4) can be defined as:

$$u_i^p = u_i - u_i^e \tag{2-9}$$

The superposition of the two extreme (elastic and fully plastic) solutions will give the elastic-plastic response only if it can be proven that ϵ^p_{ij} derives from the displacement field u^p_i.

This compatibility condition is satisfied exactly for certain geometries and loading configurations. However, this condition may not be valid in general under the above four basic hypotheses. Thus the statement,

$$J = J_e + J_p \tag{2-10}$$

has to be considered as an approximation.

Numerical computations in antiplane shear (Ref. 2.15) and p: e strain (Ref. 2.17) have shown a good agreement between the complete solution and the superposition formula (Eq. 2-10).

J-Computation and Plastic-Zone Size Correction

In J-estimation schemes for through-wall pipes, J is computed on the midsurface. The through-wall variations of J along the crack front is then neglected even for R/t ratios less than 10. For such shells under pure bending, J_e is somewhat higher on the outer diameter. The difference for J_p is smaller.

J_e and J_p may be computed using the following formulas written here for the pure bending case see Figure 2.13):

$$J_e = -\int_0^{\phi^e} \frac{\partial M}{\partial A}\bigg|_{\phi} d\phi^e \tag{2-11}$$

$$J_p = -\int_0^{\phi^p} \left(\frac{\partial M}{\partial A}\right)\bigg|_{\phi} d\phi^p \tag{2-12}$$

In Equations 2-12 and 2-1? the generalized load Q becomes the bending moment, M, and the generalized displacement q becomes the pipe rotation, ϕ.

In linear elasticity we have also,

$$J_e = \frac{K^2}{E'} \tag{2-13}$$

where

E'	=	the elastic modulus, E, for plane stress state,
E'	=	$E/(1-\nu^2)$ for plane strain state, and
K	=	Stress Intensity Factor, which may be obtained from a singular stress field characterization[a].

(a) For through-wall cracked pipe we assume that plane stress state prevails whatever the pipe thickness.

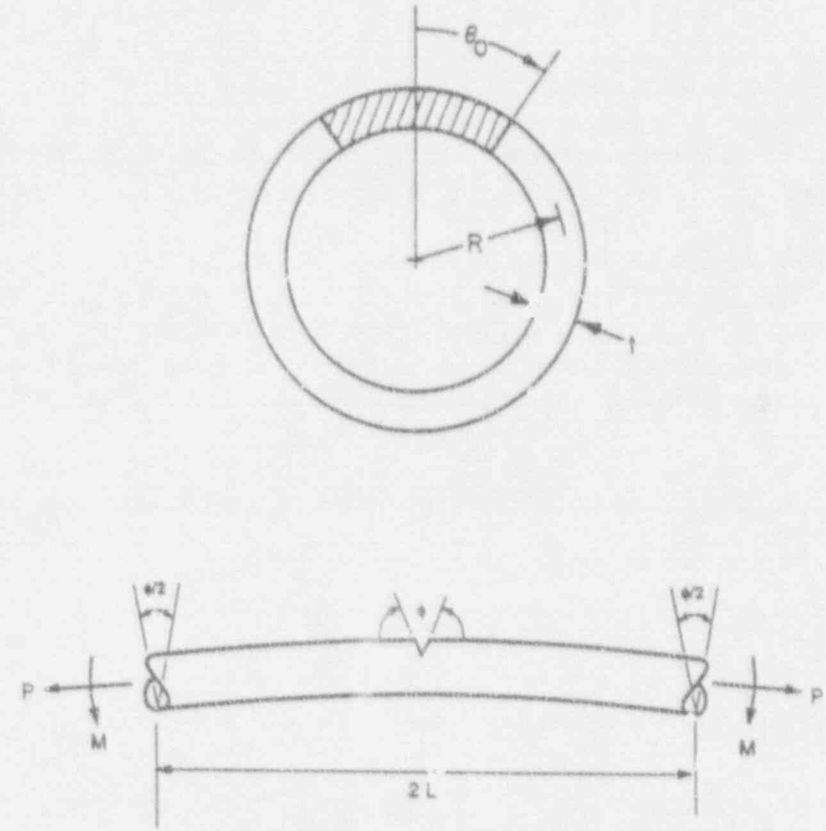

Figure 2.13 Circumferentially cracked pipe loaded in four-point bending

SC-SA-7/91-F2.13

For circumferentially through-wall-cracked pipe, recently several thin-shell solutions for J_e have been derived assuming elasticity prevails. References 2.18 and 2.19 discuss some of these solutions. All J-estimation methods have used such analytical solutions except the GE/EPRI method, which interpolates between precomputed finite element solutions.

Computing J_p is more difficult and requires the knowledge of the nonlinear behavior of the cracked body. Again, the GE/EPRI method is based on finite element fully plastic solutions. In other methods, J_p is obtained through a moment-rotation curve estimation, still assuming full plasticity.

J is given by the sum of J_e and J_p, but in small-scale yielding conditions, the fully plastic component J_p is much smaller than J_e, and ($J_e + J_p$) may be smaller than the plastic-zone corrected LEFM solutions. In order to compensate for this underestimation, Shih et al. (Refs. 2.14 and 2.15) applied an Irwin-type plastic zone size correction to J_e. This adjustment has no theoretical foundation beyond small-scale yielding and even in this case is redundant with J_p. The discrepancy noticed in GE/EPRI estimation scheme may be due to Poisson's ratio changes occurring in an elastic-plastic material, which are neglected in this simplified approach based on deformation theory of plasticity. As explained in Reference 2.20, any plastic-zone correction violates Ilyushin's theorem, which should be verified in deformation plasticity computations.

Activity 1.4.1 Improve Short-Through-Wall-Cracked Pipe Analysis and Compare to Existing Data

Objective

This activity will involve several efforts to identify shortcomings, and then to make and verify improvements in existing analyses. In general, the objective of this activity is to make needed improvements to the analyses prior to developing any new experimental data.

Approach

The four separate efforts in this activity are:

(a) Numerically assess the effect of plastic ovalization on the validity of J
(b) Determine pipe ovalization effects on limit-load analysis
(c) Improve F-, V-, and h-functions
(d) Compare predictions from improved analyses to existing data.

Activities 1.4.1(b) and 1.4.1(c) were the only active efforts during this progress report.

Activity 1.4.1(b) Determine pipe ovalization effects on limit-load analysis

One consideration is the possible effect of pipe ovalization on the maximum load-carrying capacity based on plastic buckling. Existing closed-form solutions on pipe buckling were used to estimate the load-carrying capacity and compared to that predicted by the net-section-collapse (NSC) analysis for uncracked pipe. From this, an ovalization correction function will be eventually developed. Such a function would depend on (1) the ratio of applied bending load to the maximum bending load predicted by NSC analysis, (2) the ratio of tension to bending load, (3) the pipe's R/t ratio, and (4) the strain-hardening characteristics of the pipe material.

During this reporting period existing methods used to predict the load-carrying capacity of an uncracked pipe were reviewed and compared with experimental data.

Progress

This subtask has two specific objectives. The first is to provide a simple method that can be used to account for buckling loads being below those predicted by the simple NSC equation. The second is to verify a method to predict moment-rotation response of uncracked pipe when the bending stresses are above yield. This correction is necessary if η-factor analyses are to be used to calculate the J-R curves from the short through-wall-cracked pipe experiments. The need for such a correction was first illustrated by Bruckner et al. (Ref. 2.21).

These efforts first concentrated on predictions of maximum load for uncracked pipe. The experimental results from five tests conducted at JAERI were used for this purpose (Ref. 2.22). The analysis techniques reviewed are summarized below.

(1) The NSC Method: The maximum moment, M_{nsc}, is predicted by

$$M_{nsc} = 4\sigma_f R_m^2 t F(\theta) \tag{2-14}$$

where
$\sigma_f = (\sigma_y + \sigma_u)/2$
R_m = mean radius
t = pipe thickness
$F(\theta)$ = 1 for uncracked pipe.

(2) Mesloh's Method: This method (Ref. 2.23) was empirically derived to predict the buckling strength of offshore pipelines. The maximum moment-carrying capacity is given by

$$M_{mes} = D_o^2 t \sigma_{0.005} [500/(445 + D/t)] \tag{2-15}$$

where
D_o = outer diameter
$\sigma_{0.005}$ = stress at 0.5 percent strain, $\simeq \sigma_y$.

This equation was developed for design purposes and contained some inherent safety margin.

(3) The "COLAPS" Code: This computer program was written to study buckling of pipes under bending loads (Ref. 2.24). The method incorporates strain-hardening characteristics of the material into the analysis. This code was developed at Battelle for the offshore pipeline industry.

(4) Fully Plastic Solution: This method is used to predict the moment-rotation behavior of an uncracked pipe using a fully plastic analysis. The rotation of the pipe is given by

$$\phi = \frac{2L\alpha\varepsilon_o}{R}\left[\frac{M}{4\sigma_o R^2 t\beta}\right]^n \tag{2-16a}$$

where

$$\beta = \frac{\sqrt{\pi}}{2}\frac{\Gamma\left(1+\frac{1}{2n}\right)}{\Gamma\left(\frac{3}{2}+\frac{1}{2n}\right)} \qquad (2\text{-}16b)$$

and where

L	=	pipe length.
ε_o, σ_o, α, n	=	Ramberg Osgood constants for the material
R	=	pipe radius
t	=	pipe wall thickness
Γ	=	Gamma function.

Since this method is based on the Ramberg-Osgood idealization of the material behavior, where the stress increases indefinitely with strain, it cannot be used to predict the maximum moment-carrying capacity of the pipe. However, it can be used to predict the experimental moment-rotation behavior prior to maximum load and also verify FE prediction.

(5) Finite Element Method: Three element options can be used in the ABAQUS code. These are the elbow element, shell elements, and three-dimensional brick elements. The elbow element in ABAQUS is specifically designed to study bending and buckling of pipes and elbows. It includes ovalization effects in its formulation. Straight pipe can easily be modelled by making the elbow have a zero degree bend. This method also uses the strain-hardening characteristics of the material, which are input as a either a Ramberg-Osgood or piece-wise linear function. The shell element is more accurate than the elbow element, and brick elements are considered the most accurate.

Prior to conducting the systematic analyses of the JAERI experiments, one experiment was analyzed using both the ABAQUS elbow and shell elements. The difference of the maximum load predictions was within 1 percent, but the computing cost was significantly lower for the elbow element. Use of the three-dimensional brick elements would give negligible improvement in accuracy, but would be even more expensive. Hence, the rest of the FEM analyses were conducted with only the elbow element.

Table 2.11 lists the geometry and the material properties of the five pipe experiments conducted by JAERI on uncracked stainless steel pipe. These results are given in Figure 2.14, which is a plot of calculated moment over the experimental moment (M/M_{exp}) versus the R_m/t of the pipe. The comparison of the experiments to the calculated values show that the Mesloh and the ABAQUS elbow element give virtually identical predictions. These predictions were consistently lower than the experimental results. For the five experiments, the Mesloh method averaged 77.2 percent of the experimental results and the standard deviation was 0.065. The ABAQUS elbow element had an average value of 81.2 percent of the experimental results, and a standard deviation of only 0.028. This can be contrasted to the larger scatter in the COLAPS

Table 2.11 Summary of uncracked JAERI experiments analyzed[a]

Expt. No.	Outer Diameter mm	Outer Diameter (inch)	Schedule	σ_y kg/mm^2	σ_y (ksi)	σ_u kg/mm^2	σ_u (ksi)	α	n
S-1	86.1	(3.39)	40	27.5	(39.03)	33	(46.8)	32.9	5.63
S-21	87.4	(3.44)	160	27.2	(38.6)	62.4	(88.6)	33.6	6.02
S-17	85.1	(3.35)	80	34	(48.3)	64.5	(91.5)	31.8	8.39
TT-00	168.3	(6.63)	80	24.4	(34.6)	63.4	(90.0)	1.97	5.4
TT-100	323.9	(12.75)	80	26.3	(37.33)	53.9	(76.5)	(b)	

(a) With $\sigma_0 = \sigma_y$ and $E = 26.5 \times 10^6$ psi.
(b) Stress-strain curve not available.

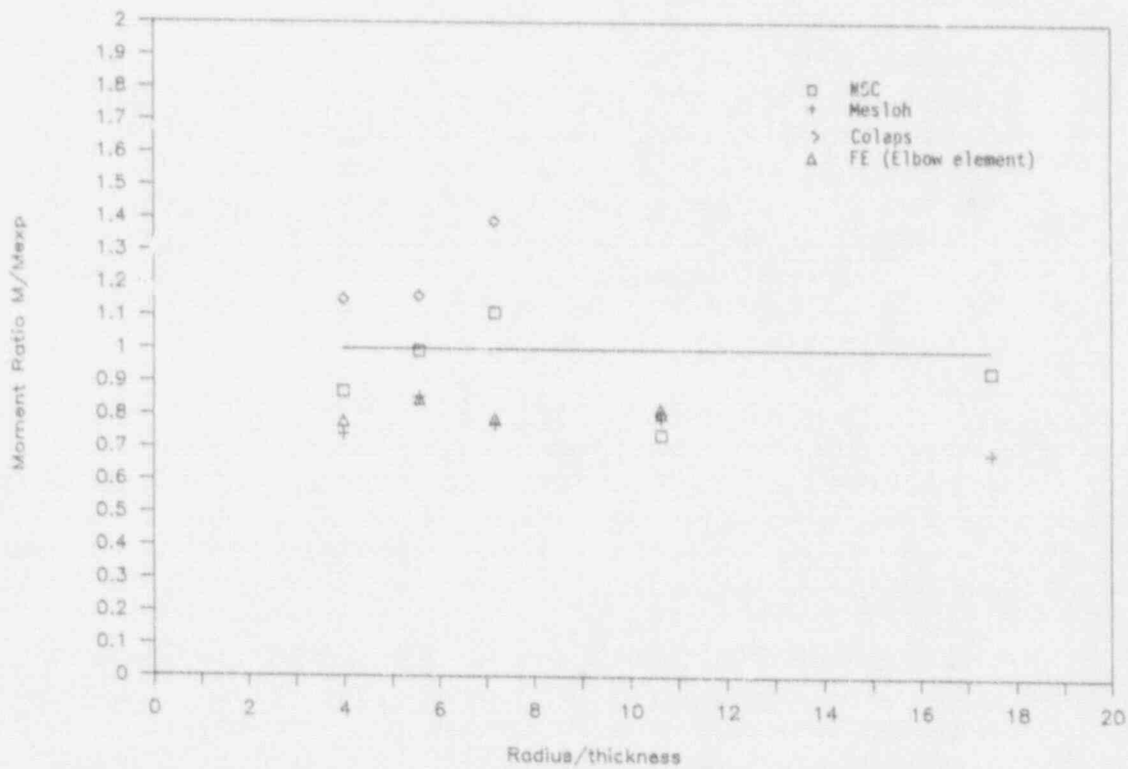

Figure 2.14 Comparison of predicted to experimental maximum moments for JAERI uncracked stainless steel unpressurized pipe bending experiments

SC-M-12/90-F4

and NSC analyses which had standard deviations of 0.29 and 0.14, respectively. The average values of the COLAPS and NSC analyses predictions were 1.11 and 0.93, respectively.

For the experiments analyzed, there was very little effect of the R_m/t ratio on the maximum loads. These experiments had R_m/t ratios of 4 to 17.5, which covers most primary and secondary LWR nuclear pipes.

The results show that the simple Mesloh formula could be used with a correction factor of 1/0.772 to give reasonable predictions for stainless steel uncracked pipe maximum loads without internal pressure. This empirical correction is probably due to the inherent safety margin in the design bases equation they developed. A further review of the past Battelle pipe buckling data gave a modified Mesloh formula for average buckling moments as

$$M_{max} = 1.8982(D_o/t)^{-0.1356} D_o^2 t \sigma_{0.005} \quad (2\text{-}17)$$

Figure 2.15 shows a comparison of the experimental moment-rotation curve from JAERI Experiment S-17 with the prediction from the FEM analysis. As seen in Figure 2.15, the FEM results are overly conservative (~20 percent) in predicting the moment beyond the elastic regime. Similar observations were made on uncracked stainless steel bars under four-point bending loads in Sweden (Ref. 2.25). A detailed analysis of this data is currently under way to explain the discrepancy between FEM results and experimental observations on uncracked stainless steel pipe.

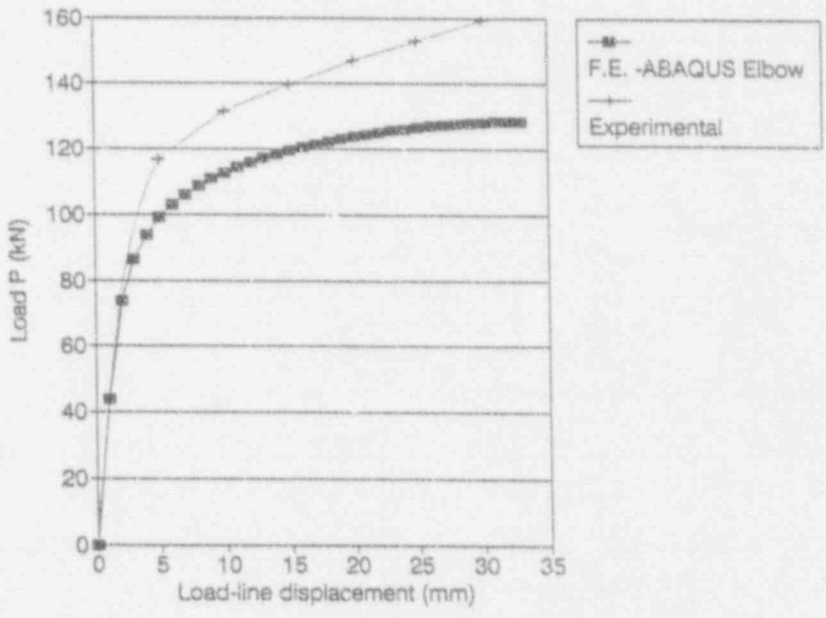

Figure 2.15 Comparison of experimental to finite element analyses of uncracked stainless steel pipe test results (JAERI Experiment S-17)

SC-SA-7/91-F2.15

Activity 1.4.1(c) Improve F-, V- and h-functions

The Sander's F-function (Ref. 2.26) is known to be applicable for relatively long crack lengths, which are longer than the lengths used in LBB analyses for large diameter pipe. Figure 2.16 shows that the Sander's solution approaches zero as the crack length approaches zero. Typically, such F-functions for other geometries approach values of 1 to 1.3 as the crack length approaches zero (Ref. 2.27). It was assumed by Paris and Tada in Reference 2.28, and subsequently by Brust in Reference 2.20, that Sander's solution should approach a value of one as the crack length approaches zero. Assessment of this assumption is one of the objectives of this activity.

The GE/EPRI Estimation Scheme

The GE/EPRI method takes advantage of the scaling properties in linear and nonlinear elasticity to interpolate over the range from small-scale yielding to large-scale yielding and to normalize fracture parameters such as J, COD, and displacements due to the crack. The elastic-plastic solution is obtained by superposition of a small-scale yielding solution and of the fully plastic solution. The stress-strain law is defined by a Ramberg-Osgood relation:

$$\frac{\varepsilon}{\varepsilon_o} = \frac{\sigma}{\sigma_o} + \alpha\left(\frac{\sigma}{\sigma_o}\right)^n \tag{2-18}$$

where σ_o is an arbitrary reference stress usually defined as the yield stress, α and n are curve fitting parameters, and $\varepsilon_o = \sigma_o/E$.

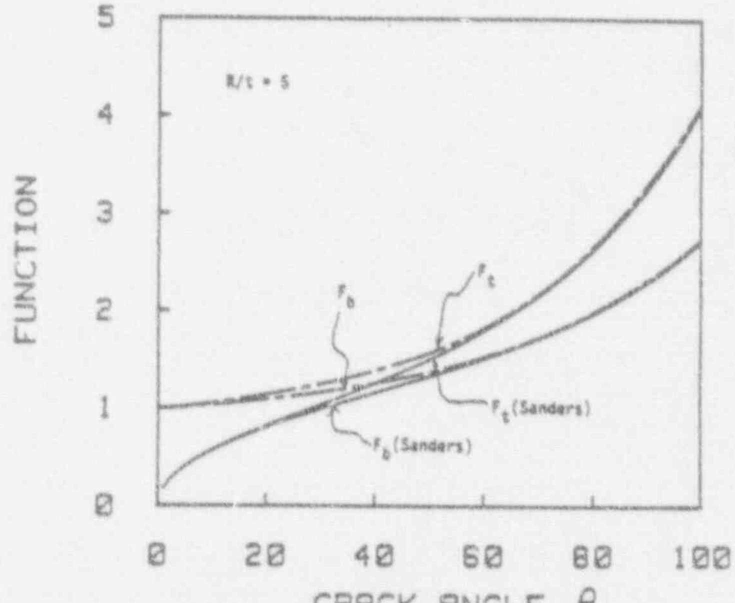

Figure 2.16 Comparison of Sanders' F-functions for F_m/t = 5 and polynominal fit assuming F = 1 as crack angle approaches zero

T-4572-FA.4

This normalization reduces the fracture parameter determination to the computation of coefficients depending, for given types of geometry and loading, only on the strain hardening coefficient n and few geometrical parameters. Tabulated values of these coefficients were computed (Refs. 2.18 and 2.19) using the finite element technique. J for a through-wall cracked pipe in bending is written in the following form:

$$J = f_1 \frac{M^2}{E} + \alpha\, \sigma_o\, \varepsilon_o\, a \left(1 - \frac{\theta}{\pi}\right) h_1 \left(\frac{M}{M_o}\right)^{n+1} \qquad \text{(2-19a)}$$

In Equation 2-19, a is half the total crack length, θ is half of the total crack angle, and M_o is the limit moment, defined in Reference 2.18. Also

$$f_1 = f_1\left(a_e\, ,\, \frac{R}{t}\right) \qquad \text{(2-19b)}$$

$$h_1 = h_1\left(\frac{\theta}{\pi}\, ,\, \frac{R}{t}\, ,\, n\right) \qquad \text{(2-19c)}$$

and are tabulated. In the pipe bending case, Q = the moment (M), and the effective crack size, a_e, based on an Irwin plastic zone correction, is written as:

$$a_e = a + \frac{r_y}{1 + \left(\frac{Q}{Q_o}\right)^2} \qquad \text{(2-20a)}$$

$$a = R\theta \qquad \text{(2-20b)}$$

$$r_y = \frac{1}{2\pi}\left[\frac{n-1}{n+1}\right]\left(\frac{K}{\sigma_o}\right)^2 \qquad \text{(2-20c)}$$

where K is a function of a and not of a_e. Other parameters such as crack opening displacement and load-point rotations were also evaluated in Reference 2.18.

Comments on the Plastic-Zone Size Correction

The linear elastic solution underestimates the actual J value when Q/Q_o exceeds 0.5 (Ref. 2.15) and the J_p component is too small, especially for large n values, to account for the difference. This is the apparent reason why Kumar et al. (Ref. 2.18) extended the plastic zone size formula established by Rice (Ref. 2.29) for the antiplane shear problem. This extended formula (Eq. 2-20a) has been developed in order to reduce the magnification of J_e when Q becomes closer to Q_o. There is no justification for the choice of the $1/(1 + (Q/Q_o)^2)$ function except ensuring continuity of partial derivatives of J with respect to applied load at $Q = Q_o$ (Ref. 2.17, p. 420). Our experience (Refs. 2.12, 2.13, and 2.20) suggests that, when using the GE/EPRI method for TWC pipes, using the plastic-zone correction in the elastic solution produces results that are far too conservative.

The GE/EPRI method, as developed for TWC pipe, appears to be too conservative, i.e., the compiled values of h_1 and hence J are too large. In fact, for the smaller crack sizes, the results appear quite inadequate. Indeed, the pipe rotations due to the crack are negative for θ/π = 1/16, as compiled in Reference 2.18 for both elastic and plastic solutions. As discussed in References 2.12, 2.13, and 2.20, this problem may be due to the use of the 9-node shell element in Reference 2.18 to produce the solutions, and overly stiff results occurred. Here we will recompile the solutions of Reference 2.18 for θ/π = 1/8 and θ/π = 1/16. In this fashion, more reliable predictions of crack instability for the smaller crack sizes using the GE/EPRI scheme are expected.

Another source of error in the current analyses is in the GE/EPRI solutions for a cracked pipe in bending. In fact, Reference 2.19 shows that the V_3 (pipe elastic-crack rotation function) and the fully plastic crack rotation function (h_4) are negative for the shorter crack lengths. It is physically impossible for the pipe to have less rotation with a crack than without a crack. This obvious error forced Brust in Reference 2.20 to make an engineering approximation for shorter crack lengths. The V_3 solutions will be determined at the same time as the Sander's elastic F-function is verified.

Progress

Six finite element meshes have been developed, one for each case listed in Table 2.12. A typical finite element mesh and geometric definitions are illustrated in Figure 2.17(a). A quarter model is used by taking advantage of symmetry. Twenty node isoparametric brick elements are being used with focussed elements at the crack tip. Only one element through the pipe wall is used, and, as such, the tabulated results should be considered as average values through the pipe wall.

The elastic solutions are developed using linear elastic properties. A deformation theory plasticity algorithm in the ABAQUS finite element code is being used to generate the plastic solution. Because a through-wall cracked pipe subjected to bending (or tension) is a plane stress problem, the special (hybrid) elements in the ABAQUS library that adequately handle plastic incompressibility are not necessary. A reduced (2 x 2) Gauss quadrature integration rule is used.

Table 2.12 Matrix of finite element calculations

Model No.	Model Name	R/t	$n^{(a)}$	θ/π	Remarks	Loading
1	CASE1A3DM	5	1,3,5,7,10	0.0625	10 Runs	Tension or Bending
2	CASE2A3DM	10	1,3,5,7,10	0.0625	10 Runs	Tension or Bending
3	CASE3A3DM	20	1,3,5,7,10	0.0625	10 Runs	Tension or Bending
4	CASE1B3DM	5	1,3,5,7,10	0.1250	10 Runs	Tension or Bending
5	CASE2B3DM	10	1,3,5,7,10	0.1250	10 Runs	Tension or Bending
6	CASE3B3DM	20	1,3,5,7,10	0.1250	10 Runs	Tension or Bending

(a) n = 1 is elastic

The GE/EPRI handbook (Reference 2.18) has tables whereby J, the crack mouth opening displacement (at the center of the crack), δ, and either the total relative load-point displacement due to the crack, Δ_c (for tension load), or the total relative rotation due to the crack, ϕ_c (for bending load) are tabulated for specific geometric parameters. The parameters include R/t, θ, and the Ramberg-Osgood power law exponent, n. For a uniaxial tensile bar, the Ramberg-Osgood relation is as written in Equation 2-18.

Here we follow the convention of Reference 2.18 and compile, for J (see Eq. 2-19), the crack opening displacement, δ, and the pipe rotation, ϕ:

$$\begin{aligned}\delta_T &= \delta_e + \delta_p \\ &= f_2 \frac{M}{E} + \alpha\varepsilon_o\, a\, h_2 \left(\frac{M}{M_o}\right)^n\end{aligned} \tag{2-21}$$

$$\begin{aligned}\phi_T^c &= \phi_e^c + \phi_p^c \\ \phi_T^c &= f_4 \frac{M}{E} + \alpha\, \varepsilon_o\, h_4 \left(\frac{M}{M_o}\right)^n\end{aligned} \tag{2-22}$$

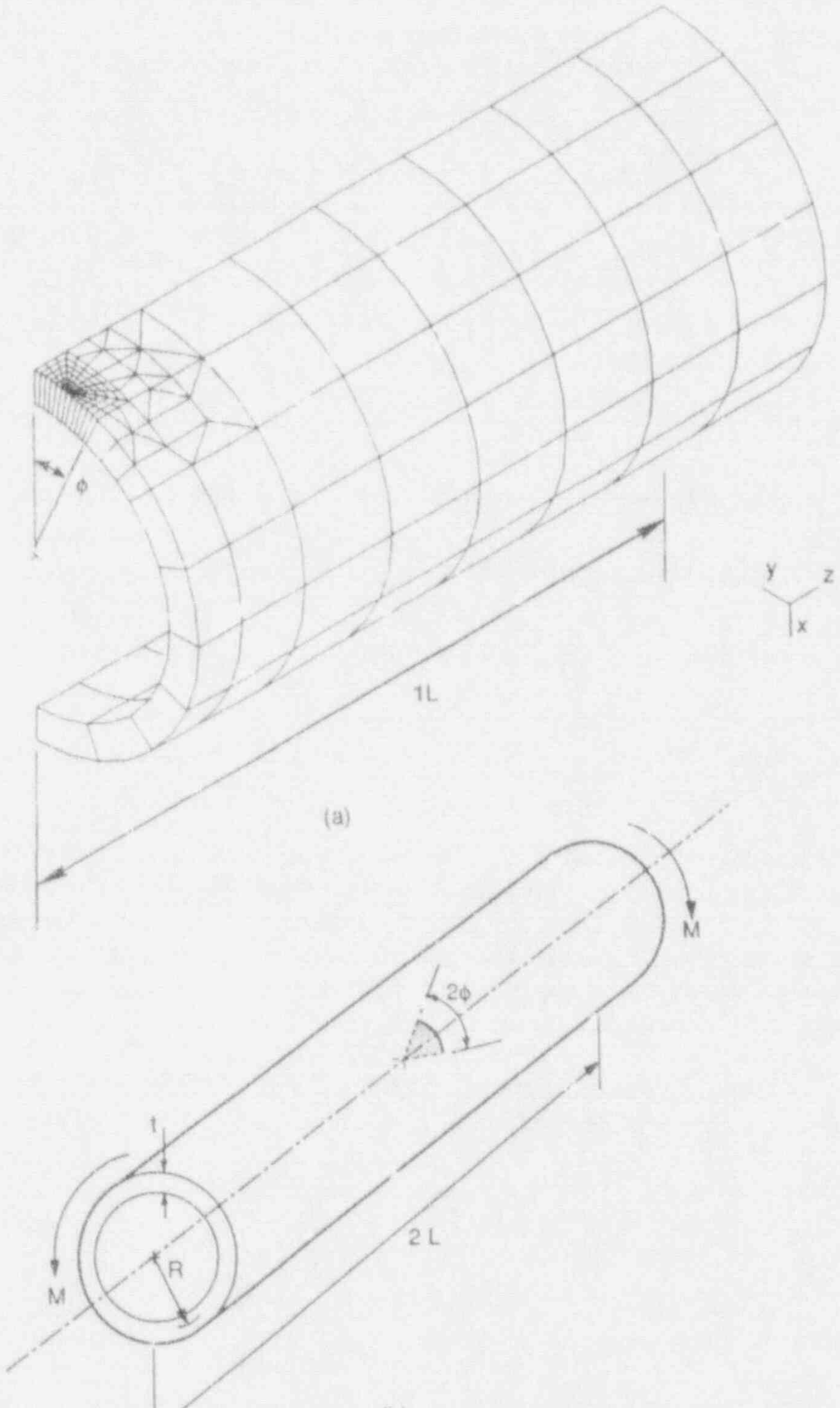

Figure 2.17 Typical finite element (a) mesh used for analysis (1/4 model), and (b) circumferential cracked pipe geometry

SC-SA-7/91-F2.17

In Equation 2-22, the "c" superscript refers to "due to crack", as defined in Reference 2.18. For the elastic contribution, using the GE/EPRI convention, we write:

$$f_1\left(\frac{\theta}{\pi},\frac{R}{t}\right) = \pi a\left(\frac{R}{I}\right)^2 F^2\left(\frac{\theta}{\pi},\frac{R}{t}\right) \tag{2-23}$$

$$f_2\left(\frac{\theta}{\pi},\frac{R}{t}\right) = 4a\,\frac{R}{I}\,V_1\left(\frac{\theta}{\pi},\frac{R}{t}\right) \tag{2-24}$$

$$f_4\left(\frac{\theta}{\pi},\frac{R}{t}\right) = 4\,\frac{R}{I}\,V_3\left(\frac{\theta}{\pi},\frac{R}{t}\right) . \tag{2-25}$$

In Equations 2-23 to 2-25, I is the moment of inertia of the uncracked section, which for large R/t is written as:

$$I = \pi R^3 t \tag{2-26}$$

and F, V_1, V_3 are compiled from the finite element solutions. Note that F is the function conventionally defined in the stress intensity factor definition as:

$$K_I = \sigma\sqrt{\pi a}\,F\left(\theta,\ \frac{R}{t}\right) \tag{2-27}$$

The plastic functions h_1, h_2, and h_4 are compiled also. Note that the axial stretch, denoted by Δ_c in Reference 2.18 and which depends on f_3 and h_3, are not compiled here for bending since these are unimportant.

The ABAQUS deformation theory routine uses a constitutive law which includes the elastic term (Eq. 2-18), i.e., it is not truly a fully plastic solution. The analyses are performed to a load level in which plastic strains greatly dominate elastic strains everywhere in the body, which effectively results in a nearly fully plastic solution. However, for completeness, we obtain the fully plastic solution by subtracting out the (separately calculated) elastic results. Hence, from Equations 2-19, 2-21, and 2-22 h_1, h_2, and h_4 are evaluated using:

$$h_1 = \frac{J_T - J_e}{\alpha\ \sigma_o\ \varepsilon_o\ a \left(1 - \dfrac{\theta}{\pi}\right)\left(\dfrac{M}{M_o}\right)^{n+1}} \tag{2-28}$$

$$h_2 = \frac{\delta_T - \delta_e}{\alpha\ \varepsilon_o\ a \left(\dfrac{M}{M_o}\right)^{n}} \tag{2-29}$$

$$h_4 = \frac{(\phi_T - \phi_e^c - \phi_e^{nc} - \phi_p^{nc})}{\alpha\ \varepsilon_o \left(\dfrac{M}{M_o}\right)^{n}} \tag{2-30}$$

In Equations 2-28 to 2-30, respectively, J_T, δ_T, and ϕ_T are results from the ABAQUS solution. Also, Equation 2-30, the "nc" superscript, refers to "no crack". The dimensionless elastic functions are compiled first (F, V_1, V_3) to determine J_e, δ_e, ϕ_e^c. Then the results of the ABAQUS solution provides J_T, δ_T, ϕ_T^c, from which Equations 2-28 to 2-30 provide h_1, h_2, h_4.

Results

Table 2.12 earlier showed the matrix of finite element calculations to be performed. A complete set of analyses was performed using ABAQUS on Battelle's VAX Computer for Model 2 (n = 1, 3, 5, 7). Both elastic and fully plastic (Deformation Theory) computations were made for bending loads.

To verify our analysis procedure, it was decided to conduct a pure tension analysis, for which the GE/EPRI solutions were believed to be accurate. Table 2.13 shows the F and V functions obtained from the ABAQUS analysis (tension - elastic). The GE/EPRI results are also included in Table 2.13 for comparison purposes.

Table 2.13 F, V_1, V_2, V_3 functions (tension - elastic)

Function	3D Solid ABAQUS	GE/EPRI
F	1.0487	1.0770
V_1	1.1786	1.0820
V_2	0.0540	0.0520
V_3	0.0198	0.0210

Table 2.14 shows the h functions obtained from the ABAQUS analysis (tension - fully plastic). The GE/EPRI results are also included in Table 2.14 for comparison purposes.

Table 2.14 h functions (tension-fully plastic) (n = 3)

Function	3D Solid ABAQUS	GE/EPRI
h_1	3.9240	4.6550
h_2	5.0080	5.1960
h_3	1.1800	0.5100
h_4	0.2950	0.3090

As Tables 2.13 and 2.14 show, the GE/EPRI solutions differ from those produced here by as much as 15 percent for J (h_1). Because of this, the matrix listed in Table 2.12, which was originally meant to be completed for the bending-only analysis, was extended to include tension loading cases also. Note that for the tension loading cases, we include an axial displacement in our compilation. This displacement is evaluated at the neutral axis of the uncracked pipe section. Again, following Reference 2.18:

$$\Delta_c = f_3 \frac{P}{E} + \alpha \, \varepsilon_o \, a \, h_3 \left[\frac{P}{P_o}\right]^n \tag{2-31}$$

where

$$f_3\left(\frac{\theta}{\pi}, \frac{R}{t}\right) = \frac{2a}{\pi R t} \, V_2 \left(\frac{\theta}{\pi}, \frac{R}{t}\right) \tag{2-32}$$

For tension loading P is the total applied tensile load and P_o is the limit load defined in Reference 2.18.

Bending solutions were also performed for the Model 2 case for n = 1, 3, 5, 7 using the ABAQUS code. Table 2.15 shows the F and V functions obtained from the ABAQUS analysis (bending - elastic). The GE/EPRI results are also included in Table 2.15 for comparison purposes.

Tables 2.16, 2.17, and 2.18 show the fully plastic h-functions obtained from the ABAQUS analysis (bending - fully plastic) for n = 3, 5, 7. The GE/EPRI results are also included in Tables 2.16, 2.17, and 2.18 for comparison purposes.

In order to obtain the h-functions, the ABAQUS calculation involved elastic and plastic analysis (Deformation Theory) for a series of bending moment loads until a fully plastic criteria was met. One check on the fully plastic h-functions reported in Tables 2.16 through 2.18 was to calculate these functions at all load levels and verify that h-functions do not vary once certain load levels

Table 2.15 F, V_1, V_3 functions[a] (bending-elastic)

Function	3D Solid ABAQUS	Shell - GE/EPRI
F	1.0490	1.0700
V_1	1.2060	1.0810
V_3	0.0351	-0.0430

(a) There is no V_2 (tension) displacement function for pure bending.

Table 2.16 h functions[a] (bending - fully plastic) (n = 3)

Function	3D Solid ABAQUS	Shell - GE/EPRI
h_1	6.207	6.7430
h_2	7.385	6.9060
h_4	1.140	0.1440

(a) There is no h_3 (tension) function for pure bending.

Table 2.17 h functions[a] (bending - fully plastic) (n = 5)

Function	3D Solid ABAQUS	Shell - GE/EPRI
h_1	6.558	7.620
h_2	7.521	7.867
h_4	1.720	0.288

(a) There is no h_3 (tension) function for pure bending.

Table 2.18 h functions[a] (bending - fully plastic) (n = 7)

Function	3D Solid ABAQUS	Shell - GE/EPRI
h_1	6.617	7.969
h_2	7.478	8.260
h_4	2.130	0.429

(a) There is no h_3 (tension) function for pure bending.

(plasticity dominates) are reached. A typical plot of the h_1 function with bending moment is given in Figure 2.18; it shows that the h_1 function levels off after some load value.

Activity 1.4.2 Analyze Large Diameter Pipe TWC Test Results

Objective

The objective in this activity is to analyze the large diameter, short through-wall-cracked pipe fracture experiments.

Rationale

These pipe fracture data were developed to assess the J-estimation schemes to be used in LBB analyses for typical fracture behavior.

Approach

The pipe fracture data will be used to assess the accuracy of J-estimation schemes in the current version of NRCPIPE and the improved versions from the analysis improvements developed in Activity 1.4.1. This effort will consider accuracy of the Ramberg-Osgood fit, different fits of the J-R curve, as well as the other improvements made in the J-estimation schemes.

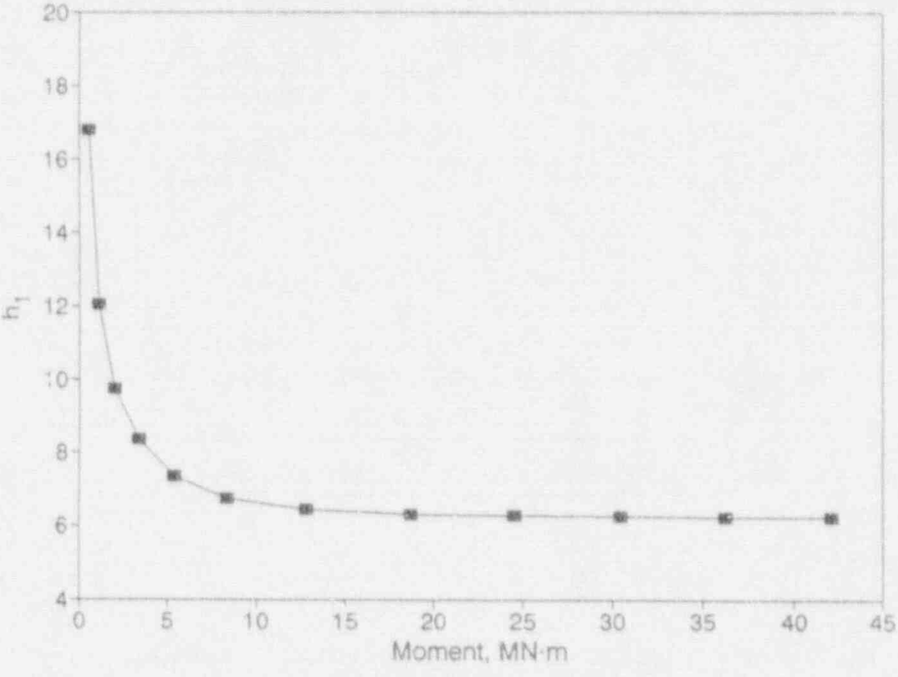

Figure 2.18 Plasticity function h_1 (ABAQUS - Solid Element Results) for pipe under bending. R/t = 10, n = 3, and θ/π = 0.0625

SC-M-5/91-F4

Comparisons will also be made between the experimental data and the following analyses: net-section-collapse, ASME Section XI flaw evaluation criteria, and the dimensionless plastic-zone criteria.

Progress

The maximum load predictions using current calculational methods were made for Experiment 1.1.1.21 and 1.1.1.23 as well as their companion Experiments from the Degraded Piping Program (4111-2 and 4111-5). The comparisons between various existing analyses and the maximum loads in the Experiments 1.1.1.21 and 4111-3 were made in the last semiannual report. All of the experiments were on 711-mm- (28-inch) diameter pipe under four-point bending at 288 C (550 F). The difference, other than pipe material, is the crack length of 6 percent (for Experiments 1.1.1.21 and 1.1.1.23) versus 37 percent of the circumference for Experiments 4111-3 and 4111-5.

The analyses evaluated were:

- The EPRI NP-192 net-section-collapse (NSC) analysis (Ref. 2.30),
- the GE/EPRI estimation scheme (Ref. 2.18),

- the Tada-Paris or NUREG/CR-3464 method (Ref. 2.28)
- the LBB.NRC method (Ref. 2.31),
- the LBB.GE method (Ref. 2.20),
- the LBB.ENG method (Ref. 2.20), and
- the ASME IWB-3640 or 3650 pipe flaw evaluation criteria (Ref. 2.32 and 2.33).

The flow stress was defined as the average of yield and ultimate strength from tensile tests on these pipe materials. The J-estimation schemes used Ramberg-Osgood parameters from a best fit of the stress-strain curve from a program called ROFIT. The ASTM deformation J-R curve, J_D-R curve, was used in the calculations, with the curve extrapolated by a power-law hardening curve for crack growth beyond 30 percent of the ligament in the C(T) specimen (Ref. 2.3).

The calculations were made for various crack lengths for all the analyses. Figure 2.19 shows the various predicted maximum loads and the data from the two carbon steel base metal experiments (1.1.1.21 and 4111-3).

Similar calculations were made for the recently completed Experiment 1.1.1.23 on the stainless steel SAW. In this experiment the base metal stress strain properties of a similar pipe (A50) were used, and the J_D-R curve of the new stainless steel SAW were used. The companion experiment from the Degraded Piping Program was on a similar pipe and although the weld in that experiment was a SMAW, it had similar properties. Figure 2.20 shows the comparison of the maximum load predictions by the various methods and the experimental maximum loads. Note that NSC calculations were made using a flow stress equal to the average of the yield and ultimate strength, whereas the ASME IWB-3640 analysis uses the definition of $3S_m$ and a Z-factor (stress multiplier)[a] of 1.612.

These comparisons show the following:

(1) The experimental maximum loads fall below the NSC analysis predicted values. This was expected since the pipe diameters are large and the J-R curve is relatively low for these materials.

(2) In Figure 2.19, the ASME IWB-3650 curve is much more conservative for the carbon steel experiment with this shorter crack length than the longer crack. This was expected since the Z-factor is based on a crack length of roughly 30 percent of the circumference where there is the largest difference between the NSC predictions and the GE/EPRI estimation scheme (Ref. 2.18). For the ASME IWB-3640 analyses of the stainless steel SAW experiments in Figure 2.20, the experimental results were only slightly above the IWB-3640 predictions for both crack sizes. Hence, for LBB analyses, such as proposed in NRC's draft Standard Review Plan 3.6.3 for elimination of dynamic effects from pipe rupture, the Z-factor approach would be perhaps too conservative for ferritic pipe, but reasonably conservative for the stainless steel pipe.

(a) The Z-factor is a correction factor to account for failure loads being below the limit-load predicted failure stress. Details can be found in Reference 2.32.

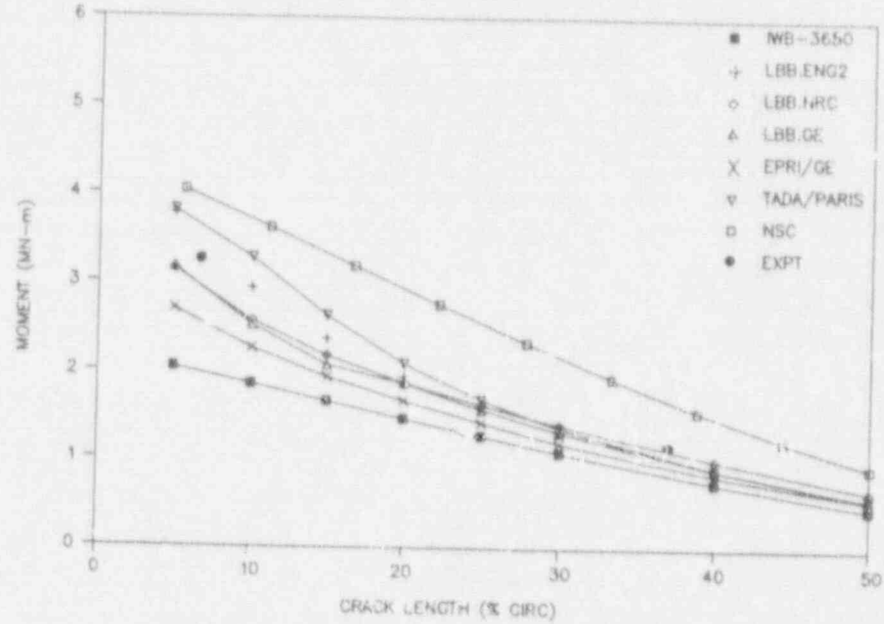

Figure 2.19 Comparison of maximum loads from Experiments 1.1.1.21 and 4111-2 on a 28-inch-diameter Schedule A516, Grade 70 pipe to predictions by various analyses

SC-M-11/90-F1

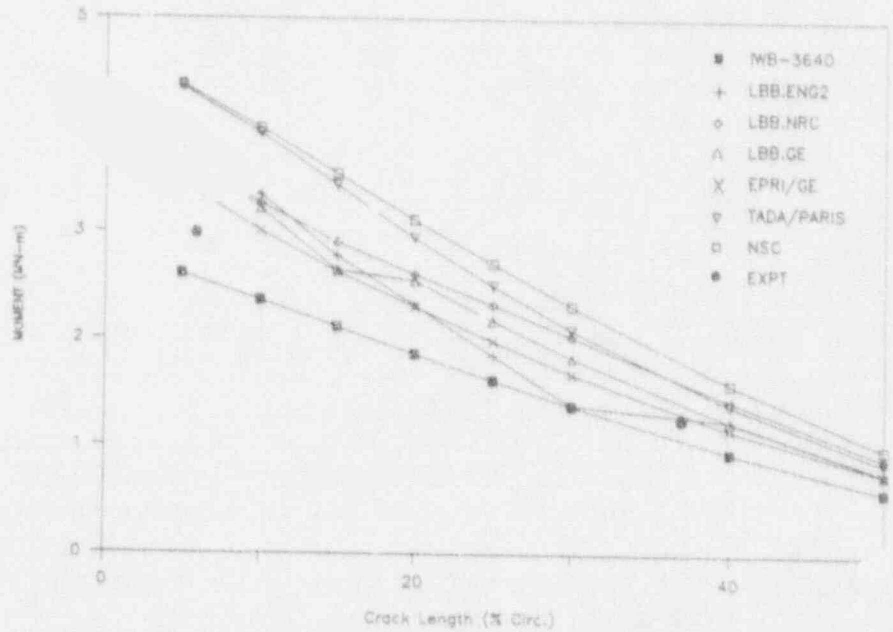

Figure 2.20 Comparison of maximum load predictions by various analyses to two 28-inch-diameter, Schedule 80, TP316 stainless steel, through-wall-cracked pipe experiments

SC-SA-7/91-F2.20

(3) The Tada-Paris method (Ref. 2.28) was developed for NRC licensing staff to check calculations by others for licensing submittals. For the ferritic pipe (Figure 2.19) it was found that this method very slightly underpredicted the long cracked pipe failure loads, but overpredicted the short crack failure loads. For the stainless steel SAW, the Tada-Paris method overpredicted the maximum experimental loads for both the short and long crack experiments.

(4) The LBB.NRC analysis is frequently used by NRC licensing staff to check calculations for licensing submittals. It is a modification of the Tada-Paris method. It was found that this method underpredicted both the long and short cracked pipe experimental maximum loads for the ferritic pipe (Figure 2.19), but overpredicted the maximum loads for both the stainless steel SAW experiments (Figure 2.20).

(5) The GE/EPRI method was the technical basis of the ASME IWB-3650 analysis, and is frequently used in licensing submittals. It was found that this was the most conservative of the J-estimation scheme predictions, but it still overpredicted both the stainless steel pipe experiments (Figure 2.20). This is consistent with predictions made in the Degraded Piping Program (Ref. 2.2).

(6) The LBB.GE method was developed at Battelle in the Degraded Piping Program and is incorporated in the NRCPIPE Code; see discussion in Task 7. The comparisons show similar agreement with the LBB.NRC analysis. It was found that the moment versus crack length curves for this analysis were not smooth. This comes from problems in the GE/EPRI plastic rotation function, V_3, being negative at short crack lengths. This problem with the V_3 function was one reason for the finite element analyses for short through-wall cracks in Activity 1.4.1(c).

(7) The LBB.ENG2 method was originally developed in the NRC's Degraded Piping program as an independent method to check the other solutions. Two versions of this analysis were developed. The LBB.ENG1 method uses a numerical integration method to calculate the area under a calculated moment-rotation curve to determine J applied. The LBB.ENG2 method uses direct integral equations of the moment-rotation functions to give an analytical solution without need for numerical integration. The LBB.ENG2 method gives much faster solutions on a PC than the LBB.ENG1, LBB.NRC, or Tada-Paris methods. The comparison of the experimental results to the existing LBB.ENG2 solution show that for the ferritic pipe experiments (Figure 2.19), the predicted maximum loads were slightly underpredicted for the long crack, and slightly overpredicted the short crack. For the stainless steel SAW experiments (Figure 2.20), the analysis overpredicted the short crack experiment significantly. The moment versus crack length curve is not smooth for crack lengths from 30 to 40 percent of the circumference. This needs to be investigated.

In general, (a) the NSC analysis overpredicted the failure loads for these pipe experiments, (b) the IWB-3650 analysis procedure appears overly conservative for short through-wall cracks, (c) the IWB-3640 analysis was slightly conservative for both short and long through-wall cracks in an SAW, and (d) as the crack becomes shorter some of the current J-estimation scheme analyses tend to become nonconservative. Corrections to the J-estimation analyses for short crack effects are being pursued as part of Subtask 1.4.1. As a result of this analysis, it appears that a modification to the Z-factor approach for LBB applications to ferritic pipe would be useful. Such a correction would be on the Z-factor as a function of crack length.

Activity 1.4.3 Analyze Through-wall Cracks in Welds

Objective

This activity involves developing a methodology to accurately assess the fracture behavior of pipe with a crack in the center of the weld.

Rationale

The current practice is to use the toughness of the weld and the strength of the base metal. Limited data from the Degraded Piping Program on as-welded and solution-annealed welds suggest that the strength of the weld metal should also be included.

Progress

The effort in this activity focuses on the development of a new estimation method for evaluating energy release rates of through-wall cracked (TWC) pipe weldments subjected to pure bending loads. The method is based on deformation theory of plasticity, constitutive law characterized by Ramberg-Osgood model, and an equivalence criterion incorporating reduced thickness analogy for simulating system compliance due to the presence of a crack in weld metal. Numerical examples are presented to illustrate the proposed technique.

The work involves considerable interaction between numerical and analytical techniques of nonlinear fracture mechanics. To date, all of these efforts have been completed. Detailed theoretical development and results of numerical applications are also reported in a recent technical paper (Ref. 2.34).

Overview

The evaluation of energy release rates of circumferentially located through-wall cracked (TWC) pipe weldments is an important issue in the assessment of structural integrity for both leak-before-break and in-service flaw acceptance criteria. Currently, there are no estimation techniques available to evaluate performance of pipes with cracks in weld metal which account for weld metal versus base metal strengths. The energy release rate J for pipe weldment cases is typically estimated using base metal stress-strain data and weld metal J-resistance curve (Ref. 2.7). In some cases this can lead to overly conservative predictions and in some cases nonconservative predictions, depending on the strength ratio of the base and weld material.

In this activity, a new methodology is developed to predict the energy release rates of TWC ductile pipe weldments subjected to remote bending loads. The method of analysis is based on (1) classical deformation theory of plasticity, (2) constitutive law characterized by Ramberg-Osgood model, and (3) an equivalence criterion incorporating reduced thickness analogy for simulating system compliance due to the presence of a crack in weld metal. The method is general in the sense that it may be applied in the complete range between elastic and fully plastic conditions. Since it is based on J-tearing theory, it is subject to the usual limitations imposed upon this theory, e.g., proportional loading, etc. This has the implication that the crack growth must be small, although in practice, J-tearing methodology is used far beyond the limits of its theoretical validity with acceptable results (Ref. 2.2). Numerical examples are presented to illustrate the proposed technique.

The Pipe Weld Crack Problem

Consider Figure 2.21, which illustrates a typical butt-welded pipe with a circumferential through wall crack of total angle 2θ. The pipe mean radius R and thickness t are shown. Figure 2.22 illustrates the typical geometry for a butt weld in a pipe. Typically, the weld layers are deposited in sequence. The example of Figure 2.22 is an actual sequence from a 4-inch (102-mm) diameter Schedule 80 pipe that required seven passes. The welding gives rise to a heat-affected zone (HAZ) that results in material properties different from those in the weld metal or base metal alone. Often cracks develop in the HAZ zones of pipe and may grow in a skewed fashion to become a through-wall crack, as illustrated in Figure 2.22. Figure 2.22 also shows a crack that grows through the weld metal, which is the type of crack assumed in the development of the method presented here. Figure 2.23 shows the pipe weld geometric assumption made here. Note that the angular and irregular nature of the actual weldment is assumed to be a straight

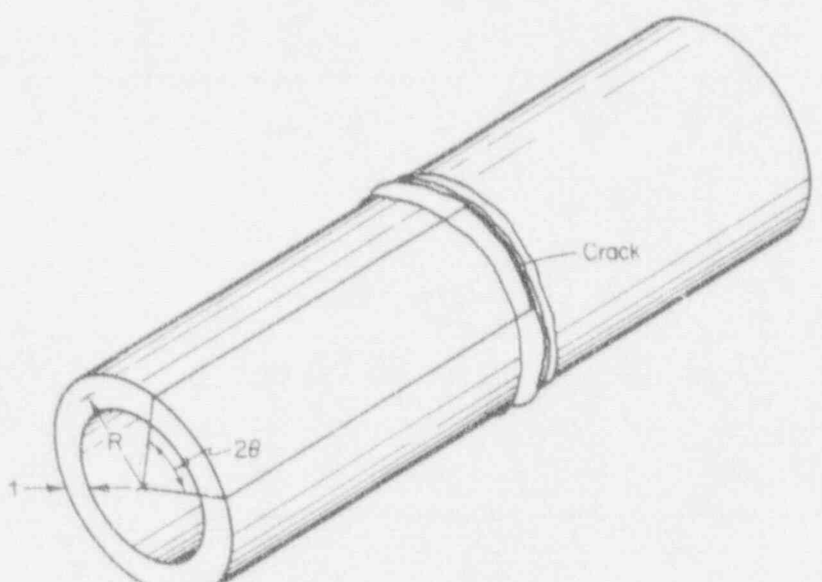

Figure 2.21 Circumferential crack in a pipe butt weld

SC-SA-7/91-F2.21

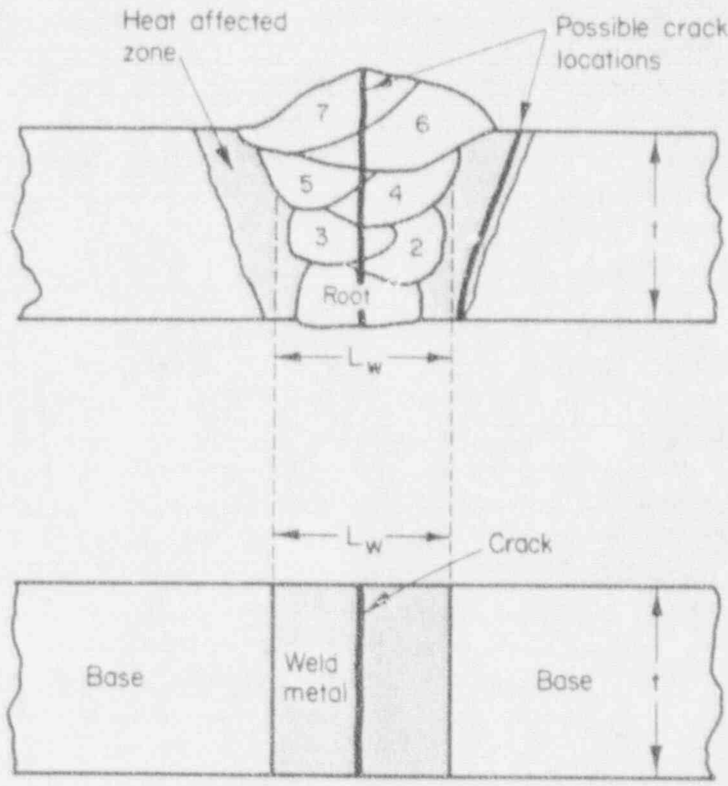

Figure 2.22 Idealized pipe weld with a crack

SC-SA-7/91-F2.22

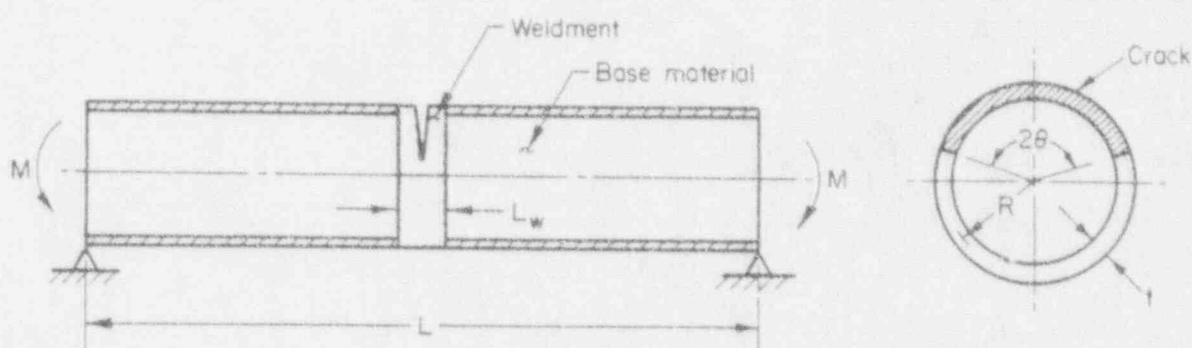

Figure 2.23 Schematics of pipe weldments with a circumferential flaw

SC-M-1/91-F8

radial bimaterial interface line for development of this model. Residual stresses and altered HAZ properties are not included, although they could be considered with rather minor modifications. The total length of the weldment (Figures 2.22 and 2.23) is assumed to be an average length, L_w which is often best approximated (as a rule of thumb) to be the pipe wall thickness (i.e., $L_w \approx t$).

General Background

Consider a simply supported TWC pipe under remote bending moment M (Figure 2.24), with length L, mean radius R, thickness t, and crack angle 2θ with the crack circumferentially located in the weld material of length L_w. In the development of a J-estimation scheme, it is generally assumed that the load point rotation due to the presence of the crack, ϕ^c, and the crack driving force, J, admit additive decomposition of elastic and plastic components

$$\phi^c = \phi^c_e + \phi^c_p \tag{2-33}$$

$$J = J_e + J_p \tag{2-34}$$

where the subscripts "e" and "p" refer to elastic and plastic contributions. In the elastic range, ϕ^c_e and M are uniquely related. In addition, if the deformation theory of plasticity holds, a unique relationship also exists between ϕ^c_p and M. Once these relationships are determined, the elastic component J_e and the plastic component J_p of the total energy release rate J can be obtained readily.

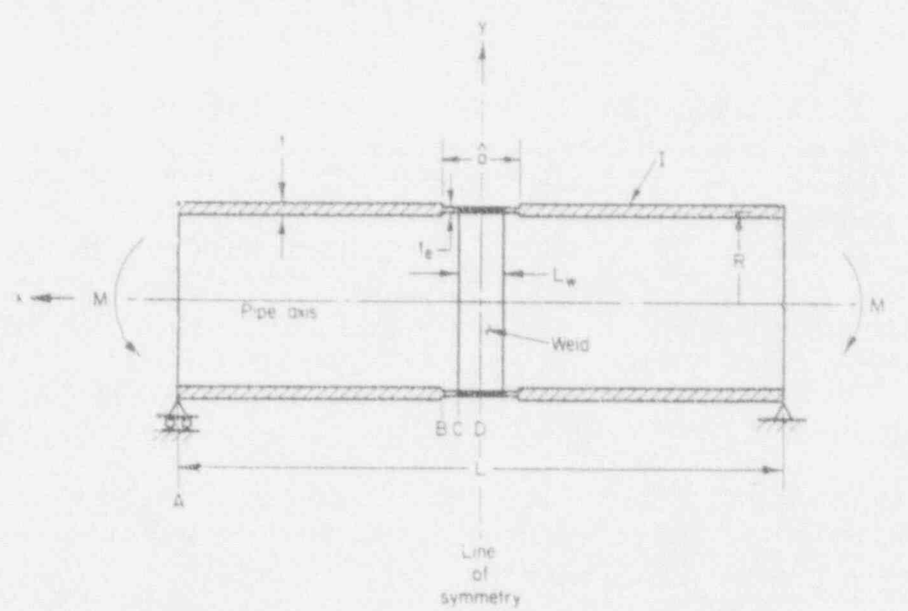

Figure 2.24 Reduced section analogy

SC-M-1/91-F9

A widely used univariate constitutive law describing the material's stress-strain (σ-ϵ) relation is the normalized Ramberg-Osgood model given by

$$\frac{\epsilon}{\epsilon_{0i}} = \frac{\sigma}{\sigma_{0i}} + \alpha_i\left(\frac{\sigma}{\sigma_{0i}}\right)^{n_i} \tag{2-35}$$

where i = 1 or 2 representing base or weld materials respectively, σ_{0i} is reference stress usually assumed to be flow stress and/or yield stress; $\epsilon_{0i} = \sigma_{0i}/E_i$ is the associated strain with elastic modulus E_i; and α_i and n_i are the parameters of model, usually chosen to fit experimental data. In applying the Ramberg-Osgood relation to the cracked-pipe problem, it is necessary to relate the stresses with rotations. Ilyushin (Ref. 2.16) showed that the field solution to the boundary value problem involving a monotonically increasing load or displacement type parameter is "proportional." Consequently, Equation 2-35 applies (minus the elastic term) and the deformation theory plasticity is assumed to be valid. Thus, it can be shown that

$$\phi^c{}_p = L_B{}^c \alpha_i\left(\frac{\sigma}{\sigma_{0i}}\right)^{n_i-1} \phi^c{}_e \tag{2-36}$$

where $L_B{}^c$ is an unknown function which needs to be determined (Refs. 2.12, 2.13, and 2.20). For the crack problem, $L_B{}^c$ may be determined via numerical method. However, no analytical method exists to obtain $L_B{}^c$ in closed form. Thus, the main task in this methodology is to establish $L_B{}^c$ in Equation 2-36.

Evaluation of $L_B{}^c$: Suppose the actual pipe can be replaced by a pipe with reduced thickness t_e which extends for a distance $\hat{\ell} \geq L_w$ at the center (Figure 2.24). Far from the crack plane, the rotation of the pipe is not greatly influenced by whether a crack exists or some other discontinuity is present, as long as the discontinuity can approximate the effects of crack. The reduced thickness section that actually results in material discontinuity is an attempt to simulate the reduced system compliance due to the presence of crack. This equivalence approach was originally suggested by Brust (Ref. 2.20) and successfully implemented to evaluate performance of TWC pipes consisting of one single material under various loading conditions (Refs. 2.12, 2.13, and 2.20). It is assumed here that the deformation theory of plasticity controls stress-strain response and that the beam theory holds.

Consider the equivalent pipe with material discontinuity in Figure 2.24 that is subjected to a bending moment (M) at both ends. Using classical beam theory, the ordinary differential equations governing displacement of beams with Ramberg-Osgood constitutive law can be easily derived. These equations, when supplemented by the appropriate boundary and compatibility conditions, can be solved following elementary operations of calculus. Details of algebra associated with these solutions are provided in Appendix B. The rotations (dy/dx in Appendix

B) provide an explicit relationship between far-field plastic rotation ϕ^d_p due to material discontinuity and the corresponding elastic rotations ϕ^d_e where the new superscript "d" refers to material discontinuity. Each of these relationships can be expressed in the form analogous to Equation 2-36 as

$$\phi^d_p = L_B{}^d \alpha_i \left(\frac{\sigma}{\sigma_{0i}}\right)^{n_i - 1} \phi^d_e \tag{2-37}$$

in which $L_B{}^d$ in general will depend on geometry, material properties of base and weld materials, t_e and the spatial coordinate x. While no attempt is made here for a formal proof, it will be assumed that $L_B{}^d$ determined from the material discontinuity solution (Eq. 2-37) approaches the actual unknown $L_B{}^c$ in Equation 2-36.

Since $L_B{}^d$ evaluated at segment CD cannot account for base material properties (see Appendix B), the appropriate choice is to write $L_B{}^d$ at either segment AB or BC. More specifically, when the spatial location is selected to be the point B (i.e., $x = \hat{a}/2$), the explicit version of Equation 2-37 becomes

$$\phi^d_p = \frac{\left(\frac{M}{M_{01}}\right)^{n_1}\left(\frac{\hat{a}}{2} - \frac{L_w}{2}\right)\left(\frac{t}{t_e}\right)^{n_1} + \left(\frac{M}{M_{02}}\right)^{n_2}\frac{L_w}{2}\left(\frac{t}{t_e}\right)^{n_2}}{\left(\frac{M}{\overline{M}_1}\right)\epsilon_{01}\left(\frac{\hat{a}}{2} - \frac{L_w}{2}\right)\frac{t}{t_e} + \left(\frac{M}{\overline{M}_2}\right)\epsilon_{02}\frac{L_w}{2}\frac{t}{t_e}}\,\phi^d_e \tag{2-38}$$

where, $\overline{M}_i = \sigma_{0i} I/R$ is the elastic bending load corresponding to flow stress σ_{0i}, and other parameters are already defined in Appendix B. Comparing Equation 2-38 with Equation 2-37 immediately gives

$$L_B{}^d = \left[\frac{\left(\frac{M}{M_{01}}\right)^{n_1}\left(\frac{\hat{a}}{2} - \frac{L_w}{2}\right)\left(\frac{t}{t_e}\right)^{n_1} + \left(\frac{M}{M_{02}}\right)^{n_2}\frac{L_w}{2}\left(\frac{t}{t_e}\right)^{n_2}}{\left(\frac{M}{\overline{M}_1}\right)\epsilon_{01}\left(\frac{\hat{a}}{2} - \frac{L_w}{2}\right)\frac{t}{t_e} + \left(\frac{M}{\overline{M}_2}\right)\epsilon_{02}\frac{L_w}{2}\frac{t}{t_e}}\right]\cdot\left(\frac{1}{\alpha_1\left(\frac{M}{\overline{M}_1}\right)^{n_1-1}}\right) \tag{2-39}$$

Determination of t_e: The equivalent reduced thickness t_e can be obtained by forcing the limit moment of reduced pipe section in

$$M_L^{\,d} = 4\sigma_{02}R^2t_e \tag{2-40}$$

to be equivalent to the limit moment of cracked pipe section

$$M_L^{\,c} = 4\sigma_{02}R^2t\left(\cos\frac{\theta}{2} \quad \frac{1}{2}\sin\theta\right) \tag{2-41}$$

giving (Ref. 2.20)

$$t_e = t\left(\cos\frac{\theta}{2} - \frac{1}{2}\sin\theta\right). \tag{2-42}$$

However, in Reference 2.20 it has been observed that Equation 2-42 provides fairly good approximation only for small crack angles (0 degrees $\leq 2\theta \leq$ 90 degrees). For large crack angles ($2\theta \leq$ 120 degrees), t_e is better represented by

$$t_e = \frac{4}{\pi}t\left(\cos\frac{\theta}{2} - \frac{1}{2}\sin\theta\right). \tag{2-43}$$

For cracks with angles in the intermediate range (90 degrees $\leq 2\theta \leq$ 120 degrees), t_e can be found from linear interpolation between these limits (Ref. 2.20).

Estimation of J_p: Having estimated the M-ϕ^c_p relationship, J_p can then be evaluated by the following algebra,

$$J_p = \frac{\pi R}{2(n_1+1)\left\{\dfrac{\alpha_1}{E_1\sigma_{01}^{\,n_1-1}}\right\}^{1/n_1}}\left[\frac{L_B^{\,d}\dfrac{\partial I_B}{\partial\theta} + I_B\dfrac{\partial L_B^{\,d}}{\partial\theta}}{(L_B^{\,d}\,I_B)^{1+1/n_1}}\right] \times \left[\frac{M^{n_1}\,L_B^{\,d}\alpha_1 I_B}{E_1\sigma_{01}^{\,n_1-1}(\pi R^2t)^{n_1}}\right]^{1-\frac{1}{n_1}} \tag{2-44}$$

where the derivatives $\partial I_B/\partial\theta$ and $\partial L^d_B/\partial\theta$ are explicitly described in Appendix C. These analytic forms are very convenient for both deterministic and probabilistic elastic-plastic fracture mechanics.

Numerical Examples

Consider two circumferential TWC pipe weldments, one with $R = 52.87$ mm and $t = 8.56$ mm ($R/t \simeq 6$), and the other with $R = 55.88$ mm and $t = 3.81$ mm ($R/t \simeq 15$), each of which is subjected to constant bending moment M applied at the simply supported ends. In both pipes, it is assumed that $2\theta = 139$ degrees and $L_w = 5.59$ mm. The constitutive law for base and weld metals are assumed to follow Ramberg-Osgood model. The numerical values of flow stress σ_{0i}, modulus of elasticity E_i, and the model parameters α_i, ϵ_{0i} are shown in Table 2.19.

Table 2.19 Parameters of material constitutive law

Material, i	σ_{0i} MPa	E_i MPa	α_i	n_i
Base Metal	303.3	175,760	30.56	3.826
Weld Metal	358.5	175,760	11.96	9.370

Figures 2.25 and 2.26 show several plots of J versus M obtained from various levels of approximation for both pipes with $R/t \simeq 6$ and $R/t \simeq 15$, respectively. Also shown in the figures are the results of finite element method (FEM) which can be used as benchmark solutions for evaluating the accuracy of analytical methods. Comparisons of the results of approximate method developed in Reference 2.12 solely based on all-base or all-weld material properties with those of FEM suggest that they provide only upper and lower bounds of actual energy release rate J at any given load M. However, neither of them can be used to predict the actual values of J reliably. The all-weld metal approximation is especially poor.

Figures 2.25 and 2.26 also exhibit the results of the proposed method for several values of $\hat{a}$ representing the length of reduced thickness section. They all show reasonably good agreement with the solutions of FEM. Although $\hat{a}$ is treated here as a free parameter, an optimum value of $\hat{a}$ needs to be determined for obtaining the best estimate.

In all the example cases, the calculation of J_p is performed here based on the proportionality factor L_B^d in Equation 2-39. It apparently indicates that L_B^d has explicit functional dependency on external load parameter M, thus violating previously invoked Ilyushin's theorem. However, it can be shown that for the variation of load magnitude in the practical range, the correlation between L_B^d and M is not of strong nature. This can be proved semi-empirically from the plots of L_B^d versus M (Equation 2-39) in Figure 2.27 for both cases of $R/t \sim 6$ and $R/t \sim 15$ in the above examples. They clearly indicate that for practical load ranges, L_B^d remains essentially invariant for various combinations of $\hat{a}$, thus verifying weak correlation with M.

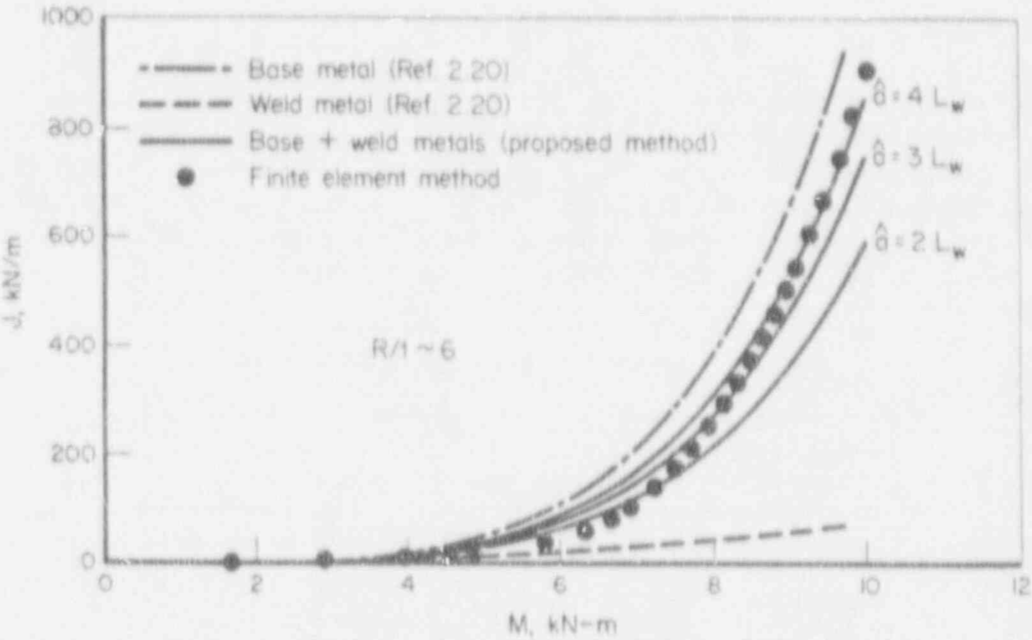

Figure 2.25 Comparisons of computed J versus M (R/t ~ 6)

SC-SA-7/91-F2.25

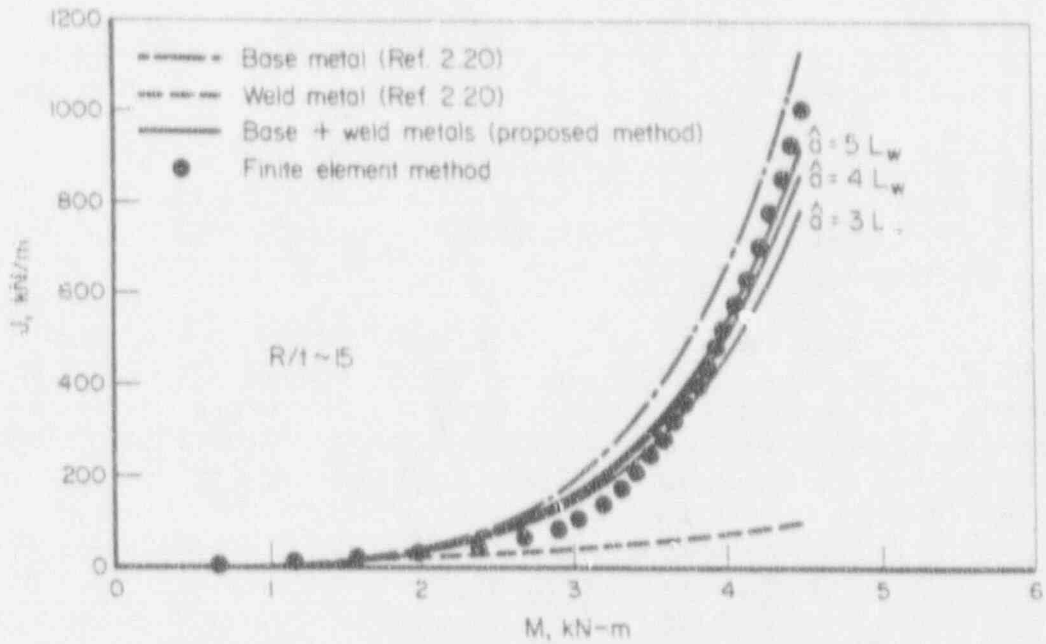

Figure 2.26 Comparisons of computed J versus M (R/t ~ 15)

SC-SA-7/91-F2.26

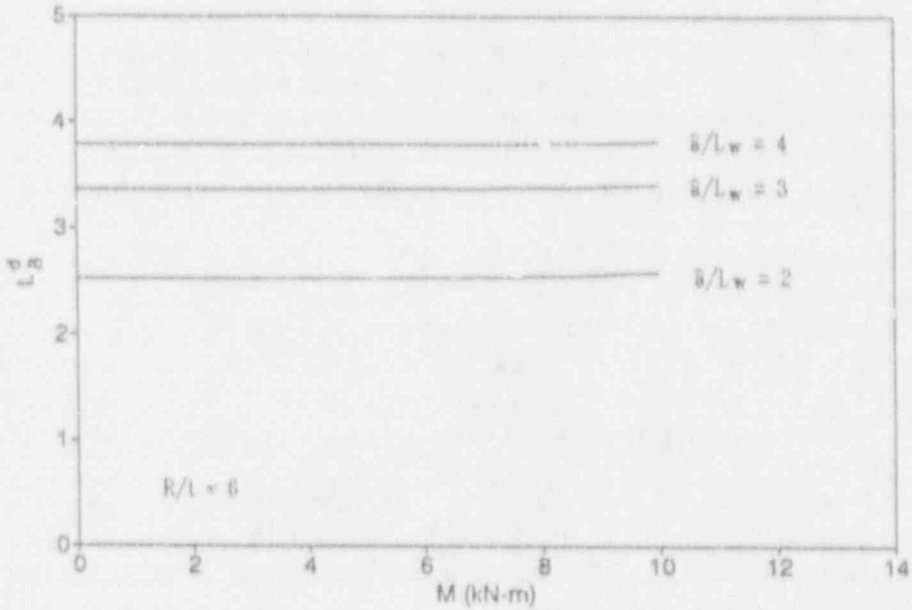

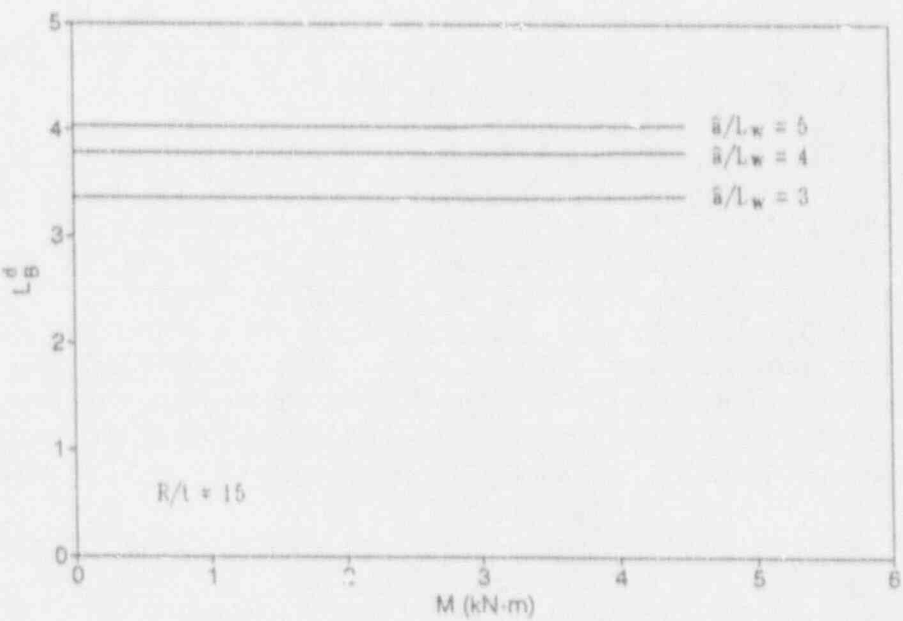

Figure 2.27 Plots of L_B^d versus M

SC-SA-7/91-F2.27

Quantification of $\hat{a}$

Several finite element analyses were carried out to determine $\hat{a}$. Following extensive comparisons with the results of finite element analysis, $\hat{a}$ was found to be relatively insensitive to the variations in the hardening parameters n_1 and n_2 of the Ramberg-Osgood models for the base and weld metals, respectively. It was also found that the optimum value of $\hat{a}/L_w$ was roughly in the neighborhood of 4 where L_w was the average length of weld metal in the pipe.

Figures 2.28 to 2.31 exhibit the plots of crack driving force J versus applied bending moment M for some of the combinations of n_1 and n_2 considered in this study. Other input parameters are kept the same as in the example problem illustrated previously. Both estimation and finite element methods are applied to compute J for a given applied moment. Comparisons of the results suggest that the estimation method with the calibrated value of $\hat{a}/L_w = 4$ (used in Figures 2.28 to 2.31) provides simple yet satisfactory measures of energy release rate J.

Note that the calibration procedure conducted here provides only a preliminary estimate of $\hat{a}$. More refined calibration will need to be performed to investigate dependency on geometry factor (e.g., R/t ratio), crack size (e.g., θ/π ratio), flow stress ratio (e.g., σ_{01}/σ_{02}), and other pertinent parameters.

Discussion

As discussed here and in References 2.12, 2.13, and 2.20, the key to developing a J-estimation scheme is to determine the reduced pipe compliance due to the presence of the crack. The reduced pipe compliance has been estimated in a number of ways including using plastic-zone correction methods in elastic solutions (Ref. 2.20), and reduced thickness sections as done here. Let us explore the consequences of this when a crack exists in a pipe weld.

Figure 2.32 shows the through-wall crack in the weld of a pipe. If the plastic zone is small in comparison to the weld width, L_w, then it is clear that an estimation scheme solution should depend only on the weld material and the corresponding Ramberg-Osgood properties. However, as the plastic zone reaches and penetrates the base metal, the far-field rotation due to the crack increases (or decreases), depending on the ratio of weld to base metal strength properties. For many types of welded nuclear piping, the base metal is of lower strength, and can accommodate more plastic flow compared to weld metal. This additional softening or plastic flow that occurs in the base metal would not occur if not for the presence of the crack. It is for this reason that the reduced thickness section included both weld and base material, i.e., the additional rotation due to crack in the base metal is caused by (weld) crack-induced plasticity.

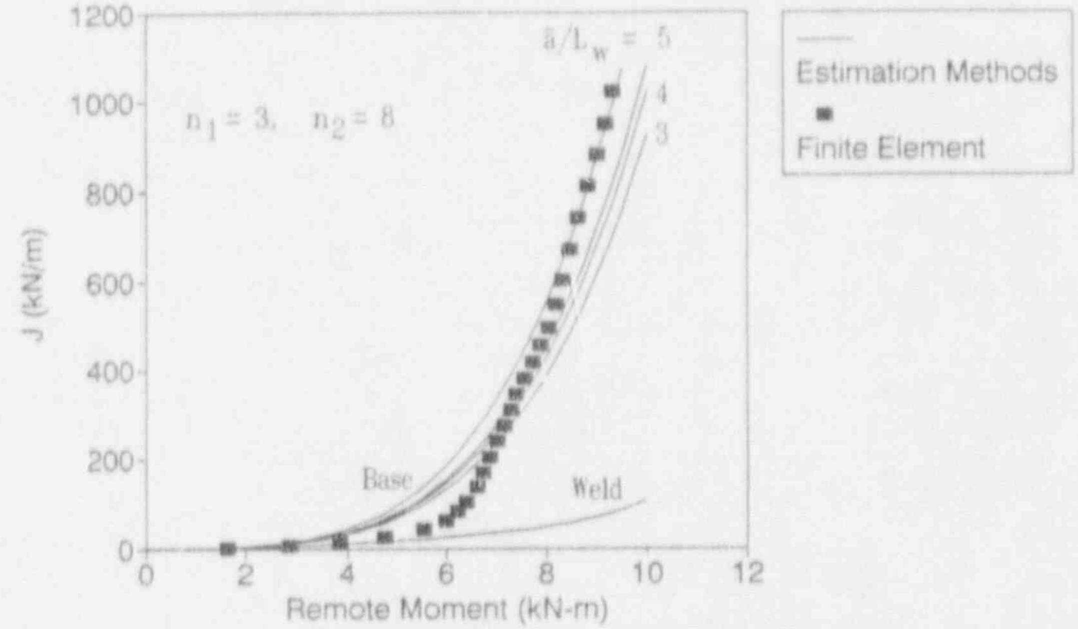

Figure 2.28 Comparisons of computed J versus M ($n_1 = 3$, $n_2 = 8$)

SC-SA-7/91-F2.28

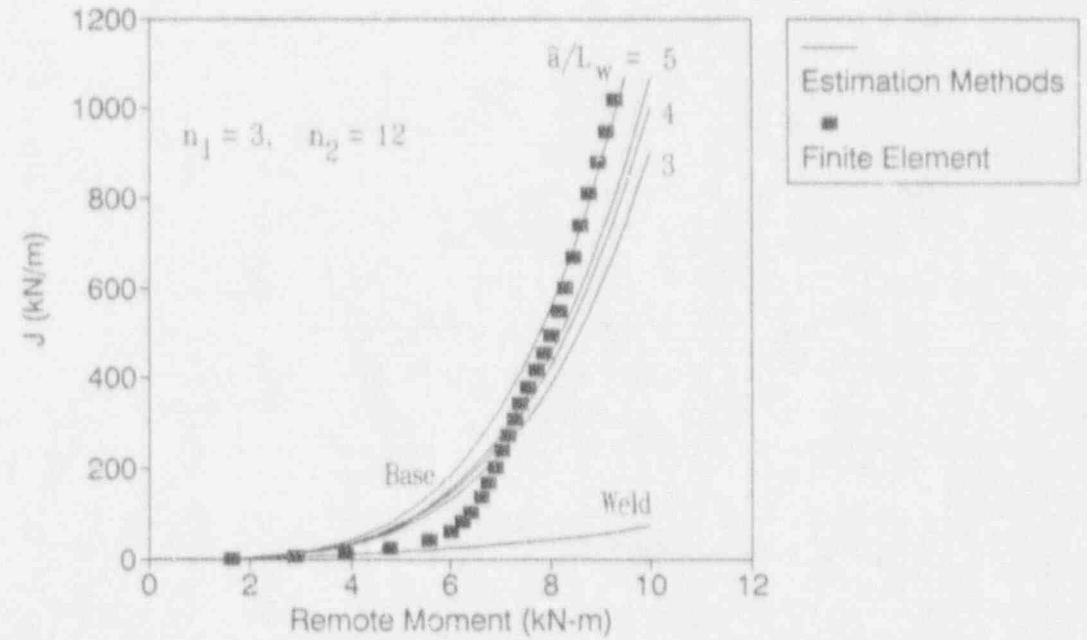

Figure 2.29 Comparisons of computed J versus M ($n_1 = 3$, $n_2 = 12$)

SC-SA-7/91-F2.29

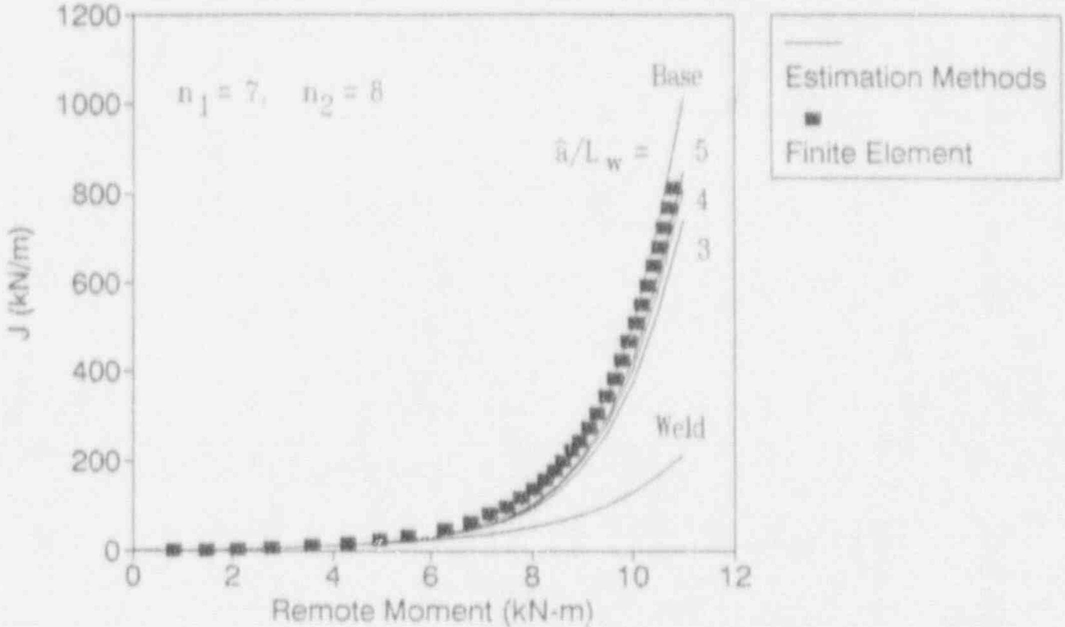

Figure 2.30 Comparisons of computed J versus M (n_1 = 7, n_2 = 8)

SC-SA-7/91-F2.30

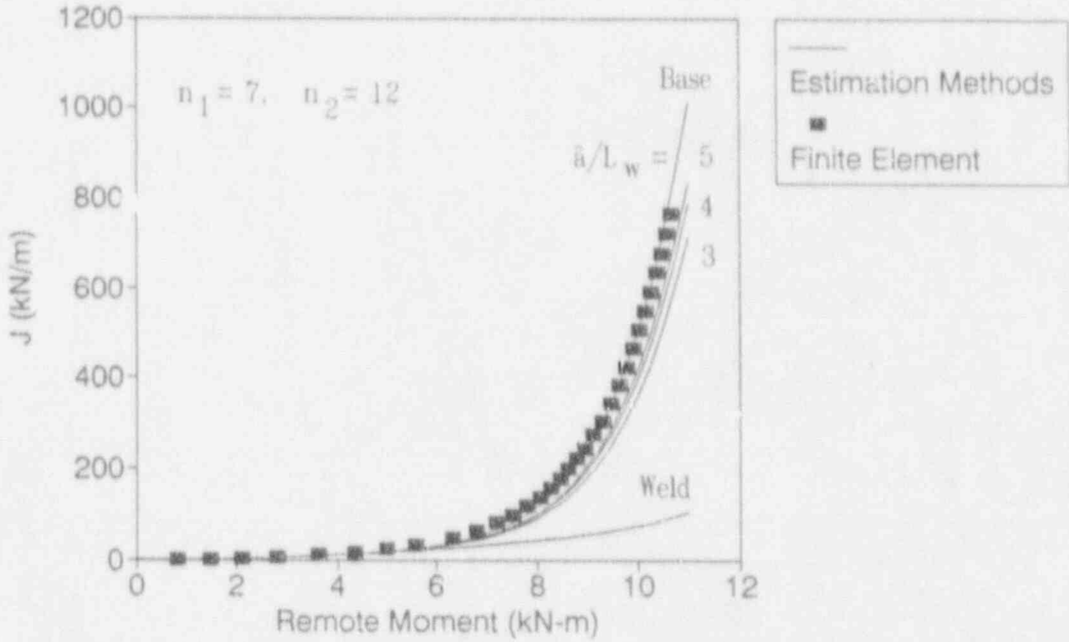

Figure 2.31 Comparison of computed J versus M (n_1 = 7, n_2 = 12)

SC-SA-7/91-F2.31

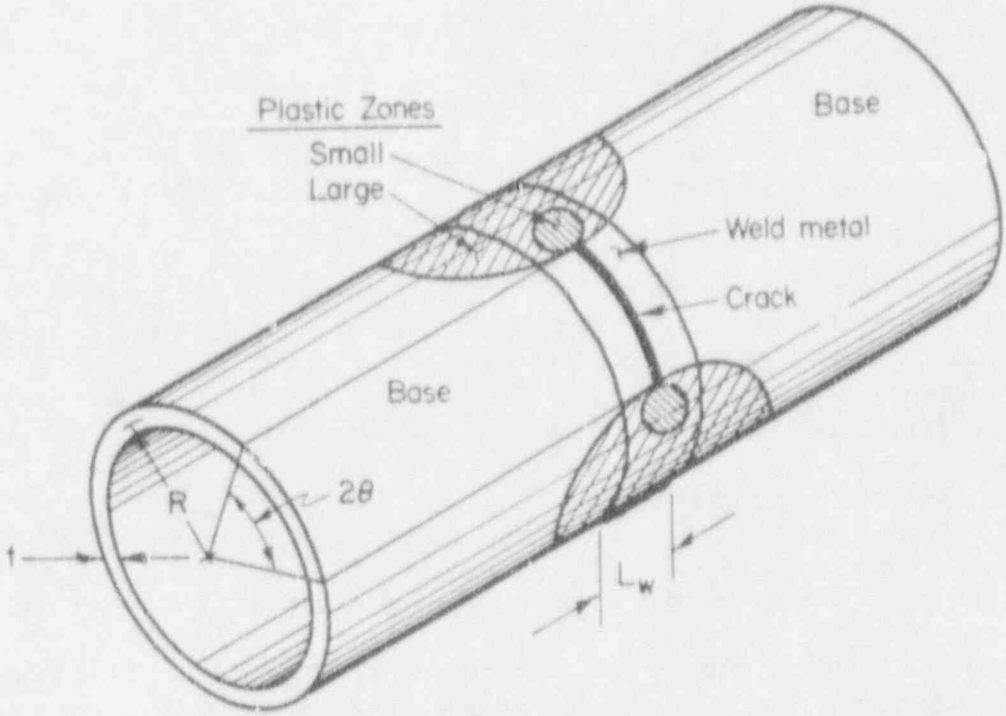

Figure 2.32 Circumferential through-wall crack in a weld showing plastic zone sizes

SC-SA-7/91-F2.32

2.4 Plans for Next Fiscal Year

During next fiscal year the following efforts will be undertaken.

2.4.1 Subtask 1.1 Material Characterization for Short TWC Pipe Experiments

Fabrication of the carbon steel weld is expected to be completed during the next fiscal year. Laboratory testing to determine material properties will probably start the beginning of FY92.

2.4.2 Subtask 1.2 Upgrading of the Large-Pipe Testing System

Upgrading of the load capacity in the current system by replacing the existing actuators and increasing local reinforcement around the actuator and end restraint locations will start in FY92.

2.4.3 Subtask 1.3 Large Diameter Pipe Fracture Experiments

The welds in the 24- and 36-inch-diameter pipes will be fabricated in FY92.

2.4.4 Subtask 1.4 Analyses for Short Through-Wall Cracks in Pipes

Various activities will continue in the next fiscal year. These include several subactivities within Activity 1.4.1 (Improve Short Through-Wall-Cracked Pipe Analysis and Compare to Existing Data).

Activity 1.4.1(a) - Numerically Assess the Effect of Plastic Ovalization on the Validity of J. Efforts next fiscal year will involve a full finite element analysis of Experiment 1.1.1.21. Review of the experimental data show that the ovalization trends reverse during the course of the experiment. This involved elongation of the pipe diameter such that the crack area extended above the circular cross section of the pipe, i.e., the vertical diameter increased, then under plastic loading the pipe flattened as it normally would for uncracked pipe in bending. This reversible behavior was postulated by Pan and can cause nonproportional loading. The nonproportional loading theoretically invalidates J, but the magnitude of this effect is not known; that is, the effect may be insignificant. Hence, this is a good experiment to analyze.

Activity 1.4.1(b) - Determine Pipe Ovalization Effects on Limit-Load Analysis. Efforts planned for next year will involve development of engineering solutions to the net-section-collapse analysis. This will be done in conjunction with the uncracked analysis in Subtask 2.4.1.

Activity 1.4.1(c) - Improve F, V, and h-Functions. The matrix of finite element analyses will be completed in FY91.

Activity 1.4.1(d) - Compare Predictions to Existing Data. This will not be initiated until all the short crack corrections have been implemented. This will be started at the end of next fiscal year, with efforts continuing the following fiscal year.

Activity 1.4.2 - Analyze Large Diameter Pipe TWC Test Results. The efforts for next year will involve analyzing the experiments completed with the current analysis methods. Once all the short crack analysis corrections have been implemented into the analyses, then all the experiments will be analyzed with those corrected methods.

Activity 1.4.3 - Analyze Through-wall Cracks in Welds. The efforts next year will involve analyzing several of the past pipe weld crack experiments from the Degraded Piping Program and Experiment 1.1.1.23.

2.4.5 Subtask 1.5 Prepare Topical Report on Short TWC Experiments and Analyses

No efforts are planned for the next fiscal year.

2.5 References

2.1 Hiser, A. L. and Callahan, G. M., "A User's Guide to the NRC's Piping Fracture Mechanics Database (PIFRAC)," NUREG/CR-4894, May 1987.

2.2 Wilkowski G. M. and others, "Degraded Piping Program - Phase II," Summary of Technical Results and Their Significance to Leak-Before-Break and In-Service Flaw Acceptance Criteria, March 1984-January 1989, by Battelle Columbus Division, NUREG/CR-4082, Vol. 8, March 1989.

2.3 Wilkowski, G. M., Marschall, C. W., and Landow, M., "Extrapolation of C(T) Specimen J-R Curves for Use in Pipe Flaw Evaluations," ASTM STP 1074, pp. 56-84, 1990.

2.4 Wilkowski, G. M. and others, "Short Cracks in Piping and Piping Welds," by Battelle, NUREG/CR-4599, Vol. 1, No. 1, May 1991.

2.5 Schmidt, R. A., Wilkowski, G. M., and Mayfield, M. E., "The International Piping Integrity Research Group (IPIRG) Program -- An Overview," SMiRT-11, Paper G12/1, August 1991.

2.6 Brust, F. W., Ahmad, J., Brickstad, B., Faidy, C., and Gilles, P., "Comparisons Between Finite Element Analysis Predictions of Fracture Experiments," in Proceedings of the Seminar on Assessment of Fracture Prediction Technology: Piping and Pressure Vessels, NUREG/CP-0037, February 1991.

2.7 Wilkowski, G. M. and others, "Analysis of Experiments on Stainless Steel Flux Welds," NUREG/CR-4878, April 1987.

2.8 Rice, J. R., "Mathematical Analysis in the Mechanics of Fracture," Fracture, Vol. II, pp. 151-311, Academic Press, 1968.

2.9 Hutchinson, J. W., J. Mech. Phys. Solids, 16, 1, pp. 13-31, 1968.

2.10 Hutchinson, J. W., J. Mech. Phys. Solids, 14, 4, pp. 337-347, 1968.

2.11 Rice, J. R. and Rosengren, G. F., J. Mech. Phys. Solids, 16, 1 pp. 1-12, 1968.

2.12 Gilles, P. and Brust, F. W., "Approximate Fracture methods for Pipes, Part 1, Theory," Nuclear Engineering and Design, 127, pp. 1-17, 1991.

2.13 Gilles, P. and Brust, F. W., "Approximate Fracture Methods for Pipes, Part II, Applications," Nuclear Engineering and Design, 127, pp. 19-31, 1991.

2.14 Shih, C. F. and Hutchinson, J. W., "Fully Plastic Solutions and Large Scale Yielding Estimates for Plane Stress Crack Problems," J. Eng. Mat. Tech., 98, pp. 289-295, 1976.

2.15 Shih, C. F., "J Integral Estimates for Strain Hardening Materials in Antiplane Shear Using Fully Plastic Solutions," ASTM STP 590, pp. 3-22, 1976.

2.16 Ilyushin, A. A., "The Theory of Small Elastic-Plastic Deformations," Vol. 10, p. 347, 1946.

2.17 Kumar, V. and Shih, C. F., "Fully Plastic Crack Solutions, Estimation Scheme and Stability Analyses for the Compact Specimen," ASTM STP 700, pp. 406-438, 1980.

2.18 Kumar, V. and others, "An Engineering Approach for Elastic-Plastic Fracture Analysis," NP 1931, EPRI, 1981.

2.19 Kumar, V. and others, "Advances in Elastic-Plastic Analysis," EPRI Final Report NP-3607, August 1984.

2.20 Brust, F. W., "Approximate Methods for Fracture Analysis of Through-Wall Cracked Pipes," NUREG/CR-4853, February 1987.

2.21 Bruckner, A., Grunmach, R., Kneifel, B., Munz, D., and Thun, G., "Fracture of Pipes with Through-Wall Circumferential Cracks in Four-Point Bending," in Circumferential Cracks in Pressure and Piping - Vol. II, ASME PVP-95, pp. 123-136, June 1983.

2.22 Shibata, K., Yasuda, Y., Onizawa, K., and Miyazono, S., "Evaluation of JAERI's Ductile Fracture Test Results on Stainless Steel and Carbon Steel Piping," in Nuclear Engineering and Design, 111, 1, pp. 135-146, 1989.

2.23 Mesloh, R. E., Sorenson, J. E., and Atterbury, T. J., "Buckling Offshore Pipelines," Gas Magazine, pp. 40-43, July 1973.

2.24 Kurjel, G. L., Sampath, S. G., Popelar, C. H., Johns, T. C., and Sorenson, J. E., "The Inelastic Collapse and Buckling of Deep Water Pipelines under Combined Moment, Pressure, and Axial Tension," Report to the Deep Water Offshore Pipeline Group, March 1976.

2.25 Öberg, H., Experimental Report No. HöB 790 7547, Department of Strength and Materials, The Royal Institute of Technology, Fack 100 44, Stockholm, Sweden, July 1990.

2.26 Sanders, J. L. Jr., "Circumferential Through-Crack in a Cylindrical Shell Under Combined Bending and Tension," Journal of Applied Mechanics, Vol. 50, p. 221, March 1983.

2.27 Tada, H., Paris, P., and Irwin, G., The Stress Analysis of Cracks Handbook, Del Research Corporation, 1973.

2.28 Paris, P. C. and Tada, H., "The Application of Fracture Proof Design Methods Using Tearing Instability Theory to Nuclear Piping Postulating Circumferential Through-Wall Cracks," NUREG/CR-3464, September 1983.

2.29 Rice, J. R., Journal of Applied Mechanics, Trans. ASME, Vol. 35, pp. 379-386, 1968.

2.30 Kanninen, M. F. and others, "Mechanical Fracture Predictions for Sensitized Stainless Steel Piping with Circumferential Cracks," Final Report. EPRI NP-192, September 1976.

2.31 Klecker, R. and others, "NRC Leak-Before-Break (LBB.NRC) Analysis Method for Circumferentially Through-Wall-Cracked Pipes Under Axial Plus Bending Loads," NUREG/CR-4572, May 1986.

2.32 "Evaluation of Flaws in Austenitic Steel Piping" (Technical basis document for ASME IWB-3640 analysis procedure), prepared by Section XI Task Group for Piping Flaw Evaluation, EPRI Report NP-4690-SR, April 1986.

2.33 "Evaluation of Flaws in Ferritic Piping," EPRI Report NP-4824M, prepared by Novetech Corporation, October 1986.

2.34 Rahman, S., Brust, F., Nakagaki, M., and Gilles, P., "An Approximate Method for Estimating Energy Release Rates of Through-Wall Cracked Pipe Weldments," in Fatigue, Fracture and Risk-1991, ASME Special Publication PVP - Vol. 215, pp. 83-92, June 1991.

3. TASK 2 SHORT SC PIPE EVALUATIONS

3.1 Task Objective

The objectives of this task are to modify and verify analyses for short surface-cracked (SC) pipe using existing and new data on large diameter pipe.

3.2 Task Rationale

These results will verify and may refine analyses that have been used for pragmatic in-service flaw evaluations such as those in ASME Section XI.

3.3 Task Approach

This task has been divided into five subtasks:

- Subtask 2.1 Material characterization for surface-cracked pipe experiments
- Subtask 2.2 Small diameter pipe fracture experiments in pure bending for limit-load ovalization correction
- Subtask 2.3 Large diameter surface-cracked pipe fracture experiment in combined bending and tension (pressure)
- Subtask 2.4 Analysis of short surface cracks in pipes
- Subtask 2.5 Topical report.

The details of each of these subtasks are presented in the following paragraphs.

3.3.1 Subtask 2.1 Material Characterization for Surface-Cracked Pipe Experiments

Some of the materials to be characterized in Subtask 2.1 were previously discussed in Task 1. Significant progress was made in Subtasks 2.2 and 2.4 during the past reporting period and is described below.

3.3.2 Subtask 2.2 Smaller Diameter Pipe Fracture Experiments in Pure Bending for Limit-Load Ovalization Correction

3.3.2.1 Objective

This effort will develop data for internally surface-cracked pipe under four-point bending that can be used to assess the ovalization correction for a limit-load failure.

3.3.2.2 Rationale

In the Degraded Piping Program, an empirical correction for the net-section-collapse (NSC) analysis of circumferentially surface-cracked pipe in pure bending was developed (Ref. 3.1). It was found that the correction was a function of the pipe R/t ratio; see Figure 3.1. Data on smaller crack sizes are needed to generalize such a correction. The correction for the limit-load case is necessary since many of the elastic-plastic fracture analyses and code flaw assessment criteria have the limit-load solutions embedded within them.

3.3.2.3 Approach

To satisfy the need for data to verify the analyses, three experiments will be conducted under pure bending. The experiments to be conducted are given in Table 3.1.

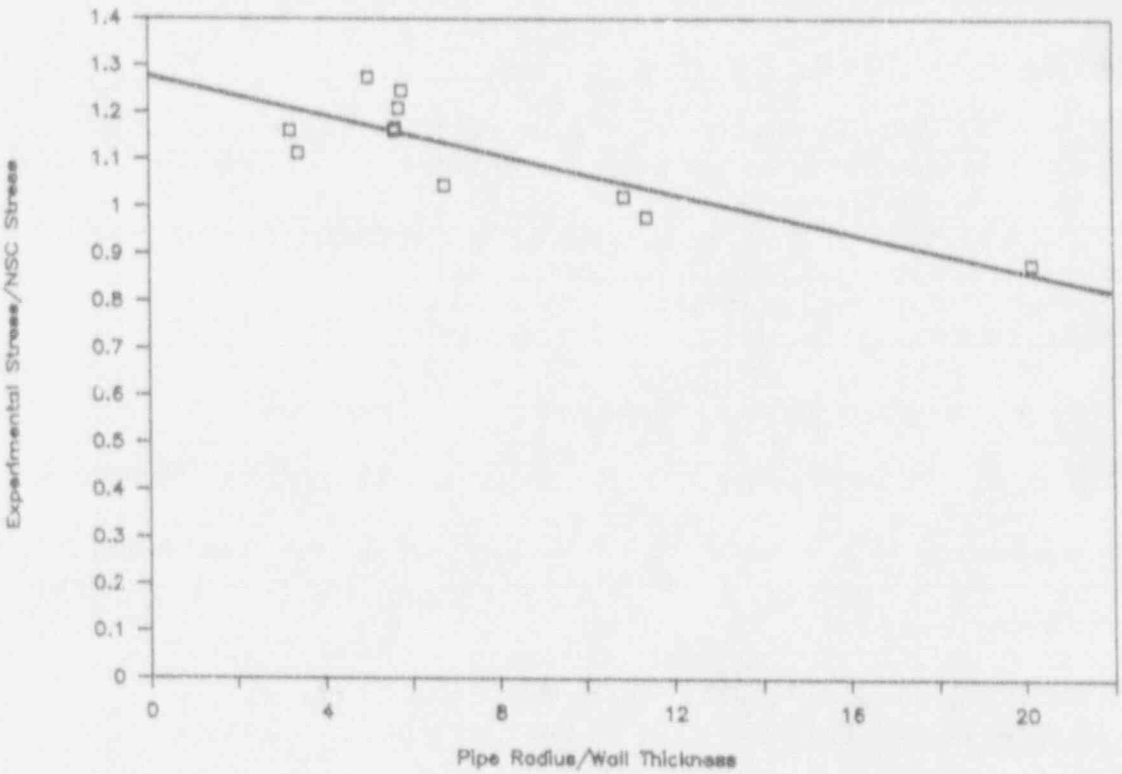

Figure 3.1 Plot of the ratio of the maximum experimental stress to the predicted net-section-collapse stress as a function of the pipe R/t ratio for a series of surface-cracked pipe experiments for which the DPZP is greater than 0.2

SC-SA-7/91-F3.1

Note that the three pipe geometries selected in this study are pipes obtained from canceled nuclear plants and, hence, represent the range of R/t geometries that may be used in nuclear piping. The largest radius to thickness (R/t) ratio is 21.3 and the smallest is 3.8.

Table 3.1 Smaller diameter pipe with short cracks under bending for Subtask 2.2

Test No.(a)	Diameter	Schedule	R/t	Material	Temperature	θ/π, a/t(b)
1.2.1.20	16 inches	40S	21.3	TP316	288 C (550 F)	0.25, 0.5
1.2.1.21	6 inches	XXS	3.8	TP304	288 C (550 F)	0.25, 0.5
1.2.1.22	6 inches	40	11.8	TP304	288 C (550 F)	0.25, 0.5

(a) Test numbers are consecutive with those in the Degraded Piping Data Record Books.
(b) d/t = surface crack depth/pipe thickness θ/π = circumferential crack length/pipe circumference.

The surface flaw size to be used will be determined by parametric analysis. The smallest flaw size that will fracture before the pipe begins to buckle will be assessed by estimating the buckling and fracture moments of the cracked pipe and comparing the two.

The data to be collected during these experiments are

- applied load,
- load-line displacement,
- rotation due to the crack and the uncracked pipe rotation,
- crack-opening displacement at the center of the surface crack (at two heights from the pipe surface),
- ovalization of the pipe in the horizontal and vertical directions at the crack plane and remote from it,
- d-c electric potential at the crack centerline and at three other locations along the surface crack, and
- temperature at various locations along the pipe.

These results will be documented in a consistent fashion with experiments from the Degraded Piping Program - Phase II. The results of these experiments will be compared with the NSC analysis and the different J-estimation schemes with and without the improvements from Subtask 2.4.

3.3.2.4 Progress

During this reporting period, the two nominal 6-inch-diameter pipe experiments have been completed. The first step was to determine the smallest size flaw that could be tested and not have the pipe fail by buckling. This procedure is described below, and is followed by the experimental results.

Determination of Surface Crack Size

Since it was desirable to conduct all the surface-cracked pipe experiments with the same nondimensional flaw size, i.e., with the same d/t and θ/π ratios, it was necessary to determine the worst case where buckling would occur. This would be for either the nominal 6-inch-diameter Schedule 40 stainless steel pipe experiment or the 16-inch-diameter Schedule 40 stainless steel pipe experiment.

The initial flaw size considered was a circumferential crack length of 25 percent of the pipe circumference and 50 percent of the wall thickness. This flaw size was considered because it is typical of the surface cracks found in service. Of additional interest, finite element analyses of this test may be conducted by the Westinghouse Savannah River staff.

To make the assessment of the acceptability of this flaw size, the pipe buckling analyses (see Section 2) were used for comparison to the NSC predicted failure loads. For the nominal 6-inch-diameter Schedule 40 pipe, the NSC predicted moment versus crack length, θ/π, is given as a function of crack depth to thickness ratio, d/t. In addition, the predicted buckling loads are given using either the ABAQUS elbow element or the Mesloh formula. Both buckling predictions were found to underpredict the actual buckling loads of stainless steel pipe; see Section 2. Hence the buckling analyses were modified by using a correction to give mean values of the JAERI uncracked stainless steel pipe experiments.

Figure 3.2 shows the calculations for the nominal 6-inch-diameter Schedule 40 pipe. The predicted buckling loads are very close for the modified ABAQUS and Mesloh methods. For a θ/π of 0.25, the buckling loads correspond to a crack depth to thickness ratio, d/t, of approximately 0.7 (Points E or D in Figure 3.2) rather than 0.5 as desired (Point C in Figure 3.2).

To make a better assessment of the reliability of this analysis, a past Degraded Piping Program experiment (Ref. 3.1) on this same pipe was evaluated. That experiment was 4112-2. The R/t of the pipe was 11.9, the θ/π was 0.5, and d/t was 0.66. As shown in Figure 3.1, the experimental to NSC predicted failure load was 0.9; see Points A and B in Figure 3.2, as well as Point 2 in Figure 3.1. Using this 0.9 correction for the $\theta/\pi = 0.25$ flaw gives a predicted failure load slightly above the buckling load; see Point F in Figure 3.2. Since the failure load relative to the NSC predicted load for a shorter crack is expected to be even lower than for the larger crack, it was decided to conduct this experiment with a crack having $\theta/\pi = 0.25$ and $d/t = 0.5$.

Similar calculations were made for all the other experiments, but this experiment was found to be the worst case.

Results of Experiment 1.2.1.22 - 6-inch-diameter Sch. 40 TP304

This was the first short surface crack experiment in this program. The pipe was used in a prior long surface crack experiment in the Degraded Piping Program (4112-2) and had a Battelle pipe number of DP2-A7. The flaw in Experiment 1.2.1.22 had a constant depth of 50 percent of the thickness, and a length of 25 percent of the circumference. The flaw was made by electric

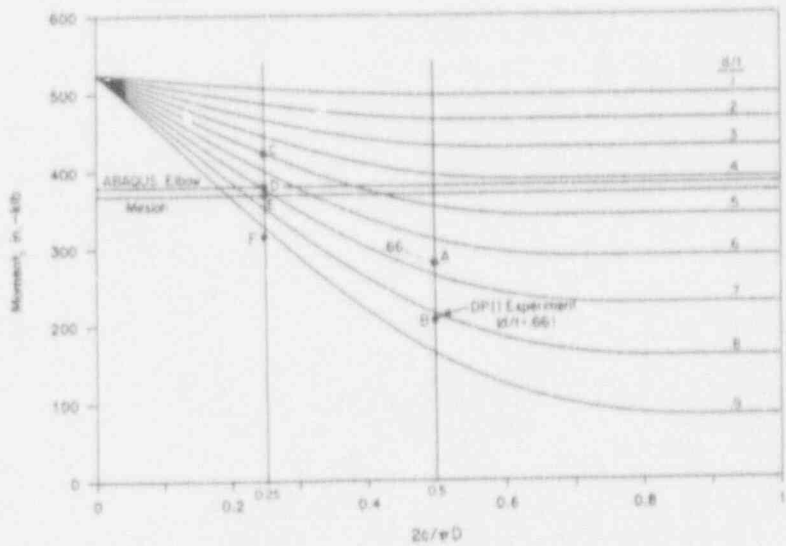

Figure 3.2 Pretest calculations for 6-inch-diameter Schedule 40 stainless steel pipe test (Experiment 1.2.1.22)

SC-SA-7/91-F3.2

discharge machining from the inside of the pipe with a notch root radius of 0.127 mm (0.005 inch). Because of the internal flaw machining and instrumentation requirements, a girth weld 100 mm (4 inches) from the crack plane was required.

The pipe was heated to 288 C, and tested without internal pressure. The pipe was loaded in four-point bending using the same apparatus as used in many of the past Degraded Piping Program and IPIRG Program experiments. The loading rate was quasi-static, and conducted in monotonic displacement control.

The data recorded were total load, load-line displacement of the test machine, center-crack-opening displacement, pipe rotation 127 mm (5 inches) either side of the crack plane, and d-c electric potential measurements across the crack. The total load versus load-line displacement data are shown in Figure 3.3. The maximum load corresponded to the start of a buckle at the girth weld 100 mm from the crack plane; see Figure 3.4. The surface crack initiated well after the buckle started, and a small instability occurred as the surface crack propagated through the wall and completely around the machined notch ligament. The crack then grew stably as a through-wall crack.

The maximum load at which buckling occurred agreed excellently with the predicted buckling loads. Interestingly, fracture still occurred. Previously it was believed that once buckling started, a fracture would not start because the energy would be going toward making the buckle. However, the CMOD data showed that the surface crack was continually loaded during the buckling process.

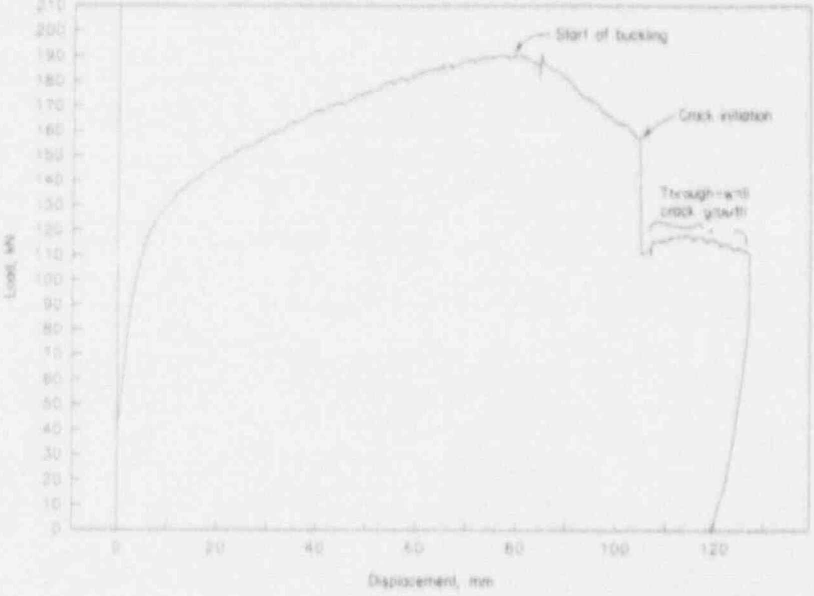

Figure 3.3 Total load versus load-line displacement of Experiment 1.2.1.22 6-inch-diameter Schedule 40 TP304 pipe with short surface crack (d/t = 0.5, θ/π = 0.25)

SC-SA-7/91-F3.3

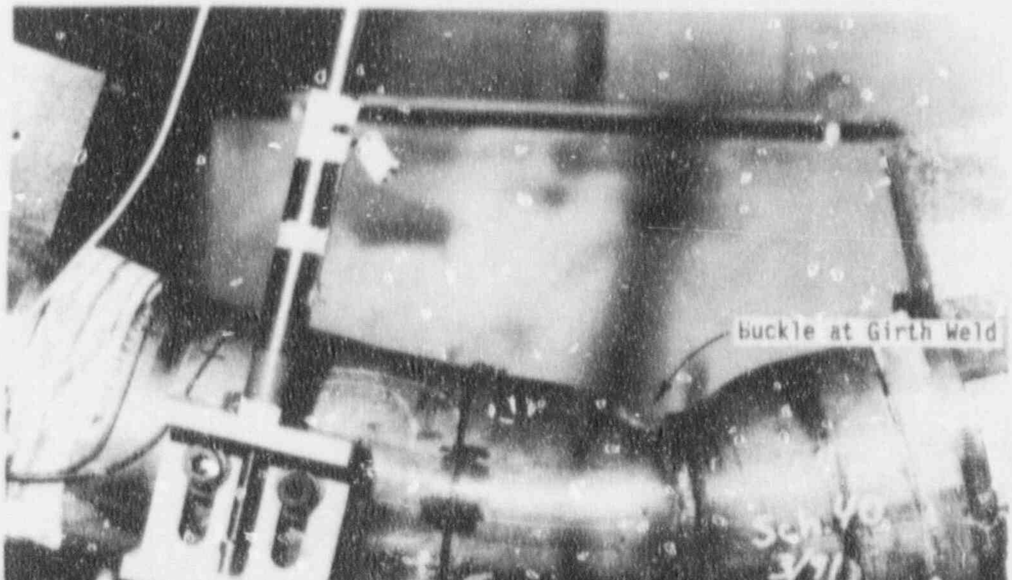

Figure 3.4 Post-test photograph of 6-inch Schedule 40 stainless steel internal surface crack showing buckling (Experiment 1.2.1.22)

SC-M-3/91-F5

Results of Experiment 1.2.1.21 - 6-inch-diameter Sch. XXS TP304

The pipe was used in a prior long surface-cracked pipe experiment in the Degraded Piping Program (4112-4) and had a Battelle pipe number of DP2-A35. The flaw in Experiment 1.2.1.21 had a constant depth of 50 percent of the wall thickness, and a length of 25 percent of the pipe circumference. The flaw was made by electric discharge machining from the inside of the pipe with a notch root radius of 0.127 mm (0.005 inch). Because of the internal flaw machining and instrumentation requirements, a girth weld 100 mm (4 inches) from the crack plane was required.

The pipe was heated to 288 C, and tested without internal pressure. The pipe was loaded in four-point bending using the same apparatus as used in many of the past Degraded Piping Program and IPIRG program experiments. The loading rate was quasi-static, and conducted in monotonic displacement control.

The data recorded were the same as Experiment 1.2.1.21. The total load versus load-line displacement data are shown in Figure 3.5. The second major unload occurred because the loads were so high that alignment pins were breaking. The specimen was unloaded and reinforcing on the test frame was made. The reloading on the second cycle occurred several days later. In this experiment, no buckling of the pipe occurred. Crack initiation occurred right at maximum load, hence limit-load requirements were met.

Analyses of these experiments are described in Activity 2.4.3.

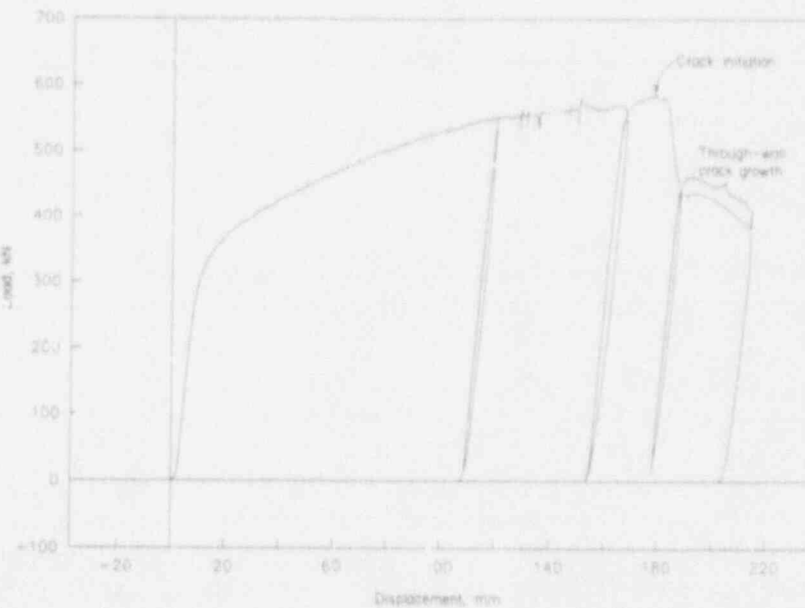

Figure 3.5 Total load versus load-line displacement of Experiment 1.2.1.21 6-inch-diameter Schedule XXS TP304 pipe with short surface crack (d/t = 0.5, θ/π = 0.25)

SC-SA-7/91-F3.5

3.3.3 Subtask 2.4 Analysis of Short Surface Cracks in Pipes

3.3.3.1 Objective

The objective of this subtask is to develop, improve, and verify the engineering analyses for short circumferential surface-cracked large diameter pipe where elastic-plastic fracture is expected.

3.3.3.2 Rationale

The short surface-cracked (SC) pipe analysis improvements are aimed at assessing and improving the ASME Section XI flaw evaluation criteria (Refs. 3.2 and 3.3).

3.3.3.3 Approach

The five activities in this subtask are:

Activity 2.4.1	Uncracked pipe analysis
Activity 2.4.2	Improve SC.TNP and SC.TKP analyses
Activity 2.4.3	Compare improved limit-load solutions to short surface-cracked small diameter pipe data
Activity 2.4.4	Analyze large diameter surface-cracked pipe test data
Activity 2.4.5	Evaluate procedures in J-estimation schemes for surface cracks in welds.

For background to the TWC analyses, the uncracked pipe analyses were presented in Section 2 for Subtask 1.4.1(b). No efforts were conducted in Activities 2.4.4 and 2.4.5.

Activity 2.4.2 Improve SC.TNP and SC.TKP Analyses.

Objective

This is the first activity involving the analyses of the SC pipe in this subtask. The objective is to improve the existing circumferential SC pipe J-estimation schemes developed in the Degraded Piping Program.

Rationale

The finite-length, SC pipe J-estimation schemes were initially developed in the Degraded Piping Program (Ref. 3.1). At the time, this development represented a major step in assessing finite-length surface-cracked pipe. However, it was recognized that several improvements were needed. Such improvements would make the existing methods more realistic (hence, defensible) for assessing the ASME Section XI flaw evaluation criteria (Refs. 3.2 and 3.3). The ASME Section XI criteria are based on a Z-factor that comes from a through-wall-cracked pipe analysis, and not a surface-cracked pipe analysis. A surface-cracked-pipe analysis basis for a Z-factor approach should lead to more realistic and defensible criteria.

Approach

Several improvements need to be made in the existing surface-cracked pipe J-estimation scheme solutions. Some of the more significant ones are:

(a) Verify J_p solutions by FEM analyses
(b) Add J_e to the SC.TNP and SC.TKP solutions
(c) Improve rotation predictions
(d) Include ovalization correction for surface-cracked pipe
(e) Extend LBB.ENG approach to circumferentially surface-cracked pipe
(f) Include pressure and bending effects in surface-cracked pipe solutions
(g) Develop a J-estimation scheme for an external surface crack.

Significant progress was completed for Activities 2.4.2.(f) and (g) and are presented below.

Activity 2.4.2(f) Include Pressure and Bending Effects in Surface-Cracked Pipe Solutions

The current SC.TKP and SC.TNP solutions are for pipe in pure bending (Ref. 3.1). The general analysis procedure can handle combined loading, but new H_n and G_n functions will be derived. A numerical integration method to determine their values will be implemented in the computer code. This is a relatively simple effort because the equations to calculate the H_n and G_n functions already exist and were published in Reference 3.1.

Since this activity and the following Activity 2.4.2(g) are closely related, progress on these two are reported together in the following section.

Activity 2.4.2(g) J-Estimation Scheme for an External Surface Crack

The objective of this effort is to develop an engineering analysis for short circumferential external SC pipe under combined bending and tension loads.

J-estimation schemes pertinent to piping have been developed principally for circumferential through-wall and internal surface cracks. However, fatigue crack loading can result in circumferentially oriented external surface cracks. Unfortunately, these are not suitable J-estimation schemes for such cracks.

The development of an external SC J-estimation scheme involves extending the analysis previously developed at Battelle in the NRC's Degraded Piping Program for internal surface cracks. This involves relatively small modifications to account for the external crack geometry, but extensive changes to account for internal pressure. To include tension-induced loading from pressure, the assumption will be made that pressure and bending are applied simultaneously in a manner that stresses in the pipe vary proportionally to the applied load. Note that this assumption is inherent in the use of any J-integral based approach to elastic-plastic fracture mechanics. In addition to the above changes, linear-elastic solutions available in the literature will be used to provide an estimate of the elastic component of J.

Progress

The technical work in this activity has been completed. Two programs EXTCRK7.EXE and INTCRK7.EXE that can be used to analyze external and internal circumferential surface cracks, respectively, were developed. Each of the programs provides the option of using either thick-wall (SC.TKP) or thin-wall (SC.TNP) analysis.

The SC.TNP and SC.TKP predictions were compared to the results from the pure bending, internal SC pipe experiments (Ref. 3.1) in the Degraded Piping Program. These results showed that SC.TKP underpredicted the experimental maximum loads by 20 to 40 percent. This effectively means that SC.TKP was overpredicting the applied J. The SC.TNP analysis was more accurate. The SC.TNP predicted maximum loads were -10 to +20 percent of the experimental maximum loads.

The estimation scheme developed in this subtask can be used to analyze surface flaws of constant depth as well as elliptically shaped flaws under either pure bending loads or under combined bending and internal pressure. Note that in the Degraded Piping Program only constant depth internal surface crack analyses were developed. Figure 3.6 shows the flaw geometries and loading configurations.

For a given pipe size, flaw geometry, and material's stress-strain curve, the analyses give the crack driving force, J, for any given value of the applied bending moment and internal pressure. To verify the code, the predictions of the code were compared with the finite element results obtained by Professor M. Kikuchi of Science University of Tokyo for Experiment No. 4131-4 of the Degraded Piping Program. This experiment involved a pipe with diameter, D_o, of 10.7 inches (272 mm), wall thickness, t, of 16.6 mm (0.654 inch), R/t of 8.2, and an internal flaw of uniform depth, a, of 10.9 mm (0.43 inch). The pipe material stress-strain curve is represented by the Ramberg-Osgood equation with $\alpha = 3.46$ and $n = 4$. The pipe was subjected to four-point bending and had an internal pressure, p, of 18.3 MPa (2650 psi). First, neglecting the effects of pressure loading, Figure 3.7 shows a plot of the predicted value of J at various values of half the applied bending load P. As can be seen up to values of P of 66.7 kN (15,000 pounds), the values of J predicted by the estimation schemes are in agreement with the FE results. At higher loads the predictions for J using the thick-wall analysis are higher than those from the FE results. The predictions from the thin-wall analysis are lower than those from the FE calculations. This is consistent with past Degraded Piping experimental comparisons (Ref. 3.1).

Results for the case of combined bending and pressure loading are shown in Figure 3.8. For this case the deviation between the FE results and the estimation scheme occurs at a lower load of about 35.6 kN (8,000 pounds). As for the case of pure bending, the predictions for J from the thick-wall analysis are significantly higher than those from FE results at the higher loads and the predictions for J from the thin-wall analysis are lower than the FE results at the higher loads.

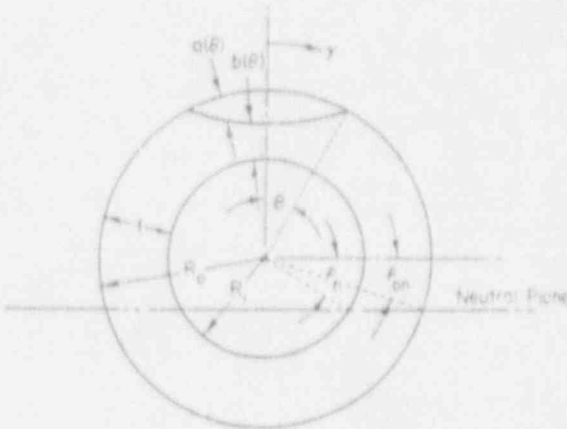

(a) External Surface Flaw Geometry

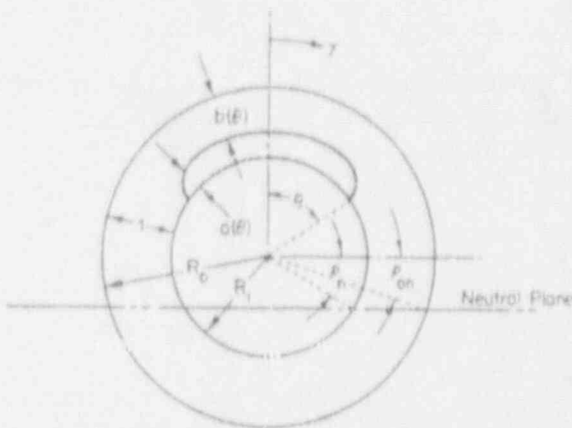

(b) Internal Surface Flaw Geometry

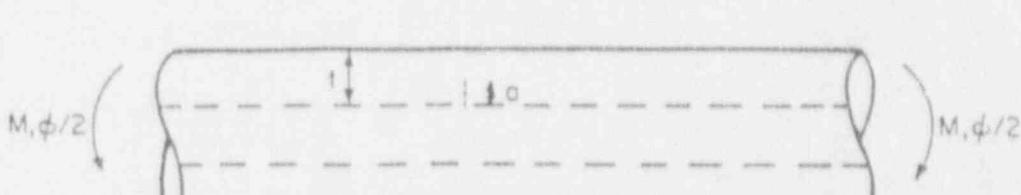

(c) Surface-cracked Pipe Under Bending and Pressure Loads

Figure 3.6 Flaw geometry and loading configuration for surface-cracked pipe

SC-SA-7/91-F3.6

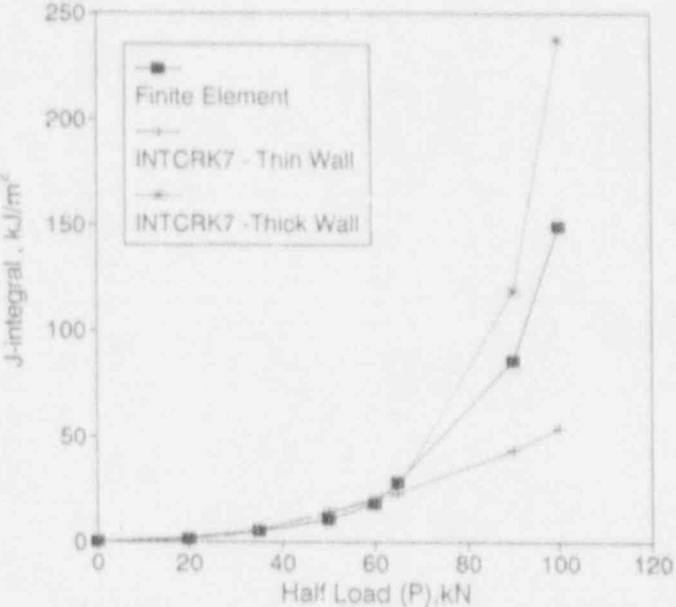

Figure 3.7 Comparison between J-estimation scheme (INTCRK7) and FE results for internal-surface-cracked pipe Experiment 4131-4, neglecting effects of internal pressure

SC-SA-7/91-F3.7

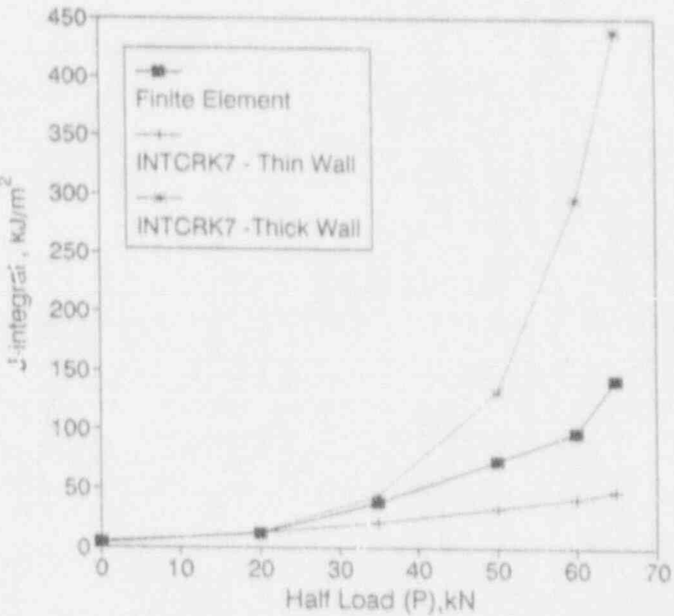

Figure 3.8 Comparison of J-estimation scheme (INTCRK7) and FE results for Experiment 4131-8, including effects of internal pressure

SC-SA-7/91-F3.8

It should be recognized that even with the current method, the error in predicting the load at a given J value would not be as large as the error in predicting J for a given load. For example, at the J_i value of 0.155 MJ/m^2 (885 pounds/inch) for the material, Figure 3.8 gives an initiation load (P_i) to be 51.2 kN (11,520 pounds) by the thick-wall estimation formula and 66.0 kN (14,830 pounds) by the finite element results. The experimental value for P_i is 73.4 kN (16,510 pounds).

Since FE results for the case of an external surface crack are not available at this time, a comparison with the predictions of the estimations scheme cannot be made. There are some older, very thick-walled, external surface-cracked pipe experiments conducted at Battelle that could be used for verification of EXTCRK7.EXE if desired (Ref. 3.4). However, the analytical development for the external and internal crack cases is very similar and should provide similar results.

One of the incentives for this work was to provide an analysis for Brookhaven National Laboratory staff to analyze the low cycle fatigue crack growth in a MITI pipe system experiment conducted in Japan. A note of caution is necessary for this application. Typically low cycle fatigue crack growth data are generated using the Dowling approach where $da/dN = C(\Delta J)^m$ (Ref. 3.5). Such data are developed from laboratory specimen tests (i.e., C(T) specimens) where J is calculated by integrating the cyclic load-displacement record. For negative load ratios (lowest/highest load in the test), the compressive load-displacement area is used only down to a point where crack closure is suspected to occur. As an example, the compressive load at which crack closure occurs for fully reverse loading can be at 30 percent of the maximum tensile load. Hence, the Dowling J value is an "operational J". This is not the same J as calculated by finite element analysis or pipe J-estimation schemes. "Adjustments" to the pipe J applied values are needed to give an operational J consistent with the Dowling values.

The computer programs initially developed, EXTCRK7.EXE and INTCRK7.EXE, will eventually be incorporated into a user-friendly framework of a surface crack version of NRCPIPE.

Activity 2.4.3. Compare Improved Limit-Load Solutions to Short-Surface-Cracked Small-Diameter Pipe Data

The objective of this activity is to determine if corrections to the net-section-collapse (NSC) analysis are needed for pipe with short circumferential surface cracks. The NSC analysis assumes the pipe remains circular. However, with short cracks the load increases, causing the pipe to ovalize. This ovalization causes the loads to be less than if the pipe remained circular.

Progress

Two short surface-cracked pipe experiments have been conducted to date. These experiments were on relatively small diameter TP304 stainless steel that were high in toughness so that limit-load, not elastic-plastic fracture, should occur. Details of the experimental data were given in Subtask 2.2.

Past efforts in the Degraded Piping Program showed that a correction to the NSC analysis, which is a function of the R/t ratio, is needed for surface-cracked pipe. This relation is shown in Figure 3.1 where, at that time, a least squares fit was drawn through the pipe test data for which the toughness was sufficient to cause failure at limit-load conditions. All of these experiments were for the same dimensionless flaw size of $d/t = 0.66$ and $\theta/\pi = 0.5$. It was felt that smaller flaws would have higher failure loads; hence, pipe ovalization may become a more significant factor in potentially reducing the experimental failure stresses. Since the NSC analysis assumes the pipe remains circular, and ovalization reduces the stiffness of the pipe, the tendency would be for the NSC analysis to overpredict the failure loads for pipe experiencing ovalization during fracture. The ovalization and pipe buckling for uncracked pipe is known to be a function of the pipe mean radius-to-thickness ratio, R_m/t.

Figure 3.9 is a plot of the ratio of the experimental maximum stress to the NSC predicted stress versus the R_m/t ratio. The NSC predictions are based on a flow stress defined as the average of the actual yield and ultimate strengths of each pipe. The upper dashed line comes from a best linear regression fit of the long surface crack data from the Degraded Piping Program. The data in Figure 3.9 represent only those experiments for which limit-load conditions should be satisfied.

The two 6-inch nominal diameter short surface crack experiments from this program are also shown in Figure 3.9, as well as two 4-inch nominal diameter short surface crack experiments from an older EPRI program conducted at Battelle (Ref. 3.6). Table 3.2 gives the data for several

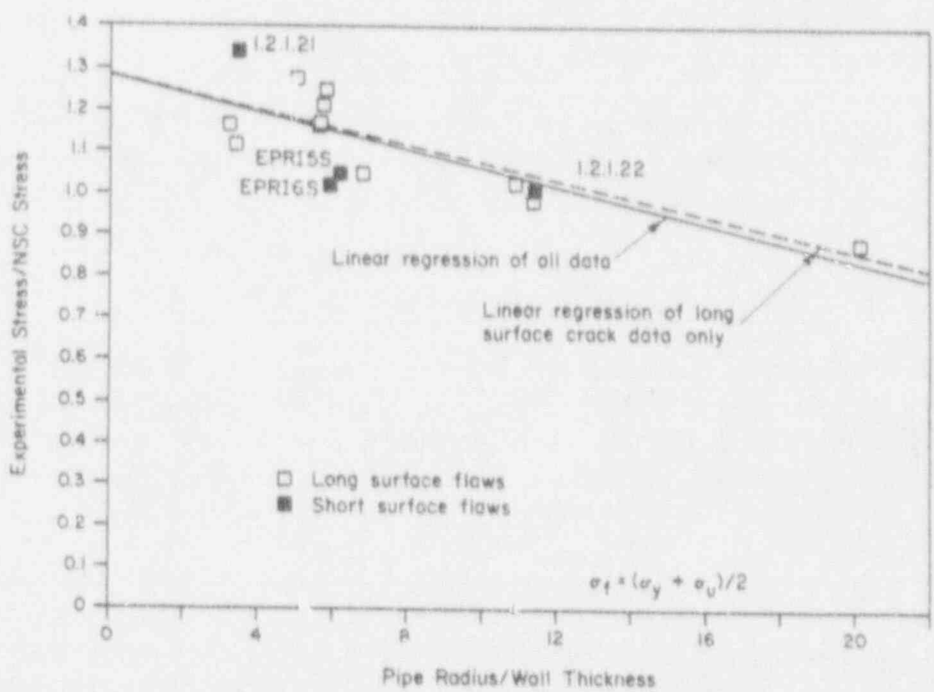

Figure 3.9 Comparison of experiment maximum moment/net-section-collapse moment versus R_m/t for short and long surface-cracked pipe experiments

SC-SA-7/91-F3.9

Table 3.2 Short versus long surface crack maximum moment/net-section-collapse predicted moments

Experiment Number	d/t	$2c/\pi D$	R_m/t	Exp/NSC[a]
4112-4[b]	0.653	0.44	3.24	1.16
4112-2[b]	0.634	0.50	11.4	0.98
1.2.1.21	0.50	0.22	3.49	1.34
1.2.1.22	0.50	0.25	11.4	1.01
5S[c]	0.39	0.25	6.20	1.05
6S[c]	0.61	0.25	5.98	1.02

(a) Experimental maximum moment/net-section-collapse predicted maximum moment ($\sigma_f = [\sigma_y + \sigma_u]/2$).
(b) From Degraded Piping Program, Ref. 3.1.
(c) From EPRI NP-2347, Vol. 2, Ref. 3.6.

short surface crack experiments reflected in Figure 3.9. It can be seen from Figure 3.9 that the short surface crack data from this program and the previous Battelle/EPRI program agree well with the long surface crack data from the Degraded Piping Program. In fact, the linear regression line for the entire data set (long and short surface cracks) agrees remarkably well with the linear regression line for the data set that includes only the long surface crack data from the Degraded Piping Program. Consequently, it appears a single correction factor (independent of flaw size) to the net-section-collapse analysis to account for ovalization effects may be appropriate. During the next reporting period a 16-inch-diameter Schedule 30 (t = 9.52 mm [0.375 inch]) stainless steel short surface crack experiment will be conducted. The R_m/t ratio for this experiment is approximately 20. This experiment, with its large R/t ratio, will provide further insight as to whether a single correction factor exists.

3.4 PLANS FOR NEXT FISCAL YEAR

The efforts described below will be undertaken during next fiscal year.

3.4.1 Subtask 2.1 Material Characterization for Surface-Cracked Pipe Experiments

During the next fiscal year, the carbon steel submerged arc welds will be fabricated and material characterization tests completed.

3.4.2 Subtask 2.2 Smaller Diameter Pipe Fracture Experiments in Pure Bending for Limit-Load Ovalization Correction

The 16-inch-diameter pipe will be procured and tested.

3.4.3 Subtask 2.3 Large Diameter Surface-Cracked Pipe Fracture Experiment in Combined Bending and Tension (Pressure)

Of the three experiments planned, the two 711-mm- (28-inch) diameter pipe experiments can be conducted on the current strongback system prior to the upgrading. These experiments will be conducted during 1991.

3.4.4 Subtask 2.4 Analysis of Short Surface Cracks in Pipes

Data from the literature on additional small diameter pipe experiments with short surface cracks from the literature will be compared to limit-load analyses.

3.5 REFERENCES

3.1 Scott, P. M. and Ahmad, J. A., "Experimental and Analytical Assessment of Circumferentially Surfaced-Cracked Pipes Under Bending," NUREG/CR-4872, May 1986.

3.2 "Evaluation of Flaws in Austenitic Steel Piping" (Technical basis document for ASME IWB-3640 analysis procedure), prepared by Section XI Task Group for Piping Flaw Evaluation, EPRI Report NP-4690-SR, April 1986.

3.3 American Society of Mechanical Engineers Boiler and Pressure Vessel Code, Edition July 1989, See Code Case N-463.

3.4 Wilkowski, G. M. and Prabhat, K., "Simplified Model for Predicting Elastic to Plastic Instability Loads for Circumferential Cracked Pipe in Bending," in ASME PVP95, pp. 79-99, June 1983.

3.5 Dowling, N. E., in Flaw Growth and Fracture, ASTM STP 631, pp. 139-158, 1977.

3.6 Kanninen, M. F. and others, "Instability Predictions for Circumferentially Cracked Type 304 Stainless Steel Pipes Under Dynamic Loadings," Final Report on EPRI Project T118-2, by Battelle Columbus Laboratories, EPRI Report Number NP-2347, April 1982.

4. TASK 3 BIMETALLIC WELD CRACK EVALUATIONS

This task was not active this fiscal year; hence there is no progress to report.

5. TASK 4 DYNAMIC STRAIN AGING

5.1 Task Objective

The objective of this task is to evaluate and predict the effects of crack instabilities, believed to be due to dynamic strain aging (DSA), on the fracture behavior of pipe. Specific objectives are to establish a simple screening criterion to predict which ferritic steels may be susceptible to unstable crack jumps, and to evaluate the ability of current J-based analysis methodologies to assess the effect of unstable crack jumps on the fracture behavior of ferritic steel pipe. If necessary, alternative procedures for predicting pipe behavior in the presence of crack jumps will be derived.

5.2 Task Rationale

The methodology developed here will be applicable to both LBB and in-service flaw evaluations. It will also be valuable for selection of materials for future advanced reactor designs.

5.3 Task Approach

The four subtasks and two optional subtasks in this task are:

Subtask 4.1	Establish a screening criterion to predict unstable crack jumps in ferritic steels
Subtask 4.2	Evaluate procedures for characterizing fracture resistance during crack jumps in laboratory specimens
Subtask 4	Assess current procedures for predicting crack jump magnitude in pipes
Subtask 4.4	Prepare interim and topical report on dynamic strain aging induced crack instabilities in ferritic nuclear piping steels at LWR temperatures
Subtask 4.5	(Optional Subtask) Refine procedures for characterizing fracture resistance during crack jumps in laboratory specimens
Subtask 4.6	(Optional Subtask) Refine procedures for predicting crack jump magnitude in pipes

Significant efforts were made only in Subtask 4.1 during the past reporting period.

5.3.1 Background

The approach in Task 4 is based on experimental data obtained in the Degraded Piping Program (Ref. 5.1). In several pipe steels tested at 288 C (550 F), both in laboratory and pipe specimens, crack instabilities were observed, interspersed between periods of stable, ductile tearing. These instabilities have been assumed to be related to a steel's susceptibility to DSA (Ref. 5.2). DSA is a pinning of dislocation movement by free nitrogen or carbon atoms in the crystallographic structure. This increases the flow properties and reduces the ductility. However, no firm proof of that tie-in between DSA and crack instabilities presently exists. Information about crack instabilities is lacking in other areas as well. Some questions include:

(1) How large must a crack instability be to significantly affect flawed-pipe safety analyses?
(2) Are J-based analysis procedures valid when crack instabilities occur?
(3) Are there simple ways to predict the occurrence and severity of crack instabilities in a particular steel?
(4) Is there a correlation between crack jumps in C(T) specimens and pipe specimens?
(5) How reproducible is the phenomenon?
(6) Do the fracture surfaces or microstructures associated with crack instabilities have any unusual features?

The significance of crack instabilities in flawed-pipe safety analyses has already been demonstrated in at least one 288 C (550 F) pipe test conducted at David Taylor Research Center. In this experiment, a crack jump of approximately one-fourth of the pipe circumference was observed for a through-wall circumferential crack. Such an instability in a nuclear plant would lead to a large loss of cooling water. Therefore, it is important in this program to determine how to predict the occurrence and magnitude of crack instabilities. Subtask 4.3 represents an attempt to tackle these issues in a logical manner.

A limited number of laboratory experiments are being conducted in Subtask 4.1. The results of those experiments, when combined with existing data, will be used to establish a direct link between crack instabilities and DSA. If that link can be established, then it should be possible to assess a steel's propensity for crack jumps by conducting a few tensile tests or, even better, a few hardness tests. Hardness tests would be especially attractive in nondestructive, in-plant testing of pipes for which no archival material exists. Within Subtask 4.1, data also are being obtained on correlating crack jumps in C(T) and pipe specimens, on determining the reproducibility of crack jumps in replicate tests, and on determining the presence of any unusual fractographic or microstructural features in specimens that display crack instabilities.

The activities involved in developing the screening criteria for dynamic strain aging in Subtask 4.1 will also determine what triggers dynamic crack jumps. From a global sense, the dynamic crack jumps could be triggered by being at the proper temperature and strain rate, and by having a material sufficiently susceptible to dynamic strain-aging. The latter can be determined by the screening criteria, ideally with a single test such as the hardness ratio at high temperature to room temperature. From a microstructural viewpoint, metallographic investigations of past fracture surfaces from Degraded Piping Program test specimens at the points of initiation and arrest of the crack jumps may shed further light on how to predict the start of an instability, or better yet, how to manufacture steels that would not produce instabilities for future plant construction.

In addition to the work in Subtask 4.1, efforts will be undertaken in Subtask 4.2 to modify analytical procedures for calculating fracture resistance in laboratory specimens during a crack instability. Included in this activity will be an evaluation of a J-resistance curve approach, an evaluation of alternate measures of fracture resistance (CTOA, for example), and an assessment of plausible analysis methods to account for crack jumps. The results of Subtask 4.2 will provide information on the variability of the toughness during the instability event and at the end of the crack jump.

The results of Subtask 4.2 will then be used in Subtask 4.3 to make engineering predictions of the length of crack jumps in pipe, using several approaches. One approach will apply the NRCPIPE code (see Task 7) and another will use an energy balance method (Ref. 5.3). The success of these engineering approaches will be evaluated and a determination will be made as to whether improved methods should be recommended for study in optional activities. The first optional subtask is aimed at improving the analytical procedures for calculating fracture resistance during unstable cracking in laboratory specimens. The second seeks to improve the ability to analyze crack jumps in pipes.

The details of the steps to be undertaken in each of the activities are given in the following sections.

5.3.2 Subtask 4.1 Establish a Screening Criterion to Predict Unstable Crack Jumps in Ferritic Steels

The establishment of a screening criterion will involve the following efforts:

Activity 4.1.1	Conduct laboratory tests to determine correlations among tensile properties, hardness, DSA, and the occurrence of crack instabilities in both C(T) specimens and pipes, and
Activity 4.1.2	Using the results of Activity 4.1.1, formulate a practical screening criterion for predicting crack instabilities in pipes.

The details of these activities are given below.

5.3.2.1 Activity 4.1.1 Conduct Laboratory Tests to Determine Correlations Among Tensile Properties, Hardness, DSA, and the Occurrence of Crack Instabilities in Both C(T) Specimens and Pipes

The objectives of this activity are to: (1) establish a direct link between crack instabilities and dynamic strain aging (DSA), thus making it possible to use tests that reveal susceptibility to DSA as screening tests for indicating susceptibility to crack instabilities, (2) examine test data and fracture specimens to correlate crack jumps in C(T) and pipe specimens, (3) investigate reproducibility of crack jumps, and (4) discern any unusual fractographic and/or microstructural features associated with crack instabilities.

In work conducted during the last six months, an attempt was made to link crack jumps to DSA and to develop simple screening tests for DSA. Several types of laboratory tests were conducted over a range of temperatures. These tests included C(T), tensile, and hardness tests. Work also was initiated on examining test records for the purpose of correlating crack jumps in C(T) specimens with those in pipe specimens. Only limited work was done to investigate the reproducibility of crack jumps, and no work was performed to discern fractographic or microstructural features associated with crack instabilities.

Experimental Procedures

Conduct Tensile Tests

Tensile tests were conducted over a range of temperatures from room temperature to 385 C (725 F) to encompass the range in which DSA effects are commonly observed. Round-bar, threaded-end tensile specimens were machined from five different carbon steel pipes, described in Table 5.1. These steels came from the Degraded Piping Program where laboratory specimen and pipe fracture experiments were conducted. They represent a range of steels that had little DSA to significant DSA, as observed by limited past tensile tests. Chemical compositions of the pipes are given in Table 5.2. Tensile tests were conducted at a strain rate of approximately 3 x 10^{-4} s^{-1} in a servohydraulic test machine. The data were analyzed to obtain 0.2-percent offset yield strength, ultimate tensile strength, elongation, and reduction of area. In addition, complete stress-strain curves were obtained from each test.

Table 5.1 Description of Activity 4.1.1 pipes used in study of dynamic strain aging

Pipe Ident. No.	Material Type	Schedule	Pipe Dimensions, mm (inch) Diameter	Wall Thickness
DP2-F9	ASTM A333 Grade 6 carbon steel	100	254 (10)	18.3 (0.719)
DP2-F11	ASTM A333 Grade 6 carbon steel	80	102 (4)	8.6 (0.337)
DP2-F26	ASTM A516 Grade 70 carbon steel	60	711 (28)	22.2 (0.875)
DP2-F30	ASTM A106 Grade B carbon steel	120	152 (6)	14.3 (0.562)
DP2-F29W	Submerged-arc girth weld in ASTM A106 Grade B[a]	100	406 (16)	26.2 (1.031)

(a) The ferritic steel girth weld was prepared by United McGill Corporation of Columbus, Ohio, using procedures recommended by Babcock and Wilcox. It was a single-Vee weld having a 6.4 mm (0.25 inch) gap; a 9.5-mm- (0.38-inch) thick steel backing strip was used for the root pass. The filler metal met Specification SFA-5.23, Class EF2 (Linde 44) and the flux was Linde 80. The weld was stress relieved at 605 C (1125 F) for 1 hour.

Table 5.2 Chemical composition of Activity 4.1.1 pipes used in study of dynamic strain aging

	Weight Percentage for Indicated Pipe				
Element	Pipe DP2-F9	Pipe DP2-F11	Pipe DP2-F26	Pipe DP2-F30	Pipe DP2-F29W
C	0.14	0.21	0.13	0.15	0.068
Mn	0.99	0.84	0.80	0.65	1.31
P	0.008	0.010	0.009	0.012	0.016
S	0.024	0.015	0.027	0.014	0.015
Si	0.20	0.19	0.25	0.20	0.57
Cu	0.076	0.035	0.12	0.28	0.14
Sn	0.014	0.001	0.007	0.018	0.028
Ni	0.12	0.006	0.13	0.14	0.59
Cr	0.12	0.027	0.13	0.18	0.027
Mo	0.042	0.012	0.040	0.055	0.43
Al	0.018	0.030	0.003	0.010	0.003
V	0.000	0.000	0.000	0.001	0.002
Cb	0.000	0.000	0.000	0.000	0.000
Zr	0.000	0.000	0.000	0.000	0.001
Ti	0.0[illegible]	0.000	0.000	0.000	0.001
B	0.0001	0.0000	0.0001	0.0000	0.0003
Co	0.006	0.000	0.006	0.008	0.007
W	0.00	0.00	0.00	0.00	N.D.
Pb	0.00	0.00	0.00	0.00	0.00
Ca	N.D.	N.D.	N.D.	N.D.	0.00

Conduct Hardness Tests

Brinell hardness tests were conducted on the same group of five carbon steels that were subjected to tensile tests. Special procedures were devised to permit these tests to be conducted over a range of temperatures, from room temperature to approximately 450 C (840 F). The upper end of that range was somewhat higher than that used in the tensile tests because it was believed that DSA effects in the hardness tests would be shifted to higher temperatures than in the tensile tests, due to the higher strain rates in the hardness tests.

Specimens for the hardness tests were flat, rectangular plates of sufficient size to permit a number of Brinell hardness impressions to be made within the requirements of Test Method ASTM E10-84, Brinell Hardness of Metallic Materials. Each plate specimen had a thickness of approximately 12.7 mm (0.5 inch) except for Pipe DP2-F11, which had a thickness of only approximately 6.4 mm (0.25 inch). A 10-mm tungsten carbide ball was used as the indenter in all tests. The applied load was 3000 kg for all of the thicker specimens and 1500 kilograms for the thinner specimens. The surface subjected to the hardness tests was the one nearer the outside surface of the pipe.

Three chromel-alumel thermocouples were spark welded to the top surface of each test piece; their approximate locations are indicated in Figure 5.1. Also shown in Figure 5.1 are locations where hardness impressions were to be made. Note that the chromel and alumel wires were spaced such that several of the thermocouple junctions encompassed the site of hardness impressions, thereby giving an accurate indication of the actual temperature existing under the hardness indenter for tests at those locations. The particular plate to be tested was placed in a circulating-air oven that was operating at approximately 540 C (1000 F). Also placed in the oven at the same time were two other steel plates, each 25.4 mm (1 inch) thick, labeled A and B. Plate A was used for preheating the Brinell tester platen for several minutes prior to conducting the actual hardness tests, and Plate B was used to support the test piece such that loss of heat from the test piece to the platen would be slowed appreciably.

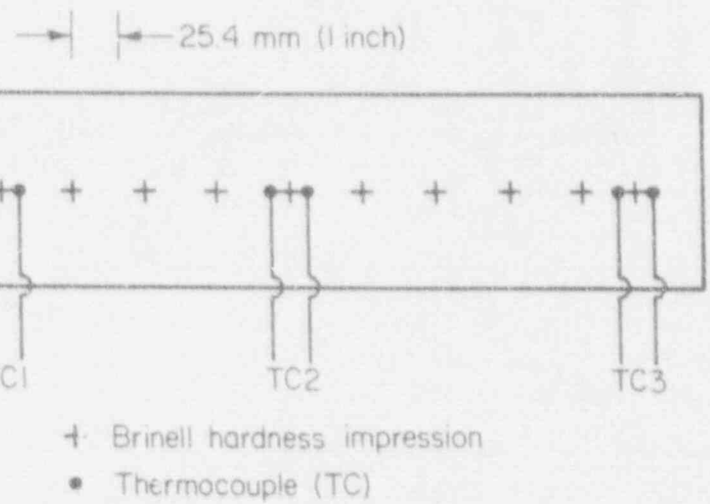

Figure 5.1 Location of thermocouples and Brinell hardness impressions on carbon steel plates

SC-SA-7/91-F5.1

Once the test piece reached the temperature of the oven, Plate A was removed from the oven and placed on the Brinell tester platen. Several minutes later, Plate A was removed from the Brinell tester and was replaced by Plate B. The test piece was then transferred quickly from the oven to the hardness tester and was placed on top of Piece B. Immediately, the hardness indenter was brought into contact with the test piece at Location 1 (Thermocouple 1) to preheat the indenter as the test piece was cooling in preparation for the first hardness test at approximately 450 C (840 F). In fact, since there was a significant temperature drop during the initial hardness test, which took approximately 11 seconds, the first test was initiated when the temperature at Thermocouple 1 was 455 to 460 C (850 to 860 F), so that the average temperature during the test was close to 450 C (840 F). The indenter was then moved to Location 2 and was again brought into contact with the specimen to keep the indenter hot. The second hardness test was begun when the temperature at Location 2, estimated from Thermocouples 1 and 2, was approximately 400 C (750 F) or slightly above. Those steps were repeated to provide hardness impressions at intervals of approximately 50 C (90 F) until the specimen achieved a temperature of approximately 100 C (210 F). Much later, another hardness impression was made when the specimen had reached room temperature. Two plates were tested in this way for each of the five carbon steels investigated. Following testing, the diameters of the hardness impressions were read with a measuring eyepiece and converted to Brinell hardness numbers. Hardness was then graphed as a function of temperature for each of the five steels.

Conduct Compact Specimen Tests

Precracked and side-grooved compact specimens were machined from three of the pipes that had been subjected to tensile and hardness tests over a range of temperatures. The three pipes were identified as DP2-F11, -F26, and -F30 (see Table 5.1 for steel types and pipe dimensions). One of those pipes, DP2-F11, appeared, on the basis of tensile and hardness tests, to be less susceptible than the other two pipes to DSA. The specimens were machined from the pipes, without flattening the pipes, such that the direction of crack extension was in the circumferential direction of the pipe (L-C orientation). The pipe dimensions dictated the size of the C(T) specimens that could be machined from each pipe. The sizes were 0.4T, 1T, and 0.5T, respectively, for DP2-F11, -F26, and -F30. In each case, the specimen thickness was the maximum attainable from the pipe wall.

The specimens were tested in crosshead control in a screw-driven Instron machine at several temperatures that ranged from 150 to 385 C (300 to 725 F). That temperature range is where DSA effects are customarily observed in tensile tests and where crack jumps have been observed to occur in compact specimen tests and in pipe tests. The crosshead speed was selected to cause crack initiation in approximately 5 to 10 minutes. Data obtained during each test included load, load-line displacement, and direct-current electric potential. The latter was collected to indicate the point of crack initiation and the amount of crack extension. To estimate the point of crack initiation, graphs of electric potential (U) versus load-line displacement (LLD) and load versus U were examined for points of slope change prior to maximum load. Engineering judgment then was applied to estimate U_o, the value of U at crack initiation. Crack growth beyond initiation was calculated from the ratio U/U_o using the Johnson expression (Ref. 5.4). Note that the term for the spacing of the voltage probes (2y) in the Johnson expression was allowed to increase in proportion to the LLD as the test progressed, because experience has shown that this procedure provides a more accurate estimate of the crack growth (Ref. 5.5).

The procedures used to calculate J values and J-resistance curves from each compact-specimen test were those specified in ASTM E1152-87, Standard Test Method for Determining J-R Curves. The value of J at crack initiation, J_i, as used in this report, refers to the onset of crack extension rather than to a finite amount of crack extension. The slope of the J-R curve, dJ/da, was calculated for crack extensions in the range of 0.15 to 1.5 mm (0.006 to 0.060 inch).

An additional important observation in the compact-specimen tests was the occurrence of crack jumps and the relation between test temperature and the nature of the crack jump phenomenon, to assess whether correlations exist between susceptibility to DSA, as revealed by tensile or hardness tests, and the occurrence of crack jumps in C(T) tests.

Correlate Crack Jumps in C(T) and Pipe Tests

Test records from both pipe tests and C(T) tests conducted on carbon steel pipes in the Degraded Piping Program, the Short Crack Program, and the IPIRG Program were examined for evidence of crack instabilities during the tests. The best indicator of a crack jump was a sudden drop in the load. The number and magnitude of individual load drops, the latter expressed as a percentage of both the existing load and the maximum load, were tabulated for each test record examined. A total of 24 pipe test records and 58 C(T) test records were examined, covering base metal tests of 10 different pipes and weld metal tests for three different pipes. The base metals included A106 Grade B, SA333 Grade 6, and A516 Grade 70. At the end of the six-month reporting period, several tests remained to be examined and the results remained to be thoroughly analyzed.

Determine Reproducibility of Crack Jumps

Six additional precracked and side-grooved C(T) specimens were prepared from Pipe DP2-F26, which had been found to exhibit significant crack jumps in C(T) specimens and pipe specimens tested at 288 C (550 F). Several of those specimens will be tested at 288 C (550 F) during the next reporting period to obtain two types of information: (1) an indication of the reproducibility of the crack jump behavior in a number of nominally identical tests, and (2) accurate load, displacement, and electric potential data during a crack jump. The instrumentation used in earlier tests was not designed to record events that occurred as rapidly as the crack jumps.

Examine Tested Specimens to Reveal Unusual Fractographic or Metallographic Features Associated with Crack Jumps

No work was done in this area during the last reporting period.

Experimental Findings

Tensile and Brinell Hardness Tests

The results of tensile and Brinell hardness tests over a range of temperatures are presented in Figures 5.2, 5.3, and 5.4. Figure 5.2 shows yield strength, ultimate tensile strength, and Brinell hardness number as functions of temperature, Figure 5.3 shows fracture elongation and reduction of area versus temperature, and Figure 5.4 shows engineering stress-strain curves for the various test temperatures.

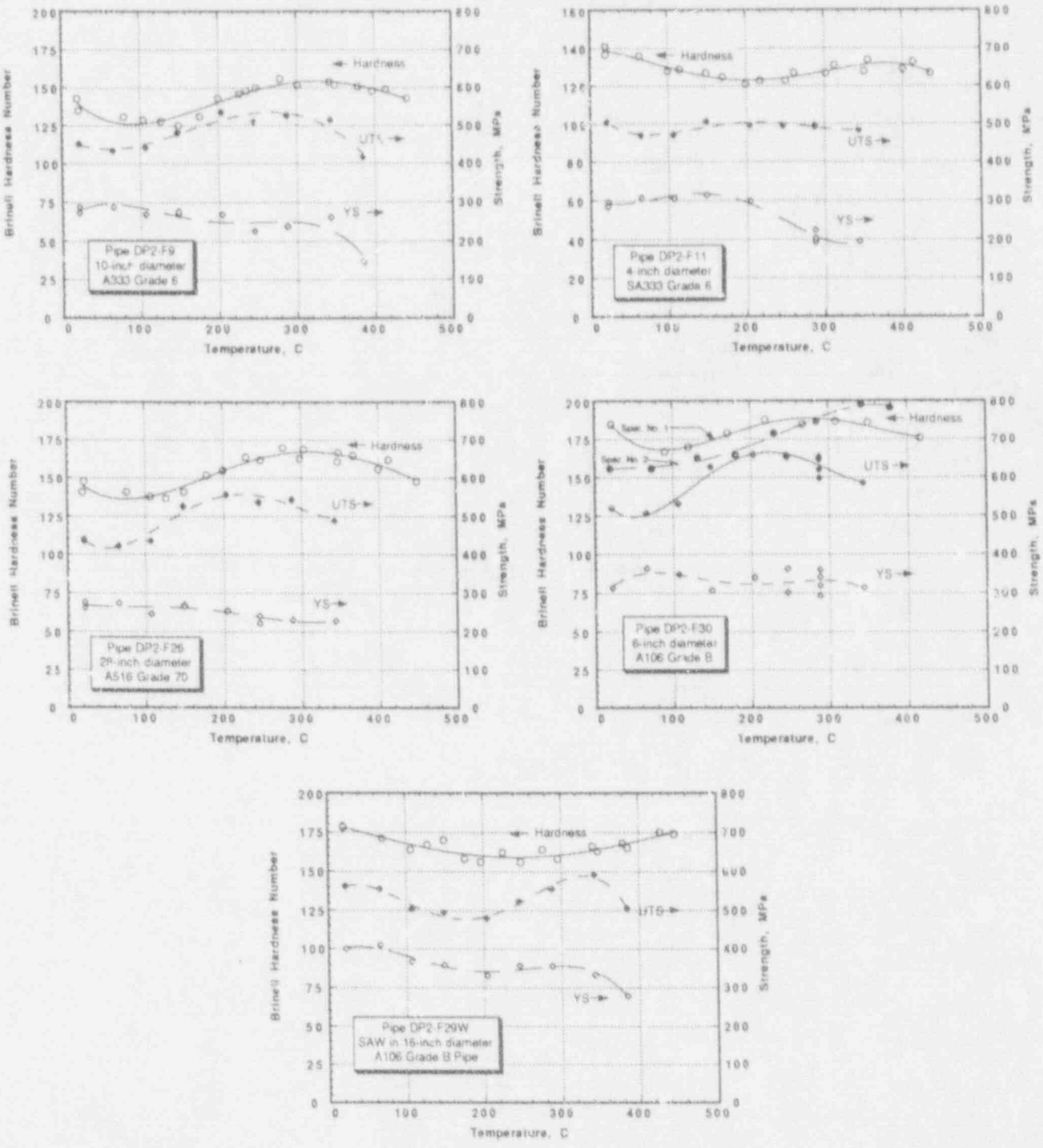

Figure 5.2 Yield strength, ultimate tensile strength, and Brinell hardness as functions of test temperature for five carbon steels

SC-SA-7/91-F5.2

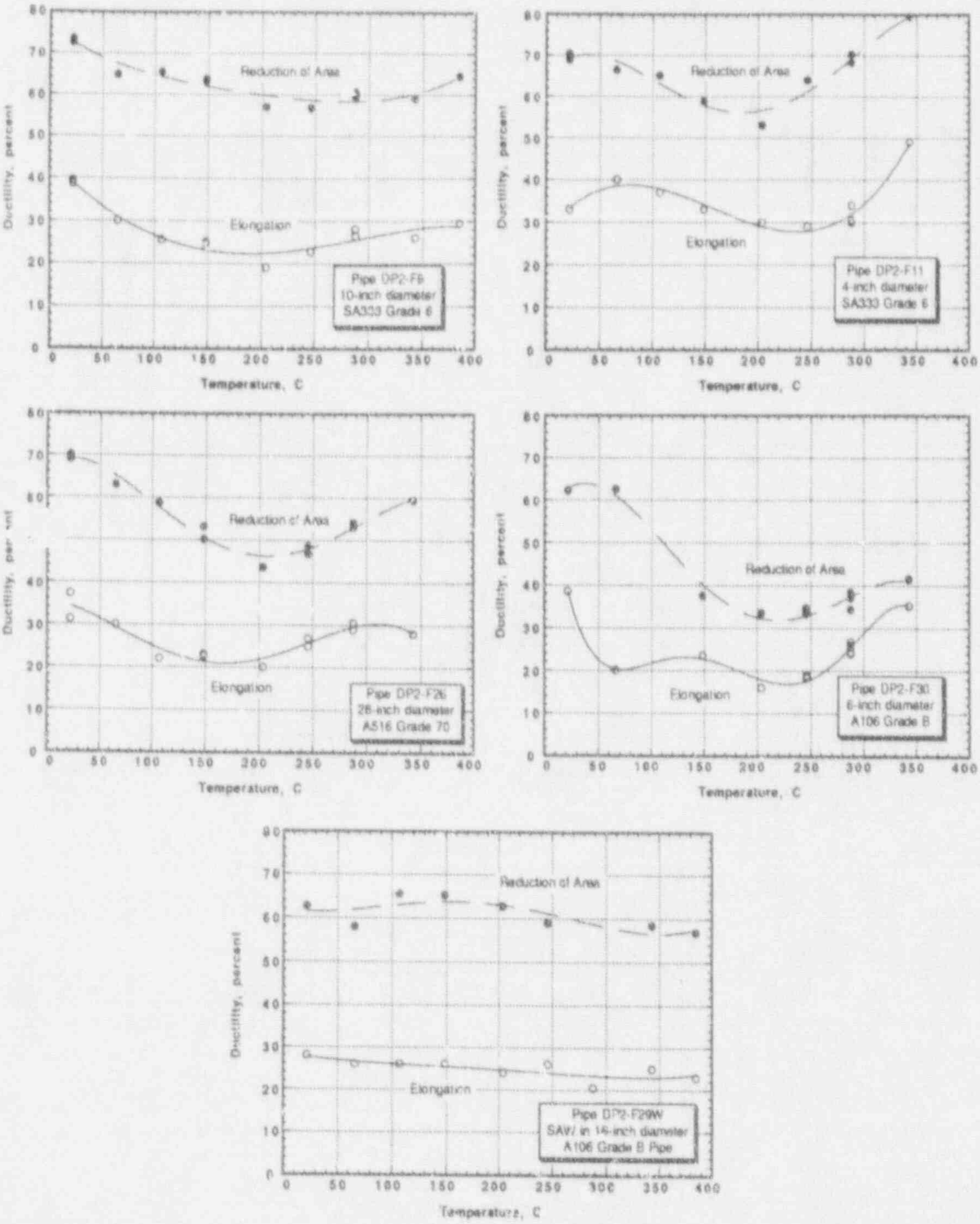

Figure 5.3 Elongation and reduction of area as functions of test temperature for five carbon steels

SC-SA-7/91-F5.3

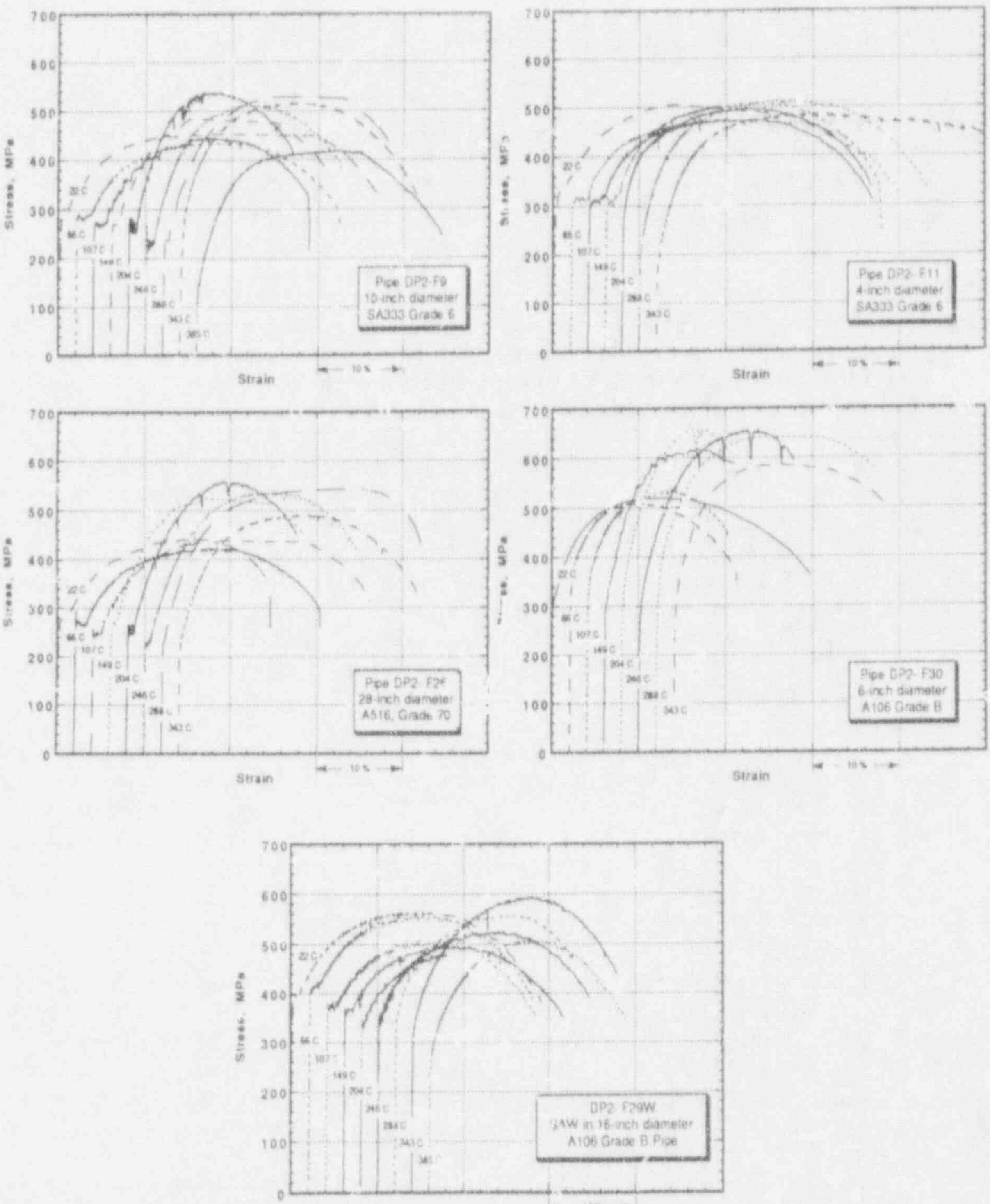

Figure 5.4 Engineering stress-strain curves at various temperatures for five carbon steels tested in tension

SC-SA-7/91-F5.4

Examination of the curves in Figure 5.2 indicates several interesting features.

- Four of the five carbon steel pipes tested exhibited a significant UTS peak, which is indicative of DSA at an elevated temperature; the fifth pipe, DP2-F11, showed a relatively flat curve of UTS versus temperature. That result indicates that Pipe DP2-F11 is less susceptible to DSA than are the other four pipes, even though it is the same type of pipe (A333 Grade 6) as Pipe DP2-F9. Note in Table 5.2 that those two pipes have slightly different chemical compositions. Pipe DP2-F11 has more carbon and aluminum and less chromium and molybdenum than does Pipe DP2-F9. However, of those differences, only the increased aluminum would be expected to make DP2-F11 less susceptible to DSA by tying up more of the nitrogen. Nitrogen along with carbon, is believed to be responsible for DSA. The other differences would be expected to have an opposite, if any, effect by making carbon increasingly available for promoting DSA.

- The submerged-arc weld metal (DP2-F29W) exhibited a peak in UTS at a temperature of approximately 340 C (645 F); the base metals (DP2-F9, -F26, and -F30) exhibited a UTS peak at a temperature in the range of 220 to 260 C (430 to 500 F). From Table 5.2, it can be seen that the chemical composition of the weld metal differs from that of the four base metals in several respects: the carbon and chromium contents are relatively low and the manganese, silicon, nickel, and molybdenum contents are relatively high. Of those differences, only the high silicon and molybdenum contents might be thought to contribute to shifting the UTS peak to a higher temperature.

- The curve of Brinell hardness number versus temperature closely resembled the curve of UTS versus temperature, except that the peak in the hardness curves was typically shifted to a higher temperature. That shift was anticipated because the hardness tests were conducted at a strain rate estimated to be one to two orders of magnitude faster than for the tensile tests. The magnitude of the shift was not consistent among the five materials tested. It ranged from approximately 30 C in Pipe DP2-F30 to more than 100 C in several of the other materials.

- In four of the five materials tested, the hardness versus temperature curves were nominally identical in duplicate tests. In Pipe DP2-F30, however, duplicate tests gave significantly different results, both in the ratio of maximum to minimum hardness and in the temperature at which the peak hardness was observed. That finding suggests that the strength and susceptibility varies significantly in Pipe DP2-F30. Other types of tests on that pipe, including pipe tests, C(T) tests, and tensile tests, also have indicated significant differences in behavior between nominally identical specimens. No attempt has been made to identify the nature of the suspected inhomogeneities. High-temperature hardness measurements at various locations around and along a section of this pipe are under way.

- For the submerged-arc weld metal (DP2-F29W), the hardness versus temperature curve had not yet reached a peak value at the highest test temperature of approximately 450 C (840 F). That result is a consequence of the unusually high peak in the UTS versus temperature curve described earlier.

With respect to the ductility versus temperature curves shown in Figure 5.3, each of the four base metals exhibited a trend toward decreased ductility as the temperature was increased from room temperature, followed by an increase in ductility as temperature was increased further. For the submerged-arc weld metal (DP2-F29W), changing the test temperature had only a modest effect on tensile ductility.

The engineering stress-strain curves in Figure 5.4 reveal, as did the UTS versus temperature curves in Figure 5.2, that Pipe DP2-F11 was less susceptible to DSA than were the other four materials and that the DSA effect was shifted to higher temperature for the submerged-arc weld metal (DP2-F29W). In addition to an increase in UTS at elevated temperatures, indicators of susceptibility to DSA include increased strain hardening rate (greater slope of the stress-strain curve between the onset of yielding and maximum load) and the appearance of serrations on the stress-strain curve within a certain range of elevated temperatures.

Compact Specimen Tests

Results of compact specimen tests at various temperatures from 149 to 385 C (300 to 725 F) are presented in Figures 5.5 through 5.9. Figure 5.5 shows load-displacement curves; Figure 5.6 shows J-resistance curves; and Figures 5.7 through 5.9 show J_i and dJ/da versus temperature for the three different carbon steel pipes investigated. The three pipes had been selected from the five pipes that had earlier been subjected to tensile and Brinell tests at various temperatures.

The load-displacement curves in Figure 5.5 reveal that two of the pipes, DP2-F26 and -F30, exhibited crack jumps, as evidenced by sharp load drops, when compact specimens were tested at a temperature near 288 C (550 F). The third pipe, DP2-F11, did not exhibit crack jumps at any of the four test temperatures investigated. It will be recalled from a previous paragraph that, on the basis of tensile and hardness tests, Pipe DP2-F11 was noticeably less susceptible to DSA than were the other two pipes. This finding lends additional support to the hypothesis that the occurrence of crack jumps is associated with the degree of susceptibility to DSA.

However, it is not known whether the small size, in particular the small thickness, of the DP2-F11 specimens (0.4T x 5.1 mm [0.2 inch] thick) might have played a role in the results by way of favoring stable crack growth over crack jumps. The DP2-F26 and -F30 specimens, which did exhibit crack jumps, were 1T x 21 mm (0.82 inch) thick and 0.5T (full thickness), respectively. The implication of these results is that a study on the effect of specimen size on the occurrence of instabilities may be of value.

J-resistance curves for the three pipe materials are shown in Figure 5.6. Values of J_i and dJ/da obtained from the curves in Figure 5.6 are presented in Figures 5.7, 5.8, and 5.9 for Pipe DP2-F11, -F26, and -F30, respectively. In Figure 5.7, Pipe DP2-F11 appears to exhibit a minimum in

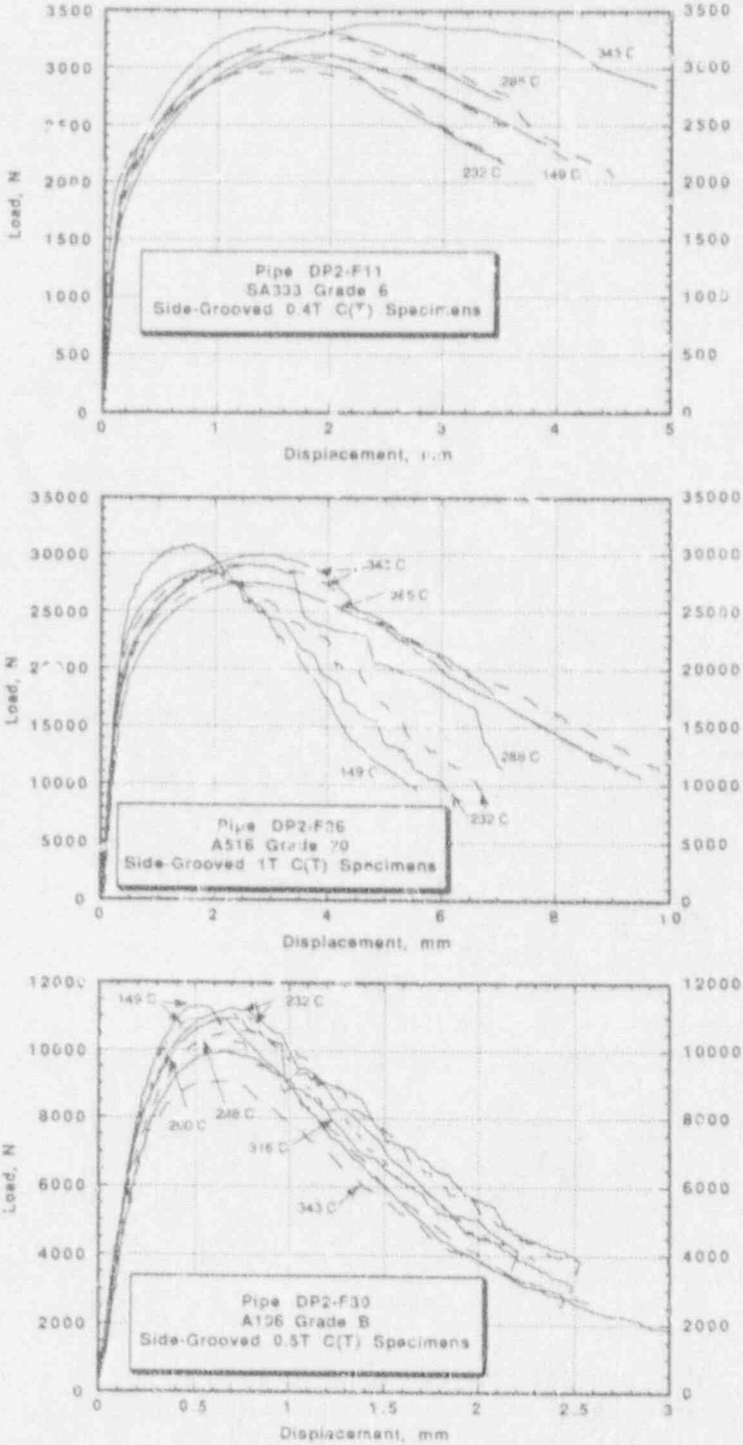

Figure 5.5 Load versus displacement curves for C(T) specimens of three different carbon steels tested at various temperatures

SC-SA-7/91-F5.5

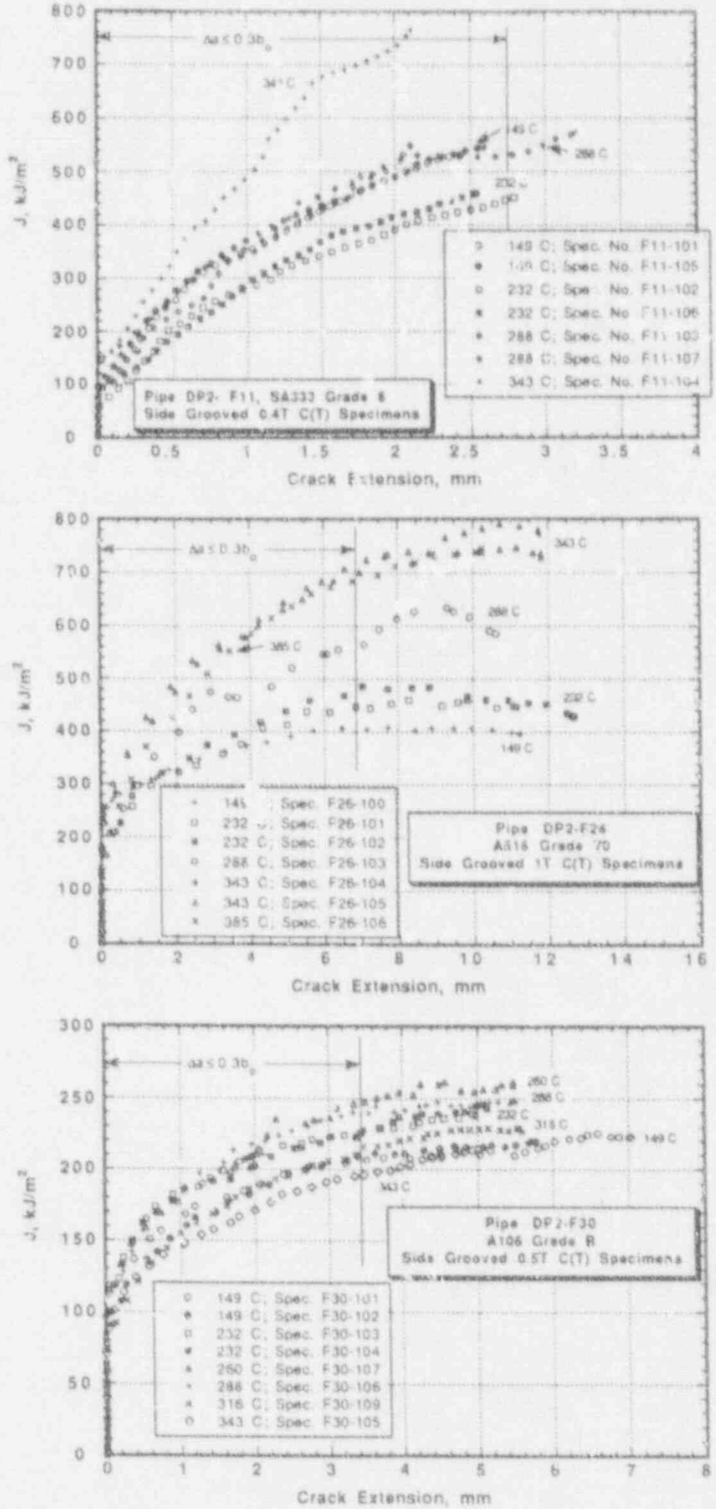

Figure 5.6 J-resistance curves for C(T) specimens of three different carbon steels tested at various temperatures

SC-SA-7/91-F5.6

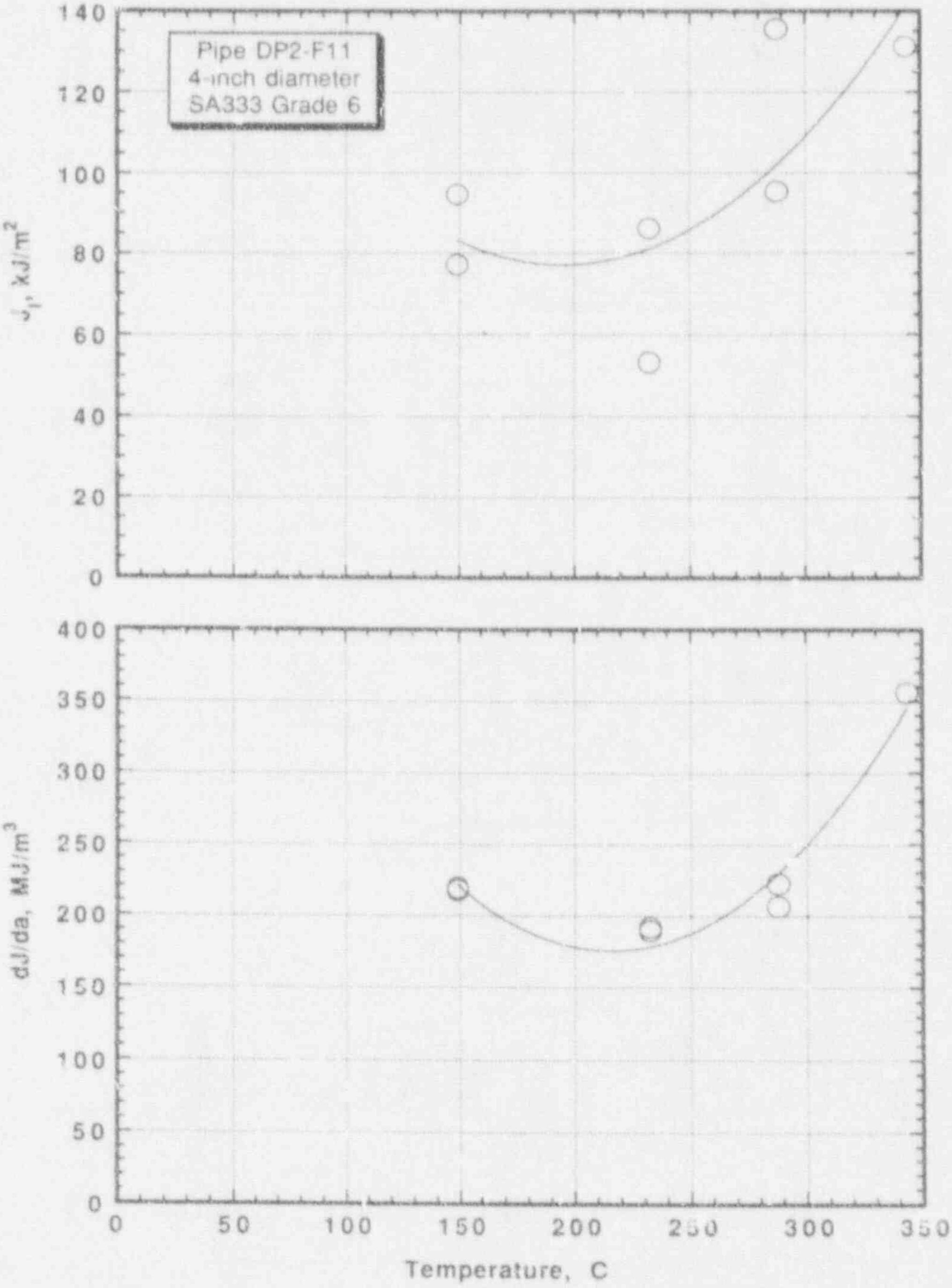

Figure 5.7 J_I and dJ/da versus test temperature for C(T) specimens from Pipe DP2-F11

SC-SA-7/91-F5.7

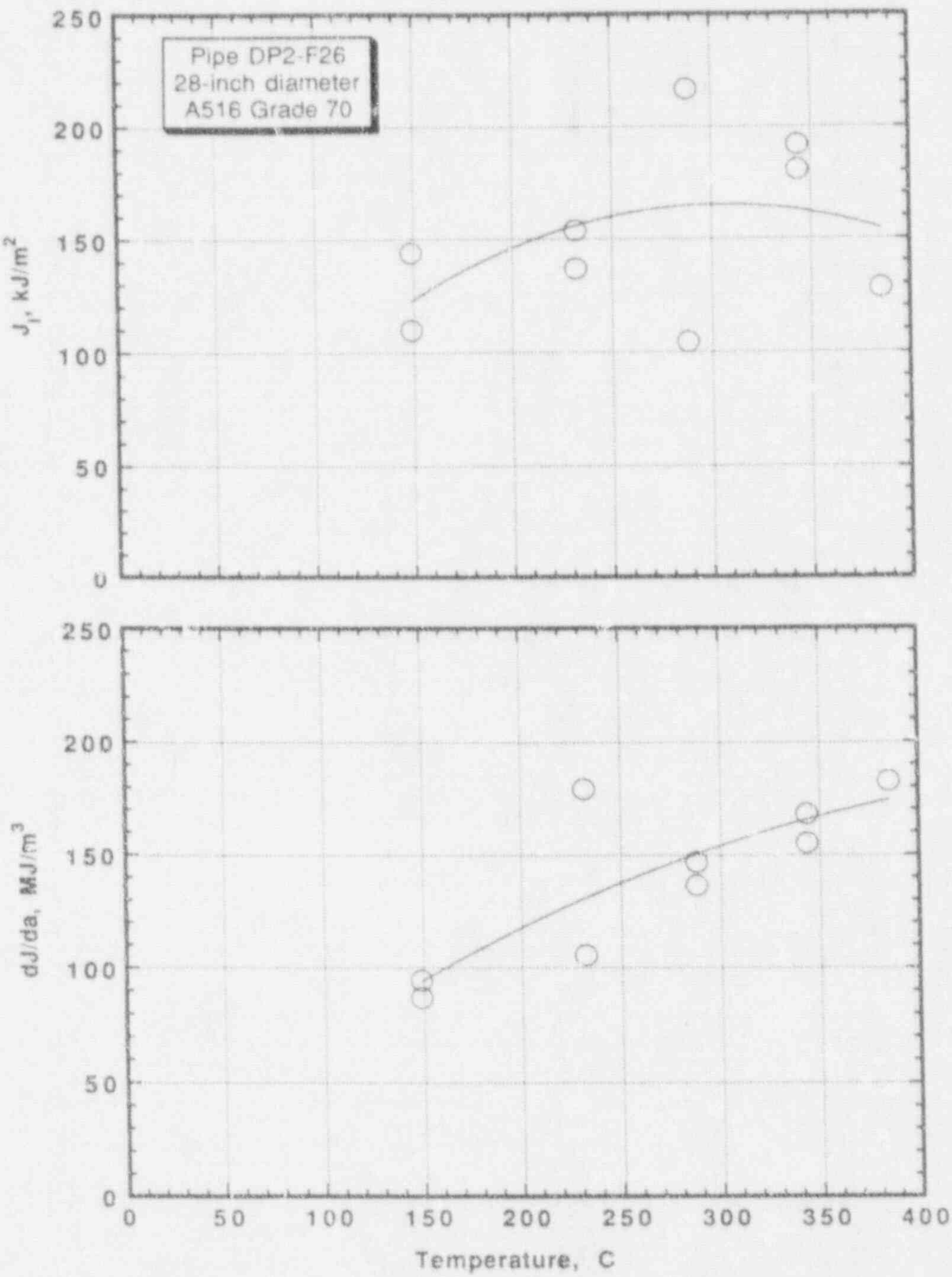

Figure 5.8 J_I and dJ/da versus test temperature for C(T) specimens from Pipe DP2-F26

SC-SA-7/91-F5.8

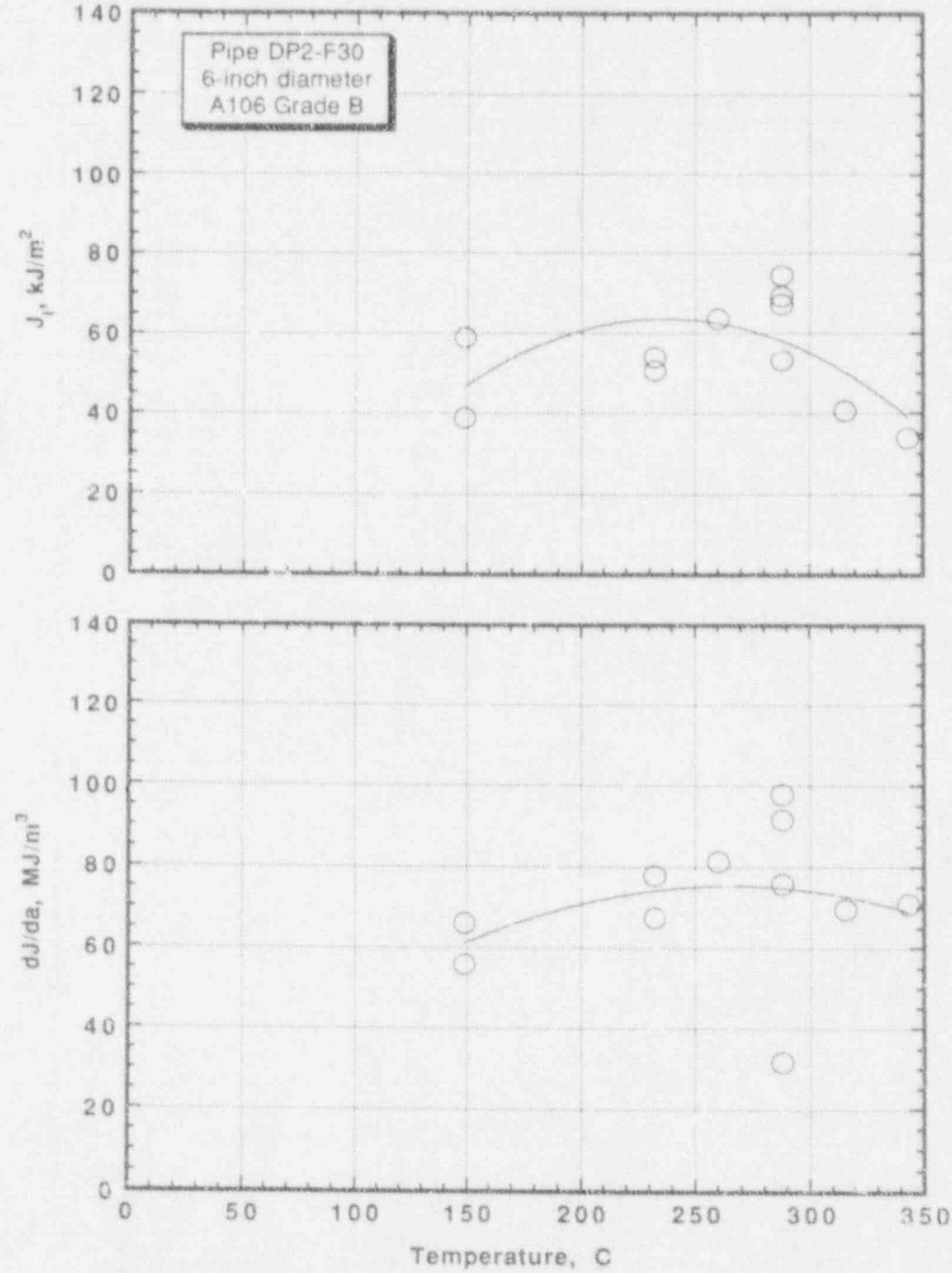

Figure 5.9 J_i **and dJ/da versus test temperature for C(T) specimens from Pipe DP2-F30**

SC-SA-7/91-F5.9

both J_i and dJ/da at a temperature near 225 C (435 F), similar to results reported in Reference 5.6 for two different heats of A106 Grade C steel. Similar trends are not discernible in Figures 5.8 and 5.9 for the other two steels tested. Hindsight suggests that it would have been worthwhile to conduct additional tests at room temperature to obtain a better assessment of the role of temperature on fracture behavior. Also note that the J-R curves are not valid after the start of an instability. Determination of the J values during and after an instability is the subject of future efforts in this program.

Correlation of Crack Jumps in C(T) and Pipe Tests

At the end of the six-month reporting period, several test records remained to be examined for evidence of crack jumps, and the results remained to be thoroughly analyzed. A first impression based on limited analysis of the results was that the occurrence of crack jumps in C(T) specimens exhibited considerable variability and that, while some correlation appears to exist between the occurrence of crack jumps in C(T) specimens and in pipes, there is no close correlation between the number of crack jumps or their magnitudes in the two cases.

5.3.2.2 Activity 4.1.2 Using the Results of Activity 4.1.1, Formulate a Practical Screening Criterion for Predicting Crack Instabilities in Pipes

The objective of this activity is to formulate a practical screening criterion, based on the results of Activity 4.1.1, that will permit prediction of crack instabilities in specific pipes.

The basic hypotheses in formulating a screening criterion are these: (1) Crack jumps at 288 C (550 F) are associated with a high degree of susceptibility to DSA. (2) The degree of susceptibility to DSA can be estimated from tensile strength ratios at selected temperatures. (3) The tensile strength ratios can be estimated from hardness ratios at selected temperatures. Therefore, if each hypothesis holds, a steel's propensity for crack jumps should be predictable from hardness tests at selected temperatures.

To test these hypotheses the data shown in Figure 5.2 were analyzed to obtain ultimate tensile strength (UTS) ratios and Brinell hardness number (BHN) ratios at selected temperatures. Several of those ratios are given in Table 5.3 for five carbon steels, along with a column indicating whether the particular steel exhibited crack jumps in C(T) tests at 288 C (550 F). The UTS ratios will be considered first.

The UTS(max)/UTS(min) ratio, which, intuitively, would seem to be the best indicator of degree of susceptibility to DSA, indicates that, for base metals, ratios in excess of 1.23 were associated with crack jumps while ratios of only 1.09 or less were not. It is possible that the weld metal (DP2-F29W) would have exhibited crack jumps if it had been tested at a temperature somewhat higher than 288 C (550 F), because it displayed manifestations of DSA at a higher temperature than did the base metals. (Note: The only C(T) test data available for DP2-F29W were obtained at 288 C (550 F) in the IPIRG Program.) The UTS(max)/UTS(min) ratio suffers from the fact

Table 5.3 Tensile strength ratios and hardness ratios for carbon steel pipes at selected temperatures

Pipe Ident. No.	Type	Crack Jumps in C(T) Tests at 288 C	UTS (max) / UTS (RT)	UTS (288) / UTS (RT)	BHN (max) / BHN (min)	BHN (288) / BHN (RT)
DP2-F9	SA333 Gr 6	Yes	1.23	1.16	1.22	1.09
DP2-F11	SA333 Gr 6	No	1.09	0.98	1.07	0.91
DP2-F26	A516 Gr 70	Yes	1.32	1.24	1.22	1.16
DP2-F30	A106 Gr B	Yes	1.30	1.20	1.26[a], 1.13[b]	1.21[a], 1.02[b]
DP2-F29W	SAW in A106 Gr B	No	1.23	0.99	> 1.10	0.90

(a) Brinell hardness Spec. No. 1.
(b) Brinell hardness Spec. No. 2.

that tensile tests are required over a relatively wide range of temperatures. Furthermore, for pipes already in service, archival material would have to be available for fabricating specimens.

Another column in Table 5.3 shows UTS(288)/UTS(RT) ratios, which would require tensile tests at only two temperatures but which would still require archival material for pipes already in service. This ratio indicates that crack jumps are associated with values of 1.16 and above, while values of 0.99 or less resulted in no crack jumps, both for base metal and weld metal.

The remaining columns in Table 5.3 show hardness ratios. Hardness tests would be preferred over tensile tests for two reasons: (1) they are simpler and less expensive to perform, and (2) it is believed that they could be conducted *in situ* on pipe already in service, though special procedures would have to be developed. If the hardness data from Specimen No. 2 of the DP2-F30 pipe were to be ignored, it could be concluded that BHN(max)/BHN(min) ratios of 1.22 or greater in base metals were associated with crack jumps at 288 C (550 F), while ratios of 1.07 or less resulted in no crack jumps. A similar conclusion could be reached for the BHN(288)/BHN(RT) ratios, except that they would apply to the weld metal as well as to the base metal. For the BHN(288)/BHN(RT) ratio, values of 1.09 or greater would be associated with crack jumps; values of 0.91 or less would not. Thus, it would appear feasible to assess a pipe's propensity for crack jumps at 288 C (550 F) simply by performing hardness tests at room temperature and at 288 C (550 F).

Inclusion of the second hardness test for Pipe DP2-F30, that on Specimen No. 2, requires some adjustment to several of the statements made above. Those adjustments would lower the BHN(max)/BHN(min) and BHN(288)/BHN(RT) values associated with crack jumps to 1.13 and 1.02, respectively, from their initial values of 1.22 and 1.09. Nonetheless, even considering the variability in the hardness data for Pipe DP2-F30, it still appears reasonable to conclude that hardness data at two temperatures can act as an indicator of crack jump tendencies in carbon steel pipes operating at 288 C (550 F).

Because work in several areas is ongoing, no conclusions can be drawn at this time with respect to: (a) the ability of C(T) tests to predict crack jumps in pipe tests, (b) the reproducibility of crack jumps in C(T) tests, and (c) the presence of unusual fractographic or metallographic features associated with crack jumps.

5.4 Plans for Next Fiscal Year

During next fiscal year the efforts described below will be undertaken.

5.4.1 Subtask 4.1 Establish a Screening Criterion to Predict Unstable Crack Jumps in Ferritic Steels

There are two specific activities in this subtask. Plans for these activities are:

Activity 4.1.1 - Conduct Laboratory Tests to Determine Correlations Among Tensile Properties, Hardness, DSA, and the Occurrence of Crack Instabilities in Both C(T) Specimens and Pipes. All the experimental efforts have been completed. Data reduction on the dynamic crack growth measurements will be completed this fiscal year.

Activity 4.1.2 - Using the Results of Activity 4.1.1, Formulate a Practical Screening Criterion for Predicting Crack Instabilities in Pipes. All of these efforts will be completed next fiscal year.

5.4.2 Subtask 4.2 Evaluate Procedures for Assessing Fracture Resistance During Crack Jumps in Laboratory Specimens

There are three specific activities in this subtask. The plans for next fiscal year for these activities are:

Activity 4.2.1 - Evaluate J-resistance Curve Approach. These efforts will be completed next fiscal year.

Activity 4.2.2 - Evaluate Alternate Material Resistance Measures. These efforts will start next fiscal year but will not be completed until the following fiscal year.

Activity 4.2.3 - Assess Plausible Analysis Methods to Account for Crack Jumps. These efforts will start next fiscal year but will not be completed until the following fiscal year.

5.4.3 Subtask 4.3 Assess Current Procedures for Predicting Crack Jump Magnitude in Pipes

There are two specific activities in this subtask. The plans for next fiscal year are:

Activity 4.3.1 - Predict the Magnitude of Crack Jumps in Pipes using Current Analysis Methods. These efforts will start in FY93.

Activity 4.3.2 - Assess the Success of the Current Approximate Approaches and Identify if Optional Efforts are Warranted. These efforts will start in FY92.

5.4.4 Subtask 4.4 Prepare Interim and Topical Reports on Dynamic Strain Aging Induced Crack Instabilities in Ferritic Nuclear Piping Steels at LWR Temperatures

These reports will be written in FY93.

5.4.5 Optional Subtask 4.5 Refine Procedures for Assessing Fracture Resistance During Crack Jumps in Laboratory Specimens

If this subtask is undertaken, it will start in FY93.

5.4.6 Optional Subtask 4.6 Refine Procedures for Predicting Crack Jump Magnitude in Pipes

If this subtask is undertaken, it will start in FY93.

5.5 References

5.1 Wilkowski, G. M. and others, "Degraded Piping Program - Phase II," Summary of Technical Results and Their Significance to Leak-Before-Break and In-Service Flaw Acceptance Criteria, March 1984-January 1989, by Battelle Columbus Division, NUREG/CR-4082, Vol. 8, March 1989.

5.2 Marschall, C. W., Landow, M. P., and Wilkowski, G. M., "Effect of Dynamic Strain Aging on Fracture Resistance of Carbon Steels Operating at Light-Water-Reactor Temperatures," in ASTM STP 1074, pp. 339-360, 1990.

5.3 Brust, F. W., "Approximate Methods for Fracture Analyses of Through-Wall-Cracked Pipes," NRC Topical Report by Battelle Columbus Division, NUREG/CR-4853, February 1987.

5.4 Schwalbe, K. H. and Hellmann, D., "Application of the Electric Potential Method to Crack Length Measurements Using Johnson's Formula," Journal of Testing and Evaluation, Vol. 9, No. 3, pp. 218-221, 1981.

5.5 Marschall, C. W., Held, P. R., Landow, M. P., and Mincer, P. N., "Use of the Direct-Current Electric Potential Method to Monitor Large Amounts of Crack Growth in Highly Ductile Metals," Fracture Mechanics: Twenty-First Symposium, ASTM STP 1074, J. P. Gudas, J. A. Joyce, and E. M. Hackett, Eds., American Society for Testing and Materials, Philadelphia, pp. 581-593, 1990.

5.6 Miglin, M. T., Van Der Sluys, W. A., Futato, R. J., and Domian, H. A., "Effects of Strain Aging in the Unloading Compliance J Test," Elastic-Plastic Fracture Test Methods: The User's Experience, ASTM STP 856, E. T. Wessel and F. J. Loss, Eds., American Society for Testing and Materials, Philadelphia, pp. 150-165, 1985.

6. TASK 5 FRACTURE EVALUATIONS OF PIPE ANISOTROPY

6.1 Task Objective

The objective of this subtask is to assess if anisotropic fracture properties (where the toughness is typically lower in a helical direction or the axial direction for ferritic seamless pipe) together with having high principal stresses in a helical direction can cause a lower failure stress than calculated using the toughness in the L-C orientation and using only the longitudinal stresses.

6.2 Task Rationale

The rationale for this task is to assess if current LBB and ASME flaw evaluation procedures could be nonconservative for out-of-plane crack growth under certain service loading conditions. If current procedures are found to be significantly nonconservative, modifications to existing fracture analysis methods will be made.

6.3 Task Approach

Five subtasks will be conducted in this task. Two of them are optional subtasks that would be started only with NRC approval after an interim report is completed. The subtasks are:

Subtask 5.1	Assess effect of toughness anisotropy on pipe fracture under combined loads
Subtask 5.2	Determine magnitude of toughness anisotropy and establish a screening criterion to predict out-of-plane crack growth
Subtask 5.3	Prepare interim and topical reports on anisotropy and mixed-mode studies
Subtask 5.4	Establish ductile crack growth resistance under mixed-mode loading (optional subtask)
Subtask 5.5	Refine J-estimation scheme analyses for pipes (optional subtask).

6.3.1 Background

The approach is based on the following two facts: (a) out-of-plane (angled) crack growth under nominally Mode I loading has been observed in both laboratory and pipe specimens of ferritic pipe materials (Refs. 6.1 and 6.2) and (b) the data and observations have not yet been adequately analyzed to assess the ramifications of the phenomenon under realistic loading conditions and for large diameter pipes.

Existing data suggest that the out-of-plane crack growth observed in the Degraded Piping Program experiments was due to toughness (or, more precisely, crack growth resistance) anisotropy (Ref. 6.2). The toughness anisotropy arises from nonmetallic inclusions, which tend to be aligned parallel to the principal working direction. In the Degraded Piping Program, an ad hoc modification to existing J-estimation analysis methods was made by using projected rather than actual crack length in J-R curve calculations for pipe experiment data. It is not known if this procedure would be reasonably accurate for larger diameter pipes under combined bending, internal pressure, and torsional loads.

A prudent overall approach is to first assess the ramifications of toughness anisotropy on the behavior of pipes under a sufficiently broad range of service loading conditions. This assessment will be accomplished using parametric analyses (Subtask 5.1). The analyses will be performed using the finite element method on a pipe involving bending, internal pressure, torsion, and combined loadings. Crack driving force will be computed under each loading type as a function of angle from the crack plane. Using existing data and engineering judgment, the results will be used to identify realistic service loading conditions, which may require modifications to existing analysis methods to avoid nonconservative predictions. So that the assessment is realistic, Subtask 5.2 is focusing on determining the realistic magnitude of anisotropy in representative ferritic piping materials. This determination will be done mostly by using available data. A minimum number of laboratory specimens are being tested to generate the necessary quantitative information for analysis. Subtask 5.2 also is attempting to develop a screening test that would make it possible to predict the occurrence of toughness anisotropy or out-of-plane crack growth in pipes.

An interim report will be prepared (Subtask 5.3) using the findings in Subtasks 5.1 and 5.2. The report will provide the technical bases for a decision by the NRC as to the subsequent course of action. For example, the findings may indicate that there is no practical need for modifying existing analysis methods. But assuming that, for certain realistic situations, modifications in analysis methods are called for, our approach contains Optional Subtasks 5.4 and 5.5. These activities are aimed at providing the NRC with a validated analysis procedure for predicting crack growth behavior in nuclear power plant piping of materials with significant material anisotropy.

Progress is reported for Subtasks 5.1 and 5.2 only, because the other subtasks are inactive.

6.3.2 Subtask 5.1 Assess Effect of Toughness Anisotropy on Pipe Fracture Under Combined Loads

The general objective of this subtask is to conduct a parametric analysis to determine if there is significant nonconservatism in current LBB analyses for service loading conditions of circumferentially through-wall cracked pipe with anisotropic fracture toughness. There are six activities within this subtask.

Activity 5.1.1	Determine driving force for angled stationary crack
Activity 5.1.2	Conduct tensile tests at different orientations, and additional skewed orientation C(T) specimens on a 4-inch-diameter pipe to assess strength and toughness variations
Activity 5.1.3	Determine driving force for angled growing crack
Activity 5.1.4	Determine angled crack principal stresses

Activity 5.1.5 Formulate approximate corrections
Activity 5.1.6 Assess if optional efforts are necessary.

The major area of progress was in Activity 5.1.2.

Analysis methods that are currently used to assess crack growth and fracture in nuclear piping assume Mode I (opening mode) conditions. Mode I crack growth requires symmetry of field variables about a plane through the crack. However, load conditions exist in nuclear piping systems that may violate the Mode I assumptions upon which J-integral analysis methods are based. Two basic conditions exist in nuclear piping that may lead to a violation of the Mode I crack growth assumption:

(1) out-of-plane (angled) crack growth, and
(2) mixed-mode loading (bending and torsion).

Most ferritic nuclear piping exhibits out-of-plane ductile crack growth from a circumferential through-wall crack. J-estimation scheme analyses from the Degraded Piping Program (which assumed straight crack growth) of experiments where the crack grew at an angle gave reasonable predictions of maximum load. However, the reasons for this success were never adequately explained. Moreover, the effect of angular crack growth under mixed-mode conditions (bending, torsion, tension) was never established.

Three important aspects of the angle-crack problem are addressed in this task:

(1) initiation under bending only and combined pressure and bending – a Mode I problem but with anisotropic toughness,
(2) initiation under bending, pressure, and torsion – a mixed-mode problem with anisotropic and isotropic toughness, and
(3) angled crack growth under mixed-mode conditions.

In addition, the effectiveness of current simplified J-estimation analysis procedures in predicting this type of crack growth is considered. This effort also includes finding proper characterization of both angled crack growth and crack growth perpendicular to the pipe axis under mixed-mode loading caused by bending and torsion. If significantly lower failure loads are predicted for loading of anisotropic toughness pipe (including combined loading) relative to analyses considering only longitudinal stresses, then optional activities, also provided here, are suggested to enable the development of a simplified procedure for mixed-mode, ductile fracture.

The details of these activities are described below.

6.3.2.1 Activity 5.1.2 Conduct tensile tests at different orientations, and additional skewed orientation C(T) specimens on a 4-inch diameter pipe to assess strength and toughness variations

The objectives of this activity are to provide tensile stress-strain curves and J-resistance curves at 288 C (550 F) at several different specimen orientations for a 4-inch-diameter seamless carbon steel pipe, DP2-F11 (SA333 Grade 6). That pipe was shown previously (Ref. 6.2) to have stringer-type inclusions that are at an angle of approximately 24 degrees to the pipe axis. The data obtained will be used in several analytical activities within Subtask 5.1.

All work under this activity was completed during the past six-month period.

Experimental Procedures

Conduct Tensile Tests

Tensile tests were conducted at 288 C (550 F) on round-bar threaded-end tensile specimens machined from Pipe DP2-F11 in four different orientations. The tensile axis in those four different orientations was at 0, 45, 66, and 90 degrees to the pipe axis, as is illustrated schematically in Figure 6.1a. Note in that figure that the 66-degree specimen had its tensile axis perpendicular to the long axis of the stringer-type inclusions. Tensile tests were conducted at a strain rate of approximately 3×10^{-4} s^{-1} in a servohydraulic test machine. The data were analyzed to obtain 0.2 percent offset yield strength, ultimate tensile strength, elongation, and reduction of area. In addition, complete stress-strain curves were obtained from each test.

Conduct Compact Specimen Tests

The crack growth resistance was assessed in four different orientations (0, 24, 45, and 90 degrees, as is illustrated schematically in Figure 6.1b). Note in the figure that the 24-degree specimen had the crack extending along the long axis of the stringer-type inclusions. The compact specimens were 0.4T x 5.1 mm (0.2 inch) thick.

Unintentionally, an additional piece of information pertaining to specimen-orientation effects was obtained for another pipe, DP2-F30 (6-inch-diameter A106 Grade B). One of the C(T) specimens machined for the dynamic strain aging study in Activity 4.1.1 was unintentionally machined in the C-L orientation, rather than the L-C orientation, that is, the crack grew in the direction of the pipe axis rather than in the circumferential direction. Metallographic examination of Pipe DP2-F30 showed that the stringer-type inclusions were aligned with the pipe axis.

The compact specimens were tested in crosshead control in a screw-driven Instron machine at 288 C (550 F). The crosshead speed was selected to cause crack initiation in approximately 5 to 10 minutes. Data obtained during each test included load, load-line displacement, and direct-current electric potential, the latter to indicate the point of crack initiation and the amount of

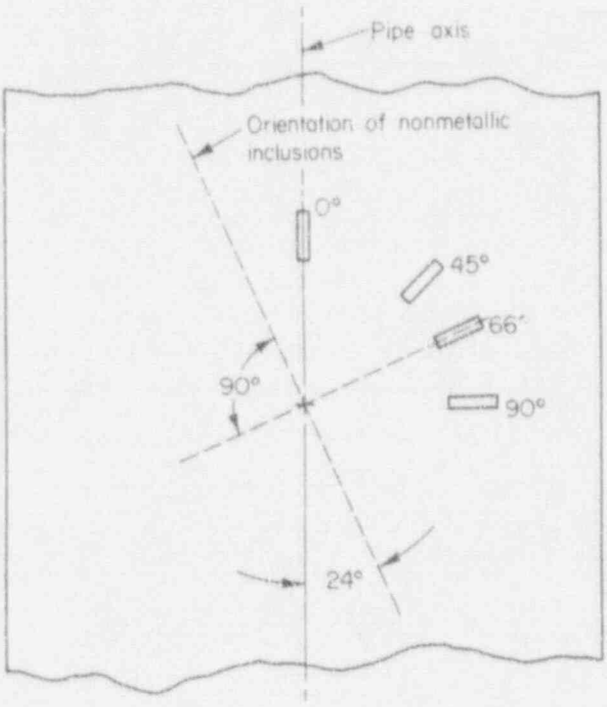

(a)

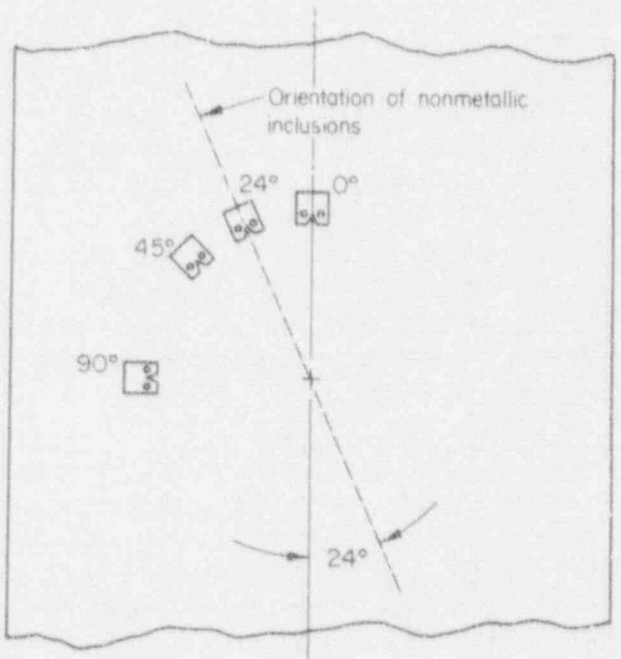

(b)

Figure 6.1 Orientation of skewed specimens machined from Pipe DP2-F11: (a) tensile specimens and (b) C(T) specimens

SC-SA-7/91-F6.1

crack extension. Analysis of the data and calculation of J values and J-resistance curves were carried out in the manner described in Activity 4.1.1.

Experimental Findings

Tensile Tests

The results of tensile tests at four different orientations are presented in Figures 6.2 and 6.3. Figure 6.2 shows yield strength, ultimate tensile strength, elongation, and reduction of area as functions of specimen angle relative to the pipe axis. Figure 6.3 shows engineering stress-strain curves for the various orientations.

The most noteworthy feature of the tensile results is the relatively high yield strength and low fracture elongation of the specimen whose tensile axis was perpendicular to the axis of the inclusions, that is, the 66-degree specimen. This would result in a much higher flow stress for fracture calculations.

Compact Specimen Tests

The results of compact specimen tests at 288 C (550 F) for various orientations for Pipe DP2-F11 are presented in Figures 6.4 through 6.6. Figure 6.4 shows load-displacement curves; Figure 6.5 shows J-resistance curves; and Figure 6.6 shows J_i and dJ/da values as a function of the angle of the crack relative to the pipe axis. Each of the three figures shows, not unexpectedly, that the specimen in which the crack was aligned with the stringer-type inclusions exhibited the lowest crack growth resistance, both in terms of J_i and dJ/da.

Results for Pipe DP2-F30, tested at two different orientations, are presented in Figures 6.7 through 6.9. Figure 6.7 shows load-displacement curves; Figure 6.8 shows J-resistance curves; and Figure 6.9 shows J_i, J at 2 mm (0.08 inch) of crack extension, and dJ/da values at the two different orientations. As would be expected, the resistance to crack extension was lower in the C-L orientation than in the L-C orientation.

6.3.3 Subtask 5.2 Determine Magnitude of Toughness Anisotropy and Establish a Screening Criterion to Predict Out-of-Plane Crack Growth

The establishment of a screening criterion is necessary to determine which materials are susceptible to out-of-plane crack growth. It involves establishing procedures that would enable an evaluation of anisotropic fracture to be made on piping in a plant without archival material. This activity requires a small amount of material property testing. The actual magnitude of this activity is much smaller than the other activities, but it has a high significance. We have divided this subtask into three activities.

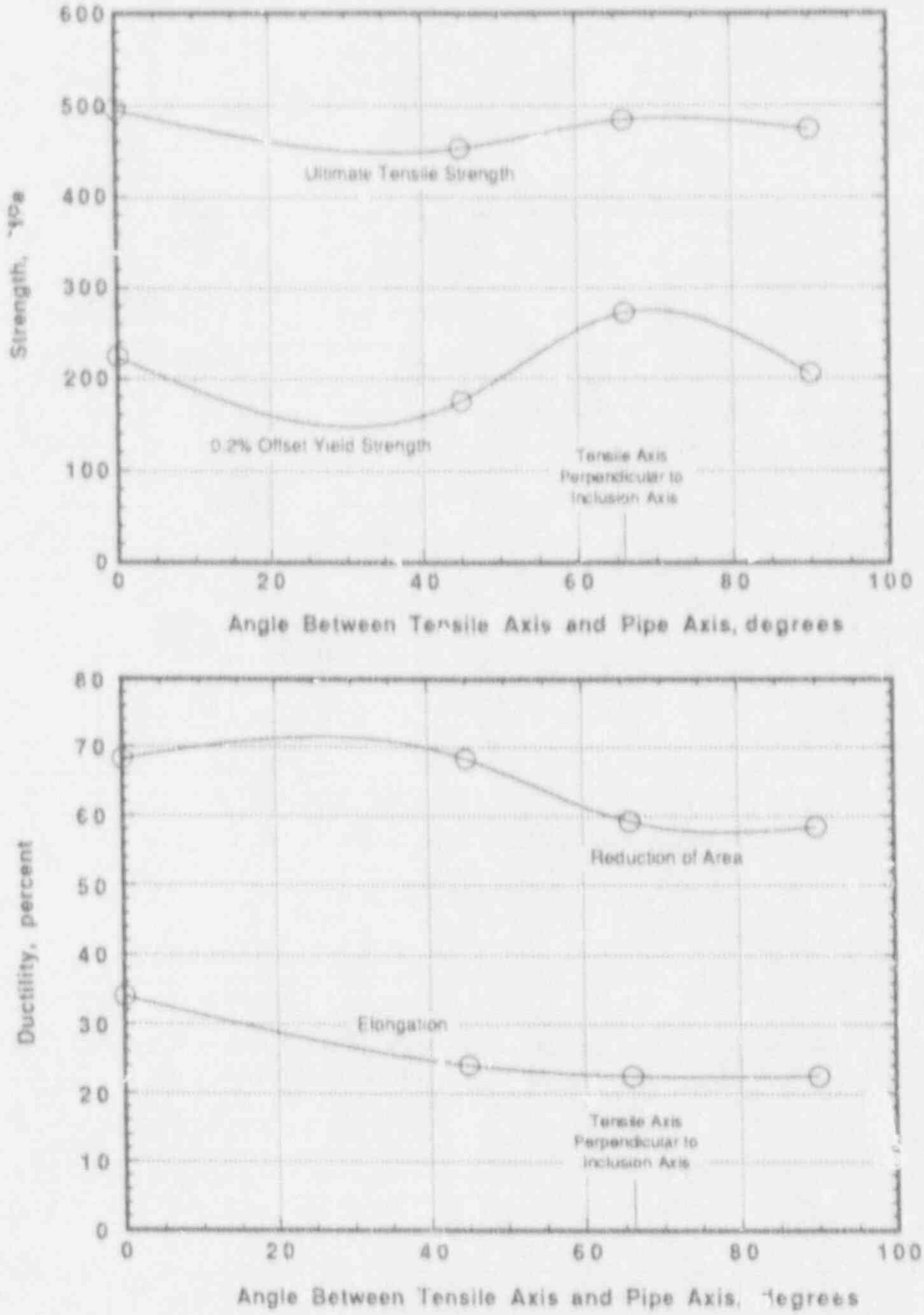

Figure 6.2 Tensile properties as functions of specimen orientation for Pipe DP2-F11 (A333 Grade 6)

SC-M-2/91-F7

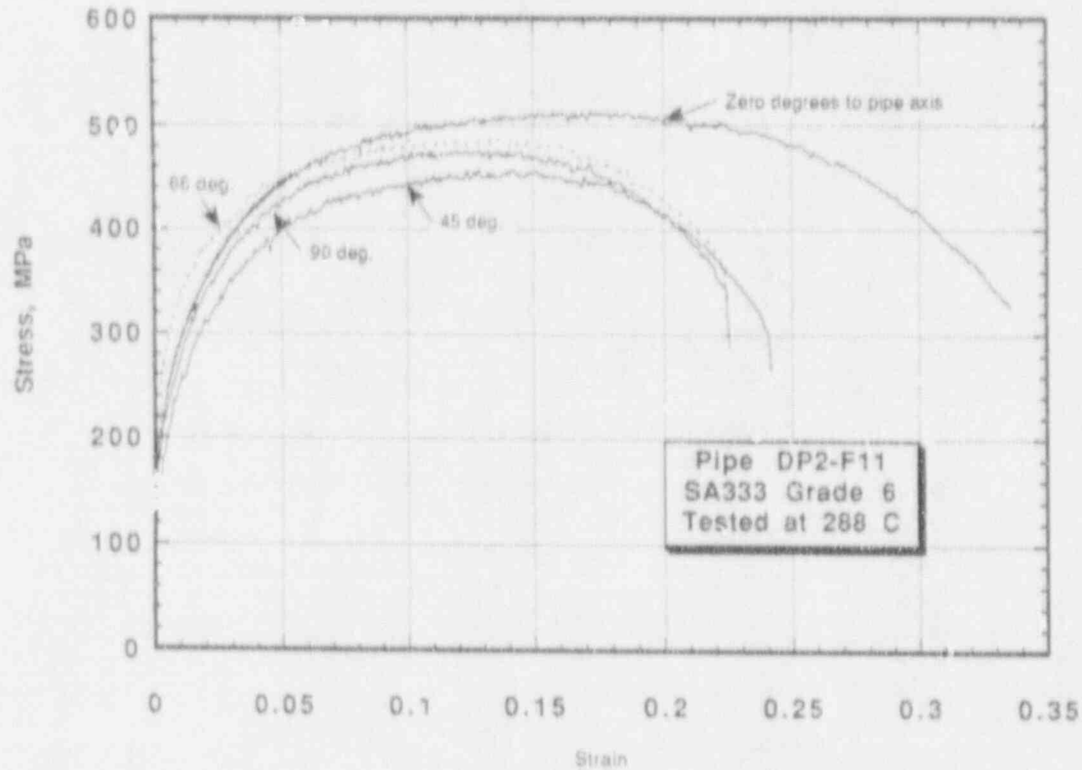

Figure 6.3 Engineering stress-strain curves for several different tensile specimen orientations in Pipe DP2-F11

SC-SA-7/91-F6.3

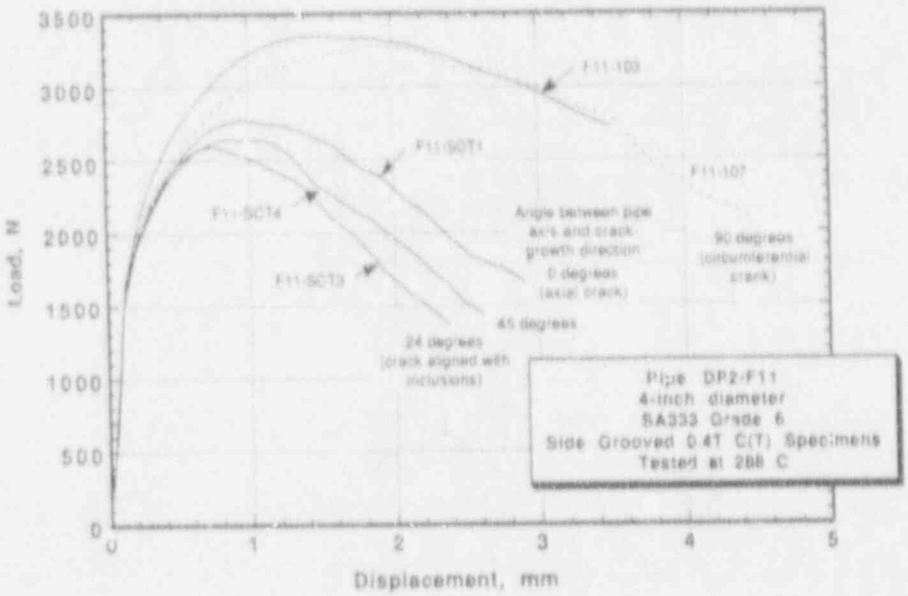

Figure 6.4 Load versus displacement curves for several different C(T) specimen orientations in Pipe DP2-F11

SC-SA-7/91-F6.4

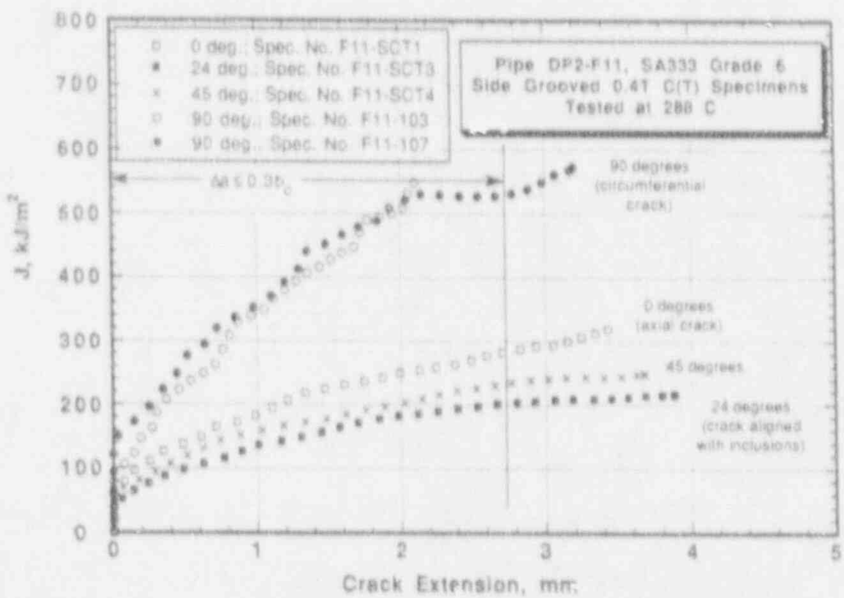

Figure 6.5 J-resistance curves for several different C(T) specimen orientations in Pipe DP2-F11

SC-SA-7/91-F6.5

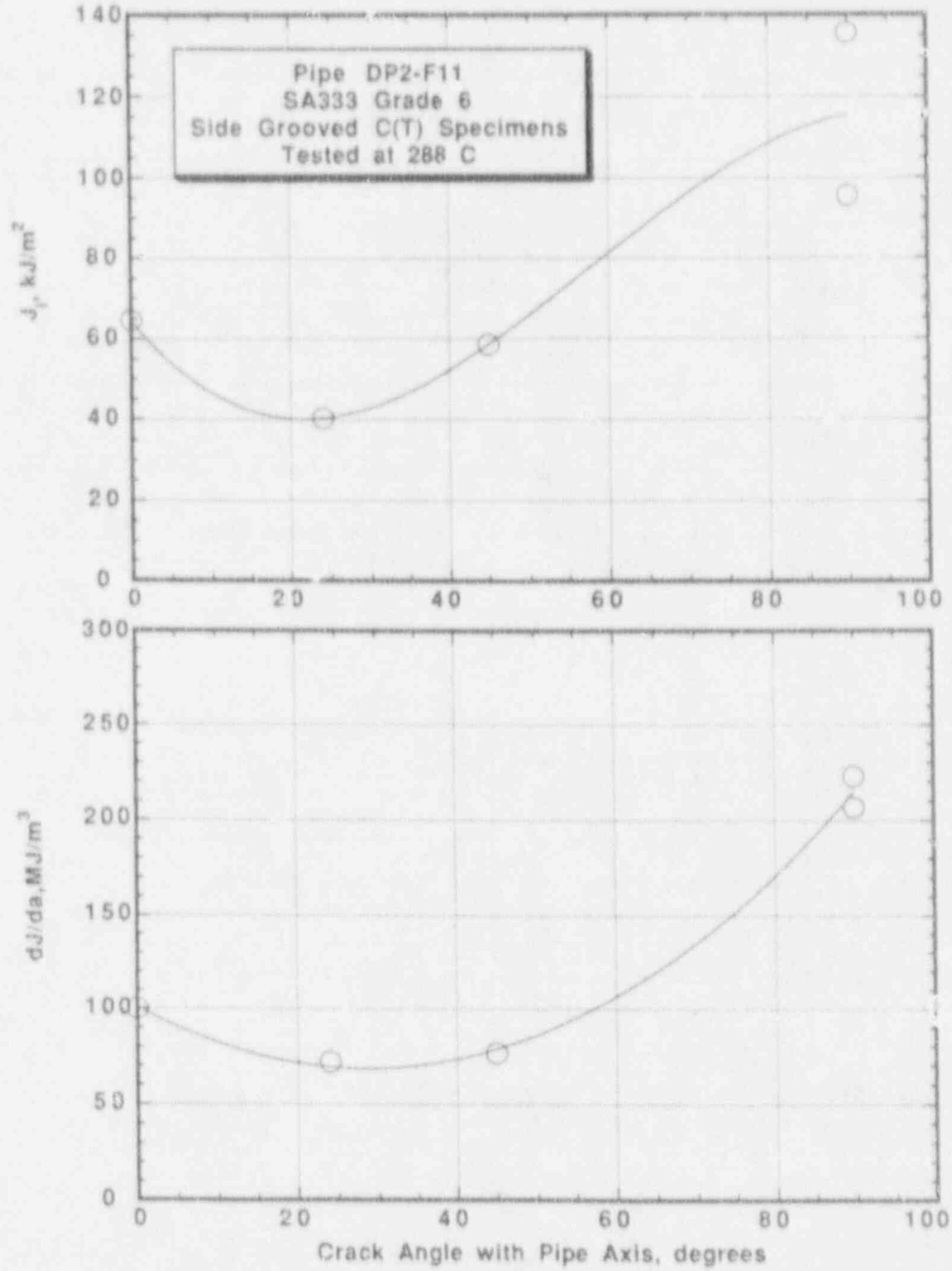

Figure 6.6 J_I and dJ/da as functions of C(T) specimen orientation in Pipe DP2-F11

SC-SA-7/91-F6.6

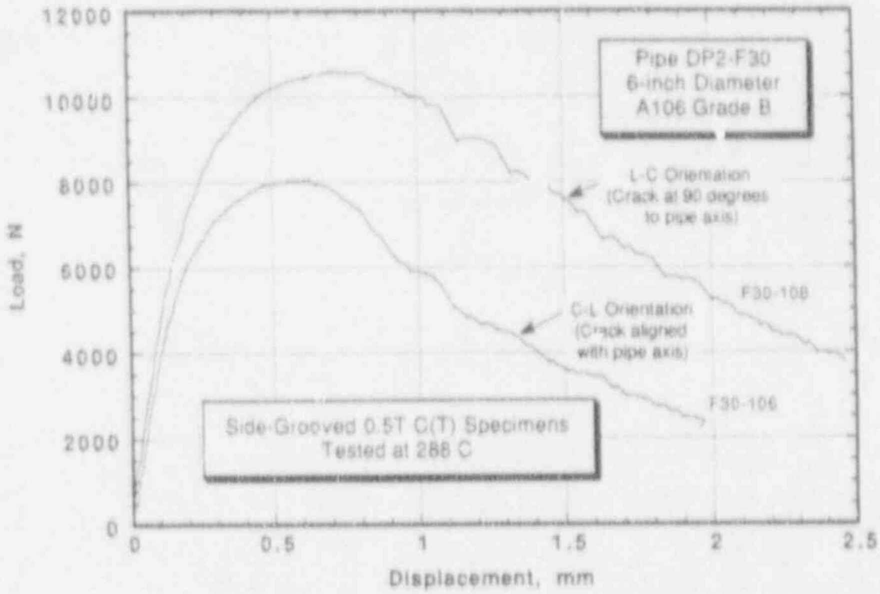

Figure 6.7 Load versus displacement curves f. r two different C(T) specimen orientations in Pipe DP2-F30

SC-SA-7/91-F6.7

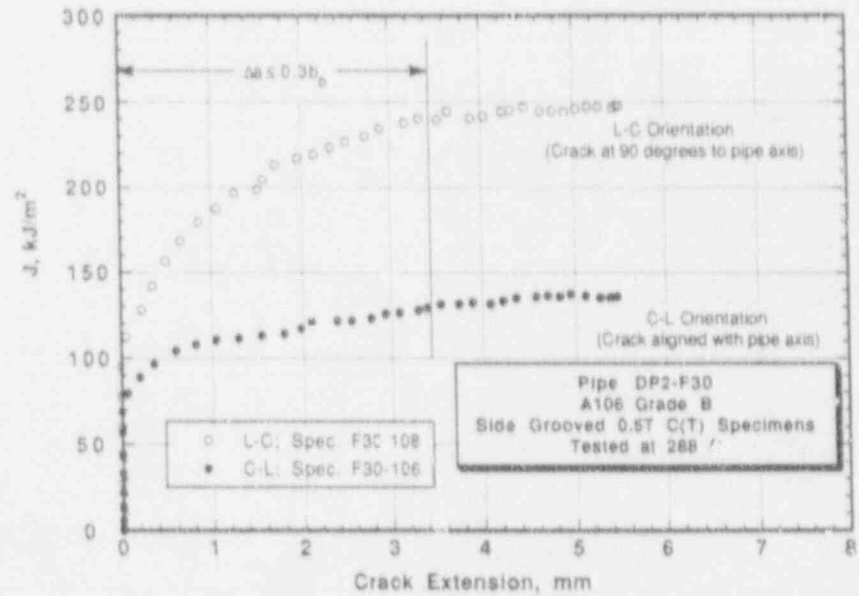

Figure 6.8 J-resistance curves for two different C(T) specimen orientations in Pipe DP2-F30

SC-SA-7/91-F6.8

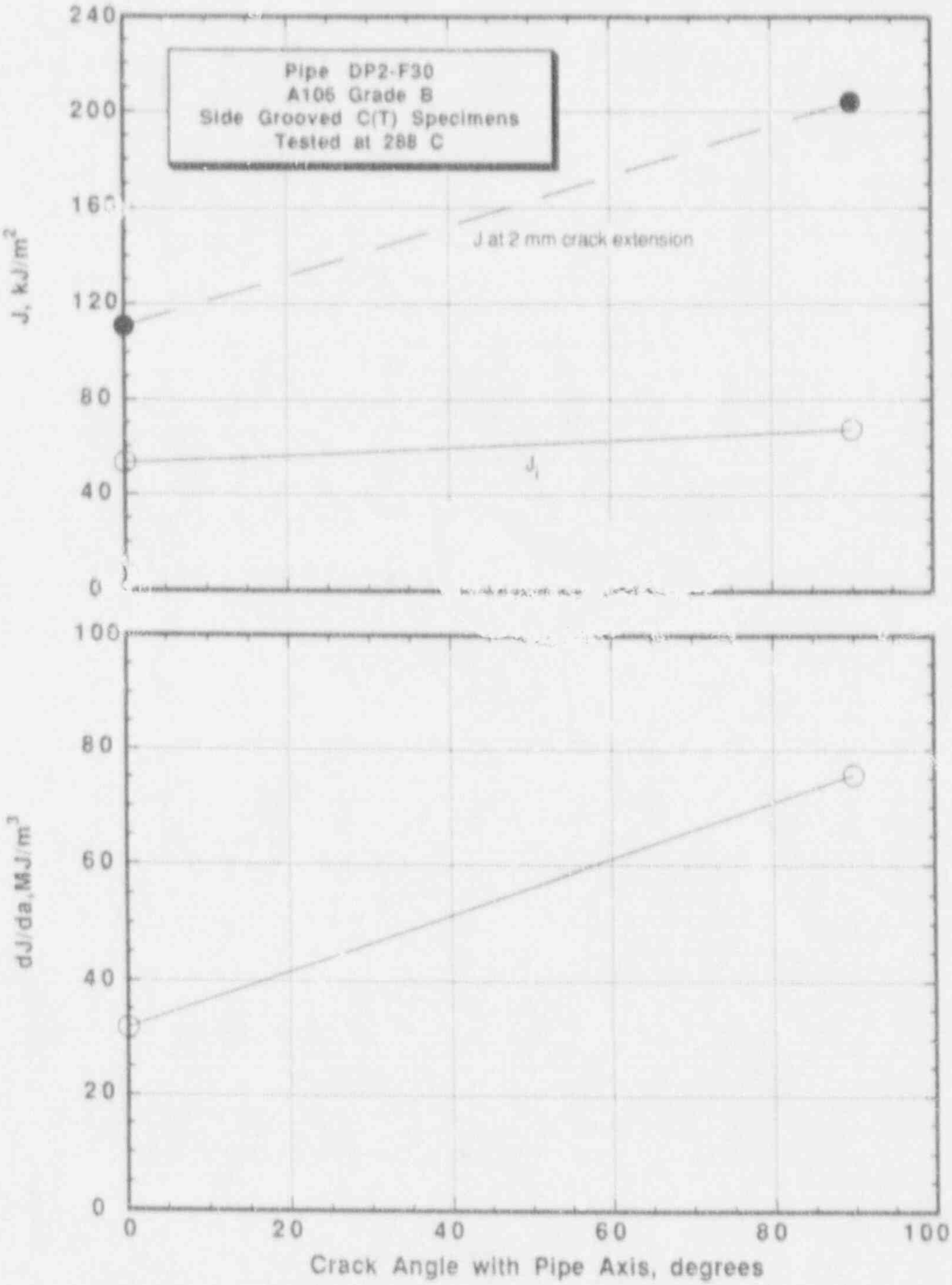

Figure 6.9 J_i, J at Δa = 2 mm, and dJ/da as functions of C(T) specimen orientation in Pipe DP2-F30

SC-SA-7/91-F6.9

Activity 5.2.1	Document inclusion size, shape, distribution, and orientation in carbon-steel pipes
Activity 5.2.2	Examine literature and conduct tests to determine toughness anisotropy as a function of inclusion characteristics
Activity 5.2.3	Assess usefulness of screening tests to predict out-of-plane crack growth

Progress during the past six-month period on each of these activities is described below.

6.3.3.1 Activity 5.2.1 Document inclusion size, shape, distribution, and orientation in carbon-steel pipes

The objective of this activity is to establish by metallographic examination the types of inclusions present and their size, shape, distribution, and orientation; to compare the inclusion characteristics with the pipes' propensity for out-of-plane crack growth; and to determine whether correlations exist.

Work conducted during the past six months included metallographic examination of specimens machined from four different carbon steel pipes to determine the inclusion characteristics. A fifth pipe had been examined earlier in the Degraded Piping Program. The five carbon steel pipes are described in Table 6.1 and their chemical compositions are given in Table 6.2. In addition to the metallographic studies, each of the carbon steel pipes tested in the Degraded Piping Program, the IPIRG Program, and the Short Cracks Program were carefully examined for skewed crack growth to see if the pipes' propensity for out-of-plane crack growth could be correlated with inclusion characteristics.

Experimental Procedures

Conduct Metallographic Examinations

Specimens that measured approximately 38 x 25 mm (1-1/2 x 1 inch) were cut from four carbon steel pipes (DP2-F9, -F26, -F29, and -F30; see Table 6.1), such that the longer dimension was parallel with the pipe axis. The outside surface of each specimen was ground flat and that surface was then prepared metallographically. The unetched polished surface was examined in an optical microscope to determine the nature of the nonmetallic inclusions. Photomicrographs at 100X and 500X magnification were taken of at least three areas selected at random on each specimen. Subsequent to the examination in the optical microscope, the specimens were subjected to imaging and X-ray mapping in a JEOL 840A scanning electron microscope to determine the chemical makeup of selected inclusions, using energy dispersive X-ray spectrometry.

Table 6.1 Description of Activity 5.2.1 pipes used in study of anisotropy

Pipe Ident. No.	Material Type	Schedule	Pipe Dimensions, mm (inch)	
			Diameter	Wall Thickness
DP2-F9	ASTM A333 Grade 6 carbon steel	100	254 (10)	18.3 (0.719)
DP2-F11	ASTM A333 Grade 6 carbon steel	80	102 (4)	8.6 (0.337)
DP2-F26	ASTM A516 Grade 70 carbon steel	N.A.	711 (28)	22.2 (0.875)
DP2-F29	ASTM A106 Grade B carbon steel	100	406 (16)	26.2 (1.031)
DP2-F30	ASTM A106 Grade B carbon steel	120	152 (6)	14.3 (0.562)

Table 6.2 Chemical composition of Activity 5.2.1 pipes used in study of anisotropy

Element	Weight Percentage for Indicated Pipe				
	Pipe DP2-F9	Pipe DP2-F11	Pipe DP2-F26	Pipe DP2-F29	Pipe DP2-F30
C	0.14	0.21	0.13	0.28	0.15
Mn	0.99	0.84	0.80	0.82	0.65
P	0.008	0.010	0.009	0.010	0.012
S	0.024	0.015	0.027	0.023	0.014
Si	0.20	0.19	0.25	0.18	0.20
Cu	0.076	0.035	0.12	0.088	0.28
Sn	0.014	0.001	0.007	0.011	0.018
Ni	0.12	0.006	0.13	0.11	0.14
Cr	0.12	0.027	0.13	0.14	0.18
Mo	0.042	0.012	0.040	0.041	0.055
Al	0.018	0.030	0.003	0.000	0.010
V	0.000	0.000	0.000	0.001	0.001
Cb	0.000	0.000	0.000	0.000	0.000
Zr	0.000	0.000	0.000	0.000	0.000
Ti	0.000	0.000	0.000	0.000	0.000
B	0.0001	0.0000	0.0001	0.0001	0.0000
Co	0.006	0.000	0.006	0.005	0.008
W	0.00	0.00	0.00	0.00	0.00
Pb	0.00	0.00	0.00	0.00	0.00
Ca	N.D.	N.D.	N.D.	N.D.	N.D.

Conduct Examinations of Fractured Pipes and C(T) Specimens

Each carbon steel pipe that had been subjected to a pipe fracture experiment in the Degraded Piping Program, the IPIRG Program, and the Short Crack Program was examined to determine the fracture path. Cracks at each end of the starting flaw were measured for length and angle and for the type of shear fracture, namely, single or double shear, as will be discussed later. Sketches were prepared to document the fracture features.

Similarly, fractured carbon steel compact specimens without side grooves, which had been tested at Battelle, were examined for skewed crack growth and sketches were prepared to document the fracture features.

Experimental Findings

Metallographic Examinations

Of the five carbon steel pipes examined (four in this study and one in the Degraded Piping Program), only one was found to have inclusions that were at a significant angle to the pipe axis. That pipe was DP2-F11, a 4-inch-diameter A333 Grade 6 pipe, which was subjected to tensile and C(T) tests in Activity 5.1.2 to determine the effect of specimen orientation on strength and crack growth resistance. The results of those tests were described previously in this report and indicated that the minimum toughness was associated with a crack growing parallel with the inclusions, which were inclined at an angle of approximately 24 degrees to the pipe axis. This pipe was also examined during the course of the Degraded Piping Program (see Appendix C in Ref. 6.2). In each of the other pipes examined, the inclusions were nominally aligned with the pipe axis.

As is indicated in Table 6.3, the general shapes of the inclusions varied among the five pipes examined. The two in which the stringer-type inclusions were the most elongated were DP2-F11 and -F30. Pipe DP2-F9 contained a mixture of short, medium, and long stringers, Pipe DP2-F29 had short to medium stringers, and Pipe DP2-F26 showed little evidence of stringer-type inclusions. Examples of inclusions in each of the five steels are shown in Figure 6.10 at a magnification of 500X.

Examination of the metallographically prepared specimens in the scanning electron microscope using energy dispersive X-ray spectrometry indicated the inclusions to be mainly manganese sulfides, along with some aluminum oxides, and occasional silicates. An example of manganese sulfide inclusions in Pipe DP2-F9 is shown in Figure 6.11a at 2000X magnification. The X-ray dot maps in Figures 6.11b, c, and d, in which the bright dots indicate the presence of manganese, sulfur, and aluminum, respectively, confirm that the inclusions shown in Figure 6.11a are, indeed, manganese sulfides.

Table 6.3 Appearance of stringer-type inclusions in pipes used in study of anisotropy

Pipe Ident. No.	Material Type	General Shapes of Stringer-Type Inclusions
DP2-F9	A333 Grade 6	Mixture of short, medium, and long stringers aligned with pipe axis
DP2-F11	A333 Grade 6	Numerous long stringers at an angle of ~24 degrees to the pipe axis
DP2-F26	A516 Grade 70	Short stringers only, aligned with pipe axis
DP2-F29	A106 Grade B	Mixture of short and medium stringers, aligned with pipe axis
DP2-F30	A106 Grade B	Numerous long stringers aligned with pipe axis

Fractured Pipe and C(T) Specimen Examinations

Mapping of fracture features on carbon-steel pipe specimens and C(T) specimens was completed during the past six-month period and detailed sketches of those features were prepared. Examples of the pipe-fracture sketches are shown in Figure 6.12 for three different carbon steel pipes in which the initial crack was circumferential. The view is from the outside of the pipe, as if the pipe had been flattened. Notice the three different crack growth patterns pictured in Figure 6.12. In Figure 6.12a, the crack path changed direction several times, such that its average direction was circumferential. In Figure 6.12b, the crack at each end of the starting flaw grew upward, whereas in Figure 6.12c, the crack grew upward at one end and downward at the other end.

Examples of the C(T) specimen sketches are shown in Figure 6.13. Figure 6.13a shows a single-shear crack that grew in the intended direction, while Figure 6.13b shows a double-shear crack that veered sharply from the intended (circumferential) direction.

Probably the most striking difference observed between C(T) tests and pipe tests was in the contribution of double-shear fracture to skewed crack growth (noncircumferential) from a crack that was originally circumferential. In C(T) specimens, if the growing crack developed as a double-shear crack, it veered off from the circumferential direction at a very steep angle. If, on the other hand, it developed as a single-shear crack, which appeared to be about equally likely, the crack extended circumferentially, although the fracture surface was tilted through the thickness.

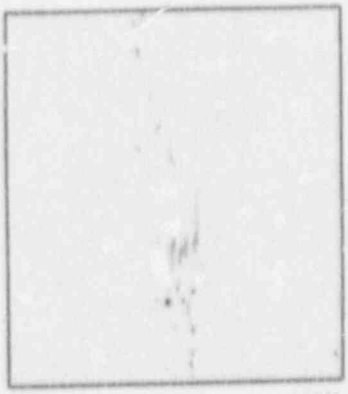

30892 385X
a. Pipe DP2-F9 (A333 Grade 6)

10876 385X
b. Pipe DP2-F11 (A333 Grade 6)

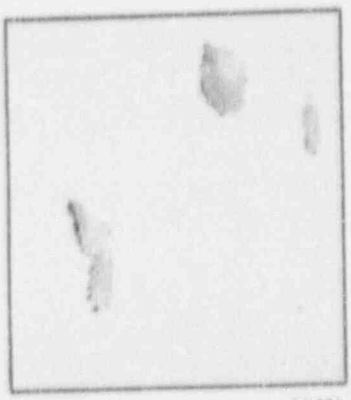

30896 385X
c. Pipe DP2-F26 (A516 Grade 70)

30906 385X
d. Pipe DP2-F29 (A106 Grade 8)

Pipe
Axis

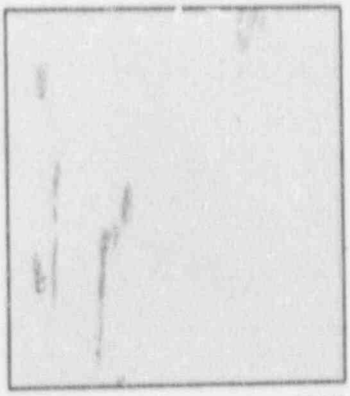

40310 385X
e. Pipe DP2-F30 (A106 Grade B)

Figure 6.10 Photomicrographs of sulfide inclusions in carbon steel pipes: (a) Pipe DP2-F9, (b) Pipe DP2-F11, (c) Pipe DP2-F26, (d) Pipe DP2-F29, and (e) Pipe DP2-F30

SC-SA-7/91-F6.10

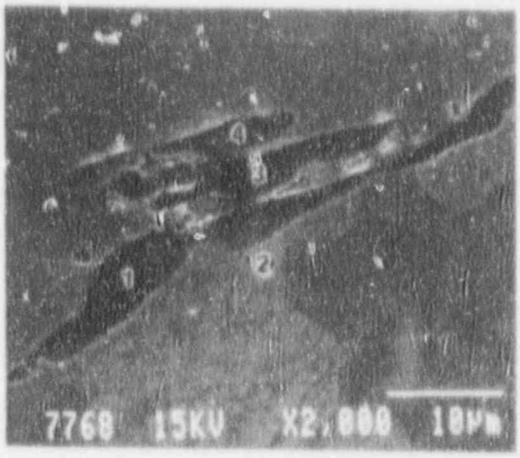

J7768 1540X
a. SEM Photographs of Inclusions

J7769 1540X
b. X-ray Dot Map for Manganese

J7770 1540X
c. X-ray Dot Map for Sulfur

J7771 1540X
d. X-ray Dot Map for Aluminum

Figure 6.11 Photographs and X-ray dot maps of selected inclusions in Pipe DP2-F9 (A333 Grade 6 carbon steel) to verify presence of manganese sulfides

SC-SA-7/91-F6.11

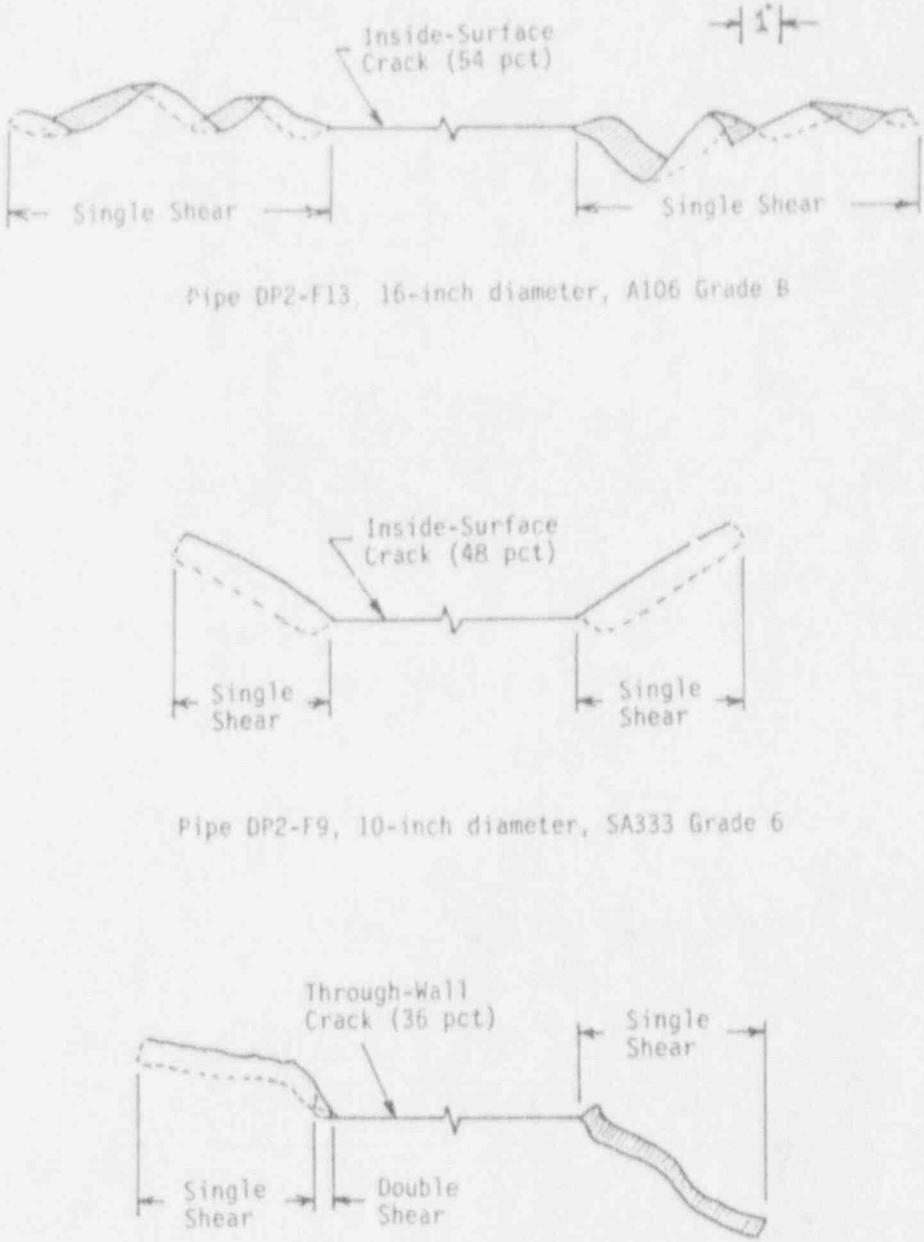

Pipe DP2-F13, 16-inch diameter, A106 Grade B

Pipe DP2-F9, 10-inch diameter, SA333 Grade 6

Pipe DP2-F30, 6-inch diameter, A106 Grade B

Figure 6.12 Examples of skewed crack extension in tests on three different carbon steel pipes

SC-M-2/91-F10

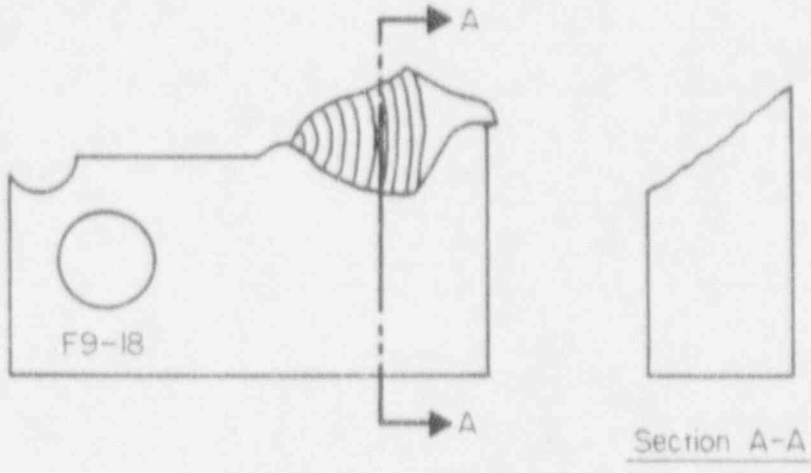

(a) Single-shear fracture

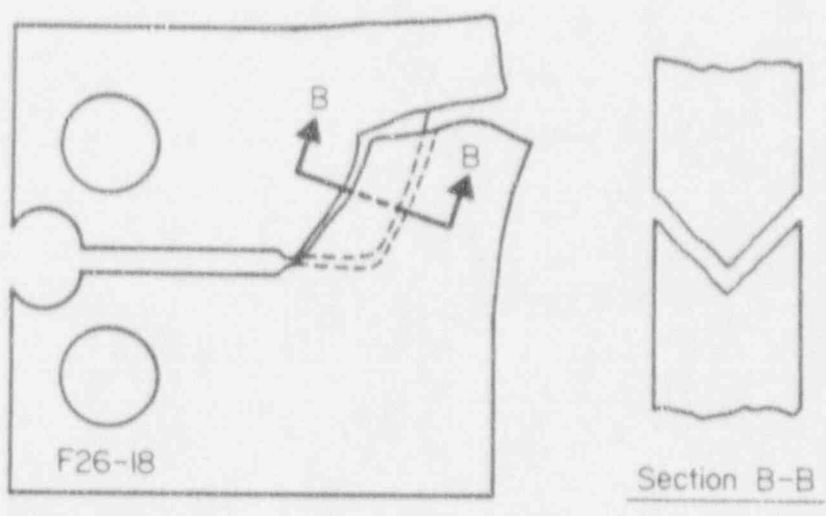

(b) Double-shear fracture

Figure 6.13 Comparison of single shear and double shear fractures in carbon steel C(T) specimens

SC-SA-7/91-F6.13

In 22 pipe specimens examined, double-shear fractures were almost nonexistent and yet the cracks in every case except one, that being a pipe loaded in axial tension, grew at an angle to the circumference. The reason for the striking difference between the C(T) specimens and the pipe specimens is not clear at this time.

These results suggest that a C(T) specimen test in which the crack extends in double shear and veers sharply from the circumferential direction probably has little relevance to pipe fracture tests, for two reasons: (1) double-shear fractures rarely occur in pipe tests and (2) the J-R curve data obtained from a C(T) test in which the crack grows in double shear are unreliable beyond crack initiation, due to the unusually flat load-displacement curve beyond maximum load and the uncertainty in the length of the growing crack. Hence, where side grooving is not an acceptable means to achieve straight crack growth in C(T) specimens, it is recommended that only results from nonside-grooved specimens in which the crack extends in single shear be used to develop J-R curves.

6.3.3.2 Activity 5.2.2 Examine Literature and Conduct Tests to Determine Toughness Anisotropy as a Function of Inclusion Characteristics

The objective of this activity is to determine the relation between inclusions and toughness anisotropy in carbon steels, based on a review of data from the technical literature and on the results of Charpy V-notch impact tests on specimens machined from pipes at several different orientations.

During the last six months, a literature review was initiated and most of the pertinent references have been obtained. Charpy V-notch impact tests at several different orientations were also completed for four different carbon steel pipes that have exhibited skewed crack growth in pipe fracture experiments.

Experimental Procedures

Conduct Literature Review

A search of the METADEX database, produced by the American Society for Metals (ASM) and the Metals Society (London) was conducted, using the DIALOG Information Retrieval Service. The resulting abstracts were reviewed and pertinent references were retrieved from the Battelle library or, if unavailable at Battelle, were ordered through interlibrary loan.

Conduct Charpy V-Notch Impact Tests

Charpy V-notch impact specimens were machined from four different carbon steel pipes at angles of 0, 30, 60, and 90 degrees to the pipe axis. Duplicate specimens were tested at a temperature that produced 100 percent shear fracture; for Pipes DP2-F9, -F26, and -F29, that temperature was 38 C (100 F), whereas for Pipe DP2-F30, that temperature was 204 C (400 F). Data recorded included absorbed energy, fracture appearance, and lateral expansion.

Experimental Findings

Literature Review

Gathering of references from the literature search was nearly completed during the past six-month period; several references requested from interlibrary loan have not yet been received. In-depth examination of the references has not yet begun, but a cursory review of information relating to rolled steel plate material indicated that transverse Charpy V-notch toughness values often are as low as 40 to 50 percent of longitudinal toughness values. Furthermore, it appears that the magnitude of the toughness anisotropy remains approximately the same, even when the sulfur content of the steel is significantly less than that present in the pipes tested in this program.

Charpy V-Notch Impact Tests

The results of Charpy V-notch impact tests for four different carbon steel pipes, conducted at temperatures that produced ductile fractures, are shown in Figure 6.14. A strong effect of specimen orientation is evident; the toughness in the transverse direction (90 degrees in Figure 6.14) ranged from approximately 30 to 55 percent of that in the longitudinal direction (zero degrees). This result is similar to that found for rolled steel plate in the literature search.

From the summary of results shown in Table 6.4, no clear picture emerges regarding the effect of sulfur content on toughness anisotropy. The greatest anisotropy, expressed as the ratio of transverse toughness to longitudinal toughness, was exhibited by Pipe DP2-F30; the least anisotropy occurred in Pipe DP2-F29, despite the fact that Pipe DP2-F30 contained the least sulfur of the four pipes evaluated. Inclusion shape, on the other hand, appears to have a predictable effect on toughness anisotropy. Pipe DP2-F30, which contains numerous, long, stringer-type inclusions, exhibited the greatest toughness anisotropy. Pipes DP2-F26 and -F29, on the other hand, which contain few, if any, long stringer-type inclusions, exhibited the least toughness anisotropy. Even in those less anisotropic pipes, however, the transverse toughness was only about half of the longitudinal toughness.

6.3.3.3 Activity 5.2.3 Assess Usefulness of Screening Tests to Predict Out-of-Plane Crack Growth

The objective of this activity is to assess the usefulness of screening tests, namely, microscopic examination of nonmetallic inclusions or Charpy V-notch tests at several different orientations, to predict the occurrence and severity of out-of-plane crack growth in pipe experiments.

It would not be prudent to draw final conclusions regarding the usefulness of the screening tests until the references from the literature search have been reviewed thoroughly. However, from the experimental results obtained in this program, it appears that microscopic examination of inclusions may provide a promising approach to predicting the degree of anisotropy. Pipes that had few, long, stringer-type inclusions (Pipes DP2-F26 and -F29) displayed significantly less toughness anisotropy than did a pipe that had numerous, long, stringer-type inclusions (Pipe

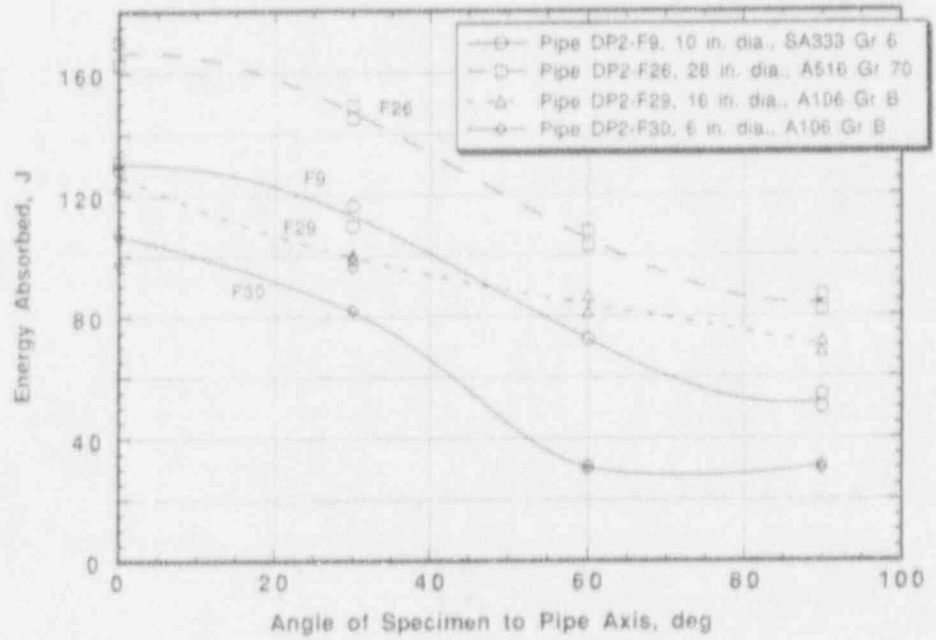

Figure 6.14 Energy absorbed by Charpy V-notch impact specimens as a function of specimen orientation
Note: All fractures were 100 percent ductile

SC-SA-7/91-F6.14

Table 6.4 Ratio of transverse to longitudinal toughness in Charpy V-notch impact specimens machined from carbon steel pipes

Pipe Ident. No.	Material Type	Sulfur Content	Inclusion Content	$CVN_{trans.}/CVN_{long.}$
DP2-F9	A333 Grade 6	.024	Mixture	0.40
DP2-F26	A516 Grade 70	.027	Short	0.51
DP2-F29	A106 Grade B	.023	Mixture	0.55
DP2-F30	A106 Grade B	.014	Long	0.29

DP2-F30). The sulfur content of the steel, however, does not appear to be a good indicator of toughness anisotropy.

It is possible that Charpy tests could provide useful screening data, but that possibility cannot be confirmed at this time because none of the carbon steel pipes evaluated to date from the Degraded Piping Program, the IPIRG Program, or the Short-Crack Program exhibited circumferential crack growth. Each pipe in which strong toughness anisotropy was observed in Charpy tests also displayed skewed crack growth in pipe tests. If a pipe were found that exhibited circumferential crack growth, and Charpy V-notch tests indicated that little toughness anisotropy was present, then the usefulness of Charpy tests to provide screening data would be confirmed. Data from other experiments and programs will be examined in the future.

6.4 Plans for Next Fiscal Year

During the next fiscal year the following efforts are scheduled.

6.4.1 Subtask 5.1 Assess Effect of Toughness Anisotropy on Pipe Fracture Under Combined Loads

There are six activities in this subtask. The plans for each of these are given below.

Activity 5.1.1 - Determine Driving Force for Angled Stationary Crack. These finite element analyses will be completed for stationary cracks of different orientations.

Activity 5.1.2 - Conduct Tensile tests at Different Orientations. This activity has been completed. The data will be put into a digital format for incorporation to the PIFRAC data base.

Activity 5.1.3 - Determine Driving Force for Angled Growing Crack. No efforts are planned for next fiscal year.

Activity 5.1.4 - Determine Angled Crack Principal Stresses. No efforts are planned for next fiscal year.

Activity 5.1.5 - Formulate Approximate Corrections. No efforts are planned for next fiscal year.

Activity 5.1.6 - Assess if Optional Efforts are Necessary. No efforts are planned for next fiscal year.

6.4.2 Subtask 5.2 Determine Magnitude of Toughness Anisotropy and Establish a Screening Criterion to Predict Out-of-Plane Crack Growth

There are three activities in this subtask. The plans for each of these are given below.

Activity 5.2.1 - Document Inclusion Size, Shape, Distribution, and Orientation in Carbon-Steel Pipes. These efforts will be completed next fiscal year.

Activity 5.2.2 - Examine Literature and Conduct Tests to Determine Toughness Anisotropy as a Function of Inclusion Characteristics. These efforts will be completed next fiscal year.

Activity 5.2.3 - Assess Usefulness of Screening Tests to Predict Out-of-Plane Crack Growth. These efforts will be started next year.

6.4.3 Subtask 5.3 Prepare Interim and Topical Reports on Anisotropy and Mixed-Mode Studies

No efforts are planned for this subtask next fiscal year.

6.4.4 Optional Subtask 5.4 Establish Ductile Crack Growth Resistance Under Mixed-Mode Loading

No efforts are planned for this optional subtask next fiscal year.

6.4.5 Optional Subtask 5.5 Refine J-Estimation Scheme Analyses for Pipes

No efforts are planned for this optional subtask next fiscal year.

6.5 References

6.1 Wilkowski, G. M. and others, "Degraded Piping Program - Phase II," Summary of Technical Results and Their Significance to Leak-Before-Break and In-Service Flaw Acceptance Criteria, March 1984-January 1989, by Battelle Columbus Division, NUREG/CR-4082, Vol. 8, March 1989.

6.2 Scott, P. and Brust, F., "An Experimental and Analytical Assessment of Circumferential Through-Wall-Cracked Pipes under Pure Bending," Battelle Topical Report from NRC Degraded Piping Program, NUREG/CR-4574, September 1986.

7. TASK 6 CRACK OPENING AREA EVALUATIONS

7.1 Task Objective

The objective of this subtask is to make improvements in the crack-opening area predictions for circumferentially cracked pipe, with particular attention to cracks in welds. The crack opening area (COA) analyses will be incorporated into the SQUIRT code.

7.2 Task Rationale

From past efforts in the Degraded Piping Program, IPIRG, and ASME Section XI round-robin efforts, it has been found that the leakage area predictions are reasonably consistent for circumferential through-wall cracked pipe in bending (with the cracks in the base metal). For the case of a crack in the center of the weld, the predictions showed more scatter in the intermediate to higher bending load levels. For the case of a crack in the base metal, but with the pipe in combined bending and tension, the scatter in the results was significantly greater. If the crack had been in a weld under combined loading, the scatter probably would have increased even more. The accuracy of the solutions for a crack in a weld and for cracked pipe under combined loading needs verification and improvement for LBB analyses.

7.3 Task Approach

The five specific subtasks in this task are:

Subtask 6.1	Create combined loading improvements
Subtask 6.2	Implement short TWC crack-opening improvements
Subtask 6.3	Improve weld crack evaluations
Subtask 6.4	Modify SQUIRT Code
Subtask 6.5	Prepare topical report on crack-opening-area improvements
Subtask 6.6	Leak rate quantification.

Progress was made in Subtasks 6.1, 6.3, and 6.6.

7.3.1 Subtask 6.1 Create Combined Loading Improvements

The three activities in this subtask are:

Activity 6.1.1	Establish LBB.ENG method for crack opening
Activity 6.1.2	Account for pressure on the crack face
Activity 6.1.3	Verify with existing data.

Progress was made in Activity 6.1.1.

7.3.1.1 Activity 6.1.1 Establish LBB.ENG Method for Crack Opening

Currently two analysis methods are widely used for the prediction of the crack-opening area for leak-rate analysis. These are the GE/EPRI method (Ref. 7.1) and the Paris or NUREG/CR-3464 method (Ref. 7.2). For fracture predictions involving the load-carrying capacity of through-wall-cracked pipe, the GE/EPRI method generally underpredicts the experimental loads, and the NUREG/CR-3464 method frequently overpredicts the experimental loads. The LBB.ENG method (Ref. 7.3) was found to give slightly conservative yet reasonably accurate predictions of the experimental loads.

This activity will involve incorporating a crack-opening-area prediction capability in the LBB.ENG method.

Progress

The leak-rate prediction models for piping (for example the SQUIRT Code) are based on knowledge of the area of crack opening (ACO). The ACO is then used as input to the thermal-fluids models to predict leak rates through the cracks. Thus, it is important to be able to accurately predict the ACO in the J-estimation models.

Reference 7.4 shows that accurate ACO predictions are obtained if an elliptic opening shape is assumed. Thus, if we can estimate the total center-crack-opening displacement, δ, with, of course, knowledge of the total crack length, 2a, the ACO is easily obtained (major ellipse axis = 2a, minor axis = δ). Hence, the problem boils down to needing an accurate predictive method for the crack-opening displacement. Previously, methods for evaluating δ were provided for by the GE/EPRI method.[a] Here methods are provided for predicting δ, and hence ACO, for other J-estimation techniques for bending, pressure, and combined loadings. Additionally, predictions of the crack-opening displacement for a weld crack are generally based on assuming that base metal Ramberg-Osgood properties prevail throughout and by using a weld metal J-resistance curve. Here we provide an improved methodology based on the LBB.ENG method, which accounts for both the base and weld metal properties.

COD Predictions, Base Metal

Bending

In order to make predictions of the area of crack opening so that leak rates may be determined, it is necessary to predict the center-crack-opening displacement (COD). Reference 7.5 shows that the area of crack opening is accurately estimated by fitting an elliptic crack opening shape through the predicted COD and crack length. Thus, our task is to develop the COD for methods other than the GE/EPRI technique.

(a) The Paris and LBB.NRC (Ref. 7.5) J-estimation methods predict ACO directly using a plastic correction to the elastic solution.

The COD may be separated into the elastic and plastic components as:

$$\delta = \delta_e + \delta_p \quad . \tag{7-1}$$

The elastic component (δ_e) may be obtained from any known solution such as the Sanders (Ref. 7.6 solution, as interpreted by Yoo and Pan (Ref. 7.7). However, when this closed form solution (based on Shell theory) is compared with both experimental data and the GE/EPRI finite element solutions, the elastic COD is underpredicted by a factor of about three. Because Reference 7.4 shows that the GE/EPRI solutions compare well with both experimental data and separate finite element solutions, we use these solutions for δ_e in Equation (7-1) for the present method.

It now remains to determine the plastic component of displacement, δ_p. After attempting to develop several techniques based upon the works of Smith (Ref. 7.8) and Hasegawa et al. (Ref. 7.9), the following alternative technique was developed. We assume that the plastic component of COD (δ_p) may be obtained by assuming

$$\delta_p = \{R_m(1 + \sin\theta/2)\}\ \phi_{pc} \quad , \tag{7-2}$$

where R_m is mean pipe radius, 2θ is the total crack angle, and ϕ_{pc} is the total plastic rotation of the pipe due to the crack. The term in brackets in Equation (7-2) represents the distance from the rigid plastic neutral axis to the center of the crack. Hence, it is clear that Equation (7-2) should, at worst, represent a conservative prediction.

Numerical Example

Bending Analyses: Crack-opening-displacement predictions are provided for the LBB.ENG2 method in Figures 7.1, 7.2, and 7.3. Figures 7.1, 7.2, and 7.3 correspond, respectively, to Experiments 4111-1, 4111-2, and 4111-3 from the Degraded Piping Program (Ref. 7.10). It is seen that comparison between experiment, GE/EPRI, and the LBB.ENG2 method is quite good. Pipe properties and material data are taken from Reference 7.4.

Combined Loading Analyses: COD predictions can now be implemented into NRCPIPE for all analysis methods with the exception of the R6 and η-factor analysis.

For the Paris (NUREG/CR-3464) and LBB.NRC methods, the center-crack-opening displacement is evaluated by calculating the crack-opening area using the equation supplied in References 7.2 and 7.5, and assuming an elliptical, crack-opening shape.

For the LBB.GE, LBB.ENG1, and LBB.ENG2 analyses, the center-crack-opening displacement is calculated using Equation (7-1) with the following changes. As before, δ is the total center-crack-opening displacement and the subscripts "e" and "p" refer to elastic and plastic components of the center-crack-opening displacement. δ_e contributions can be determined

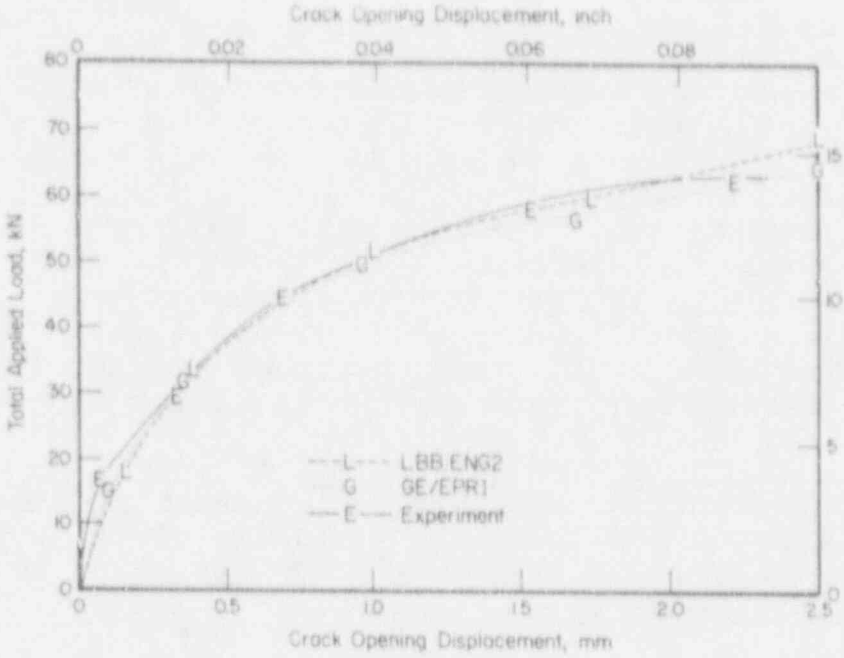

Figure 7.1 Crack-opening displacement in Experiment 4111-1 up to load at crack initiation

SC-M-11/90-F2

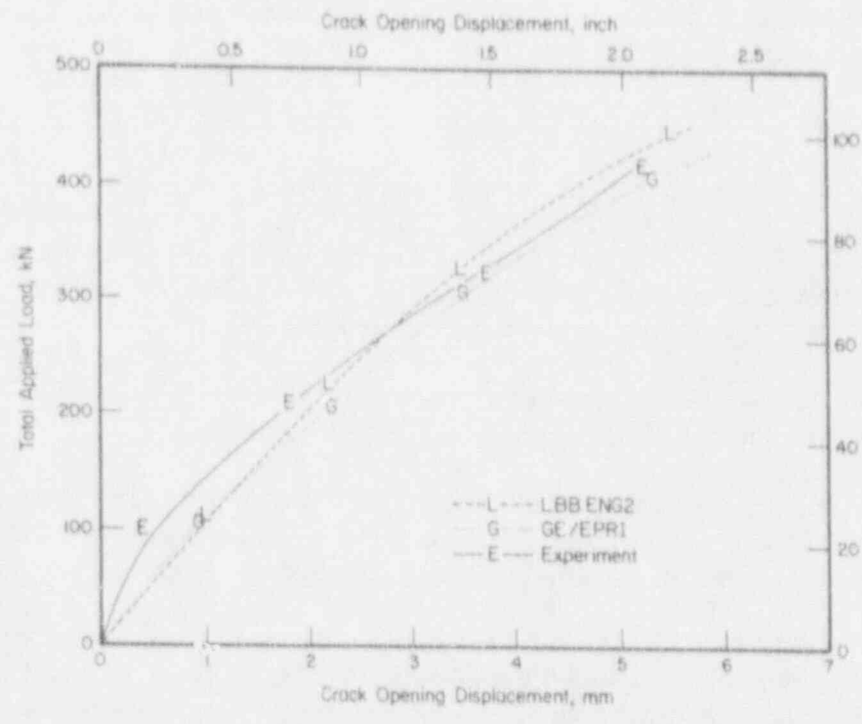

Figure 7.2 Crack-opening displacement in Experiment 4111-2 up to load at crack initiation

SC-M-11/90-F3

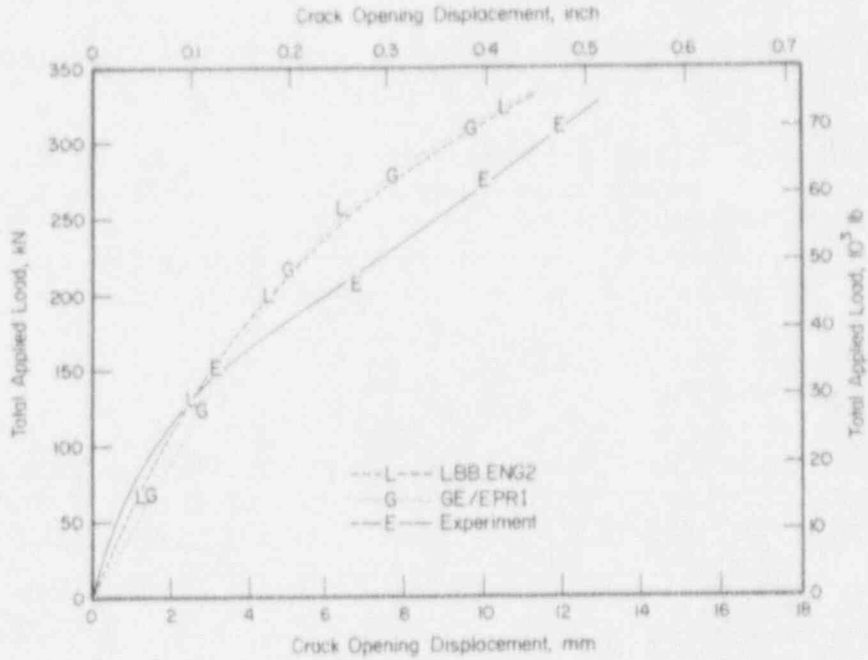

Figure 7.3 Crack-opening displacement in Experiment 4111-3 up to load at crack initiation

SC-M-11/90-F4

by several different methods. In our approach we used the GE/EPRI displacement functions. Note that for combined bending and tension loading, δ_e has separate contributions for the bending and tension solutions, which are summed.

The δ_p contribution is evaluated using;

$$\delta_p = \Delta_{cpt} + [R_m(1 + \sin\beta)]\phi_{pc} \quad (7\text{-}3)$$

In Equation (7-3), Δ_{cpt} is the tension component that naturally arises in the LBB.ENG2 mathematical solution method, R_m is the mean radius, and ϕ_{pc} is the plastic rotation of the pipe due to the crack. For the pure bending case Δ_{cpt} is equal to zero.[a] For pure pressure, both Δ_{cpt} and ϕ_{pc} are non-zero. This is because the pressure has an induced bending contribution. The term $R_m(1 + \sin\beta)$ is the moment arm used in the assumption that the bending induced component of δ_p may be obtained by multiplying the distance from the rigid plastic neutral axis to the center of the crack in the pipe by the plastic rotation due to the crack. With the above assumption β is given by:

$$\beta = \theta/2 + (\pi/2)(\sigma_t/\sigma_f) \quad (7\text{-}4)$$

(a) Δ_{cpt} is not available with the LBB.ENG1 and LBB.GE methods, and thus is not active in Equation (7-3) for these methods.

where θ is the half crack angle, σ_t is the tensile stress applied to the pipe, and σ_f is the flow stress. Equations (7-3) and (7-4) reduce to Equation (7-2) for pure bending.

Note that in the LBB.ENG2 solution it is possible to account for the possibility that the rotation of the pipe is restrained for the pressure contributions. This is a possibility that may occur for a crack in a pipe system where terminal ends at nozzles or other restraints from elbows, tees, etc. could restrain induced bending from pressure loads. This restraint could have implications by reducing the crack-opening area under normal conditions below that calculated by existing LBB analyses.

Comparisons to Experimental Data

In Figures 7.1 to 7.3 comparisons of predicted and experimental COD were presented for the case of pure bending. It was shown that Equation (7-3) provides reasonable results for pure bending. Here we provide comparisons for one pressure and two combined pressure and bending cases.

For pressure only, geometric and material property data are provided in Table 7.1 for the pipe analysis. The stress-strain data and the J-resistance curve data came from the Degraded Piping Program data record book for Experiment 4121-1. Figure 7.4 provides a comparison of the applied pressure versus center-crack-opening displacement for the GE/EPRI and LBB.ENG2

Table 7.1 Crack-opening displacement analysis of past Degraded Piping Program data

Exp. No.	Loading	O.D.[(a)], mm	t, mm	θ/π [(b)]	Ramberg-Osgood Data[(c)] α	n	σ_o, MPa	E, MPa	J at Initiation, (N/mm)
4121-1	Pressure	168.1	12.9	0.386	42.5	3.88	294.1	179,330	1,090
4131-1	Pressure & Bending	166.4	13.4	0.37	42.5	3.88	294.1	179,330	1,090
4131-9	Pressure & Bending	274.1	18.7	0.37	14.4	3.64	383.3	179,240	298

(a) O.D. = Outer diameter.
(b) θ is half the crack angle.
(c) Ramberg-Osgood formula

$$\frac{\varepsilon}{\varepsilon_o} = \frac{\sigma}{\sigma_o} + \alpha\left(\frac{\sigma}{\sigma_o}\right)^n$$

where $\sigma_o = (\sigma_y + \sigma_u)/2$.

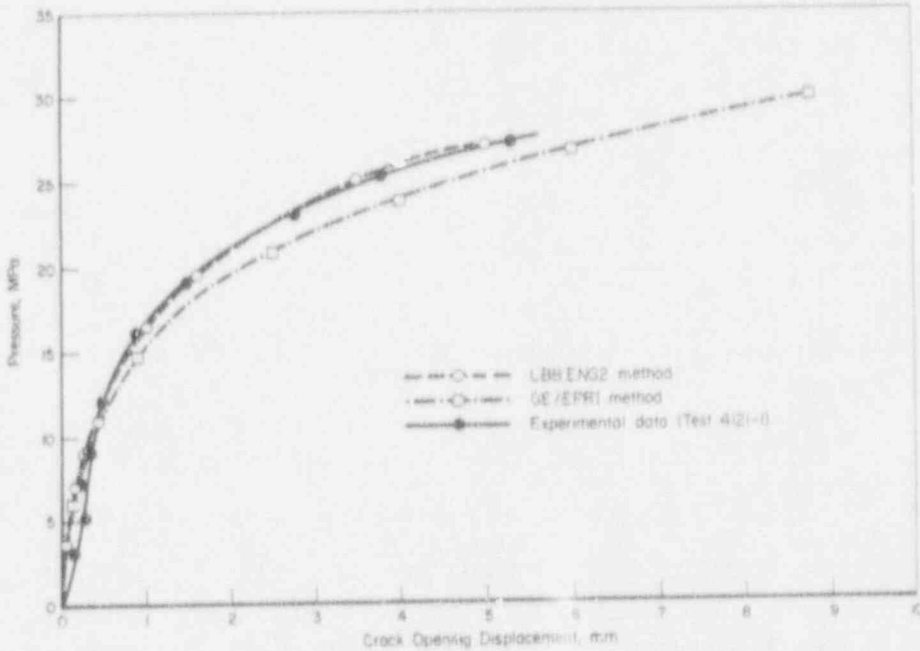

Figure 7.4 Comparison of various analyses to center-crack-opening displacement for pressurized pipe Experiment 4121-1 on 6-inch-diameter TP304 stainless steel pipe

SC-M-12/90-F6

methods[a] with experimental data up to crack initiation. Extremely good agreement was found.

Pressure and bending Experiments 4131-1 and 4131-9 from the Degraded Piping Program were also analyzed. Pertinent material property and geometry data for these experiments are given in Table 7.1. Comparisons between the experiments and the various analyses are given in Figures 7.5 and 7.6 for Experiments 4131-1 and 4131-9, respectively. For Experiment 4131-1 (Figure 7.5) it is seen that all methods overpredicted the center-crack-opening displacements compared to the experimental data. The Paris and LBB.NRC solutions gave the worst predictions, while the LBB.ENG2 method gave the best.

For Experiment 4131-9 (see Figure 7.6) it is seen that the Paris and LBB.NRC methods overpredicted the experimental data, while the LBB.GE and LBB.ENG2 methods underpredicted the center-crack-opening displacement. Note that the curves should not begin at the origin (see Figures 7.5 and 7.6), since the pipe was pressurized, then loaded in bending. These comparisons show that for combined pressure and bending, the Paris and LBB.NRC methods provided overpredictions in Figures 7.5 and 7.6. The LBB.GE and LBB.ENG2 methods overpredicted the case in Figure 7.5 and underpredicted the case in Figure 7.6.

(a) These are the only two methods currently available for pressure only analyses.

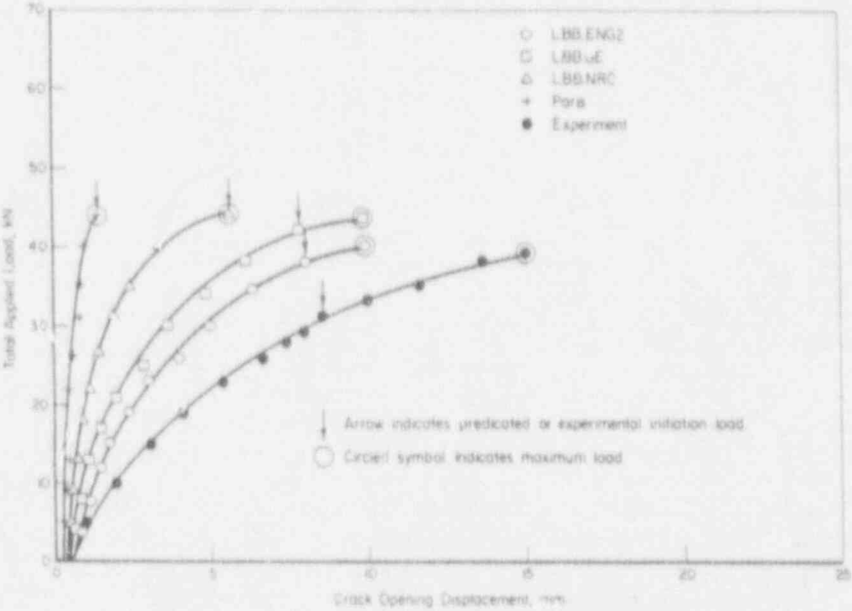

Figure 7.5 Comparison of predictions of various analyses to experimental center-crack-opening displacement for pressure and bend Experiment 4131-1 on 6-inch-diameter TP304 stainless steel pipe

SC-M-12/90-F7

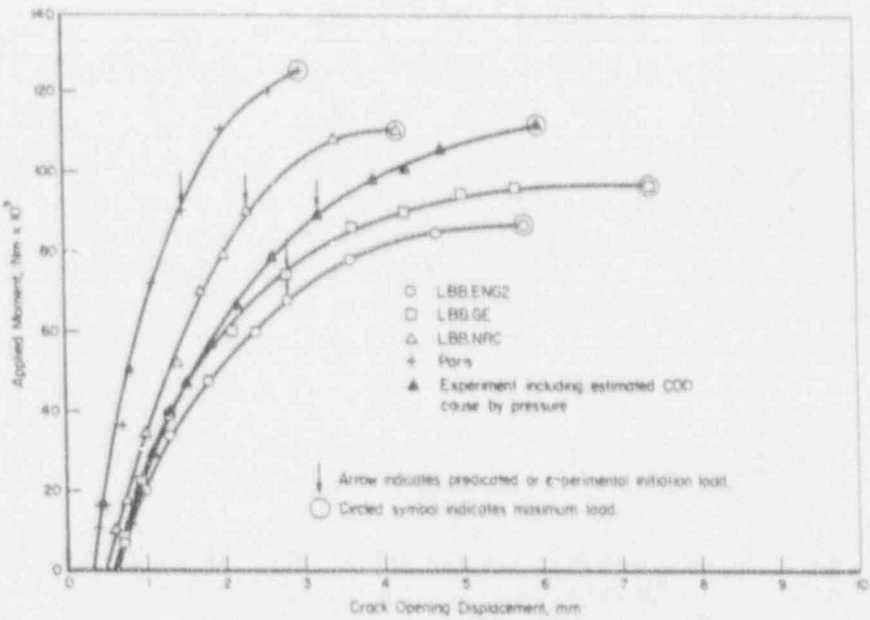

Figure 7.6 Comparison of predictions of various analyses to experimental center-crack-opening displacement for pressure and bend Experiment 4131-9 on 10-inch nominal diameter A333 Grade 6 pipe

SC-M-12/90-F8

No other base-metal through-wall-cracked pipe experiments under combined pressure and bending were available from the Degraded Piping Program (Ref. 7.10) for comparison. However, there are two pressure and bending, through-wall cracked pipe fracture experiments with the cracks in the weld available for future comparisons.

7.3.2 Subtask 6.3 Improve Weld Crack Evaluations

The two specific activities in this subtask are:

Activity 6.3.1 Incorporate weld corrections in crack-opening displacement analyses
Activity 6.3.2 Compare with recent Degraded Piping Program and Task 1 data.

Progress was made mainly for Activity 6.3.1.

7.3.2.1 Activity 6.3.1 Incorporate Weld Corrections in Crack-Opening Displacement Analyses

The second major improvement suggested from the 1987 ASME PVP leak-rate round-robin results is to make better predictions for a crack in the center of a weld. In some LBB applications, it has been proposed to use the upper bound for the material Ramberg-Osgood curve. This is believed to be conservative for crack-opening-area predictions, but inconsistent with the pipe fracture analyses for maximum load predictions.

To eliminate the inconsistencies between the load and crack-opening-area analyses and improve the accuracy of both analyses, the rule-of-mixture approach or other approaches from Activity 1.4.3 for fracture mechanics load predictions will be incorporated into the area of crack opening analyses. This will be specifically applicable to through-wall, weld-metal cracks.

Progress

COD Predictions for Weld Cracks

An approximate method for evaluating crack-opening displacement of through-wall cracks in the center of a pipe girth weld is provided here. This method is based on the extension of the LBB.ENG2 method (Ref. 7.11).

Leak-rate estimation models are important elements in developing a leak-before-break (LBB) analysis for piping integrity and safety. Crack-opening area and displacement models are currently used in evaluating performance of cracked pipe weldments. Predictions are usually based on base metal stress-strain data and a weld metal J-resistance curve (Ref. 7.12). This can lead to mispredictions depending on th[illegible]ngth ratio of the base versus weld material.

Here, a methodology was develope[illegible] predict the crack-opening displacement (COD) of through-wall-cracked (TWC) duct[illegible] pipe weldments subjected to constant bending loads. The method of analysis is based on

(a) classical deformation theory of plasticity,
(b) constitutive law characterized by Ramberg-Osgood model, and
(c) equivalence criteria incorporating reduced thickness analogy for simulating system compliance due to the presence of a crack in weld metal.

The method is general in the sense that it may be applied in the complete range between elastic and fully plastic conditions. See Section 2 for more details about the J-estimation portion of the method.

In the development of an estimation scheme for elastic-plastic fracture mechanics, it is generally assumed that the generalized displacements, energy release rate, crack-opening displacement, and other fracture parameters admit an additive decomposition of elastic and plastic components. For example, the total crack-opening displacement, δ, can be separated into an elastic part, δ_e, and a plastic part, δ_p. The elastic solution is well-established and can be obtained from the current literature (Refs. 7.6 and 7.7). It now remains to determine the plastic component δ_p of COD for welds.

Consider a TWC pipe under constant bending moment M in Figure 7.7 which has length L, mean radius R, thickness t, and crack angle 2θ with the crack circumferentially located in the weld material of length L_w. Suppose, the actual pipe can be replaced by a pipe with reduced thickness t_e which extends for a distance $\hat{a} \geq L_w$ (Figure 7.8). The reduced thickness section which actually results in material discontinuity is an attempt to simulate the reduced system compliance due to the presence of the crack. A similar equivalence method has been successfully implemented to evaluate performance of TWC pipes under various loading conditions (Refs 7.3, 7.11, 7.13, and 7.14). These assumptions are applied to develop a closed-form solution for plastic rotation ϕ_p of the pipe at the crack plane. Assuming a rigid body rotation, a conservative estimate of δ_p can be obtained as using Equations (7-3) and (7-4), where here Δ_{cpt} and ϕ_{pc} come from the LBB.ENG2 method for weldments, described in Section 2.

Numerical Examples

Bending

Consider two circumferential TWC pipe weldments, one with R = 52.87 mm and t = 8.56 mm (R/t = 6), and the other with R = 55.88 mm and t = 3.81 (R/t = 15), each of which is subjected to constant bending moment M applied at the simply supported ends. In both pipes, it is assumed that 2θ = 139 degrees and L_w = 5.59 mm. The constitutive law for base and weld metals are assumed to follow the Ramberg-Osgood model.

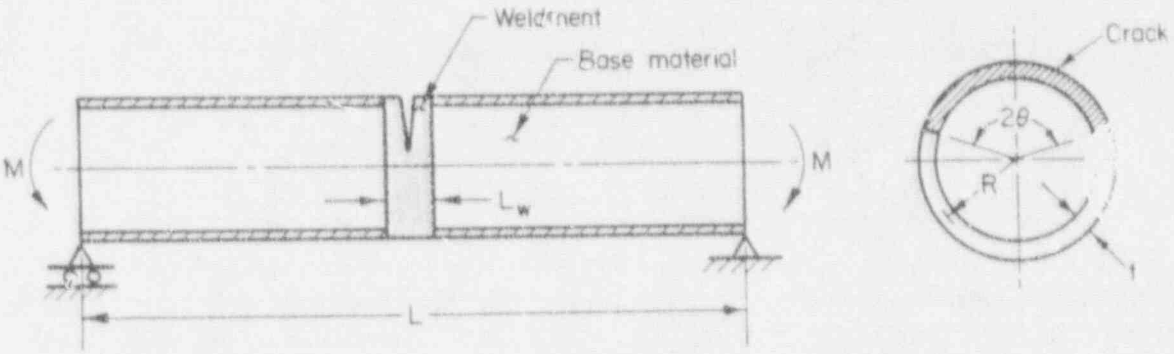

Figure 7.7 Schematics of pipe weldments with a circumferential flaw

SC-SA-7/91-F7.7

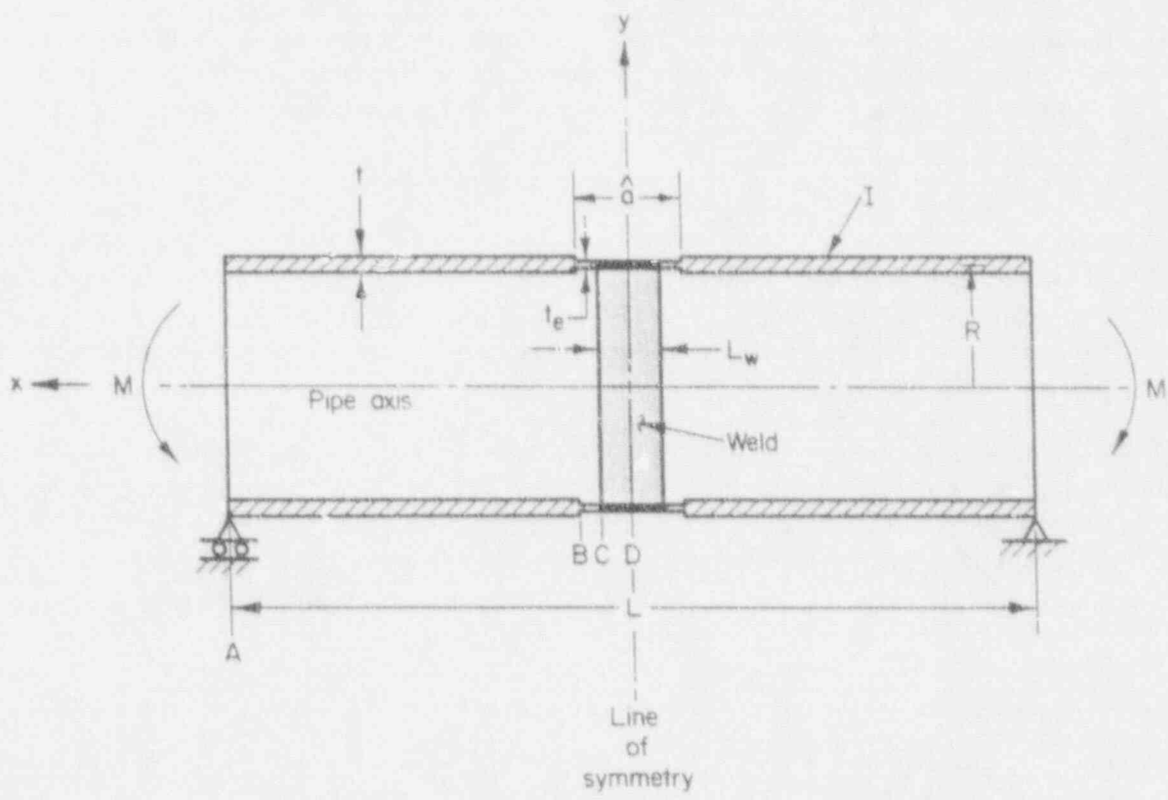

Figure 7.8 Reduced section analogy

SC-SA-7/91-F7.8

The numerical values of flow stress σ_o, modulus of elasticity E, and the Ramberg-Osgood constants α and n are shown in Table 7.2.

Table 7.2 Ramberg-Osgood coefficients of experiment analyzed

Material	σ_o, MPa	E, GPa	α	n
TP304 Base Metal	303.3	175.76	30.56	3.826
SAW Metal	358.5	175.76	11.96	9.370

Figures 7.9 and 7.10 show several plots of total M versus COD obtained from various levels of approximation for both pipes with R/t = [illegible] and R/t = 15, respectively. Also shown in the figures are the results of finite element analyses (FEM), which can be used as reference solutions for evaluating the accuracy of analytical methods. Comparisons of the results of approximate method solely based on all base or all weld material properties with those of FEM suggest that they provide only lower and upper bounds of actual COD at any given load M. However, neither of them can be used to predict the actual values of δ precisely.

Figures 7.9 and 7.10 also exhibit the results of the proposed method for several values of $\hat{a}$ representing the length of reduced thickness section. They all show reasonably good agreement with the solutions of FEM. Although, $\hat{a}$ is treated here as a free parameter, an optimum value $\hat{a}_{opt} = 4\ L_w$ appears adequate, and this is the value chosen for the estimation scheme described in Section 2.0.

Pressure

Figure 7.11 shows several plots of total applied load (P) versus COD (δ) obtained from estimation methods and finite element method (FEM). Comparisons with FEM suggest that the results of current methods such as LBB.ENG2 based on either all-base or all-weld material properties may not be satisfactory.

Figure 7.11 also exhibits the results of the proposed method for several representative values of $\hat{a}$. As observed earlier when comparing the energy release rates, COD estimates with $\hat{a}/L_w = 2$ provide reasonably good agreement with FEM. For larger values of $\hat{a}/L_w$, the values of COD are found to depart significantly from those obtained from FEM. However, in all cases, the proposed method provides better estimates than those based on current methods.

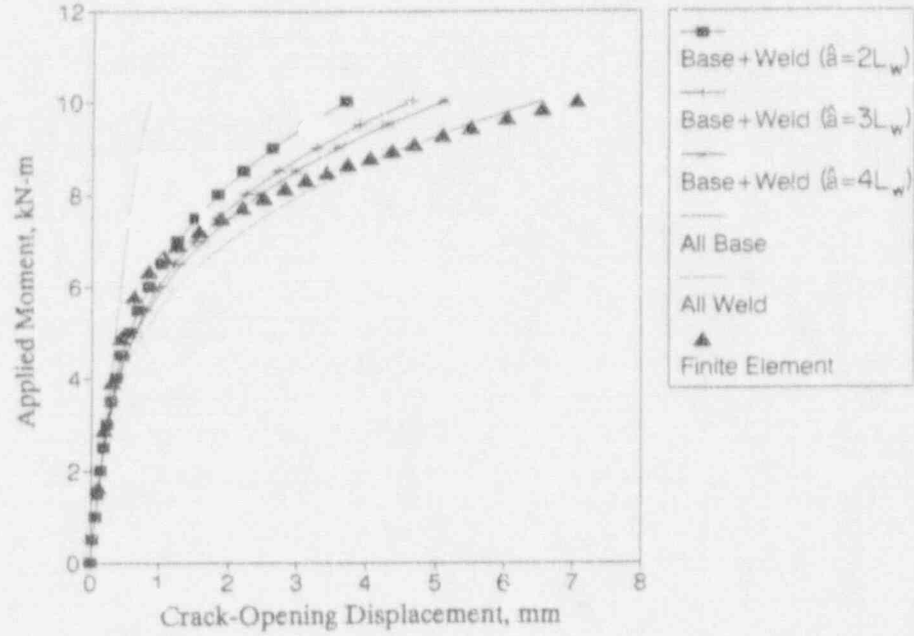

Figure 7.9 Comparisons of M versus COD (R/t ≅ 6)

SC-M-1/91-F11

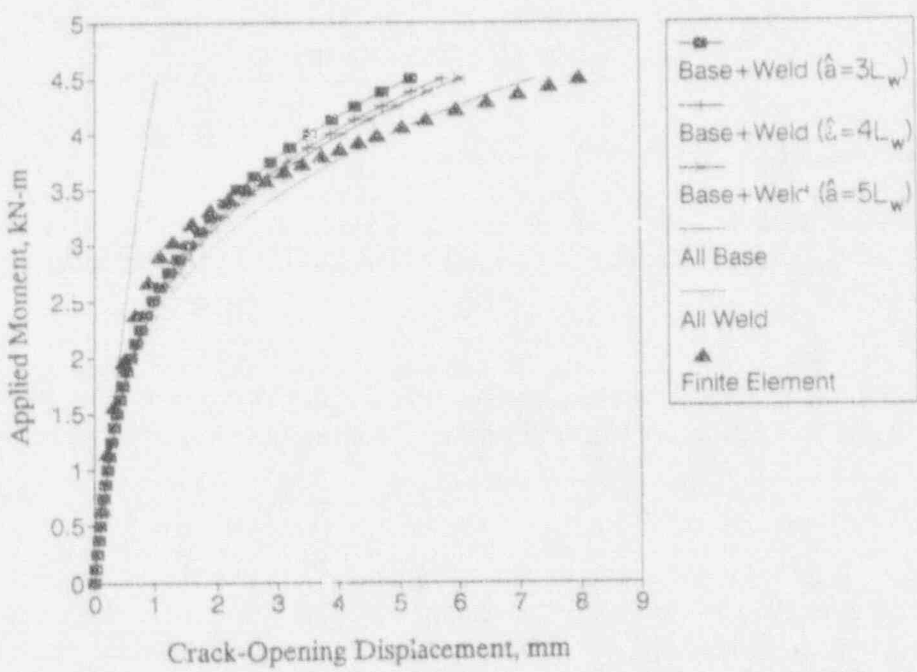

Figure 7.10 Comparisons of M versus COD (R/t ≅ 15)

SC-M-1/91-F10

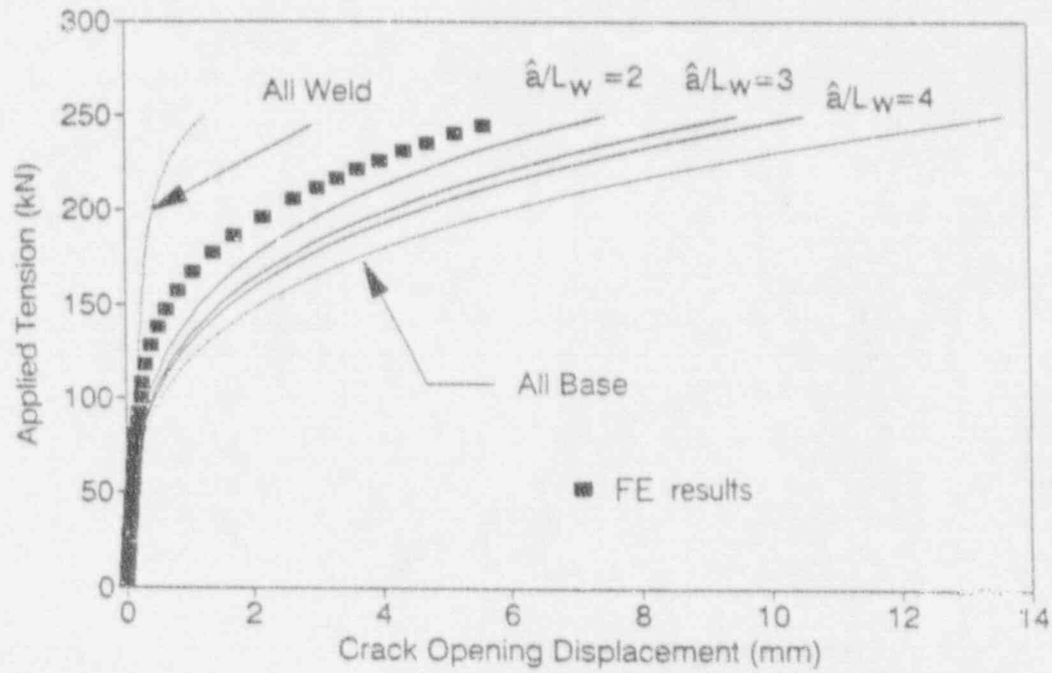

Figure 7.11 Comparisons of applied load versus computed crack-opening displacement

SC-M-4/91-F10

7.3.3 Subtask 6.6 Leak Rate Quantification

This is a new subtask created since the last semiannual report. Its objective, rationale, and approach are given below, since they were not given in the first semiannual report (Ref. 7.15).

7.3.3.1 Objective

The objective of this effort is to perform analyses to support changes to the NRC's current Regulatory Guide 1.45, "Reactor Coolant Pressure Boundary Leakage Detection Systems."

7.3.3.2 Rationale

Regulatory Guide 1.45 was published in May 1973, and is now considered outdated. The NRC currently wants to update this procedure taking into account the current leak-detection instrumentation capabilities, experience from the accuracy of leak detection systems in the past, and current analysis methods to assess the significance of the detectable leakage relative to the structural integrity of the plant. Leak-detection capabilities at normal operating conditions are used in current leak-before-break (LBB) analyses. The consistency of the LBB procedures needs to be considered in any changes to Regulatory Guide 1.45, and the impact of such changes on structural integrity of piping not approved for LBB needs to be considered.

7.3.3.3 Approach

The analyses to be performed shall build on other work being done in Task 6. The specific work to be performed shall include the following activities.

- Activity 6.6.1 Develop the technical background information for verification of analyses to be used
- Activity 6.6.2 Evaluate the proposed changes in leak detection requirements in terms of the potential impact on LBB analyses
- Activity 6.6.3 Evaluation of the proposed changes on leak rate for "non-LBB" piping systems
- Activity 6.6.4 Coordination with NRC-RES and NRC-NRR staff
- Activity 6.6.5 NUREG report

The approach for the first three activities is described below. Progress to date is limited to item 2(c) in Activity 6.6.1.

Activity 6.6.1 Develop the Technical Background Information for Verification of Analyses

The efforts involved in this activity include:

(1) Obtaining typical system normal plus safe shut-down earthquake (SSE) stresses. This shall be done by reviewing information in technical reports, and through guidance from NRC-NRR staff.

Material property data to be used shall come from the NRC's PIFRAC database (Ref. 7.16), the Degraded Piping Program (Ref. 7.10), and the IPIRG program (Ref. 7.17) as applicable.

(2) Verification analyses shall be conducted to define the areas of uncertainty in the analyses prior to conducting the necessary sensitivity studies. Such verification analyses shall include:

(a) Comparisons of predictions and experimental data for center-crack-opening displacement and failure loads for complex-cracked pipe.

(b) Evaluation of crack morphology effects on the leak-rate analyses. This shall involve examining photographs of fracture surfaces from various reports and actual surfaces where obtainable, to assess the different parameters necessary in the leak-rate analyses.

(c) Evaluation of the effect of restraint of induced bending for pressure/tension loads for TWC pipe. This effect could lower the crack opening displacement from that calculated in typical LBB analyses.

(3) To establish confidence in the analysis procedures, benchmark leak-rate and failure load predictions shall be conducted for cracks that have been found by leakage in service.

Activity 6.6.2 Evaluate the Proposed Changes in Leak Detection Requirements in Terms of the Potential Impact on LBB Analyses

This activity will establish leak-rate detection limits for different size piping in the BWR and PWR systems, assuming a simple through-wall circumferential crack in the piping systems. This procedure shall consider keeping a safety margin of √2 on the normal plus SSE stresses for flaw stability. The NRCPIPE code shall be used with the LBB.ENG2 analysis method employing lower-bound tensile properties and J_d-R curves to predict the maximum loads. The leak rates at the normal operating stresses shall be determined using the SQUIRT code with average strength properties. These calculated leak rates shall be reduced by a safety factor that shall account for uncertainties in the SQUIRT leak-rate model as determined from comparison to existing test data. This safety factor may differ from the current NRC safety factor of 10 on leakage in LBB analyses. The final leak rate that will have safety margins on failure stress and leakage detection requirements will be established for selected piping systems in BWR's and PWR's. This procedure will establish a maximum allowable leak rate for piping systems that are approved for LBB, and will then set a limit on the smallest diameter pipe where LBB can be accepted.

Activity 6.6.3 Evaluation of the Proposed Changes on Leak Rate for "Non-LBB" Piping Systems

Once Activity 6.6.2 is completed, evaluation of the proposed changes on leak rate for "non-LBB" piping systems shall be made. This involves assessing the crack sizes that can be detected from the proposed new leakage detection limits. This shall be done using both the leak-rate limits defined in Activity 6.6.2 and the current Reg. Guide 1.45 leak-rate limits to detect flaws in non-LBB approved piping systems.

Such calculations shall be somewhat similar to the LBB-approved-pipe sensitivity studies, but shall consider both long circumferential surface crack and complex-crack geometries (Ref. 7.18). This sensitivity study shall define the family of cracks that could be safely detected by leakage, and how changes in the Reg. Guide 1.45 leak-rate limits affect the inherent flaw detection capability.

Sensitivity studies shall also be conducted to assess the change in leakage rate. This shall be done by considering subcritical crack growth rates for the crack at normal operating stresses. This shall provide a basis for the change in leak-rate requirements in the Reg. Guide 1.45.

7.3.3.4 Progress

The progress in this subtask to date involves evaluation of the effect of induced bending restraint for axial tension loads for circumferentially cracked pipe, Activity 6.6.1(2-c). Current analyses assume that for axial stresses (generally pressure induced) the pipe is free to rotate. The restraint of the rotation increases the failure stresses (Ref. 7.19), but can decrease the crack opening at a given load. If the pipe system restrains the bending (i.e., from cracks being close to a nozzle or restraint from the rest of the piping system) then the leak rate will be less than that calculated by using analyses that assume that the pipe is free to rotate. This will cause the actual crack to be larger than calculated by the current analyses methods for the same leak rate. Since normal operating stresses have a large component of the total stress being the pressure stress, this can have a significant effect on LBB analyses.

As a numerical example, consider a TWC pipe with mean radius R = 355.6 mm (14 inches), thickness t = 35.56 mm (1.4 inch), R/t = 10, and two distinct cases of initial crack angle 2θ with $\theta/\pi = 1/8$ and $\theta/\pi = 1/4$. For material properties, it is assumed that the modulus of elasticity E = 200 GPa and the Poisson's ratio $\nu = 0.3$. The pipe is subjected to remote pressure with the resultant force applied at the centroid of uncracked pipe cross section. Linear elastic analyses by finite element method (FEM) are performed to examine the effects of restraint due to induced bending in a piping system when the pressure load is applied. Figure 7.12 shows a mesh representing finite element discretization of the pipe under consideration.

Figure 7.13 presents the results of crack opening displacements (COD) as a function of "restraint length" normalized with respect to the mean pipe diameter D_m (where $D_m = 2R_m$). The restraint length defined here simply represents the location of restrained pipe cross section from the cracked plane. The COD values are also normalized with reference to the crack opening displacement when no external constraints are present in the pipe (i.e., when the restraint length becomes infinity), allowing free rotation and ovalization.

The results suggest that when the crack angle is "small" ($\theta/\pi = 1/8$), the restraint effects may be neglected. However, for larger crack angles ($\theta/\pi = 1/4$), the restrained COD can be significantly different than the unrestrained COD and, hence, cannot be ignored in the crack opening area analysis for leak rate quantification. It is interesting to note that a significant input parameter like the "restraint length" is not considered in either the current versions of the thermohydraulic codes SQUIRT or PICEP (Ref. 7.20) or in any other leak-rate analyses.

7.4 Plans for Next Fiscal Year

The plans for efforts in the next fiscal year are summarized below.

7.4.1 Subtask 6.1 Create Combined Loading Improvements

There are three activities in this subtask.

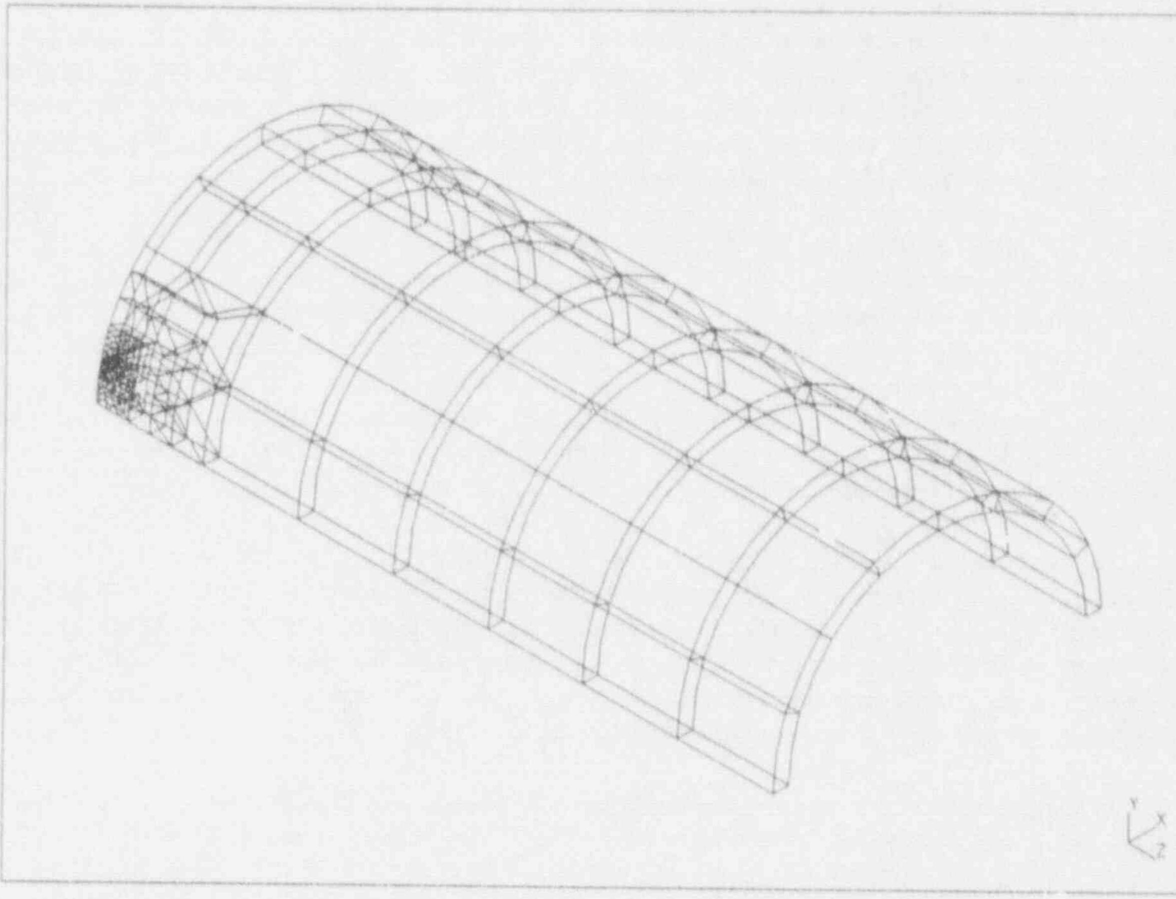

Figure 7.12 Finite element analysis in linear elastic restraint of COD study

SC-M-5/91-F5

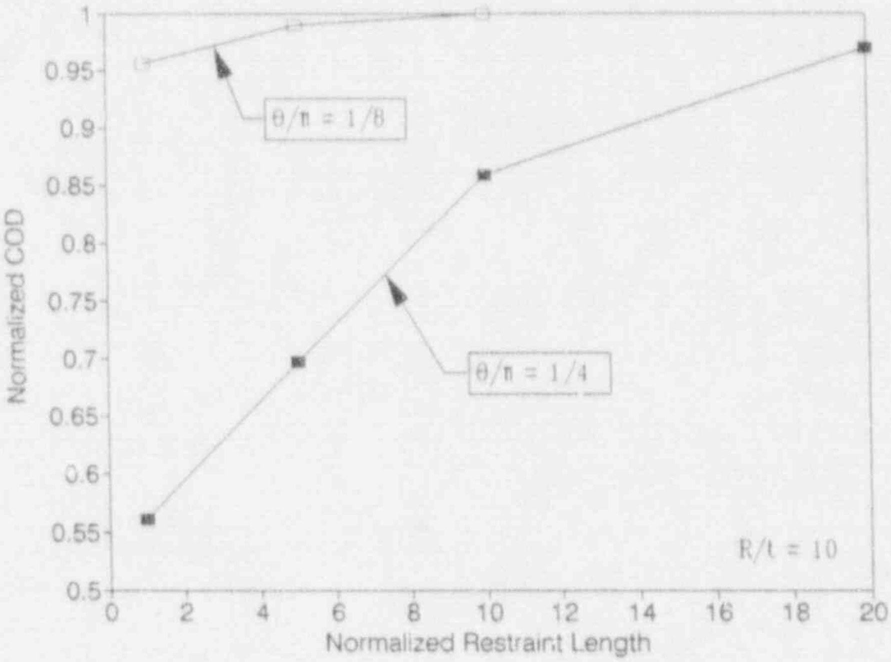

Figure 7.13 Effect of fully restrained bending conditions from crack location on COD normalized by unrestrained COD

SC-M-5/91-F6

Activity 6.1.1 and 6.1.3 have been completed.

Activity 6.1.2 - Account for Pressure on the Crack Face. This activity will be started in fiscal year 1991.

7.4.2 Subtask 6.2 Implement Short TWC Crack-Opening Improvements

This subtask will not start in fiscal year 1991.

7.4.3 Subtask 6.3 Improve Weld Crack Evaluations

There are two activities in this subtask. Activity 6.3.1 was completed, and Activity 6.3.2 (compare with recent DP^{3}II and Task 1 data), has started and will continue as data become available.

7.4.4 Subtask 6.4 Modify SQUIRT Code

This subtask will not start in fiscal year 1991.

7.4.5 Subtask 6.5 Prepare Topical Report on Crack-Opening-Area Improvements

This subtask will not start in fiscal year 1991.

7.4.6 Subtask 6.6 Leak Rate Quantification

This subtask will be completed in fiscal year 1991.

7.5 References

7.1 Kumar, V. and others, "An Engineering Approach for Elastic-Plastic Fracture Analysis," NP 1931, EPRI, 1981.

7.2 Paris, P. C. and Tada, H., "The Application of Fracture Proof Design Methods Using Tearing Instability Theory to Nuclear Piping Postulating Circumferential Through-Wall Cracks," NUREG/CR-3464, September 1983.

7.3 Brust, F. W., "Approximate Methods for Fracture Analysis of Through-Wall Cracked Pipes," NUREG/CR-4853, February 1987.

7.4 Paul, D. D. and others, "Evaluation and Refinement of Leak-Rate-Estimation Models," NUREG/CR-5128, February 1991.

7.5 Klecker, R. W. and others, "NRC LBB (LBB.NRC) Analysis Method for Circumferentially Through-Wall Cracked Pipes Under Axial Plus Bending Loads," NUREG/CR-4572, May 1986.

7.6 Sanders, J. L. Jr., "Circumferential Through-Crack in a Cylindrical Shell Under Combined Bending and Tension," Trans. ASME, Journal of Applied Mechanics, Vol. 50, No. 1, 1983, p. 221.

7.7 Yoo, S. H. and Pan, J., "Closed Form Displacement Solutions for Circumferentially Cracked Pipes in Bending and Tension," University of Michigan Report No. UM-MEAM-88-06, October 10, 1988.

7.8 Smith, E., "The Opening of Through-Wall Cracks in BWR Coolant Lines Due to the Application of Severe Overloads," Int. J. Pres. Vessel and Piping, 11, 1983, pp. 19-31.

7.9 Hasegawa, K. and others, "Crack Opening Area for Leak-Before-Break Evaluation," LBB Seminar, Tokyo, Japan, May 14-15, 1987.

7.10 Wilkowski, G. M. and others, "Degraded Piping Program, Phase II," Final Report, NUREG/CR-4082, Vol. 8, March 1989.

7.11 Gilles, P. and Brust, F. W., "Approximate Methods for Fracture Analysis of Tubular Members Subjected to Combined Tensile and Bending Loads," Proceedings of the 8th OMAE Conference, Hague, The Netherlands, March 1989.

7.12 Wilkowski, G. M. and others, "Analysis of Experiments on Stainless Steel Flux Welds," NUREG/CR-4878, April 1987.

7.13 Brust, F. W., "Approximate Methods for Fracture Analyses of Through-Wall Cracked Pipes", NRC Topical Report by Battelle Columbus Division, NUREG/CR-4853, February 1987.

7.14 Rahman, S., Brust, F. W., Nakagaki, M., and Gilles, P., "An Approximate Method for Estimating Energy Release Rates of Through-Wall Cracked Pipe Weldments," in ASME PVP, Vol. 215, pp. 87-92, June 1991.

7.15 Wilkowski, G. M. and others, "Short Cracks in Piping and Piping Welds," by Battelle, NUREG/CR-4599, Vol. 1, No. 1, May 1991.

7.16 Hiser, A. L. and Callahan, G. M., "A User's Guide to the NRC's Piping Fracture Mechanics Database (PIFRAC)," NUREG/CR-4894, May 1987.

7.17 Schmidt, R. A., Wilkowski, G. M., and Mayfield, M. E., "The International Piping Integrity Research Group (IPIRG) Program -- An Overview," SMiRT-11, Paper G12/1, August 1991.

7.18 Kramer, G. and Papaspyropalous, V., "An Assessment of Circumferentially Complex-Cracked Pipe Subjected to Bending," NUREG/CR-4687, October 1986.

7.19 Wilkowski, G. M. and others, "Degraded Piping Program -- Phase II," Semiannual Report, October 1984-March 1985, NUREG/CR-4082, Vol. 2, July 1985, see Section 2.5.

7.20 Norris, D. and others, "PICEP: Pipe Crack Evaluation Program," EPRI report NP-3596-SR, 1984.

8. TASK 7 NRCPIPE IMPROVEMENTS

8.1 Task Objective

The main objective of this task is to incorporate the analysis improvements from Subtasks 1.4 and 2.4 into the NRCPIPE code. A secondary objective is to make the NRCPIPE Code more efficient and also to restructure the code to allow for ease of implementation of the activities described below.

8.2 Task Rationale

In the Degraded Piping Program, the computer code NRCPIPE was developed for circumferential through-wall-cracked pipe fracture analyses. Numerous J-estimation schemes were developed or modified. The improvements developed in this program need to be incorporated into this code to take advantage of the technology developments, as well as to facilitate the comparisons with the experimental results.

8.3 Task Approach

To accomplish the objectives of this task, four subtasks are to be undertaken:

Subtask 7.1	Improve efficiency of current version
Subtask 7.2	Incorporate TWC improvements in NRCPIPE
Subtask 7.3	Make surface crack version of NRCPIPE
Subtask 7.4	Provide new user's manual.

The crack-opening-area analysis improvements will be incorporated into the SQUIRT code in Subtask 6.4.

Before and after each of the changes in the following activities, quality assurance calculations will be made. These will involve cases where experimental data exists, data are being generated in Tasks 1 and 2, or hypothetical cases, which check critical parameters of interest.

Although some progress was made, the results are not significant to report as yet. These will be reported in the next program report when there are more results.

8.4 Plans for Next Fiscal Year

Efforts scheduled for the rest of fiscal year 1991 are discussed below.

8.4.1 Subtask 7.1 Improve Efficiency of Current Version

Efforts in this subtask will continue next year, including any corrections to the current version of NRCPIPE.

8.4.2 Subtask 7.2 Incorporate TWC Improvements in NRCPIPE

There are four activities in this subtask.

Activity 7.2.1 - Incorporate F-, V_3, and h_4-Function Improvements. This activity will start at the end of fiscal year 1991.

Activity 7.2.2 - Incorporate Ovalization for Short Cracks. No efforts are scheduled for fiscal year 1991.

Activity 7.2.3 - Incorporate Bending and Tension Improvements. These efforts will be ongoing in fiscal year 1991.

Activity 7.2.4 - Incorporate Improved Analyses of Weld and Fusion Line Cracks. These efforts will be ongoing in fiscal year 1991.

8.4.3 Subtask 7.3 Make Surface Crack Version of NRCPIPE

There are seven activities within this subtask.

Activity 7.3.1 - Make Circumferentially Surface-Crack Pipe PC Code of NRCPIPE. The initial framework of the program will be taken from the current TWC version of NRCPIPE in fiscal year 1991.

Activity 7.3.2 - Incorporate ASME Section XI Criteria in NRCPIPE. This effort will start in fiscal year 1991.

Activity 7.3.3 - Add J_e to SC.TNP and SC.TKP. This effort will be started and completed in fiscal year 1991.

Activity 7.3.4 - Add Ovalization. This effort will not start in fiscal year 1991.

Activity 7.3.5 - Incorporate New LBB.ENG Surface-Cracked Pipe Solution. This effort will not start in fiscal year 1991.

Activity 7.3.6 - Add Pressure and Bending Solutions. This activity will be completed in fiscal year 1991.

Activity 7.3.7 - Add Surface-Cracked Pipe Weld Criteria. This activity will not start in fiscal year 1991.

8.4.4 Subtask 7.4 Provide New User's Manual

This subtask will not start in fiscal year 1991.

United McGill Corporation
Columbus Operations 2400 Fairwood Avenue, P.O. Box 820, Columbus, Ohio 43216, 614/443-0192, Telex: 245-384

QW-482 SUGGESTED FORMAT FOR WELDING PROCEDURE SPECIFICATION (WPS)
(See QW-201.1, Section IX, ASME Boiler and Pressure Vessel Code)

Company Name UNITED McGILL CORP. By: [illegible]
Welding Procedure Specification No. 5.1.400 Date 4-18-85 Supporting PQR No.(s) 5.1.400-1,2,3
Revision No. 0 Date 4-18-85
Welding Process(es) GTAW-SMAW-SAW Type(s) MANUAL & MACHINE-SAW
(Automatic, Manual, Machine, or Semi-Auto.)

JOINTS (QW-402)
Joint Design SINGLE or DOUBLE GROOVE & FILLET
Backing (Yes) YES (No) --
Backing Material (Type) ARGON/GTAW; WELD/SMAW & SAW

Sketches, Production Drawings, Weld Symbols or Written Description should show the general arrangement of the parts to be welded. Where applicable, the root spacing and the details of weld groove may be specified.

(At the option of the Mfgr., sketches may be attached to illustrate joint design, weld layers and bead sequence, e.g. for notch toughness procedures, for multiple process procedures, etc.)

Details

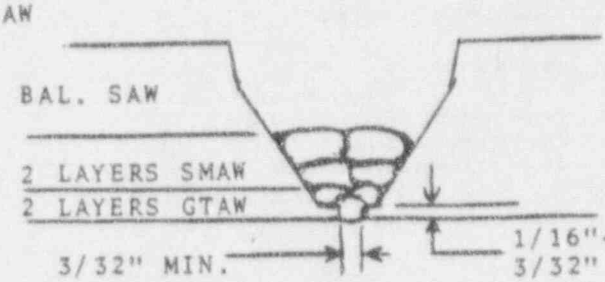

*BASE METALS (QW-403)
P-No. 8 Group No. 1 to P-No. 8 Group No. 1

Base Metal Thickness Range 3/16" to 2".
For GTAW and SMAW
Pipe Dia. Range Any.

For Submerge Arc-Pipe Dia. Range 6" and over.

Deposited Weld Metal Range
Groove GTAW 3/16"-7/16" Fillet ANY
Groove SMAW 3/16"-5/16" Fillet ANY
Groove SAW 3/16"-1-¼" Fillet ANY
Other

*FILLER METALS (QW-404)
F-No. F-6 for GTAW & SAW Other F-5 for SMAW
A-No. A-8 Other A-8
Spec. No. (SFA) SFA-5.9 for GTAW & SAW SFA-5.4 for SMAW
AWS No. (Class) ER-308 E-308
Size of filler metals 3/32" for GTAW 1/8" for SMAW
1/8"- 3/32" For SAW
(Electrode, Cold Wire, Hot Wire, etc.)

Electrode-Flux (Class) ER-308/ST-100
Flux Trade Name LINCOLNWELD
Consumable Insert N/A

*Each base metal-filler metal combination should be recorded individually.

United McGill Corporation

Columbus Operations 2400 Fairwood Avenue, PO Box 820, Columbus, Ohio 43216, 614/443-0192, Telex 245-384

QW-484 MANUFACTURER'S RECORD OF WELDER OR WELDING OPERATOR QUALIFICATION TESTS

Welder Name RICHARD COOPER Check No. 1323 Stamp No. U4

Welding Process SUBMERGED ARC (SAW) Type MACHINE

In accordance with Welding Procedure Specification (WPS) 5.1.400 REV.0

Backing (QW-402) YES WELD METAL

Material (QW-403) Spec. SA-240 to SA-240 of P No. 8 GROUP 1 to P No. 8 GROUP 1

Thickness 1" PLATE Dia. N/A

Filler Metal (QW-404) Spec. No. SFA- 5.9 Class No. ER-308/ST-100 F No. 6

Other DEPOSITED WELD METAL SAW 5/8"

Position (QW-405) (1G, 2G, 6G) 1G

Gas (QW-408) Type N/A % Composition --

Electrical Characteristics (QW-409) Current DIRECT Polarity REVERSE

Weld Progression (QW-410) --

Other --

For Information Only

Filler Metal Diameter and Trade Name 1/8" L-18/8 LINCOLNWELD

Submerged Arc Flux Trade Name ST-100 LINCOLNWELD

Gas Metal Arc Welding Shield Gas Trade Name N/A

Guided Bend Test Results QW-462.2(a), QW-462.3(a), QW-462.3(b)

Type and Fig. No.	Result	
SIDE BEND QW-462.2 (a)		
SIDE BEND QW-462.2 (a)	PASSED NO TEARS	QW-163
SIDE BEND QW-462.2 (a)	PASSED NO TEARS	QW-163
SIDE BEND QW-462.2 (a)	PASSED NO TEARS	QW-163
--	PASSED NO TEARS	QW-163
	--	

Radiographic Test Results (QW-304 & QW-305)

For alternative qualification of groove welds by radiography

Radiographic Results: N/A

Fillet Weld Test Results [See QW-462.4(a), QW-462.4(b)]

Fracture Test (Describe the location, nature and size of any crack or tearing of the specimen)

N/A

Length and Per Cent of Defects -- inches -- %

Macro Test—Fusion --

Appearance—Fillet Size (leg) -- in. x -- in. Convexity -- in. or Concavity -- in.

Test Conducted by Philip A. Chainey Laboratory—Test No. UMC/QA

We certify that the statements in this record are correct and that the test welds were prepared, welded and tested in accordance with the requirements of Sections IX of the ASME Code.

Date 4-26-85

Organization UNITED McGILL CORP.

By Orville Tucker

United McGill Corporation

Columbus Operations 2400 Fairwood Avenue, P.O. Box 820, Columbus, Ohio 432 . 14/443-0192, Telex 245-384

QW-484 MANUFACTURER'S RECORD OF WELDER OR WELDING OPERATOR QUALIFICATION TESTS

Welder Name TOM M. SHAW Check No. 1737 Stamp No. 91
Welding Process GTAW & SMAW Type MANUAL
In accordance with Welding Procedure Specification (WPS) 5.1.400 REV. 0
Backing (QW-402) YES ARGON/GTAW WELD/SMAW
Material (QW-403) Spec. SA-240 to SA-240 of P No. 8 GROUP 1 to P No. 8 GROUP 1
Thickness 1" PLATE Dia. N/A
Filler Metal (QW-404) Spec. No. SFA-5.9 SFA-5.4 Class No. ER-308 E-308 F No. 6, 5
Other DEPOSITED WELD METAL GTAW 7/32" SMAW 5/32"
Position (QW-405) (1G, 2G, 6G) 1G
Gas (QW-408) Type ARGON % Composition 100%
Electrical Characteristics (QW-409) Current DIRECT Polarity STRAIGHT/GTAW REVERSE/SMAW
Weld Progression (QW-410) --
Other --

For Information Only

Filler Metal Diameter and Trade Name 3/32" McAY 1/8" LINCOLN
Submerged Arc Flux Trade Name N/A
Gas Metal Arc Welding Shield Gas Trade Name N/A

Guided Bend Test Results QW-462.2(a), QW-462.3(a), QW-462.3(b)

Type and Fig. No.	Result
SIDE BEND QW-462.2 (a)	PASSED NO TEARS QW-163
SIDE BEND QW-462.2 (a)	PASSED NO TEARS QW-163
SIDE BEND QW-462.2 (a)	PASSED NO TEARS QW-163
SIDE BEND QW-462.2 (a)	PASSED NO TEARS QW-163
--	--

Radiographic Test Results (QW-304 & QW-305)
For alternative qualification of groove welds by radiography

Radiographic Results: N/A

Fillet Weld Test Results [See QW-462.4(a), QW-462.4(b)]

Fracture Test (Describe the location, nature and size of any crack or tearing of the specimen)
N/A

Length and Per Cent of Defects -- inches -- %
Macro Test—Fusion --
Appearance—Fillet Size (leg) -- in. X -- in. Convexity -- in. or Concavity -- in.

Test Conducted by Philip A. Yeaman 4/26/85 Laboratory—Test No. UMC/QA

We certify that the statements in this record are correct and that the test welds were prepared, welded and tested in accordance with the requirements of Sections IX of the ASME Code.

Organization UNITED McGILL CORP.
Date 4-26-85 By Orville Tackett

United McGill Corporation

Columbus Operations 2400 Fairwood Avenue, P.O. Box 820, Columbus, Ohio 43216, 614-443-0192, Telex 245-384

QW-484 MANUFACTURER'S RECORD OF WELDER OR WELDING OPERATOR QUALIFICATION TESTS

Welder Name JOHN HARNESS Check No 2304 Stamp No. 40

Welding Process GTAW and SMAW Type MANUAL

In accordance with Welding Procedure Specification (WPS) 5.1.04 Rev. 0

Backing (QW-402) ARGON BACKING

Material (QW-403) Spec SA-240 TP 316 to SA-240-TP 316 of P No. 8 GROUP 1 to P No. 8 GROUP 1

Thickness 3/8" Dia PLATE

Filler Metal (QW-404) Spec. No. SFA.5.9 & 5.4 Class No ER-308L E-308-16 F No. 6 and 5

Other -----

Position (QW-405) (1G, 2G, 6G) 1G

Gas (QW-408) Type ARGON 100 % Composition WELDING GRADE

Electrical Characteristics (QW-409) Current DIRECT Polarity DCSP-GTAW/DCRP-SMAW

Weld Progression (QW-410) -----

Other -----

For Information Only

Filler Metal Diameter and Trade Name 3/32" N-S EP-308L & 1/8" E-308-16

Submerged Arc Flux Trade Name N/A

Gas Metal Arc Welding Shield Gas Trade Name N/A

Guided Bend Test Results QW-462.2(a), QW-462.3(a), QW-462.3(b)

Type and Fig. No.	Result	
FACE BEND QW-452 & QW-466	SATISFACTORY	NO TEARS
ROOT BEND QW-452 & QW-466	SATISFACTORY	NO TEARS

Radiographic Test Results (QW-304 & QW-305)

For alternative qualification of groove welds by radiography

Radiographic Results: N/A

Fillet Weld Test Results [See QW-462.4(a), QW-462.4(b)]

Fracture Test (Describe the location, nature and size of any crack or tearing of the specimen) N/A

Length and Per Cent of Defects ______ inches ----- %

Macro Test—Fusion ______

Appearance—Fillet Size (leg) ______ in. X ______ in. Convexity ---- in. or Concavity ______ in.

Test Conducted by Phly B. Green QA 8/26/82 Laboratory—Test No. N/A

We certify that the statements in this record are correct and that the test welds were prepared, welded and tested in accordance with the requirements of Sections IX of the ASME Code.

Date 8-26-82

Organization United McGill Corporation

By Orville Tackett

QW-483 (Back)

PQR No. 5.1.400-1,2,3

Tensile Test (QW-150)

Specimen No.	Width	Thickness	Area	Ultimate Total Load lb.	Ultimate Unit Stress psi	Type of Failure & Location
A	.503	1.013	.5095	46,850	91,950	DUCTIL AT
						EDGE OF WELD
B	.495	1.011	.5004	45,980	91,890	DUCTIL AT
						EDGE OF WELD

Guided Bend Tests (QW-160)

Type and Figure No.	Result
SIDE BEND QW-462.2 (a)	PASSED QW-163 NO TEARS
SIDE BEND QW-462.2 (a)	PASSED QW-163 NO TEARS
SIDE BEND QW-462.2 (a)	PASSED QW-163 NO TEARS
SIDE BEND QW-462.2 (a)	PASSED QW-163 NO TEARS

Toughness Tests (QW-170)

Specimen No.	Notch Location	Notch Type	Test Temp.	Impact Values	Lateral Exp. % Shear	Lateral Exp. Mils	Drop Weight Break	Drop Weight No Break
N/A								
--								
--								
--								
--								

Fillet Weld Test (QW-180)

Result — Satisfactory: Yes N/A No -- Penetration into Parent Metal: Yes -- No --

Macro—Results --

Other Tests

Type of Test N/A

Deposit Analysis --

Other --

Welder's Name RICHARD COOPER/SAW THOMAS M. SHAW /GTAW & SMAW Clock No. 1323 1737 Stamp No. U4 91

Tests conducted by: Phil Thomas 4-15-85 Laboratory Test No. UMC/QA

We certify that the statements in this record are correct and that the test welds were prepared, welded and tested in accordance with the requirements of Section IX of the ASME Code.

Manufacturer UNITED McGILL CORP.

Date 4-22-85 By Orville Tackett

(Detail of record of tests are illustrative only and may be modified to conform to the type and number of tests required by the Code.)

QW-483 SUGGESTED FORMAT FOR PROCEDURE QUALIFICATION RECORD (PQR)
(See QW-201.2, Section IX, ASME Boiler and Pressure Vessel Code)
Record Actual Conditions Used to Weld Test Coupon.

Company Name: UNITED McGILL CORP.
Procedure Qualification Record No.: 5.1.400-3 Date: 4-18-85
WPS No.: 5.1.400 rev. 0
Welding Process(es): SUBMERGED ARC (SAW)
Types (Manual, Automatic, Semi-Auto.): MACHINE

JOINTS (QW-402)

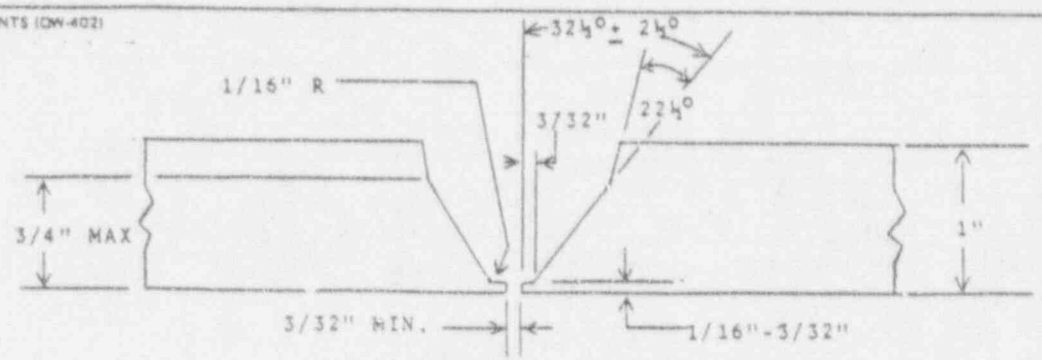

Groove Design of Test Coupon
(For combination qualifications, the deposited weld metal thickness shall be recorded for each filler metal or process weld.)

BASE METALS (QW-403)
Material Spec.: SA-240 to SA-240
Type or Grade: 304 to 304
P-No.: 8, GROUP 1 to P-No.: 8, GROUP 1
Thickness of Test Coupon: 1"
Diameter of Test Coupon: PLATE
Other: ONLY 5/8" of GROOVE WELDED

POSTWELD HEAT TREATMENT (QW-407)
Temperature: NONE
Time: --
Other: --

GAS (QW-408)
Type of Gas or Gases: N/A
Composition of Gas Mixture: --
Other: --

FILLER METALS (QW-404)
Weld Metal Analysis A-No.: 8
Size of Filler Metal: 1/8"
Filler Metal F-No.: 6
SFA Specification: 5.9
AWS Classification: ER-308
Other: DEPOSETED WELD METAL
12 PASSES 5/8" COMPLETE

ELECTRICAL CHARACTERISTICS (QW-409)
Current: DIRECT
Polarity: DCRP
Amps: 385 Volts: 29
Tungsten Electrode Size: N/A
Other: --

POSITION (QW-405)
Position of Groove: 1G
Weld Progression (Uphill, Downhill): --
Other: --

TECHNIQUE (QW-410)
Travel Speed: 18" - 20" I.P.M.
String or Weave Bead: STRING
Oscillation: N/A
Multipass or Single Pass (per side): MULTIPASS
Single or Multiple Electrodes: SINGLE
Other: --

PREHEAT (QW-406)
Preheat Temp.: 60° F MIN.
Interpass Temp.: 350° F MIN.
Other:

QW-483 SUGGESTED FORMAT FOR PROCEDURE QUALIFICATION RECORD (PQR)
(See QW-201.2, Section IX, ASME Boiler and Pressure Vessel Code)
Record Actual Conditions Used to Weld Test Coupon.

Company Name UNITED McGILL CORP.
Procedure Qualification Record No. 5.1.400-2 Date 4-18-85
WPS No. 5.1.400 rev. 0
Welding Process(es) SHIELDED METAL ARC (SMAW)
Types (Manual, Automatic, Semi-Auto.) MANUAL

JOINTS (QW-402)

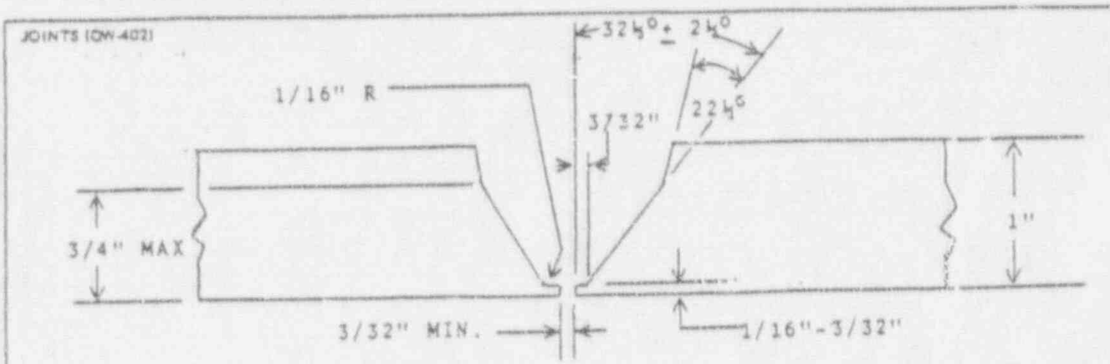

Groove Design of Test Coupon
(For combination qualifications, the deposited weld metal thickness shall be recorded for each filler metal or process used.)

BASE METALS (QW-403)
Material Spec. SA-240 to SA-240
Type or Grade 304 to 304
P-No. 8, GROUP 1 to P-No. 8, GROUP 1
Thickness of Test Coupon 1"
Diameter of Test Coupon PLATE
Other ONLY 5/32" of GROOVE WELDED

POSTWELD HEAT TREATMENT (QW-407)
Temperature NONE
Time --
Other --

GAS (QW-408)
Type of Gas or Gases N/A
Composition of Gas Mixture --
Other

FILLER METALS (QW-404)
Weld Metal Analysis A-No. 8
Size of Filler Metal 1/8"
Filler Metal F-No. 5
SFA Specification 5.4
AWS Classification E-308-16
Other DEPOSETED WELD METAL
4 PASSES 5/32" COMPLETE

ELECTRICAL CHARACTERISTICS (QW-409)
Current DIRECT
Polarity DCRP
Amps 85 Volts 24
Tungsten Electrode Size N/A
Other --

POSITION (QW-405)
Position of Groove 1G
Weld Progression (Uphill, Downhill) --
Other --

TECHNIQUE (QW-410)
Travel Speed 10" I.P.M.
String or Weave Bead STRING
Oscillation N/A
Multipass or Single Pass (per side) MULTIPASS
Single or Multiple Electrodes SINGLE
Other --

PREHEAT (QW-406)
Preheat Temp. 60° MIN.
Interpass Temp. 350° F MAX.
Other --

QW-483 SUGGESTED FORMAT FOR PROCEDURE QUALIFICATION RECORD (PQR)
(See QW-201.2, Section IX, ASME Boiler and Pressure Vessel Code)
Record Actual Conditions Used to Weld Test Coupon.

Company Name: UNITED McGILL CORP.
Procedure Qualification Record No.: 5.1.400-1 Date: 4-18-85
WPS No.: 5.1.400 rev. 0
Welding Process(es): GAS TUNGSTEN ARC (GTAW)
Types (Manual, Automatic, Semi-Auto.): MANUAL

JOINTS (QW-402)

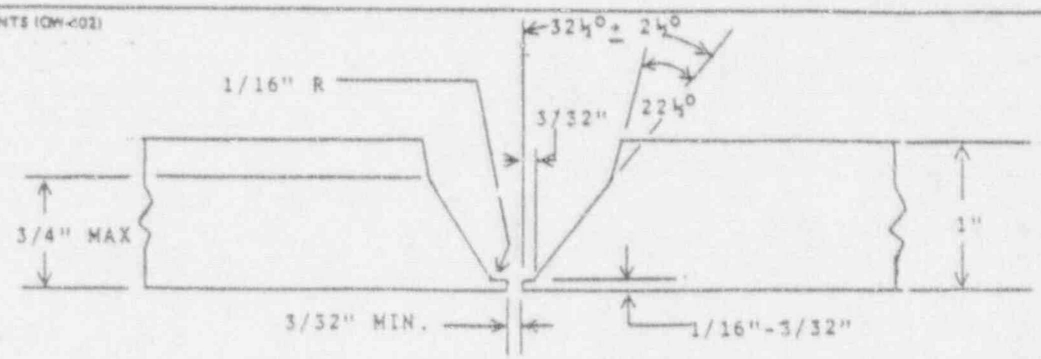

Groove Design of Test Coupon

(For combination qualifications, the deposited weld metal thickness shall be recorded for each filler metal or process used.)

BASE METALS (QW-403)
Material Spec.: SA-240 to SA-240
Type or Grade: 304 to 304
P-No.: 8 GROUP 1 to P-No.: 8 GROUP 1
Thickness of Test Coupon: 1"
Diameter of Test Coupon: PLATE
Other: ONLY 7/32" of GROOVE WELDED

POSTWELD HEAT TREATMENT (QW-407)
Temperature: NONE
Time: --
Other: --
--

GAS (QW-408)
Type of Gas or Gases: ARGON
Composition of Gas Mixture: 100% WELDING GRADE
Other: 22 CHF FLOW, # 7 CUP
ARGON for PURGING BACKSIDE
10 CHF FLOW

FILLER METALS (QW-404)
Weld Metal Analysis A-No.: 8
Size of Filler Metal: 3/32"
Filler Metal F-No.: 6
SFA Specification: 5.9
AWS Classification: ER-308
Other: DEPOSETED WELD METAL
ROOT PASS FIRST LAYER - 2nd & 3nd
PASS 7/32" COMPLETE

ELECTRICAL CHARACTERISTICS (QW-409)
Current: DIRECT
Polarity: DCSP
Amps.: 105 Volts: 15
Tungsten Electrode Size: 3/32
Other: 2% THORIATED

POSITION (QW-405)
Position of Groove: 1G
Weld Progression (Uphill, Downhill): --
Other: --

TECHNIQUE (QW-410)
Travel Speed: 2" - 3" I.P.M.
String or Weave Bead: STRING
Oscillation: N/A
Multipass or Single Pass (per side): MULTIPASS
Single or Multiple Electrodes: SINGLE
Other: --

PREHEAT (QW-406)
Preheat Temp.: 60° F MIN.
Interpass Temp.: 350° F MIN.
Other: --

QW-482 (Back)

WPS No. 5.1.400 Rev. 0

POSITIONS (QW-405)
Position(s) of Groove 1G
Welding Progression: Up N/A Down N/A
Position(s) of Fillet 1F & 2F

POSTWELD HEAT TREATMENT (QW-407)
Temperature Range NONE
Time Range --

PREHEAT (QW-406)
Preheat Temp. Min. 50° F
Interpass Temp. Max. 450° F
Preheat Maintenance TORCH NEUTRAL FLAME
(Continuous or special heating where applicable should be recorded)

GAS (QW-408)
Shielding Gas(es) N/A
Percent Composition (mixtures) --
Flow Rate --
Gas Backing --
Trailing Shielding Gas Composition --

ELECTRICAL CHARACTERISTICS (QW-409)
Current AC or DC DIRECT Polarity REVERSE
Amps (Range) PER TABLE Volts (Range) PER TABLE
(Amps and volts range should be recorded for each electrode size, position, and thickness, etc. This information may be listed in a tabular form similar to that shown below.)

MACHINE
SUBMERGED ARC WELDING
(SAW)

Tungsten Electrode Size and Type N/A
(Pure Tungsten, 2% Thoriated, etc.)
Mode of Metal Transfer for GMAW N/A
(Spray arc, short circuiting arc, etc.)
Electrode Wire feed speed range 50 - 60 I.P.M. 1/8", 55-65 I.P.M. 3/32"

TECHNIQUE (QW-410)
String or Weave Bead STRING
Orifice or Gas Cup Size N/A
Initial and Interpass Cleaning (Brushing, Grinding, etc.) ONLY WITH STAINLESS STEEL BRUSHES AND ALUMINUM OXIDE GRINDING WHEEL
Method of Back Gouging AIR ARC and/or GRIND IF REQUIRED
Oscillation N/A
Contact Tube to Work Distance 5/8" - 1-¼"
Multiple or Single Pass (per side) MULTIPLE
Multiple or Single Electrodes SINGLE
Travel Speed (Range) 14" - 14" I.P.M. 1/8", 12-22 I.P.M. 3/32"
Peening NONE
Other --

Weld Layer(s)	Process	Filler Metal		Current		Volt Range	Travel Speed Range	Other (e.g., Remarks, Comments, Hot Wire Addition, Technique, Torch Angle, Etc.)
		Class	Dia.	Type Polar.	Amp. Range			
1 & UP	SAW	ER-308	1/8"	DCRP	350-400	28-30	14-24 I.P.M.	
1 & UP	SAW	ER-308 ST-100 FLUX	3/32"	DCRP	275-325	24-26	12-22	

QW-482 (Back)

WPS No. 5.1.400 Rev. 0

POSITIONS (QW-405)
Position(s) of Groove 1G - 6G
Welding Progression: Up YES Down NO
Position(s) of Fillet 1F - 5F

POSTWELD HEAT TREATMENT (QW-407)
Temperature Range NONE
Time Range --

PREHEAT (QW-406)
Preheat Temp. Min. 50° F
Interpass Temp. Max. 450 F
Preheat Maintenance TORCH NEUTRAL FLAME
(Continuous or special heating where applicable should be recorded)

GAS (QW-408)
Shielding Gas(es) N/A
Percent Composition (mixtures) --
Flow Rate --
Gas Backing --
Trailing Shielding Gas Composition --

ELECTRICAL CHARACTERISTICS (QW-409)
Current AC or DC DIRECT Polarity REVERSE
Amps (Range) PER TABLE Volts (Range) PER TABLE
(Amps and volts range should be recorded for each electrode size, position, and thickness, etc. This information may be listed in a tabular form similar to that shown below.)

MANUAL
SHIELDED MATAL ARC WELDING
(SMAW)

Tungsten Electrode Size and Type N/A
(Pure Tungsten, 2% Thoriated, etc.)
Mode of Metal Transfer for GMAW N/A
(Spray arc, short circuiting arc, etc.)
Electrode Wire feed speed range N/A

TECHNIQUE (QW-410)
String or Weave Bead EITHER or BOTH
Orifice or Gas Cup Size N/A
Initial and Interpass Cleaning (Brushing, Grinding, etc.) ONLY WITH STAINLESS STEEL BRUSHES AND ALUMINUM OXIDE GRINDING WHEELS
Method of Back Gouging AIR ARC and/or GRIND IF REQUIRED
Oscillation MANUAL 2 FILLER DIA./ STRING 5-FILLER DIA./ WEAVE MAX.
Contact Tube to Work Distance N/A
Multiple or Single Pass (per side) MULTIPLE
Multiple or Single Electrodes SINGLE
Travel Speed (Range) 4" - 12" I.P.M.
Peening NONE
Other NO SINGLE PASS TO EXCEED ½" in THICKNESS

Weld Layer(s)	Process	Filler Metal		Current		Volt Range	Travel Speed Range	Other (e.g., Remarks, Comments, Hot Wire Addition, Technique, Torch Angle, Etc.)
		Class	Dia.	Type Polar.	Amp. Range			
1 -2	SMAW	E-308-16	1/8"	DCRP	80-110	22-26	4"-12" I.P.M.	
1-2	SMAW	E-308-16	3/32"	DCRP	60-80	18-22		

QW-482 (Back)

WPS No. 5.1.400 Rev. 0

POSITIONS (QW-405)
Position(s) of Groove: 1G - 6G
Welding Progression: Up: YES Down:
Position(s) of Fillet: 1F - 5F

POSTWELD HEAT TREATMENT (QW-407)
Temperature Range: NONE
Time Range: - -

PREHEAT (QW-406)
Preheat Temp. Min.: 50° F
Interpass Temp. Max.: 450° F
Preheat Maintenance: TORCH, NEUTRAL FLAME
(Continuous or special heating where applicable should be recorded)

GAS (QW-408)
Shielding Gas(es): ARGON
Percent Composition (mixtures): 100%
Flow Rate: 20 - 25 CFH
Gas Backing: 8 - 12 CFH
Trailing Shielding Gas Composition: N/A

ELECTRICAL CHARACTERISTICS (QW-409)
Current AC or DC: DIRECT Polarity: STRAIGHT
Amps (Range): PER TABLE Volts (Range): PER TABLE
(Amps and volts range should be recorded for each electrode size, position, and thickness, etc. This information may be listed in a tabular form similar to that shown below.)

MANUAL
GAS TUNGSTEN ARC WELDING
(GTAW)

Tungsten Electrode Size and Type: 3/32" 2% THORIATED
(Pure Tungsten, 2% Thoriated, etc.)
Mode of Metal Transfer for GMAW: N/A
(Spray arc, short circuiting arc, etc.)
Electrode Wire feed speed range: N/A

TECHNIQUE (QW-410)
String or Weave Bead: STRING
Orifice or Gas Cup Size: # 6 - # 7
Initial and Interpass Cleaning (Brushing, Grinding, etc.): ONLY WITH STAINLESS STEEL BRUSHES AND ALUMINUM OXIDE GRINDING WHEELS
Method of Back Gouging: N/A
Oscillation: MANUAL 2 FILLER DIAMETERS MAX.
Contact Tube to Work Distance: 1/16" - 3/32"
Multiple or Single Pass (per side): MULTIPLE
Multiple or Single Electrodes: SINGLE
Travel Speed (Range): MANUAL 2 - 4 I.P.M.
Peening: NONE
Other:

Weld Layer(s)	Process	Filler Metal Class	Filler Metal Dia.	Current Type Polar.	Current Amp. Range	Volt Range	Travel Speed Range	Other (e.g., Remarks, Comments, Hot Wire Addition, Technique, Torch Angle, Etc.)
1-2	GTAW	ER-308	3/32"	DCSP	90-130	14-18	2-4 I.P.M.	
1-2	GTAW	ER-308	1/16"	DCSP	50-90	10-14		

APPENDIX B PLASTIC SOLUTION OF EQUIVALENT PIPE

Using classical beam theory for small deformation, the governing differential equations for the pipe shown in Figure 2.24 are:

1. Segment AB ($\hat{a}/2 \le x \le L/2$)

$$\frac{d^2y}{dx^2} = \frac{1}{R}\left(\frac{M}{M_{01}}\right)^{n_1} \tag{B-1}$$

$$\frac{dy}{dx} = \frac{1}{R}\left(\frac{M}{M_{01}}\right)^{n_1} x + C_1 \tag{B-2}$$

$$y = \frac{1}{R}\left(\frac{M}{M_{01}}\right)^{n_1} \frac{x^2}{2} + C_1 x + C_2 \tag{B-3}$$

2. Segment BC ($L_w/2 \le x \le \hat{a}/2$)

$$\frac{d^2y}{dx^2} = \frac{1}{R}\left(\frac{M}{M_{01}}\right)^{n_1}\left(\frac{t}{t_e}\right)^{n_1} \tag{B-4}$$

$$\frac{dy}{dx} = \frac{1}{R}\left(\frac{M}{M_{01}}\right)^{n_1}\left(\frac{t}{t_e}\right)^{n_1} x + C_3 \tag{B-5}$$

$$y = \frac{1}{R}\left(\frac{M}{M_{01}}\right)^{n_1}\left(\frac{t}{t_e}\right)^{n_1}\frac{x^2}{2} + C_3 x + C_4 \tag{B-6}$$

3. Segment CD ($0 \le x \le L_w/2$)

$$\frac{d^2y}{dx^2} = \frac{1}{R}\left(\frac{M}{M_{02}}\right)^{n_2}\left(\frac{t}{t_e}\right)^{n_2} \tag{B-7}$$

$$\frac{dy}{dx} = \frac{1}{R}\left(\frac{M}{M_{02}}\right)^{n_2}\left(\frac{t}{t_e}\right)^{n_2} x + C_5 \tag{B-8}$$

$$y = \frac{1}{R}\left(\frac{M}{M_{02}}\right)^{n_2}\left(\frac{t}{t_e}\right)^{n_2}\frac{x^2}{2} + C_5 x + C_6 \tag{B-9}$$

where

$$M_{0i} = \frac{4K_i I \hat{K}_i}{\pi R},\; K_i = \frac{\sigma_{0i}}{({}_i\epsilon_{0i})^{1/n_i}},\; \hat{K}_i = \frac{\sqrt{\pi}}{2}\,\frac{\Gamma\left(1 + \frac{1}{2n_i}\right)}{\Gamma\left(\frac{3}{2} + \frac{1}{2n_i}\right)} \tag{B-10}$$

with the gamma function

$$\Gamma(u) = \int_0^{\infty} \xi^{u-1} \exp(-\xi)\, d\xi \tag{B-11}$$

and $I \simeq \pi R^3 t$ is the moment of inertia of original pipe cross-section. Enforcing appropriate bounuary and compatability conditions, the constants C_1-C_6 can be easily determined as:

$$C_1 = -\frac{1}{R}\left(\frac{M}{M_{01}}\right)^{n_1}\left[\frac{\hat{a}}{2}\left\{1-\left(\frac{t}{t_e}\right)^{n_1}\right\}+\frac{L_w}{2}\left(\frac{t}{t_e}\right)^{n_1}\right]+\frac{1}{R}\left(\frac{M}{M_{02}}\right)^{n_2}\left[\frac{L_w}{2}\left(\frac{t}{t_e}\right)^{n_2}\right] \tag{B-12}$$

$$\begin{aligned} C_2 = {} & \frac{1}{R}\left(\frac{M}{M_{01}}\right)^{n_1}\left[-\frac{L^2}{8}+\frac{L}{2}\frac{\hat{a}}{2}\left\{1-\left(\frac{t}{t_e}\right)^{n_1}\right\}+\frac{L}{2}\frac{L_w}{2}\left(\frac{t}{t_e}\right)^{n_1}\right] - \\ & \frac{1}{R}\left(\frac{M}{M_{02}}\right)^{n_2}\left[\frac{L}{2}\frac{L_w}{2}\left(\frac{t}{t_e}\right)^{n_2}\right] \end{aligned} \tag{B-13}$$

$$C_3 = -\frac{1}{R}\left(\frac{M}{M_{01}}\right)^{n_1}\left[\frac{L_w}{2}\left(\frac{t}{t_e}\right)^{n_1}\right]+\frac{1}{R}\left(\frac{M}{M_{02}}\right)^{n_2}\left[\frac{L_w}{2}\left(\frac{t}{t_e}\right)^{n_2}\right] \tag{B-14}$$

$$C_4 = \frac{1}{R}\left(\frac{M}{M_{01}}\right)^{n_1}\left[-\frac{L^2}{8} + \frac{L}{2}\frac{\hat{a}}{2}\left\{1 - \left(\frac{t}{t_e}\right)^{n_1}\right\} + \frac{L}{2}\frac{L_w}{2}\left(\frac{t}{t_e}\right)^{n_1} - \frac{\hat{a}^2}{8}\right] - \frac{1}{R}\left(\frac{M}{M_{02}}\right)^{n_2}\left[\frac{L}{2}\frac{L_w}{2}\left(\frac{t}{t_e}\right)^{n_2}\right] \tag{B-15}$$

$$C_5 = 0 \tag{B-16}$$

$$C_6 = \frac{1}{R}\left(\frac{M}{M_{01}}\right)^{n_1} \times$$

$$\left[-\frac{L^2}{8} + \frac{L}{2}\frac{\hat{a}}{2}\left\{1 - \left(\frac{t}{t_e}\right)^{n_1}\right\} + \frac{L}{2}\frac{L_w}{2}\left(\frac{t}{t_e}\right)^{n_1} - \frac{\hat{a}^2}{8} - \frac{L_w^2}{8}\left(\frac{t}{t_e}\right)^{n_1}\right] - \frac{1}{R}\left(\frac{M}{M_{02}}\right)^{n_2}\left[\frac{L_w^2}{8}\left(\frac{t}{t_e}\right)^{n_2} - \frac{L}{2}\frac{L_w}{2}\left(\frac{t}{t_e}\right)^{n_2}\right] \tag{B-17}$$

APPENDIX C PARTIAL DERIVATIVES $\partial I_B/\partial\theta$ AND $\partial L^d_B/\partial\theta$

The expression for the derivatives $\partial I_B/\partial\theta$ and $\partial L^d_B/\partial\theta$ are given below:

$$\frac{\partial I_B}{\partial\theta} = 4\theta F_B(\theta)^2 \tag{C-1}$$

$$\frac{\partial L_B{}^d}{\partial\theta} = \frac{1}{[A_3G_1(\theta)]^2}\{A_3G_1(\theta)[A_1G_{n1}(\theta) + A_2G_{n2}(\theta)] - A_3G_1(\theta)[A_1G_{n1}(\theta) + A_2G_{n2}(\theta)]\} \tag{C-2}$$

in which

$$\begin{aligned} G_k(\theta) &= \left(\cos\frac{\theta}{2} - \frac{1}{2}\sin\theta\right)^{-k} \\ G_k(\theta) &= \frac{k}{2}\left(\sin\frac{\theta}{2} + \cos\theta\right)G_{k+1}(\theta) \end{aligned} \tag{C-3}$$

$$\begin{aligned} A_1 &= \left(\frac{M}{M_{01}}\right)^{n_1}\left[\frac{\hat{a}}{2} - \frac{L_w}{2}\right]C^{-n_1}\cdot\frac{1}{\alpha_1\left(\frac{M}{M_1}\right)^{n_1-1}} \\ A_2 &= \left(\frac{M}{M_{02}}\right)^{n_2}\left[\frac{L_w}{2}\right]C^{-n_2}\frac{1}{\alpha_1\left(\frac{M}{M_1}\right)^{n_1-1}} \\ A_3 &= \left(\frac{M}{M_1}\right)\epsilon_{01}\left[\frac{\hat{a}}{2} - \frac{L_w}{2}\right]C^{-1} + \left(\frac{M}{M_2}\right)\epsilon_{02}\left[\frac{L_w}{2}\right]C^{-1} \end{aligned} \tag{C-4}$$

where $C = 1$ or $C = 4/\pi$ according to whether $0° \leq 2\theta \leq 90°$ or $2\theta \geq 120°$, respectively. When $90° \leq 2\theta \leq 120°$, C can be interpolated from the above two limits (Brust, NUREG/CR-4853, 1987).

NRC FORM 335 (2-89) NRCM 1102, 3201, 3202

U.S. NUCLEAR REGULATORY COMMISSION

BIBLIOGRAPHIC DATA SHEET

(See instructions on the reverse)

1. REPORT NUMBER (Assigned by NRC. Add Vol., Supp., Rev., and Addendum Numbers, if any.)

NUREG/CR-4599
BMI-2173
Vol. 1, No. 2

2. TITLE AND SUBTITLE

Short Cracks in Piping and Piping Welds
Semiannual Report
October 1990 - March 1991

3. DATE REPORT PUBLISHED

MONTH: April
YEAR: 1992

4. FIN OR GRANT NUMBER

B5702

5. AUTHOR(S)

G. M. Wilkowski, F. Brust, [illegible] Francini, N. Ghadiali, T. Kilinski, P. Krishnas[illegible], M. Landow, C. W. Marschall, S. Rahman, P. Scott

6. TYPE OF REPORT

Technical

7. PERIOD COVERED (Inclusive Dates)

Oct. 1990-March 1991

8. PERFORMING ORGANIZATION — NAME AND ADDRESS (If NRC, provide Division, Office or Region, U.S. Nuclear Regulatory Commission, and mailing address; if contractor, provide name and mailing address.)

Battelle
505 King Avenue
Columbus, OH 43201-2693

9. SPONSORING ORGANIZATION — NAME AND ADDRESS (If NRC, type "Same as above"; if contractor, provide NRC Division, Office or Region, U.S. Nuclear Regulatory Commission, and mailing address.)

Division of Engineering
Office of Nuclear Regulatory Research
U.S. Nuclear Regulatory Commission
Washington, D.C. 20555

10. SUPPLEMENTARY NOTES

11. ABSTRACT (200 words or less)

This is the second semiannual report of the U.S. Nuclear Regulatory Commission's Short Cracks in Piping and Piping Welds research program. The program began in March 1990 and will extend for 4 years. The intent of this program is to verify and improve fracture analyses for circumferentially cracked large-diameter nuclear piping with crack sizes typically used in leak-before-break analyses or in-service flaw evaluations. Only quasi-static loading rates are evaluated since the NRC's International Piping Integrity Research Group (IPIRG) program is evaluating the effects of seismic loading rates on cracked piping systems.

Progress for through-wall-cracked pipe involved (1) conducting a 28-inch diameter stainless steel SAW and 4-inch diameter French TP316 experiments, (2) conducting a matrix of FEM analyses to determine GE/EPRI functions for short TWC pipe, (3) comparison of uncracked pipe maximum moments to various analyses and FEM solutions, and (4) development of a J-estimation scheme that includes the strength of both the weld and base metals.

Progress for surface-cracked pipe involved (1) conducting two experiments on 6-inch diameter (Sch. 40 and XXS) pipe with d/t = 0.6 and θ/π = 0.25 cracks, (2) comparisons of the pipe experiments to Net-Section-Collapse predictions, and (3) modification of the SC.TNP and SC.TKP J-estimation schemes to include external surface cracks.

High-temperature hardness testing appears to be a useful screening criteria parameter for assessing the susceptibility of ferritic pipe to dynamic strain aging. For anisotropic fracture evaluations, it was found that only one of five ferritic pipes had the low toughness direction in a helical direction, the rest had low toughness in the axial direction.

For crack-opening area analyses, predictive capabilities were expanded so that load versus crack opening can be calculated from the LBB.NRC, GE/EPRI, LBB.GE, LBB.ENG, and Tada/Paris analyses. These include loading due to tension, bending, and combined tension and bending. The LBB.ENG analysis was also modified to account for the weld and base metals strengths. Elastic FEA showed that for pressure loading, a crack close to a terminal end (i.e., a nozzle) will have lower crack opening due to restraint of the induced bending. This could affect LBB analyses.

12. KEY WORDS/DESCRIPTORS (List words or phrases that will assist researchers in locating the report.)

Pipe, Fracture Mechanics, Cracks, J-Integral/Tearing Modulus, Elastic-Plastic Fracture Mechanics, Nuclear Piping Steels

13. AVAILABILITY STATEMENT

Unlimited

14. SECURITY CLASSIFICATION

(This Page)
Unclassified

(This Report)
Unclassified

15. NUMBER OF PAGES

16. PRICE

NRC FORM 335 (2-89)

UNITED STATES
NUCLEAR REGULATORY COMMISSION
WASHINGTON, D.C. 20555

OFFICIAL BUSINESS
PENALTY FOR PRIVATE USE, $300

SPECIAL FOURTH-CLASS RATE
POSTAGE AND FEES PAID
USNRC
PERMIT NO. G-67